Studies of Aryl Ether Linked Polybenzimidazole for the Use in Fuel Cell

A Thesis Submitted for the Degree of

DOCTOR OF PHILOSOPHY

BY

Sandip Ghosh

School of Chemistry
University of Hyderabad
Hyderabad-500 046
INDIA

June 2011

Dedicated
to
Ma & Baba

DECLARATION

I hereby declare that the matter embodied in the thesis entitled "**Studies of Aryl Ether Linked Polybenzimidazole for the Use in Fuel Cell**" is the result of investigations carried out by me in the School of Chemistry, University of Hyderabad, Hyderabad, India under the supervision of **Dr. Tushar Jana** and it has not been submitted elsewhere for the award of any degree or diploma or membership, etc.

In keeping with the general practice of reporting scientific investigations, due acknowledgements have been made wherever the work described is based on the findings of other investigators. Any omission or error that might have crept in is regretted.

June 2011 **Sandip Ghosh**

UNIVERSITY OF HYDERABAD
Central University (P.O.), Hyderabad-500046, INDIA

Dr. Tushar Jana
Associate Professor
School of Chemistry

Tel: 91-40-23134808 (Office)
91-9440127016 (Mobile)
Fax: 91-40-23012460
E-mail: tjsc@uohyd.ernet.in
tjscuoh@gmail.com
Web: http://chemistry.uohyd.ernet.in/~tj/

CERTIFICATE

This is to certify that the work described in this thesis entitled "**Studies of Aryl Ether Linked Polybenzimidazole for the Use in Fuel Cell**" has been carried out by Mr. Sandip Ghosh under my supervision and the same has not been submitted elsewhere for any degree.

Dean
School of Chemistry
University of Hyderabad
Hyderabad-500 046
India

Dr. Tushar Jana
(Thesis supervisor)

PREFACE

The present thesis entitled *"Studies of Aryl Ether Linked Polybenzimidazole for the Use in Fuel Cell"* has been divided into seven chapters. ***Chapter 1*** provides a brief introduction on polybenzimidazoles type of heterocyclic polymers, common synthesis procedure, their various properties and applications. The most advanced application of phosphoric acid doped polybenzimidazole membrane as a polymer electrolyte membrane in high temperature PEM fuel cell has also discussed. ***Chapter 2*** deals with synthesis of series of poly(4,4'-diphenylether-5,5'-bibenzimidazole) (OPBI) polymers by varying the initial monomer concentration. The effects of the initial monomer concentration on the various molecular properties of the synthesized OPBI polymers are investigated. In ***Chapter 3*** discusses the effect of solvent protic character on aggregation behavior of the OPBI. A conformational transition of OPBI chains in polar aprotic solvent like N,N-dimethyl acetamide (DMAc) with aggregation is observed and monitored. ***Chapter 4*** deals with the development of thermoreversible gel of OPBI in formic acid (FA). The PA doped OPBI membrane is fabricated from this gel which shows high acid doping level and proton conductivity due to porous nature of the membrane. ***Chapter 5*** describes the synthesis of nanocomposites of OPBI with two structurally different clays (MMT and Kao) by solution blending process. The influences of incorporation of nanosized clays on the properties of OPBI are evaluated. ***Chapter 6*** describes the formation of nanocomposite of OPBI with silica nanoparticle by solution blending process. The influences of incorporation of nanosized silica particle on the properties of OPBI are evaluated. ***Chapter 7*** summarizes the findings of the present investigations, presents a concluding remark and the future scope and upcoming challenges.

June, 2011

School of chemistry,
University of Hyderabad
Hyderabad 500 046, India

Sandip Ghosh

Acknowledgement

It is my immense pleasure to express my sincere gratitude to my research supervisor Dr. Tushar Jana, for his constant cooperation, encouragement and kind guidance. He has been quite helpful to me in both academic and personal fronts. It has been great pleasure and fortune to work with him who introduced me to the field of Polymer Chemistry. His discipline working style and honesty for the research has paved a new path in my career. I am also indebted to him for the work freedom he has given me during the last five years.

I would like to thank the former and present Dean, School of Chemistry, for their constant inspiration and for allowing me to avail the available facilities. I am extremely thankful individually to all the faculty members of the school for their kind help and cooperation at various stages of my stay in the campus. I am also grateful to all my former teachers for their help.

I am very grateful to Dr. R. Nagarajan and Dr. R. Chandrasekhar for their constant support throughout my research career.

Financial assistance from CSIR, New Delhi for providing Research Fellowship as well as various instrumental facilities, is sincerely acknowledged.

I would also like to express my sincere gratitude to Mr. Pavan of central Instrumental Laboratory (CIL), UoH for their help with SEM experiments. I sincerely acknowledge Mr. Durgaprasad (Centre for Nanotechnology, UOH) for helping me with TEM experiments.

I am deeply predicated to all my teachers starting from my school to the university for their wonderful teaching and education throughout my academics.

I felt very lucky and proudy to have labmates like Arindam, Arun, Murali, Mousumi, Sudhangshu, Malkappa and Shuvra in my ph.d life. Arindam, Arun and Murali are very good friends of mine, they are always with me in my difficult time. I am thankful to Arindam for his support and help at the initial stage of my research. I acknowledge my junior brothers and sisters Sudhangshu, Malkappa, Mousumi, Shuvra and Raju for maintaining the friendly and cooperative atmosphere in the lab. I am really lucky to have them as my juniors. My special thanks to project students Bidhan, Seenimeera, Subhramaniyam, Subhadip, Ashok keerthi, Apparao, Niranjan, Swami, Chandrasekhar, Ajay Krishnan, Sweta, Arghya, Anmol and Chinmoy.

I also thank all non-teaching staff for their timely help, Mr. Shetty in particular.

I would also like to express my sincere thanks to all my dadas and didis with whom I have some wonderful memories in Hyderabad during my Ph.D life. The senior dadas and didis who still matter are Rahulda, Dinuda, Binoyda, Sandyda, Abhikda, Sunirbanda, Archanda, Subhashda, Manabda, Saikatda, Prasunda, Moloyda, Masumda, Aniruddhada, Abhijitda,

Prashantda, Utpalda, Bipulda, Pradipda, Ghanada. Shatabdidi, Bhaswatidi, Aninditadi, Sriparnadi, Suparnadi with whom I have shared many unforgettable moments in this campus and who were never really like 'dada & didi' to me..

I am really lucky for my close association with 'the gang' of HCU Bongs which include Tapta, Tanmoy, Subrata, Susanta, Pati, Vasudhara, Rumpa. My special thanks to Tapta and Tanmoy who are more than a friend of mine. I am really lucky to have juniors like Susruta, Rishi, Dinesh, Palash, Tanmoy, Sandip, Meheboob, Anup, Nayan, Raja, Supratim, Satyajit, Tulika, Chandrani, Paramita, Sanghamitra, Pramiti, Sutanuka, Poulumi and so many others.

A note of thanks also goes to Madhu anna, Biju anna, Teja bhai, Anji, Satpal, Rajeshwar, Vignesh, Ganesh, Chandrashekar, Viji, Ramu, Rajesh, Ramesh, Gupta, Shiva, Ravi, DK Srinivas, Chaitanya, Naba, Ranjeet, Sanjib and Tridib.

It's my pleasure to thank my best friends Krishanu and Sandip for their help and encouragement.

My parents – my beloved 'Ma r Baba', without their sacrifice and mental support I would not have reached to this stage of my life. I am greatly indebted from the bottom of my heart to my baba for his spiritual guidance and stay as a philosopher of my life. My ma deserves special mention for her inseparable support and prayers. This thesis would have not been possible without the selfless love and support of my dada, baudi and bhaiji (Ananya). I value the blessings of my Dadu, Didun, pan didun, grand father and grand mother.

Words are not enough to express my appreciation, gratitude earnest feelings to my wife Munmun for giving me her constant mental support and encouragement in the last period of my Ph.D life and my little princess, Simantika who is a blessing in the guise of daughter.

June 2011 **Sandip Ghosh**

University of Hyderabad,

Hyderabad-500 046

India

Common Abbreviations

OPBI	poly(4,4'-diphenylether-5,5'-bibenzimidazole); as aryl ether linked polybenzimidazole
DSC	differential scanning calorimeter
FA	formic acid
DMAc	N,N-dimethylacetamide
DMF	N,N-dimethylformamide
DMA	dynamic mechanical analyzer
FTIR	fourier transform infrared spectroscopy
IPA	isophthalic acid
NMR	nuclear magnetic resonance
$\overline{M}_n$	number average molecular weight
$\overline{M}_w$	weight average molecular weight
NMP	N-methyl-2-pyrrolidone
MEA	membrane electrode assembly
PA	phosphoric acid
PBI	polybenzimidazole
MEA	membrane electrode assembly
PEMFC	polymer electrolyte membrane fuel cell
SEM	scanning electron microscopy
T_g	glass transition temperature
TAB	3, 3', 4, 4' – tetraaminobiphenyl
TGA	thermogravimetric analyzer
t	time
T	temperature
TEM	transmission electron microscopy
MWNT	multiwalled carbon nanotube
XRD	X-ray diffraction
GP	graphene

CONTENTS

Chapter 1

Introduction

1.1. History of Polybenzimidazole (PBI)

Insulating and protecting astronauts from temperature extremes, from the 3 K (-270°C) of deep space to the 1,533 K (1260°C) of atmospheric environment, is essential to NASA's human space flight program. NASA had spent great deal of efforts on developing and refining fire-resistant materials for use in space vehicles, flight suits, and other applications which demands extreme thermal tolerances, and kept a close eye on the high temperature stable polymers for its entire 50-years history. Prof. Marvel from University of Illinois first synthesized Polybenzimidazole (PBI) while studying the creation of high-temperature stable polymers for the U.S. Air Force. In 1961, PBI was further developed by Marvel and Vogel,[1-4] correctly anticipating that the polymers have exceptional thermal and oxidative stabilities. Polybenzimidazoles are class of linear aromatic heterocyclic polymers with benzimidazole as a repeating unit which show excellent thermal stability as well as flame retardation property, radiative stability, excellent mechanical, thermal stabilities, and strength retention over wide range of temperatures, toughness, chemical inertness and adhesion characteristics.[1,2] In 1963, NASA and the Air Force Materials Laboratory sponsored considerable work with PBI for aerospace and defense applications as a nonflammable and thermally stable textile fiber. Then, NASA sponsored the Celanese Corporation to develop a series of PBI textiles for use in space suits and vehicles.[5,6] Celanese engineers developed heat and flame resistant PBI fabric based on the fiber for high temperature applications.[5-7] The fibers formed from the PBI polymer exhibited a number of highly desirable characteristics, such as inflammability, no melting point, and retention of both strength and flexibility after exposure to flame. Polybenzimidazole with meta phenylene linkage, poly[2,2'-(m-phenylene)-5,5'-bibenzimidazole] was commercialized by Celanese as "PBI" for the use in wide range of textile fibers. In 1980s the low molecular weight PBI was marketed under the name of Celazole® as molding resins. Due to the wide range of applications of the polybenzimidazole, it has received significant attention by many researchers during last 15 years or so.[1-14]

1.2. Different Synthetic Routes of Polybenzimidazole

Polybenzimidazoles, a category of aromatic heterocyclic polymers, exhibit excellent thermal stability as well as other physicochemical properties to be widely used in different fields, are generally synthesized by the polycondensation or step growth polymerization of an aromatic bis(*o*-diamine)s with an aromatic diacids (or diacid derivate such as a diacid chloride or diacid diphenylester).[1,2,5,9] Varieties of polycondensation techniques have been reviewed by several authors for the synthesis of polybenzimidazole are as follows

(i) Melt polymerization[1-3] was carried out under nitrogen atmosphere by heating the equimolar amount of tetraamine (TAB) with diphenyl isophthalate (DPIP), isothalic acid (IPA), dimethyl isophthalate or isophthalonitrile followed by second stage heating of the solid prepolymer at an elevated temperature (Scheme 1.1) and the temperature was gradually increased from about 200 to 300°C. The initial low molecular weight materials were pulverized immediately and reheated under high vacuum for several hours at 350-400°C.

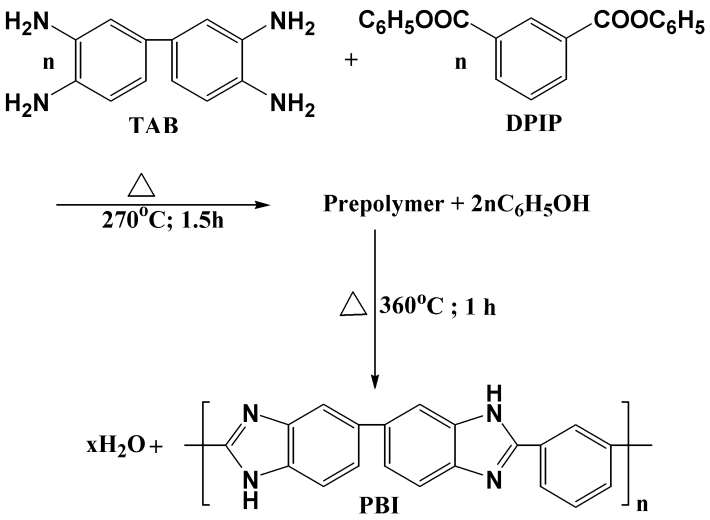

Scheme 1.1. *Melt condensation used for polybenzimidazole (PBI) synthesis.*

(ii) Solution polymerization[15-17] was carried out under nitrogen atmosphere by taking the equimolar tetraamines and aromatic dicarboxylic acids or its derivatives and then dissolved in polyphosphoric acid (PPA) at 140°C in a three necked round-bottomed flask equipped with a nitrogen inlet and outlet and mechanical stirrer. The reaction mixture is then heated to at 180-210°C for about 18-20 h with stirring and finally poured into the water and neutralized by alkaline solution and dried under vacuum oven (Scheme 1.2). Iwakura et al.[18] introduced polyphosphoric acid in 1964 as a solvent for solution polymerization technique where polyphosphoric acid has been used as a solvent as well as catalyst for large numbers of polyheterocyclization systems.[5,19-22]

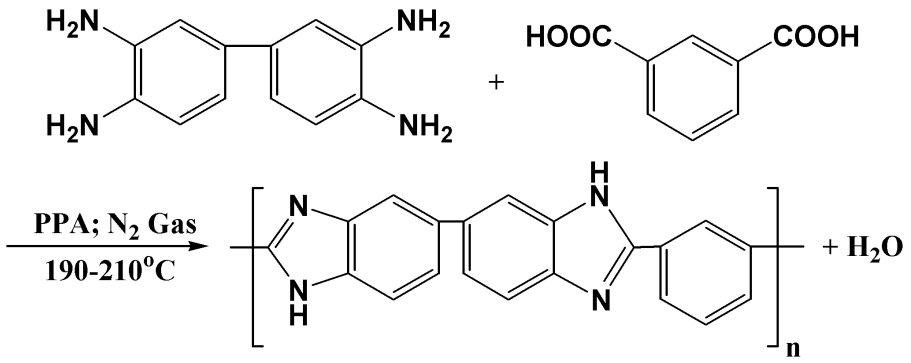

Scheme 1.2. *Solution polymerization of polybenzimidazole (PBI) in polyphosphoric acid (PPA) medium.*

(iii) Catalytic polymerization[5,19,23-28] was carried out with tetramine and aromatic diacid derivatives in presence of catalysts such as ammonium chloride, hydrochloric acid, *p*-toluensulfonic acid, phosphoric acid, triphenyl phosphate, etc (Scheme 1.3). Phosphorus containing catalysts like phosphoric acid, triphenyl phosphate, dipheny phosphate, triphenylphosphine oxide are found to be very much effective for producing the PBI with high molecular weight.

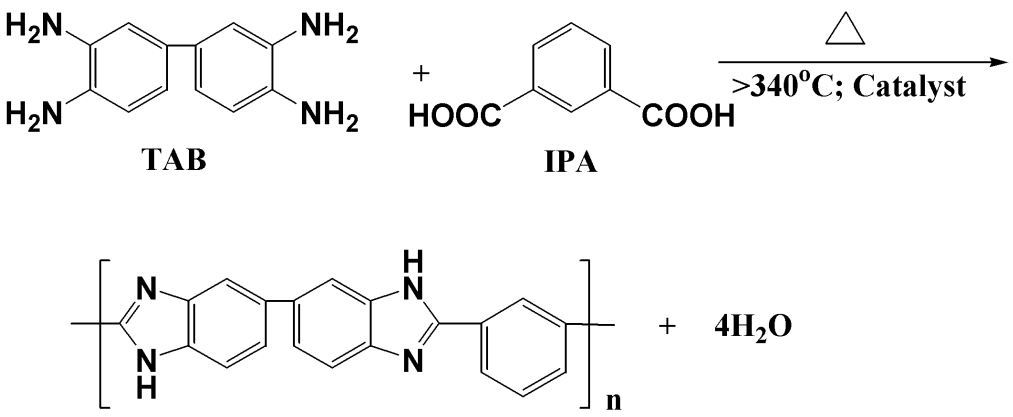

Scheme 1.3. *Catalytic polymerization for polybenzimidazole (PBI) synthesis.*

1.3. Varieties of Polybenzimidazole

Synthesis of PBI polymers with varieties of structures still remains an important area of investigation for the researchers working in the area of polybenzimidazole chemistry. Since the early discovery of PBI in 1961 by Marvel et al., large numbers of high-temperature resistance PBI polymer with different structures have been synthesized and studied. The commercially available PBI, poly [2,2'-(1,3-phenylene)-5,5'-benzimidazole][29] (known as *m*-PBI) is the most widely used structure among all PBI polymers. Other varieties include poly [2,2'-(1,4- phenylene)-5,5'-benzimidazole] (known as *p*-PBI)[9], poly(4,4'-diphenylether-5,5'-bibenzimidazole) (OPBI),[30-32] poly(2,5-benzimidazole) (AB-PBI),[33] pyridine based PBI,[34,35] sulfonated PBI,[36] hyperbranched polybenzimidazole (HPBI),[37] naphthalene based PBI,[38] fluorinated PBI,[39] meta and para PBI copolymer,[40] PBI with sulfone or sulfonic acid groups in the backbone[41] and many others. Few important types of PBI structures have been listed in Scheme 1.4. The poor solubility of PBI resulting from the highly rigid polymer backbones and the strong intra-interchain hydrogen bonding interactions makes them hard to process. Modifying the polymers to impart solubility without sacrificing the desirable properties of the aromatic polymers has therefore been a priority. Several attempts have been made through the

modification of the polymer backbone as well as side chain to solve the solubility issues.[42-44] Many investigators have incorporated flexible spacers such as methylene and arylmethylenes, arylamide and ether linkages in the polymer backbone.[45,46] Substitution of the nitrogen atom on the PBI backbone destroys its rigid-rod nature and also systematic structural variation of PBI by N-substitution by alkyl groups offer improved solubility in volatile solvents (chloroform and 1,1',2,2'-tetrachloroethane), which would ease processibility.[5,47] Among the various structures of PBI, poly(4,4'- diphenylether-5,5'-bibenzimidazole) (OPBI) exhibits distinct properties due to presence of flexible aryl ether linkage. The incorporation of aryl ether linkages into rigid heterocyclic polymer backbones can improve solubility while preserving many of the desired thermal and mechanical properties.[32] It is found that polybenzimidazoles containing fluorinated groups serves to increase the free volume, thereby improving various properties like solubility, electrical insulating properties, etc as well as reduces moisture absorption due to the hydrophobic character of fluorinated groups.[39] The presence of sulfonated groups in polybenzimidazole backbone or in side chains also improved membrane properties, such as water retention, ionic conductivity, and mechanical strength.[36] Again in order to improve properties such as mechanical strength, acid doping levels, conductivity and stability, copolymers of polybenzimidazole with various structure have been synthesized. Few important types of PBI copolymer structures have been listed in Scheme 1.4. Recently our group has developed a series of *m*-phenylene-*p*-phenylene based polybenzimidazole random copolymers and shown how to tune the properties of polybenzimidazole such as glass transition temperature (T_g), absorption and emission maxima, thermal stability, molecular weight, etc.[35,40] Also it enhances the conjugation and flexibility of the polymers due to incorporation of p-linkage in copolymer. The higher reactivity ratio of terephthalic acid (TPA) than isophthalic acid (IPA) obtained from the proton NMR studies provides the proof for the positive deviation of the *m*-phenylene-*p*-phenylene based polybenzimidazole random copolymers composition from the monomer feed ratio.[40]

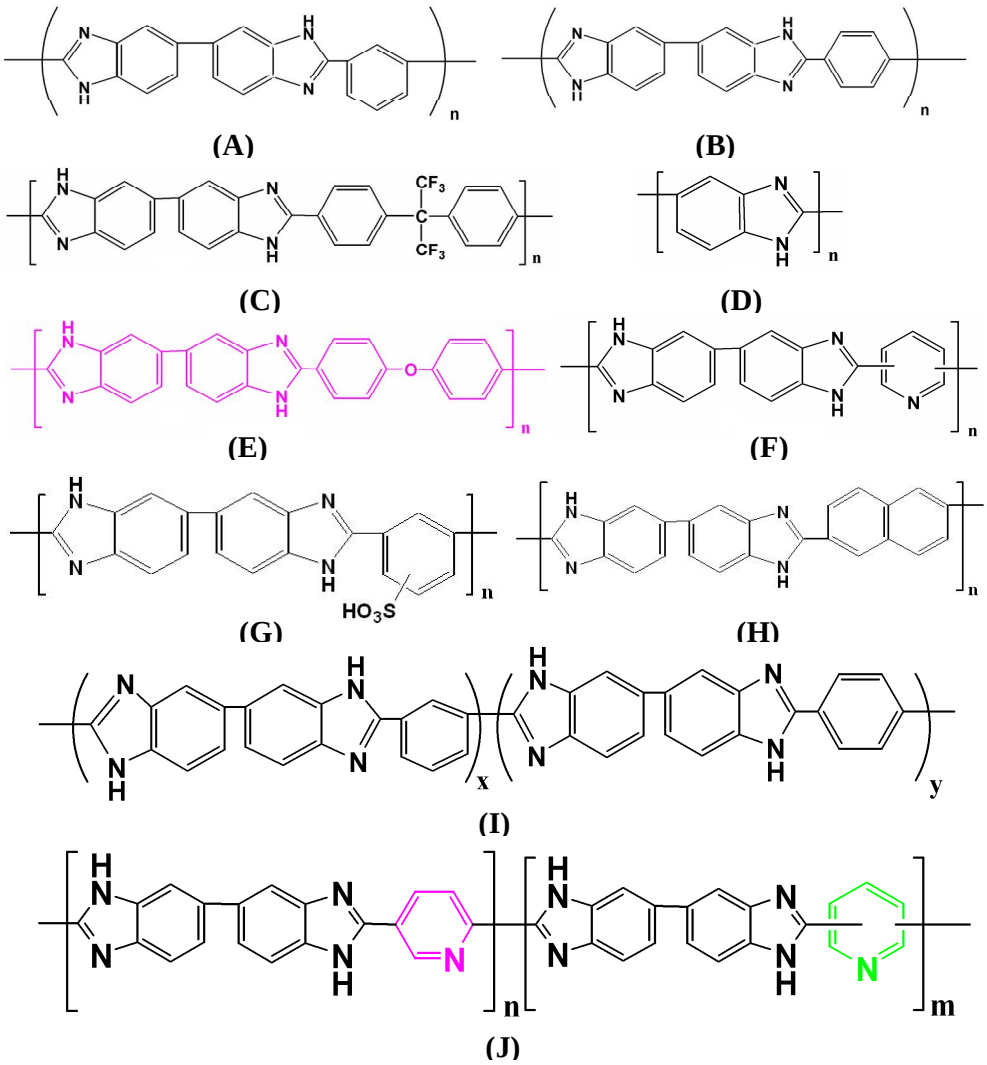

Scheme 1.4. *Various structures of Polybenzimidazole; (A) m-PBI, (B) p-PBI, (C) fluorinated PBI, (D) AB-PBI, (E) aryl ether linked PBI (OPBI), (F) pyridine based PBI, (G) sulfonated PBI, (H) naphthalene based PBI, (I) m-PBI-co-p-PBI, (J) pyridine based m-PBI-co-p-PBI.*

1.4. Physical Properties

Polybenzimidazole (PBI) is an amorphous aromatic heterocyclic polymer which possesses both proton donor (-NH-) and acceptor (-N=) hydrogen bonding sites which

shows some specific interactions with both protic and aprotic polar solvents.[48-51] PBI exhibits high proton conductivity at high temperature when doped with acids, radiative stability, excellent mechanical, thermal stabilities, and strength retention over wide range of temperatures, toughness, chemical inertness and adhesion characteristics.[5] All the aromatic polybenzimidazole obtained in the various synthetic procedures are surprisingly similar in their general chemical and physical behavior, although it has been observed in several instances that these properties of polybenzimidazole alter with the structural modification of the polymer backbone. The polybenzimidazoles are all colored polymers varying from deep golden yellow to black, usually without a melting point and glass transition temperature (T_g) around 400°C.[1,4,9,18] They vary in crystallinity and solubility depending upon the backbone structure. All have been found to be soluble in sulfuric acid, and a few in trifluoroacetic acid. Those polymers which are not crystalline as shown by x-ray patterns, are soluble in aprotic solvents such as N,N-dimethyl sulfoxide, N,N-dimethyl formamide, N,N-dimethyl acetamide, N-methyl pyrrolidone and hexamethyl phosphoramide.[1,4,9,18] They are extremely stable to hydrolysis and are not attacked by hot strong sulfuric acid solutions or hot 25% potassium hydroxide solutions.

1.4.1. Solubility

The solubility of the polybenzimidazole is mostly governed by the structural variation of the polymer backbone, polymer chain rigidity, symmetry, and intermolecular attraction. Majority of the aromatic PBI are not soluble in most of the common laboratory organic solvents owing to their rigid backbone structure. Mostly the linear aromatic PBIs dissolve partially and entirely soluble in strong protonic acids such as concentrated sulphuric acid (H_2SO_4), methanesulfonic acid (CH_3SO_3H), formic acid (HCO_2H) and in phosphoric acid (H_3PO_4) while heating and in polar aprotic solvent such as N,N-dimethyl acetamide(DMAc), N,N-dimethyl formamide (DMF) ,N,N-dimethyl sulfoxide (DMSO), N-methyl-2-pyrrolidone (NMP).[1,4,9,18,52] The presence of hetero atoms such as oxygen, sulfur, sulphone in between the aromatic units of the polymer backbone also increases the solubility of PBI due to enhancement of the chain

flexibility.[9,53,54] The functional modification of polybenzimidazoles by incorporating of the sulfonic groups into the polymer backbones[41] and the substitution of imine hydrogen (N-H) of the benzimidazole unit by alkyl group[5] also enhance the solubility behavior in the common laboratory organic solvents. Gieselman et al.[47] have prepared water soluble PBI by substituting the reactive benzimidazole N-H groups with alkylsulfonated or arylsulfonated halide. In addition these methods, various structural modifications of polybenzimidazole main backbone have been attempted to improve its solubility. These attempts include introduction of isopropylidene and oxymethylene groups,[55] methyl on the aromatic ring,[56] methylene,[57] cardo fluorene groups,[58] nitro,[59] methylsiloxane,[60] silane,[61] hexafluoroisopropylidene,[62] etc.

1.4.2. Thermal Properties

Thermal property is an important parameter to understand the structure-property relationship, the thermal degradation of different kinds of materials which can stable up to elevated temperature. Polybenzimidazole is an aromatic heterocyclic polymer which has found wide application in those ranges of technologies where the high resistance towards high temperature is required. Marvel established by thermogravimetric analysis (TGA) that most of the aromatic polybenzimidazoles show no change in properties on heating at 550°C and less than 5% weight loss after several hours at 600°C in nitrogen.[1] The exceptional retention of the thermal properties of polybenzimidazole in a high temperature environment depends upon several factors;[1,4,9,14,18] (i) presence of strong bonds in the PBI backbone, (ii) extendable electronic delocalization, (iii) low flexibility nature of PBI chain and (iv) bond healing capabilities. Thermogravimetry and differential temperature analysis (TG-DTA) has been, so far, the mostly used tool to determine the thermal stability under inert, vacuum, air and pure oxygen conditions. Thermal and oxidative stabilities of different PBIs have been reported by various research groups and they have found that PBI polymers have exceptional thermal stability up to 600°C, initial 5% wt loss at 100-120°C is due to loosely bound water molecules associated for hygroscopic nature of the polymer.[9,52,63,64] Marvel and Vogel[1,2] established that the variation of the aromatic linking units had only marginal effect on

the stability in inert or oxygen atmosphere. Substitution of alkyl or aryl groups on the imine proton of the benzimidazole moiety produces very little change in thermal stability.[5,47] Recently, our group has demonstrated that the differences in the thermal stability exist due to the *m*- and *p*-phenylene groups in the chain and introduction of *p*-phenylene groups in the polymer backbone by copolymerization enhances the thermal stability of the polymer.[35,40] The high thermal stability of polybenzimidazole with different types of structures results to poor processing characteristics. Therefore, the incorporation of the flexible linkage such as oxygen, sulfur, sulphone either in amine or acid moiety, is generally less thermally stable than all the ring systems and their decomposition temperatures in inert atmospheres or air range between 450° to 500°C.[9,53,54] We have observed that para connected aromatic PBI is always display higher thermal stability than meta connected PBI.[35,40]

PBI is a thermoplastic polymer, having the glass transition temperature varied between 350-450°C depending on the structure. The polymer is almost completely amorphous in nature; crystallinity can be induced only under some specific conditions such as hydrogen bonding interaction with polar solvent,[48-51] blending with some crystalline polymer[65,66] etc. Menczel estimated the glass transition temperature of *m*-PBI (Scheme 1.4) fiber using differential scanning calorimeter (DSC) and dynamical mechanical analysis (DMA) and calculated the T_g of the *m*-PBI fiber is 387°C and also allocated the β-relaxation at 290°C associated with loss of water while the γ-transition at 20°C was not identified clearly and assigned the δ-transition at 90°C correspond to rotation of the *m*-phenylene ring.[67] We have also correlated the glass transition temperature of OPBI and *p*-PBI and confirmed that T_g not only depends on the flexibility of the polymer chain but also the molecular weight of the corresponding polymer.[32] The glass transition temperature (T_g) of the N-substituted polybenzimidazole depends on the flexibility and length of the substituted moiety of the polybenzimidazole. Recently, Kumbharkar et al. synthesized series of N-substituted polybenzimidazoles using a series of alkyl groups with varying bulk and flexibility, such as, methyl, n-butyl, methylene trimethylsilane and 4-tert-butylbenzyl and showed

that methyl substituted PBI had highest T_g while the 4-tert-butyl benzyl substituted PBI was showing the lowest T_g.[68] Hence, N-substitution in PBI makes the polymer flexible and ease to process.

1.4.3. Photophysical Property

Photophysical studies of polybenzimidazole have been utilized as an efficient approach for the exploration of inter- and intramolecular interactions and molecular motions of the chains and their aggregations. The benzimidazole moiety of polybenzimidazole acts as fluorescence chromophore. There are very few reports in the literature about the photophysical studies of polybenzimidazole due to its poor solubility in common organic solvents.[48,50,51] The absorption and emission spectra of polybenzimidazole provide information on the conformation and microenvironment of polymer in solution. All the aromatic polybenzimidazoles in N,N-dimethyl acetamide (DMAc) solution give an intense absorption band typically at 340 nm and 440 nm due to π-π^* transition of imidazole moiety and n-π^* transition of imidazole moiety, respectively.[9,48,50,51] Recently, our group has published several articles[32,35,40,50,51] regarding the photophysical studies of various structure of polybenzimidazole. Sannigrahi et al. also showed that the incorporation of the *p*-phenylene linkage into the polymer backbone enhances the conjugation between the imidazole and the phenylene ring which results the bathochromic shift of the π-π^* absorption maxima.[35,40] Polybenzimidazole is a highly fluorescent polymer with high quantum yield (>0.5). The major two emission bands of polybenzimidazole at 398 and 415 nm were assigned by Kojima as a *0-0* and *0-1* transitions from the excited ^1L_b state of the benzimidazole rings present in the PBI chain.[47] In our recent publication, we have shown that the protic character of the solvents also has a huge impact on the photophysical properties of the OPBI by the formation of aggregated structures in both DMAc and formic acid (FA) solutions at higher concentration.[51]

1.4.4. Mechanical and Oxidative Stability

Maintaining the chemical and mechanical stability of the membrane over the anticipated lifetime is a key requirement for the use of membrane for example better mechanical stability or strength is one of the major issue for the progress of proton exchange membrane for the use in fuel cell. In maximum cases, problem associated with common PBI is the poor mechanical strength at high acid doping levels, which is essential for achieving high-proton conductivity. The commercial PBI, for example, becomes too weak at high-doping levels to fabricate into membrane electrode assemblies (MEAs), and it is recommended that the doping levels should be controlled at 5–6 to balance the proton conductivity and the mechanical strength of membranes.[21] More efforts have recently been made to increase the mechanical property of the PEM. One motivation of these efforts is to compromise the properties such as high molecular weight, good solubility and processibility, which are of significance for mechanical stability and functionalisation processing of PBI membranes with different backbones[30-39] and crosslinking is another effective way to suppress membrane swelling and to improve the mechanical properties. Up to now, there have been a few reports on the crosslinked PBIs. Li et al. have reported that the commercial PBI could be crosslinked by thermal treatment at 160–300°C in the presence of a crosslinker (α,α'-dibromo-p-xylene) and the resulting crosslinked membranes displayed high tensile strength of 21–23 MPa at the doping level of 8.5 mols.[20] The same group has also reported that the commercial PBI could be crosslinked with another kind of crosslinker, dichloromethylphosphonic acid, and the relevant crosslinked membranes displayed significantly higher tensile strength than the linear PBI at similar doping levels.[69] Xu et al.[70] have also reported that crosslinked hyperbranched PBI membranes could maintain reasonably high-mechanical strength at high acid doping levels, which is superior to the commercial PBI membranes.

Strong durability of PEMs has been recognized as one of the most important issues for the performance of PEM fuel cell systems. The stability of the PEM in oxidative environment has been documented as an indication of long-term durability of

the membranes in fuel cells.[71,72] Gaudiana and Conley[73] showed that the weakest part of the PBI in an oxidative atmosphere is the benzenoid ring bearing the nitrogen function and the amine portion of the molecule. The rupture of the bulk polymer backbone occurs through an attack on the carbon in the imidazole ring linked with the phenylene group towards the amine nitrogen (–NH–). An FT-IR study of the thermo-oxidative degradation of PBI in air at 350 °C by Musto et al.[74] revealed that two new absorption peaks were formed, indicating the stretching vibrations of the product or intermediate of the polymer oxidative degradation. It was concluded that the oxidative attack resulted in the cleavage of imidazole rings and eventually led to the formation of aromatic nitriles. Under fuel cell conditions, oxidative radicals originate from the oxygen diffusion through the membrane. Attack of peroxide radicals such as $^{\cdot}OH$ and $^{\cdot}OOH$ on the hydrogen containing bonds in polymer membranes is believed to be a principal degradation mechanism of membranes.[72] Experimentally the peroxide radicals can be generated by the decomposition of H_2O_2 with transition metal ions, e.g. Fe^{2+}, as a catalyst.[75] The so-called Fenton reagent consists of a solution of hydrogen peroxide with a trace of ferrous ions to create highly reactive $^{\cdot}OH$ or $^{\cdot}OOH$ radicals. Soaking membrane samples in Fenton solution is frequently used as a method to evaluate the stability of PEMFC membranes under fuel cell conditions. Daletou et al.[76] treated PBI/sulfonated polysulfone (SPSF) blends in 3% H_2O_2 aqueous solution containing 4 ppm $FeCl_2$ at 80°C for 72 h, however, no notable effect was observed on the mechanical and the thermal properties of the blend membranes. Similarly, Lobato et al.[29] examined FTIR spectra of high molecular weight PBI membranes before and after the treatment in Fenton solutions, however, without finding significant changes in the spectra between 2000 and 4000 cm^{-1} associated with the N–H stretching modes and between 1000 and 1700 cm^{-1} associated with benzimidazole rings. On the other hand, significant weight losses have been reported for membranes after the Fenton test in 3% H_2O_2 containing 4 ppm Fe^{2+} at 68°C,[20] ranging from 10% to 40% depending on the initial molecular weight of the polymer. Under even harsher conditions, i.e. in 30% H_2O_2 containing 20 ppm Fe^{2+} at 68°C after 24 h, Chang et al.[77] reported a weight loss of about 9% accompanied by a significant intrinsic viscosity decrease of the polymer from 0.98 to

0.11 dL/g. They suggested a degradation mechanism by molecular chain scission rather than group dropping, similar to the thermo-oxidative degradation of PBI proposed by Musto et al.[74]

1.5. Polyelectrolyte

Polyelectrolytes are polymer carrying ionic charges in the polymer chains. Depending upon the charge, these polymers are anionic or cationic. The major focus of various research group over the years has concerned the basic physical properties of polyelectrolytes in solution which includes scattering phenomenon, interactions, conformations and hydrodynamics.[78-81] Polyelectrolytes have practical importance for their applications as processing aids such as flocculation or precipitation, dewatering agents, demulsifiers, as drag reduction agents, as additives in detergents and cosmetics, in the manufacture of membranes, ion-exchange resins, gels, and modified plastics.[80-83] The behavior, in terms of conformation, structure, etc. of the polyelectrolyte in dilute solution is entirely different from the non-electrolyte polymer owing to presence of the ionizable electrolyte groups in the polymer chains. This is because of the charges of the polyelectrolyte chains repel each other through the coulombic repulsion, which causes the conformations of polyelectrolyte chains to alter very readily.[78-81] The characteristics features of polyelectrolytes in dilute solution is expressed in the polyelectrolytic effect as the non-linear change in the reduced viscosity (η_{red}) with the decrease in the concentration for a very high degree of dilution. Therefore, it is very complicated to determine intrinsic viscosity ([η]) for the polyelectrolyte due to the huge dependency intrinsic viscosity on the conformation of polymer chains in solution. The major challenges are to determine the intrinsic viscosity of polyelectrolyte solution.[80,84-87] The linear relationship of the reduced viscosity and the concentrations of the uncharged polymer solutions are defined through well known Huggins equation,[88] as follows:

$$\frac{\eta_{sp}}{C} = \eta_{red} = [\eta] + k_H[\eta]^2 C \qquad (1.1)$$

where, $[\eta]$, η_{sp} and η_{red} are the intrinsic viscosity, specific viscosity and reduced viscosity, respectively. k_H and C are the Huggins constant and concentration of the polymer in solution, respectively. Since in case of polyelectrolyte η_{red} increases with decreasing concentration of polyelectrolyte in solution and often reashes to a maxima, it is not possible to extrapolate the η_{red} to zero concentration to obtain $[\eta]$ as it is done in case of uncharged polymer using equation 1.1. Also since linear fitting is not possible, hence k_H cannot be determined. The values of $[\eta]$ and k_H are important parameter to understand the conformation and solution properties of polymers in solution. Therefore it remains a challenge to determine the $[\eta]$ and k_H for any newly developed polyelectrolytes.

Schafgen and Triwisonna[89,90] observed the polyelectrolytic effect of polycaproamide in anhydrous formic acid at the beginning of investigations of polyamides. McCormick et al.[91,92] synthesized 3-acrylamido-3-methylbutanoic acid and observed the same effect in aqueous solution. In addition to that a enormous number of studies have been devoted to polyelectrolytic effect of poly(carboxy1ic acid), poly(acrylic acid) (PAA) and poly(ethy1ene-oxide) (PEO).[93-98] Various dilution techniques[99,100] have been applied on the polyelectrolyte solution to measure the intrinsic viscosity and Huggins constant. Among these all dilution techniques, isoionic dilution method[101,102] in which the effective ionic strength of the system is kept constant, is a very well known technique. There are huge numbers of reports for the measurement of intrinsic viscosity through the isoionic dilution method for varieties of polymeric systems.[101-104] The molecular conformation of a polyelectrolyte depends upon the net charge of the molecules which directly proportional with the degree of counterion binding. The isoionic dilution technique actually keep the counterion binding constant, by maintaining the same effective ionic strength which give the linear dependency of reduced viscosity on the concentration. A full theoretical description of size and structure of the polyelectrolyte molecules in dilute solutions is still indefinable,[105-108] due to the presence of many different length scales such as the persistence length for backbone in dilute solution. Regarding the effect of electrostatic

interactions on chain dimensions, there have been two qualitatively different ways of theoretical description. In the first, pioneered by Odijk[109] and Skolnick and Fixman,[110] electrostatic interaction leads to an enhancement of the persistence length. The net persistence length of the polyelectrolyte can be treated as a sum of intrinsic persistence length and the electrostatic persistence length. But the dependence of the conformation of the polyelectrolyte chain on the concentrations of the polyelectrolyte and salt are not understood. Muthukumar first demonstrated theoretically the dependencies of the thermodynamic properties of polyelectrolyte solutions on the polyelectrolyte concentration, solvent quality, strength of the electrostatic interaction, and the salt concentration which decides the range of the electrostatic interaction.[111,112]

1.6. Polymer Aggregates

Molecular aggregation of polymers and biopolymers in solution represents an important phenomenon in material science and molecular biology. The self-assembly of the molecules, which is a thermodynamically controlled association of molecules into structurally ordered, stable aggregates, uses the classical noncovalent interactions such as hydrogen bonding, electrostatic, van der Waals, and hydrophobic interactions which are the driving force of the self-aggregation process.[113-115] Generally, the molecular aggregation behavior in polymer solutions are affected by many factors, such as the temperature, molecular weight, concentration of the polymer and the nature of the solvents. There are plenty of investigations reported in the literature on the molecular aggregation of the synthetic polymers.[116-119] However, most of these reports were focused on vinyl polymers, polypeptides, and other simple structure polymers.[116-119] Po-Da Hong et al. demonstrated that polyvinyl alcohol showed different aggregation behavior in two different solvent and also light scattering studies on aggregation behavior of polyvinyl chloride/dioxane solutions.[120] Therefore, it must have pointed out that the interactions between polymer and solvent plays an important role in the conformational transition and aggregation behavior of the polymer chains in the solution state. The aggregation behavior of polystyrene-b-poly(ethylene/butylene)-b-

polystyrene triblock and poly(N-isopropylacrylamide-b-styrenes) diblock copolymer have been studied by Ogata et al.[121] and Nuopponen et al.,[122] respectively. They have explored the connection between solvent polarity and aggregation behavior of the copolymer by comparing with the aggregations in several solvents.

1.7. Polymer Gels

Polymers or biopolymers gels have drawn a significant attention to explore its various properties.[123,124] A polymer gel is a macroscopic network of polymer chains joined at a number of connection sites which is surrounded by the solvent molecule. These joints can be either irreversible chemical bonds or reversible physical associations, which are called chemical or physical gels, respectively. Chemical associations are usually introduced by crosslinking, while physical gels are formed and stabilized in the solvent mostly through hydrophobic interactions, hydrogen bonds, and electrostatic interactions between certain segments of the polymer chains.[123-126] All these driving forces for the physical gel processes are non-covalent, in the order of kT and hence these processes become reversible in nature with respect to concentration, temperature, etc i.e. systems are thermoreversible as they can be melted and reformed through heating and cooling cycles respectively without significantly changing the chemical structure. Also the mechanism of the thermoreversible physical gelation process depends on the nature of the polarity of the solvent.[127-131] The main attraction of the thermoreversible physical gel to the various research groups lie on the following concerns; (i) the crystal structure and morphology, (ii) the mechanism of gel formation and gel kinetics and (iii) the relation between structure and thermal study to understand several physical properties of the gel.

1.8. Polymer Nanocomposites

Polymer nanocomposites are the combination of two materials in which one of the components, known as nanofiller, embedded in the macroscopic polymer matrix. Polymer nanocomposites are emerging as a new class of industrially important

materials. In contrast to conventional composites, very low concentrations of nano-sized filler particles can lead to remarkable improvements in performance, such as increased strength and heat resistance, decreased gas permeability and flammability, and increased biodegradability of biodegradable polymers[132-150] due to properties of nanofillers, such as, (i) low percolation threshold, (ii) particle-particle correlation (orientation and position) arising a low volume fraction, (iii) large number of density of particles per particle volume, (iv) extensive interfacial area (communication between matrix and filler) per volume of particles, (v) short distances between the particles, and (vi) comparable size scales among the rigid nanoparticles inclusion.

At the same time, these improvements can be realized without significantly increasing the density of the polymer or changing its optical properties, and the resulting materials still retain their processibility due to the low loadings of the fillers. For these reasons, polymer nanocomposites have attracted interest in both industrial and academic laboratories in recent years. Huge numbers of literatures about the polymer nanocomposites with different nanofillers (buckyballs,[141-143] carbon nanotubes,[144,145] clays,[136,146] different types of silica particles,[147-149] graphene[150]) have been reported by several research groups. The properties of nanocomposites are greatly influenced by the size scale of its component phases (nanofillers) and the degree of mixing between the two phases (polymer and nanofiller). The degree of mixing depends on the dispersion of the nanofiller and adhesion at the nanofiller-matrix interface acts an important role in determining the physical properties of polymer nanocomposites. Nanofillers used in polymeric nanocomposites have been divided into three categories defined in terms of the number of dimensions of their nanometer size, i.e., one dimension (e.g. clay), two dimensions (e.g. carbon nanotubes, graphene), and three dimensions (e.g. silica particles). Among the various kinds of nanocomposites polymer-clay nanocomposites and polymer-silica nanocomposites have been studied extensively in recent years.

1.8.1. Polymer-Clay Nanocomposites

Polymer nanocomposites with varieties of clays have been widely investigated due to their low cost, easy availability, high aspect ratio, very high surface area and stiffness. Different types of layered silicates are very interesting because they have different crystallite sizes and aspect ratios. The most commonly used layered silicate in polymer-clay nanocomposites is montmorillonite (MMT); a 2:1 aluminosilicate smectite clay which are composed of a sandwich type structure with two tetrahedral sheets fused to a central octahedral sheet (Figure 1.1). In the case of montmorillonite, the tetrahedral sheets are composed of oxide of silica while the octahedral sheet is comprised of Al, Mg, and Fe oxides and hydroxides.[151-153] Also kaolinite (Kao), a 1:1 aluminosilicate illite clay has been used extensively where the hydroxyl group is sandwiched in between each layers made up with one tetrahedral sheet of silica oxide and one octahedral sheet of aluminum oxide (Figure 1.2).[154-156] The size and aspect ratio of kaolinite are larger than those of montmorillonite. Consequently, the interactions at the interfaces between kaolinite and polymers should be very different from those of smectite type clays and polymer systems. Besides of the above two clays, there are also several other clays which are used as nanofiller in PLSNs such as bentonite (2:1),[157] laponite (2:1),[158] halloysite (1:1),[159] etc.

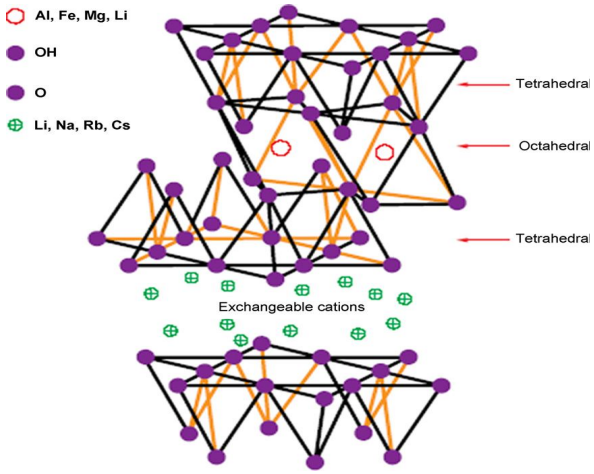

Figure 1.1. *Structure of sodium montmorillonite. (Adapted from Google image)*

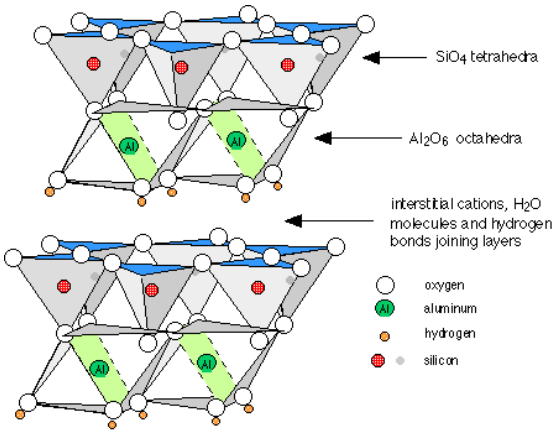

Figure 1.2. *Structure of kaolinite. (Adapted from Google image)*

Generally, the hydrophilic silicate surface of clay needs to be converted into a relatively organophilic surface for being potentially more compatible with the polymer for the preparation of the polymer-layered silicate Nanocomposites (PLSNs). Organic modification of montmorillonite (MMT) and kaolinite (Kao) occurs by ion exchange of the sodium ions present in between the silicate layers with organic alkyl ammonium or phosphonium[160-163] and by substituting hydroxyl groups with any organic solvents such as dimethyl sulfoxide, dimethyl formamide,[162-164] etc. respectively. These modifications not only converts the normally hydrophilic clay to organophilic clay, but it also increases the distance of Basal plane of the silicate layers, where the polymer chains can go easily in between the silicate layers and produce a new kind of material, known as polymer-organoclay nanocomposites.[165,166]

Polymer-organoclay nanocomposites can be basically classified as immiscible, intercalated and exfoliated according to the status of the organoclay dispersion as shown in Figure 1.3.

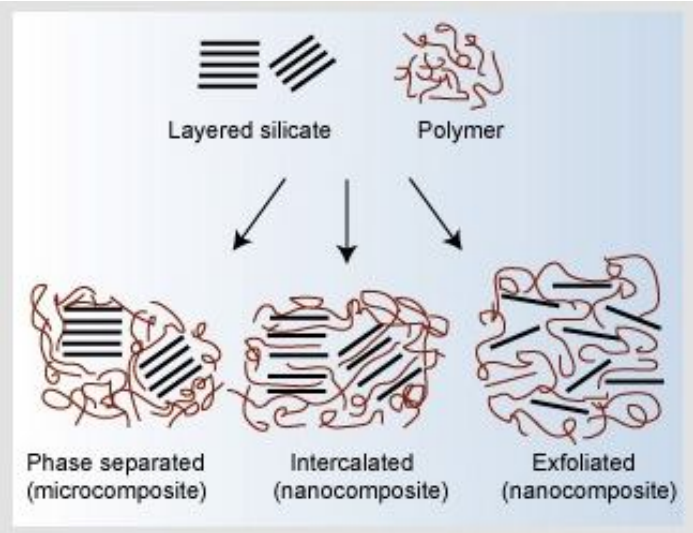

Figure 1.3. *Formation of polymer organoclay nanocomposites.*

Polymer-clay nanocomposites can be prepared mainly by three techniques, viz., in situ polymerization, solution mixing and melt mixing. In melt mixing,[167-172] nanoclays are added directly into the polymer matrix (solid state), solution mixing[173-176] involves dispersion of the nanoclay in an organic solvent followed by dissolution of the polymer matrix and solvent casting and in-situ mixing involves the incorporation of nanoclay during the polymerization. It has been observed from earlier studies that solution mixing brings about better exfoliation/delamination and dispersion of nanoclays in a polymer.[138,171-173] Hence, often solution mixing process is chosen to make nanocomposites. Thus, in solution mixing, solvent plays an important role in determining the properties of polymer–filler nanocomposites.

1.8.2. Polymer-Silica Nanocomposites

Polymer-silica nanocomposites[147-149] are the new class of organic–inorganic hybrids materials based on organic and inorganic species combined at a nanoscale level has gained huge attention during the last decade. These Nanocomposites hybrid materials combine the advantages of the inorganic material (e.g., rigidity, thermal stability) and the organic polymer (e.g., flexibility, dielectric, ductility, and processability). Also the interfacial area of the silica nanoparticle creates a significant

volume fraction of polymer matrix with properties different from the bulk polymer even at low loadings. Therefore, polymer/silica nanocomposites[147-149] have attracted substantial academic and industrial interest to receive much attention in recent years and have been employed in a variety of applications. There are several other interesting candidates as a inorganic nanosized particles with potentially unique properties such as heteropoly acids,[177,178] carbon nanotube,[144,145] fullerene,[141-143] zeolite[179] and graphene,[180,181] are extensively studied by several authors. Among them the applications of silica particles is continuously increasing due to their high specific area, large porous volume, high mechanical and thermal stability and easy surface modification. By the organic modification of the surface of the inorganic nanofiller the weak interaction between the nanofiller and the polymeric matrix can be improved. Because of the high bond energy in the Si-O bond, SiO_2 has extremely high thermal stability. SiO_2 also possesses a very low thermal expansion coefficient.[182]

Two classes of techniques have been developed for silica nanoparticle formation: the sol-gel method and the microemulsion method.[183] In 1968, Stöber[184] reported a simple synthesis of monodisperse spherical silica particles by means of hydrolysis of a dilute solution of tetraethyl ortho silicate (TEOS) in ethanol at high pH. Silica nanoparticles are also available from commercial sources now, and they usually exist as powder or colloid. Nanosilica powder is mainly produced by the fuming method and the precipitation method in industry. Fumed silica is a fine, white, odorless, and tasteless amorphous powder. It is manufactured by a high-temperature vapor process in which $SiCl_4$ is hydrolyzed in a flame of oxygen-hydrogen.[185] The commercial colloidal silica spheres, they are usually in the form of a sol, with water or alcohol as the dispersing medium. The structure of nanosilica shows a three-dimensional network. Silanol and siloxane groups are created on the silica surface, leading to hydrophilic nature of the particles. The hydrophilic surface of silica needs to be converted into a relatively organophilic surface for being potentially more compatible with the polymer for the preparation of the polymer nanocomposites.[186] Some typical silane coupling agents used for surface modification of nanosilica are listed in Table 1.1.

Table 1.1. *Typical silane coupling agents used for surface modification of silica nanoparticles.*

Name	Structure
Aminopropyl methydiethoxysilane	$H_2N(CH_2)_3(CH_3)Si(OC_2H_5)_2$
3-aminopropyltriethoxysilane	$H_2N(CH_2)_3Si(OC_2H_5)_3$
Aminophenyltrimethoxysilane	$H_2NPhSi(OCH_3)_3$
3-glycidoxypropyltrimethoxysilane	$CH_2(O)CHCH_2O(CH_2)_3Si(OCH_3)_3$
3-(trimethoxysilyl)propyl methacrylate	$CH=C(CH_3)COO(CH_2)_3Si(OCH_3)_3$
Methacryloxymethyltriethoxysilane	$CH=C(CH_3)COOCH_2Si(OC_2H_5)_3$

These silica nanocomposites can be prepared by following three main synthetic routes;

(i) Sol-gel methods,[187-191] whereby metal alkoxides such as TEOS are carried out to undergo catalyzed hydrolysis under mild conditions and followed by polycondensation reactions to form the nanosilica particles in the presence of a polymer or simultaneously during the polymerization of the monomer.

(ii) Solution blending[192-195] of dispersion of the silica in an organic solvent followed by dissolution of the polymer matrix and solvent casting.

(iii)Melt blending[196-199] of silica and polymer matrix in solid state.

1.9. Advanced Novel PBI Materials

Polybenzimidazoles are a class of thermally stable polymers that have been commercially developed as textile fibers, high temperature matrix resins, adhesives, and foams.[5] Polybenzimidazole was commercialized by the Celanese Corporation in 1983 and is widely used in firefighter's protective clothing, high-temperature gloves, and astronaut flight suits due to its excellent chemical and thermal stability.[5-7] Great efforts

have been dedicated to develop high temperature fuel cell membranes for operation at temperatures above 100°C.[21,34,200-202] Also PBI microporous resin beads, commonly known as Aurorez®, diameter from 50-500 μm and porous internal structure with 85% void have unique separation capacities.[5] But the PBI membranes are difficult to process because of its high degree of rigidity and poor solubility. Hence, several attempts have been carried out to improve the solubility, including incorporating a side chain into the polymer backbone and making the polymer with flexible monomer units.[9,52-62] Inspiteof the huge studies of several properties of polybenzimidazole, there is a deficiency of reports of polybenzimidazole. The following section briefly highlights various properties of PBI.

1.9.1. PBI Aggregates

PBI possesses both proton donor (-NH-) and acceptor (-N=) hydrogen bonding sites which exhibit specific interaction with both protic and aprotic polar solvents.[48-51] PBI is an interesting type of materials for the preparation of polymer aggregates due to their well-defined structures and different morphological behavior. They exhibit various morphological properties in different solvent systems.[50,51] Helminiak et al.[203] reported the solution properties of low molecular weight PBI such as intrinsic viscosity behavior as a function of temperature and LiCl salt concentrations in DMAc. Kojima have focused on the solution properties of different structures of polybenzimidazoles in DMAc by obtainin their molecular parameters, intrinsic viscosity, and hydrodynamic chain dimensions[204] as well as on understanding their molecular aggregation in solution.[47] PBI chain conformation was studied by Shogbon et al.[49] using viscosity measurements and static light scattering techniques, varying polymer or salt (LiCl) concentrations in the solution. They have shown the reduced viscosity as a function of varying polymer concentration and found that the polymer behaves like a polyelectrolyte in solution and the conformational changes occurred at higher concentrations. Very recently, Sannigrahi et al.[50] have carried out a systematic study on the aggregation behavior of meta structured polybenzimidazole in polar aprotic solvent, dimethyl acetamide (DMAc) using viscosity, steady state and time dependent

fluorescence techniques. They have demonstrated that the meta structure polybenzimidazole (*m*-PBI) chains undergo a coil to rodlike conformational transition in solution with increasing concentration due to the molecular aggregation driven by the self-organization process through intra- and intermolecular interactions (Figure 1.4). Upon increasing temperature the rodlike PBI aggregates dissociates and goes back to coil like conformation. We have reported the aggregation behavior of poly(4,4′-diphenylether-5,5′-bibenzimidazole) (OPBI) in polar aprotic (dimethyl acetamide, DMAc) and protic (formic acid, FA) solvents as a function of the polymer concentration and solution temperature (Chapter 4). We have found that in both the solvents the aggregations proceeds through intermolecular processes though their mechanisms are different owing to the polyelectrolytic nature of OPBI in FA medium.[51]

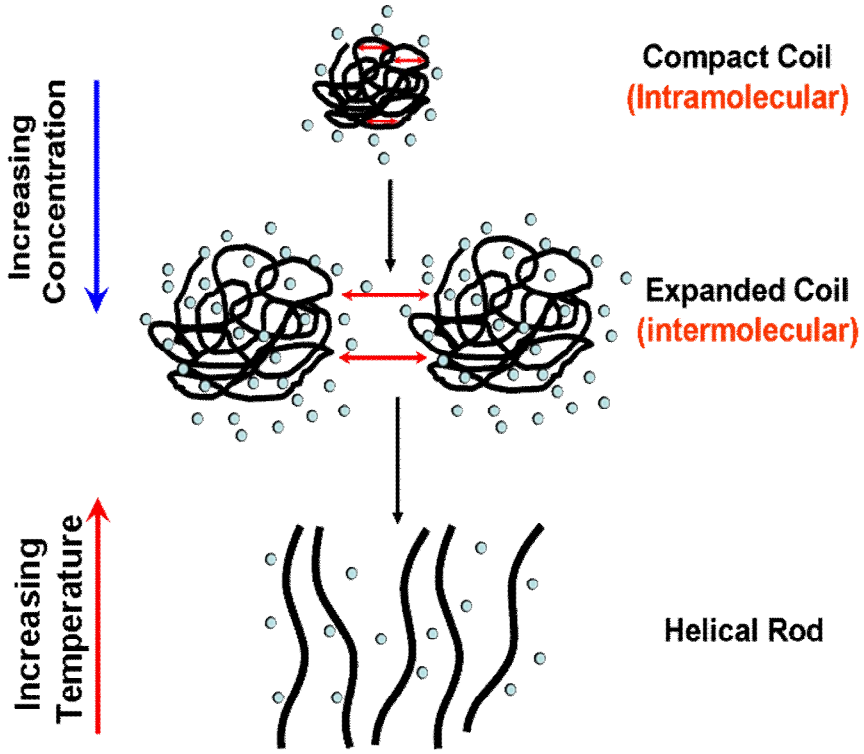

Figure 1.4. *Schematic presentation of the aggregation of m-PBI in DMAc solution with conformational transition. Tiny circles represent the solvent molecules. (Adapted from reference 50)*

1.9.2. PBI Gels

Phosphoric acid (PA) doped PBI membranes have been achieved inspiring progresses in development of high temperature proton exchange membrane fuel cells, because it allows a fuel cell to operate at temperatures up to 200^{o}C under low relative humidity.[21,34,200-202] Several attempts have been made so far for the fabrication of the PA doped *m*-PBI membranes. These include casting of *m*-PBI membrane from dimethyl acetamide (DMAc) solution followed by soaking in phosphoric acid (PA),[200-202] via sol–gel process by direct casting of the high molecular weight *m*-PBI solution in polyphosphoric acid (PPA)[21,34,205,206] and leaching out low molecular weight compound (porogen) from polymer / porogen mixture and then soaking it in PA solution.[207] Now-a-days focus has been on to the preparation of superior quality PBI membrane, having the high acid doping level hence high proton conductivity and superior mechanical strength as well. Recently, from our group Sannigrahi et al.[208] have reported the formation of thermoreversible gelation of *m*-PBI in PA solution (Figure 1.5). They have studied the gelation kinetics, thermodynamics, gel morphology and structures. The *m*-PBI gel exhibited fibrillar network morphology and semicrystalline in nature due to the strong hydrogen bonding interaction between *m*-PBI and PA molecules in the gel which has been shown by using the single crystal structure analysis of phosphate salt of benzimidazole (Figure 1.6).[209] They illustrated that the PA doped *m*-PBI gel membrane showed the high PA loading and excellent thermo-mechanical stability. This novel membrane obtained from PBI gel in PA displays very high acid loading (~35–40 mol per PBI repeat unit) and very high proton conductivity. The tensile strength of this membrane is 6.05 MPa, which is enough for the use in fuel cell.

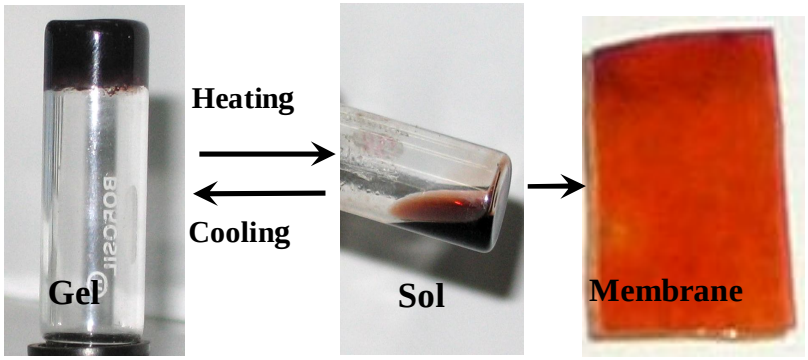

Figure 1.5. *Thermoreversible gelation of polybenzimidazole (PBI) in phosphoric acid (PA). (Adapted from reference 207)*

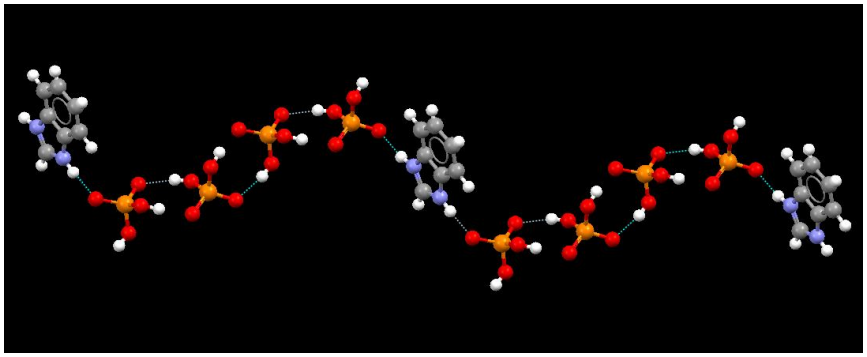

Figure 1.6. *Structural analysis of phosphate salt of benzimidazole. (Adapted from reference 208)*

1.9.3. PBI Composites and Nanocomposites

At very high PA doping capacity, PBI membrane forms soft plastic type material as well as the thermo-mechanical stability of the membrane decreases. Several efforts have also been dedicated to improve the performance and the thermo-mechanical properties of PBI membranes as well as to develop novel composite membranes with various inorganic reinforcing materials like zirconium phosphate (ZrP),[210] phosphotungstic acid (PWA),[211] silicotungstic acid (SiWA),[212] boron phosphate

(BPO_4),[213] zirconium tricarboxybutylphosphonate [$Zr(O_3PC(CH_2)_3(COOH)_3)_2$,[214] $Sn_{0.95}Al_{0.05}P_2O_7$[215] etc. But very few are reported about the preparation of the PBI nanocomposite membranes. Chuang et al. prepared polybenzimidazole (PBI)/ montmorillonite (MMT) by solution blending method[216] and polybenzimidazole (PBI)/silica nanocomposite membranes via sol–gel process[217] from an organosoluble fluorine-containing PBI. They have shown that with increasing the percentage loading of nanofillers, the thermo-oxidative stability, mechanical properties and the methanol permeability of the PBI membranes were improved. Liu et al.[218] showed that incorporation of sulfonated silica nanoparticles to PBI membranes increased tremendously the proton conductivities of the PBI membranes. Pu et al.[219] employed solvent-exchange method for the preparation of organic/inorganic composite membranes based on polybenzimidazole (PBI) and nano-SiO_2. Shao et al.[220] prepared the multiwalled carbon nanotubes (MWNTs) reinforced OPBI hybrid is proposed by combining the functionalization of the MWNTs and in situ polymerization in one reaction bottle, which is called ‘‘one pot synthesis’’. The nanocomposites exhibited an obvious reinforcing effect in mechanical properties, including higher yield strength, tensile strength and enhanced young’s modulus, as well as an improvement in the thermal stability. Very recently, Wang et al.[221] prepared graphene (GP)-based OPBI nanocomposites by in situ blending method. They have observed that compared to pure OPBI, the resulting OPBI/GP nanocomposites show simultaneously improved mechanical and thermal stability with the addition of extremely small amounts of GP. Also few research groups have recently investigated the different properties of polybenzimidazole nanocomposite membrane by incorporating single-walled or multi-walled carbon nanotube in the polymer matrix.[222] They have shown that the resulting nanocomposite membranes displayed tremendous increament of mechanical integrity and also reduced the acid leaching from the polymer matrix to achieve increased durability.

1.9.4. PBI Blends

Due to the presence of both proton donor (- NH -) and proton acceptor (- N =) hydrogen bonding sites PBI display specific interaction upon blending with variety of polymers. The main objectives for PBI blending are to improve the properties and performance for the high performance materials. Huge numbers of PBI miscible or partially miscible blends with several polymers such as polyimides (PI),[223] polyamideimide (PAI),[224] polyarylate (PAr),[225] high-modulus aramide (HMA),[225] Poly(ether imide),[225] poly(4-vinyl pyridine) (PVP),[226] sulfonated poly sulfone,[226] aromatic polyethers,[227] Nafion[228] have been investigated. In all the cases the driving forces for the formation of blend are the specific interactions between the proton donating and accepting groups of PBI and functional groups of other polymers. Blend miscibility was evidenced in the form of IR spectra, Raman spectra, solid state NMR, single T_g, and well-defined single tan delta relaxations from DMA.[223-228] Recently our group has reported the study of PBI/PVDF blend systems and their potential to use as a proton exchange membrane in PEMFC.[65] Due to the presence of hydrophobic PVDF in the PBI/PVDF blend, it absorbs more phosphoric acid (PA) by pushing out the water molecule from the membrane. Also Hazarika et al.[229] has investigated the blends of PBI and spherical PSS and shown the core–shell type morphology in which core is the sulfonated polystyrene (SPS) and shell is the PBI (Figure 1.7).

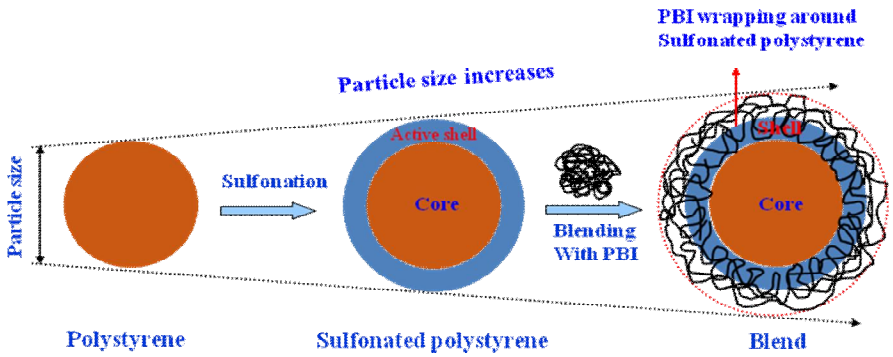

Figure 1.7. *Formation of core (polystyrene)–shell (polybenzimidazole) nanoparticles. (Adapted from reference 229)*

1.10. Application of PBI Membrane in Fuel Cell

Fuel Cells have emerged as one of the most promising technologies for the power source of the future. Though Sir William Grove first introduced the concept of a fuel cell in 1839, the fuel cell research has emerged as a potential field in recent decades. Fuel cell and its different varieties are briefly discussed in the following.

1.10.1. Fuel Cell

Fuel cells offer the promise of a low-polluting, highly efficient energy source which can be designed to utilize an almost limitless abundance of fuel. In their most basic form, fuel cells use hydrogen and oxygen from the air to create water and electricity. Basically, fuel cells are electrochemical energy conversion devices that convert chemical energy directly to electrical energy via a chemical reaction.[230-233] However, fuel cells found their first major application when NASA utilized hydrogen-powered fuel cells to produce electricity for the Gemini space missions. The high cost and short lifetimes of these systems has prevented the use of fuel cells in mass markets. Although the comparison between fuel cells and batteries is obvious because most often they serve similar applications but fuel cells differ from batteries in two distinct characteristics. First, fuel cells are considered to be energy conversion devices whereas batteries are both energy storage and energy devices. Fuel cells do not need to be recharged with an external source of power such as batteries, they simply need to be replenished or refilled with an appropriate fuel. This brings up the second major difference between batteries and fuel cells; the fuel in a battery is stored internally whereas a fuel cell stores its fuel externally to its core components. The fuel cell is not a heat engine and it is not subjected to the Carnot Cycle limitations.[232-234] Therefore, almost all the chemical energy of the fuel may in theory is converted to electricity.

A fuel cell consists of a cathode (negatively charged electrode), an anode (positively charged electrode), an electrolyte and an external load.[235,236] The anode provides an interface between the fuel and the electrolyte, catalyses the fuel reaction, and provides a path through which free electrons are conducted to the load via the

external circuit. The cathode provides an interface between the oxygen and the electrolyte, catalyses the oxygen reduction reaction, and provides a path through which free electrons are conducted from the load to the electrode via the external circuit. The electrolyte acts as the separator between hydrogen and oxygen to prevent mixing and therefore, preventing direct combustion. It completes the electrical circuit of transporting ions between the electrodes. The fuel cell operating temperature plays an important role in dictating the physicochemical and thermo-mechanical properties of materials chosen as cell components, as well as the type of fuel and oxidant that can be used in a fuel cell.

A number of different types of fuel cells are currently under development. Figure 1.8 describes the operation of typical fuel cells with their different kinds of applications. The chemical reaction involved in fuel cell is as follows:

$$\text{Anode: } H_2 \longrightarrow 2H^+ + 2e^-$$
$$\text{Cathode: } 1/2\ O_2 + 2H^+ + 2e^- \longrightarrow H_2O$$
$$\text{Overall reaction: } H_2 + 1/2\ O_2 \longrightarrow H_2O + \text{Electrical Energy} + \text{Heat}$$

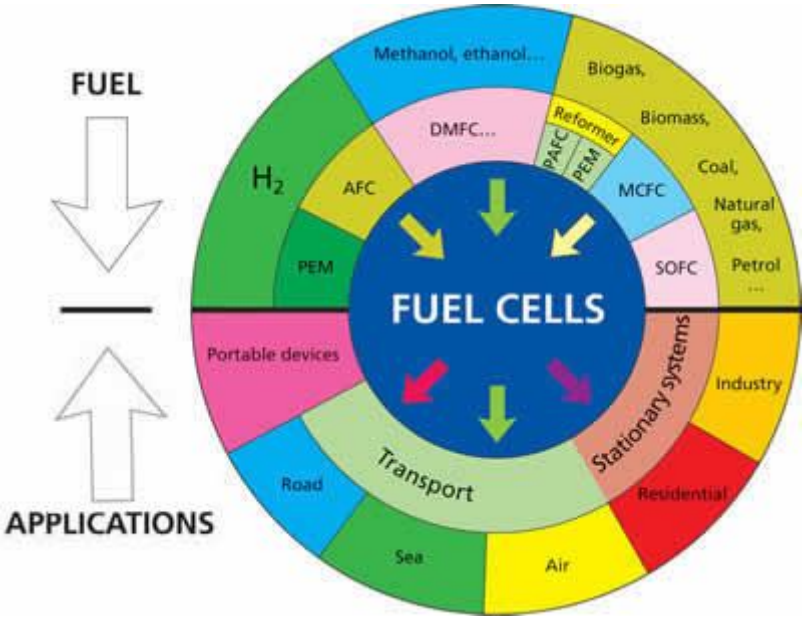

Figure 1.8. *Different types of fuel cells and their applications.*

The major types of fuel cells, classified by the type of electrolyte, are outlined in Table 1.2. Among different types of electrolytes, solid polymer electrolyte membranes [i.e., proton exchange membranes (PEM) or polymer electrolyte membrane fuel cell (PEMFC)][237-239] have attracted major recent research activities (Figure 1.9).

Table 1.2. *An Overview of Fuel Cells. (Adapted from reference 236)*

Fuel Cell	Electrolyte	Operating Temperature (°C)	Electrochemical Reactions
Polymer Electrolyte Membrane (PEMFC)	Solid organic polymer	80 - 200	Anode: $H_2 \rightarrow 2H^+ + 2e^-$ Cathode: $\frac{1}{2}O_2 + 2H^+ + 2e^- \rightarrow H_2O$ Cell: $H_2 + \frac{1}{2}O_2 \rightarrow H_2O$
Alkaline (AFC)	Aqueous solution of potassium hydroxide soaked in a matrix	90-100	Anode: $H_2 + 2(OH^-) \rightarrow 2H_2O + 2e^-$ Cathode: $\frac{1}{2}O_2 + H_2O + 2e^- \rightarrow 2(OH^-)$ Cell: $H_2 + \frac{1}{2}O_2 \rightarrow H_2O$
Phosphoric Acid (PAFC)	Phosphoric acid soaked in a matrix	175-200	Anode: $H_2 \rightarrow 2H^+ + 2e^-$ Cathode: $\frac{1}{2}O_2 + 2H^+ + 2e^- \rightarrow H_2O$ Cell: $H_2 + \frac{1}{2}O_2 \rightarrow H_2O$
Molten Carbonate (MCFC)	Solution of lithium, sodium, and/or potassium carbonates soaked in a matrix	600-1000	Anode: $H_2 + CO_3^{2-} \rightarrow H_2O + CO_2 + 2e^-$ Cathode: $\frac{1}{2}O_2 + CO_2 + 2e^- \rightarrow CO_3^{2-}$ Cell: $H_2 + \frac{1}{2}O_2 + CO_2 \rightarrow H_2O + CO_2$ (CO_2 is consumed at anode and produced at cathode, thus it is included in each side of the equation)
Solid Oxide (SOFC)	Solid zirconium oxide with a small amount of yttria	600-1000	Anode: $H_2 + O^{2-} \rightarrow H_2O + 2e^-$ Cathode: $\frac{1}{2}O_2 + 2e^- \rightarrow O^{2-}$ Cell: $H_2 + \frac{1}{2}O_2 \rightarrow H_2O$

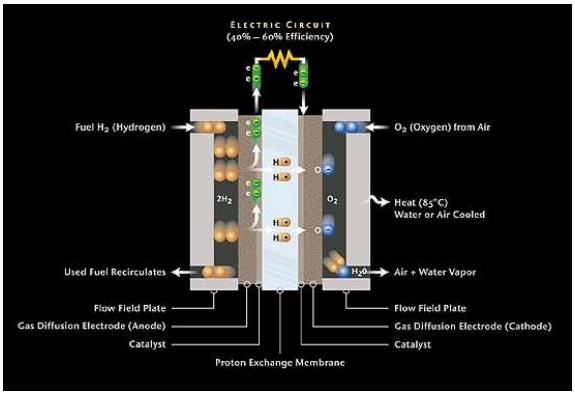

Figure 1.9. *Polymer Electrolyte Membrane Fuel Cell (PEMFC).*

1.10.1.1. Proton Exchange Membrane Fuel Cell

Proton exchange membrane or polymer electrolyte membrane fuel cell (PEMFC) is the most promising candidates and attractive among all fuel cell systems due to its simplicity in uses in automobile, stationary and portable power applications.[237-239] The PEMFC was first developed for the Gemini space vehicle. The main features of the PEMFC are high power density, low operational temperature, pollution free operation, and all-solid construction and therefore less corrosion.[239-244] The basic principle of PEMFC technology involves the oxidation of the fuel (e.g., hydrogen) at the anode and the oxygen reduction at the cathode.[230-234] The electrons, which cannot pass through the membrane, must travel through an external circuit and thus create the source of a direct electrical current. The protons, on the other hand, flow directly through the proton exchange membrane electrolytes and combine with oxygen molecules and the returning electrons to form water. The PEM fuel cell is a thin layer of proton exchange membrane that has electrodes on both sides termed as the membrane electrode assembly (MEA) unit, shown in Figure 1.10.

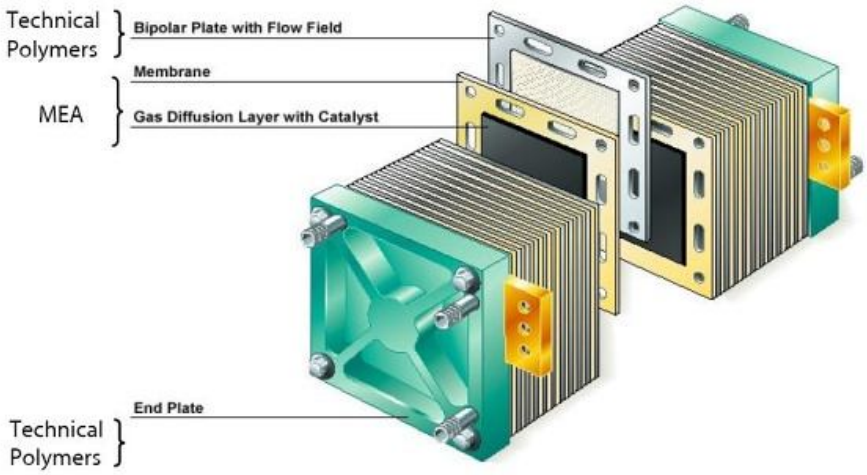

Figure 1.10. *MEA of Polymer Electrolyte Membrane Fuel Cell (PEMFC).*

1.10.1.2. Requirements for Fuel Cell Polymer Electrolyte Membranes

The polymer electrolyte membrane not only transports the protons from anode to cathode and thereby completes the cell electrical circuit, but also provides a physical barrier to prevent the fuel and oxidant gas streams from direct mixing. Hence, the following properties of polymeric membranes are critical for their use in fuel cells[236-244] such as (i) high proton conductivity, (ii) high mechanical stability, (iii) high thermal and chemical stability, (iv) low gas permeability, (v) good film-formation capacity, (vi) low cost, (vii) capable of fabrication into MEAs, and (viii) mechanical durability at high temperature (80–140^{o}C).

Moreover, there are usually significant interactions between the desired properties of the membrane. It should be emphasized that all the desired membrane properties are required for practical fuel cell applications and may not be compromised under operational conditions.

1.10.1.3. Proton Conducting Polymer Membranes

In general, proton-conducting polymer membranes are based on polymer electrolytes, which have negatively charged groups attached to the polymer backbone. Perfluorinated structures (Nafion and Dow type membranes, commercialized by DuPont in 1968 and Dow respectively) have emerged as standard materials for low-temperature fuel cell applications due to high proton conductivity and, their excellent chemical and thermal stability due to presence of teflon-like backbone[245,246] (Scheme 1.5). It also displays a much greater stability in a fuel cell environment and thus increasingly longer fuel cell lifetimes. No other type of materials could replace perfluorinated ionomers for decades because of inability to provide high proton conductivity with high chemical and thermal stability.[234,237] The most general drawbacks of perfluorinated membranes arise from the fact that these materials are proton-conducting only when they are hydrated, which results in a maximum operating temperature of ~100°C that in turn limits activity and CO tolerance of the electro catalyst. Other limitations of these types of membranes are the need of permanent humidification, high methanol crossover, and limited

mechanical stability due to its low glass transition temperature (T_g) (80-120^{o}C). In addition to these factors, which decrease the total efficiency of the system, the high price as well as difficult recycling or disposal of the perfluorinated material, has slowed widespread and economical applications.[243,244,248,249]

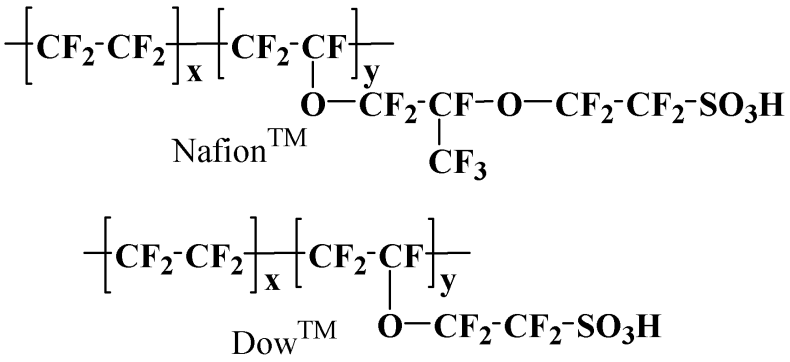

Scheme 1.5. *The chemical structures of perfluorosulfonic acid-based PEM.*

All of these factors have triggered an extensive research for alternative PEMFC materials for operation at high temperature and low degree of hydration. A variety of approaches have been attempted to improve the temperature stability of polymer electrolyte membranes.[232,237,239,241] The major approach has been the attachment of sulfonic acid groups to highly stable aromatic polymers in order to obtain alternative proton-conductive membranes. Up to now, a large number of sulfonated polymers such as polystyrenesulfonic acids,[250] sulfonated poly(ether ether ketone),[251] sulfonated polysulfone,[252] sulfonated poly(phenylene ethers),[253] sulfonated polymers[254] have been reported. Examples of this type of sulfonated ionomers are shown in Scheme 1.6. The polymer electrolyte membranes based on sulfonated aromatic polymers generally show thermal degradation between 200-400^{o}C.

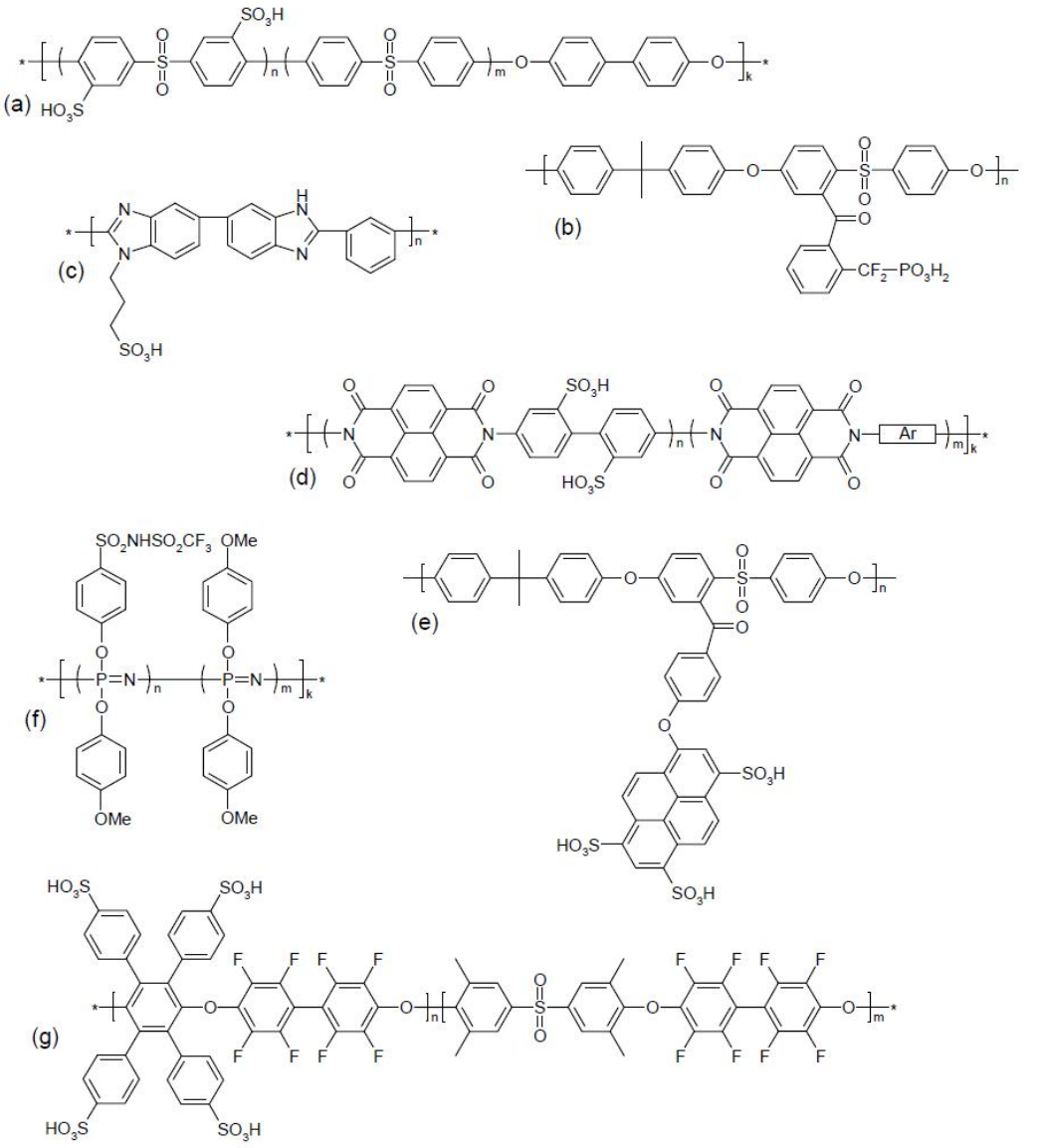

Scheme 1.6. *Examples of proton-conducting polymers designed for PEM materials: (a) sulfonated poly(arylene ethersulfone); (b)polysulfone; (c) sulfopropylated PBI; (d) sulfonated naphthalenic polyimide; (e) polysulfone carrying trisulfonated arylene ether side chains; (f) poly(aryloxyphosphazene); and (g) partially fluorinated and sulfonated poly(arylene ether sulfone) copolymer.*

A second approach investigated is the incorporation of hydrophilic, inorganic fillers into the perfluorinated membranes to increase the binding energy of water. Nanoscale oxides and heteropolyacids have been the most commonly used types of additives. The organic/inorganic composite membranes were prepared either by impregnation of pre-formed perfluorosulfonic acid (PFSAs) membranes (e.g., Nafion 115) via sol-gel processing of a polymeric oxide, or by recasting film using solubilized PFSAs and an inorganic component.[232,237,239,241] This concept is alleged to help retain the water content of the membrane at elevated temperatures. Practical implementation of this approach to date has seen limited success, primarily because of poor interactions between the inorganic phase and the proton conductor. But, all the membranes prepared via these two methods still relied on absorbed water for proton conductivity and remained vulnerable to the loss of conductivity upon loss of water. Long-term, high temperature stable membranes may require a completely different type of membrane that does not rely on water as the electrolyte. A third approach involves the use of a non-aqueous high boiling solvent to replace water completely. Alternative proton carriers have been demonstrated in membranes with phosphoric acid, imidazole, butyl methyl imidazolium triflate, and Brönsted acid-base ionic liquids.[255-261] The basis is that other liquid solvents can perform the function of water in proton conduction but with improved physical characteristics.

1.10.1.4. Phosphoric Acid (PA) Doped PBI Fuel Cell Membranes

Polybenizimidazole (PBI) is an amorphous thermoplastic polymer with a glass transition temperature of 425-436°C. It has a good chemical resistance and excellent textile fiber properties. Acid doped polybenzimidazole (PBI), first introduced by Savinell et al.,[258] has emerged as a promising candidate for a low-cost and high performance membrane material for high temperature PEM fuel cells. It combines the advantages of the inherently high thermal and chemical stability of PBI polymers with the low volatility of phosphoric acid. Significant progress has been achieved in the development of PBI based membranes over the past decade.[262,263] It has been demonstrated that this polymer electrolyte membrane exhibits high ionic conductivity at

temperatures up to 200^{o}C, low gas permeability, excellent oxidative and thermal stability, and nearly zero water drag coefficient.[201,202] In phosphoric acid (PA) doped PBI, PA is the most interesting because they are more amphoteric, thermally stable and having low vapor pressure at elevated temperatures and due to the formation of 3D polyphosphoric acid network for proton transport at high temperatures and anhydrous environment.[264] PA is the best solvent for proton at high temperatures and anhydrous conditions. Savadogo[265] compared the protonic conductivity of acid doped PBI membrane in different acids and found that the conductivity changes are in the order of H_2SO_4 > H_3PO_4 > $HClO_4$ > HNO_3 > HCl for high doping levels. Wasmus et al.[266] used solid state NMR for characterization of H_3PO_4 doped PBI to show the PA absorbed by the PBI membrane is relatively immobile compared to free PA and revealed that there is an interaction between PBI and PA. Gilpa et al.[267] confirmed using IR spectroscopy that the proton transfer was happened from H_3PO_4 to the imino groups of PBI and the presence of undissoociated H_3PO_4 at higher doping level. Kawahara et al.[268] concluded from FTIR data that except H_3PO_4 others (H_2SO_4, CH_3SO_3H, $C_2H_5SO_3H$) protonate basic N moiety on the imidazole groups of PBI but in case of H_3PO_4 strong hydrogen bonding interaction exist between the OH group of acid and imino group of imidazole ring. The higher thermal stability of the PBI/PA suggests that the hydrogen bonding interaction imparts stability to the polymer/acid complex. Siebert developed a microscopic model based on IR spectroscopy study and suggesting that proton transfer from one imide site to another in which the anionic species participates by Grotthuss mechanism.[269] Pu et al.[270] proposed that proton transfer in PA doped PBI membrane was the consequences of the two contributions: one was based on rapid proton exchange (hopping) between phosphate and imidazole moieties via hydrogen bonds (Grotthuss type mechanism), and the other on self-diffusion of phosphate moieties (Vehicular type mechanism) (Scheme 1.7).

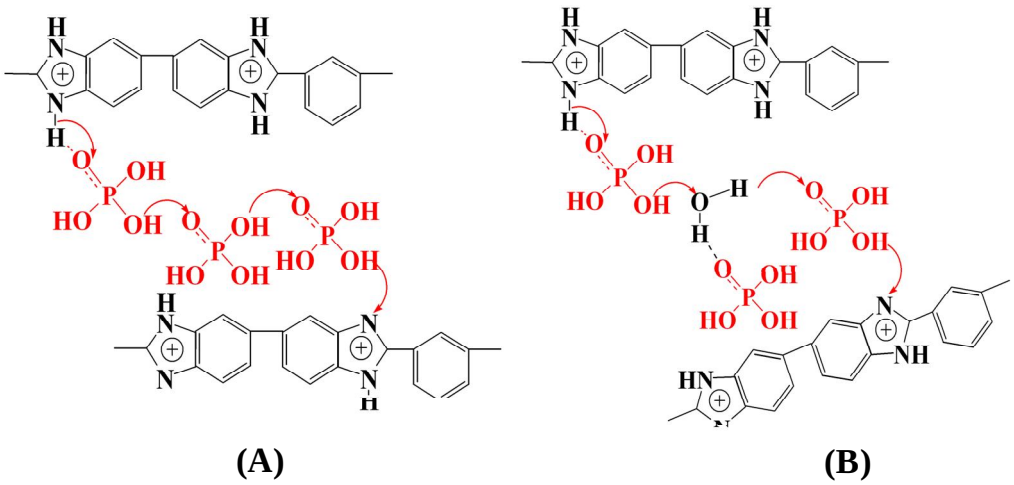

(A) **(B)**

Scheme 1.7. *Proton transfer process (A) acid- PBI- acid (B) acid- water-acid PBI.*

Wainright reported[202,256] that PA doped *m*-PBI (I.V=0.6 dl/g) with 5.0 moles PA per repeating unit (PRU) and showed the conductivity of 2×10^{-2} Scm^{-1} at 130°C and 2.5×10^{-2} Scm^{-1} at 150°C. Pu et al. reported[270] *m*-PBI/PA doped membrane with 6.0 moles PA per repeating unit had conductivity 4.5×10^{-5} $S.cm^{-1}$ at 25°C. Li et al.[257] reported m-PBI/PA complex with 16 moles PA/PRU and the conductivity of 0.13 $S.cm^{-1}$ at 160°C. It has been observed that the conductivity of PA doped PBI membrane increased with higher PA doping but the mechanical strength decreased proportionally with the increase in doping level, leading to loss of mechanical properties at higher doping levels. He et al.[20,210] conducted a study on gas permeability, volume swelling, mechanical integrity, and conductivity of PA doped PBI membranes and observed that the mechanical strength increased slightly due to hydrogen-bonding, then decreased sharply as acid loading increased. They conclude that for pure PBI membranes, the hydrogen bonding between –N and –NH– groups is the dominating force that determines its mechanical strength but when phosphoric acid is introduced, the molecular cohesion of PBI is decreased but stronger hydrogen bonds between –N and phosphoric acid molecules are formed than that of between –N and –NH– groups as a result of the acidity of phosphoric acid.

1.10.1.5. Fabrication of Phosphoric Acid (PA) Doped PBI Membranes

Various attempts have been made for fabrication of PA doped PBI membrane and these are as follows:

(i) Casting of PBI membranes from dimethyl acetamide (DMAc) solution and followed by soaking in PA acids, known as imbibing process. This conventional method to prepare acid doped PBI membranes, pioneered by Savinell et al., involved first dissolving the commercially available PBI in an appropriate solvent, such as dimethyl acetamide (DMAc) with lithium chloride as dissolution stabilizer in a pressurized Parr bomb reactor, then casting the membrane film and subsequently doping the membrane with the desired phosphoric acid (PA) electrolyte. The organic solvent, such as DMAc, were generally poisonous to the platinum fuel cell catalyst. Unfortunately, the polar groups in PBI interacted strongly with the DMAc solvent. Hence, the cast film had to be boiled in distilled water and vacuum-dried exhaustively to eliminate trace amounts of solvent. The mechanical property is good enough for the fabrication of membrane electrode assembly (MEA).[200-202]

(ii) Trifluoroacetic acid (TFA) casting method where trifluoroacetic acid (TFA) as an acid solvent in combination with phosphoric acid not only facilitated the dissolution of PBI polymers and the direct casting of acid-doped PBI membrane, but also enhanced the proton conductivity of the resulting membranes than the conventional imbibing method. But, the membranes cast from TFA solution gave poor mechanical properties.[202,258]

(iii) Sol–gel process by direct casting of membrane from the high molecular weight PBI solution in polyphosphoric acid (PPA) was developed by Xiao et al. where the hot PBI solutions in PPA are cast directly without isolation of the polymer and the PPA hydrolyzed in-situ to phosphoric acid. After casting, the hydrolysis of PPA to phosphoric acid is allowed to take place by absorbing the moisture from the surrounding environment which induces a sol–gel transition, resulting in phosphoric acid-doped PBI membranes (Figure 1.11). These membranes have high PA doping

levels, good mechanical properties, high conductivities, and excellent long term stabilities.[34]

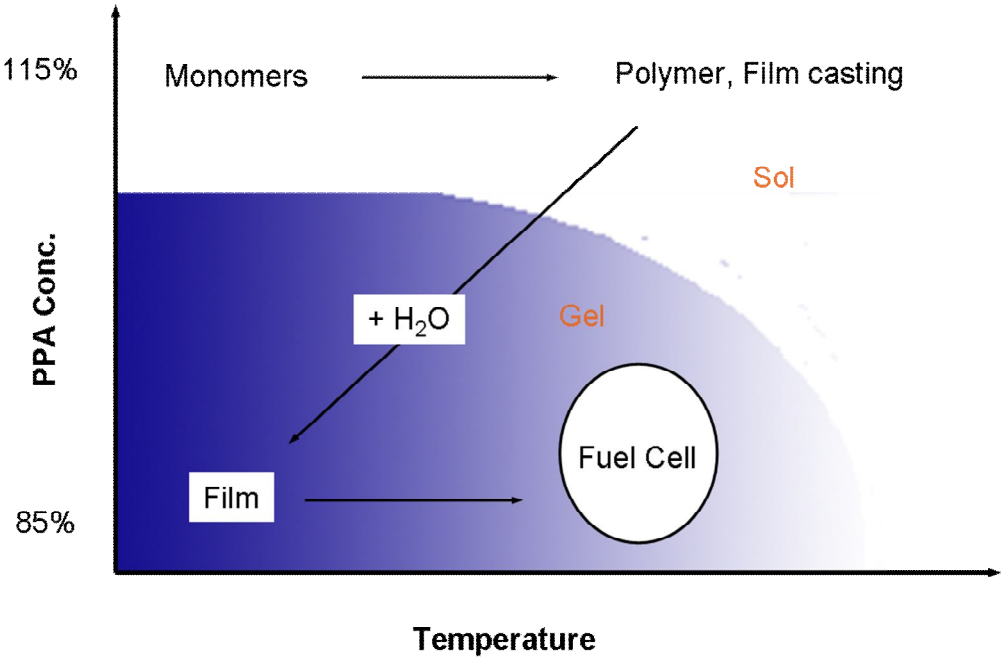

Figure 1.11. *Fabrication of PA doped PBI membrane by PPA process. (Adapted from reference 34).*

(iv) The another approach is the introduction of the porosity in the PBI by leaching out a low molecular weight compound using selective solvent for porogen followed by soaking the film in PA where Then the porous PBI membranes were soaked in phosphoric acid solution to obtain the PA doped PBI membrane (Figure 1.12). In this method different phthalates such as dimethyl, diethyl, dibutyl and diphenyl, as well as triphenyl phosphate were used as porogen.[206]

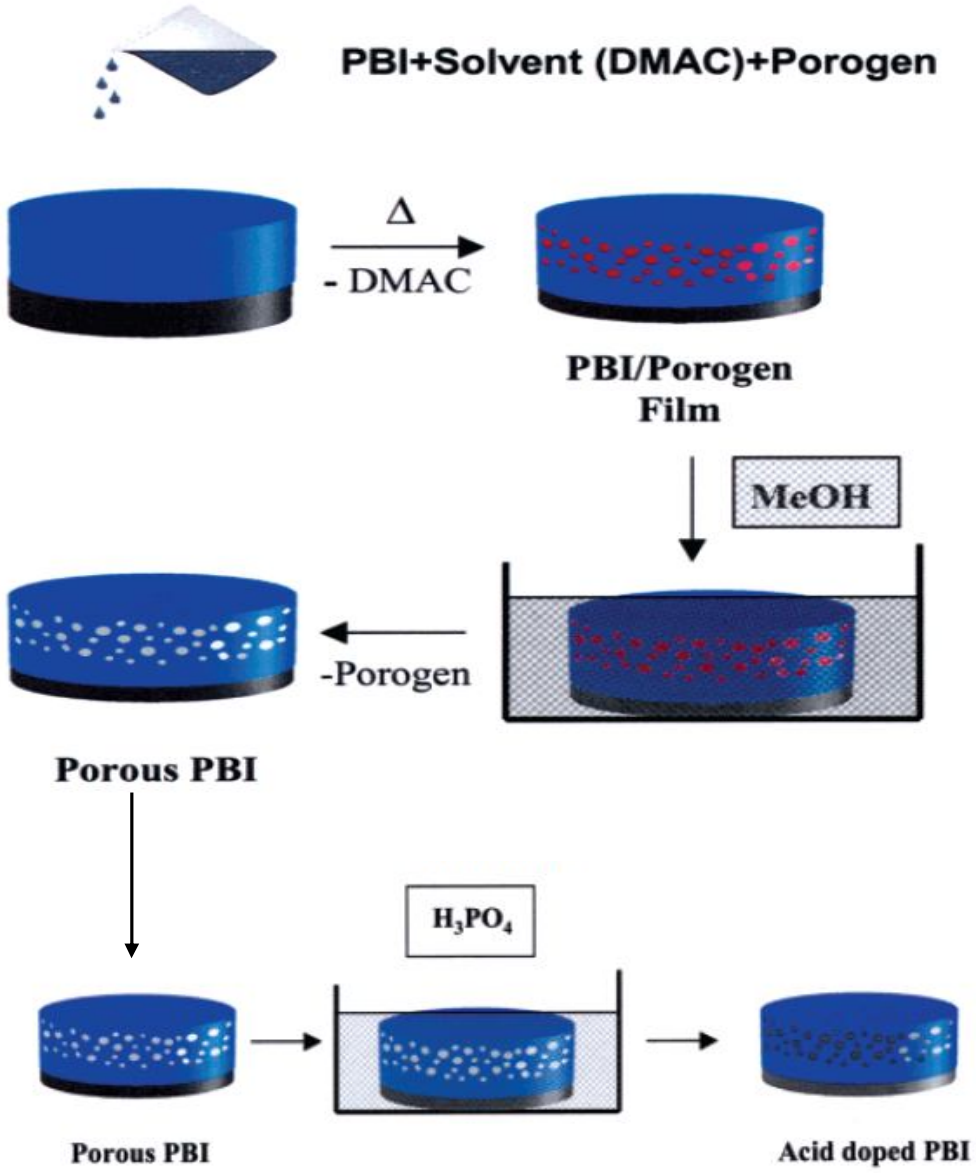

Figure 1.12. *Fabrication of PA doped PBI membrane by porous PBI process. (Adapted from reference 207).*

(v) Gel casting method (preparation of thermoreversible gel of PBI in PA and followed by casting the PA doped membranes), developed by our group where PBI gel was prepared by taking require amount of solid PBI powder, dissolved in H_3PO_4. The mixture was then heated at 180^{o}C for 1 to 2 hour to get homogeneous reddish *m*-PBI

solution in H_3PO_4. This hot solution was poured in petridish and within 2 minutes it forms the gel. This gel material can be easily pilled off from the glass surface as a strong free standing PA doped PBI film. In this process, the PBI membrane showed not only good acid doping levels, but it has also a good mechanical stability. The overall gelation mechanism is presented in Figure 1.13[209] and the whole process is presented in Figure 1.14.

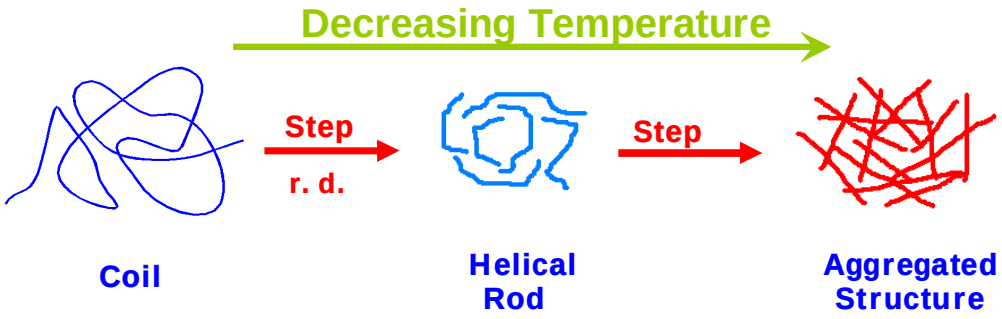

Figure 1.13. *Schematic representation of the gelation mechanism. (Adapted from reference 209)*

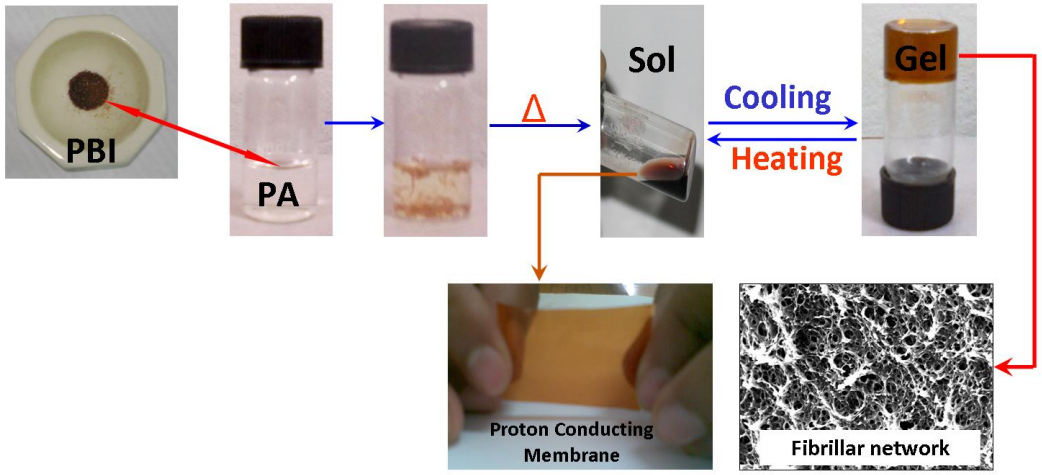

Figure 1.14. *Schematic representation of the whole gelation process. (Adapted from reference 209).*

1.11. AIMS of the Thesis

The above discussions in this chapter about the PBI types of polymers offer many opportunities to study the PBI chemistry. Despite the presence of huge literature on the PBI type materials, we found out that there are many issues which were not addressed with and discussed in the literature adequately. Large numbers of efforts have been made to synthesize variety of PBI backbone structure; however no attempts have been made regarding the influences of various properties of polybenzimidazole with the initial monomer concentration of polymerization process. Hence we have attempted to explore these aspects in Chapter 2 with an aryl ether linked polybenzimidazole namely poly(4,4'-diphenylether-5,5'-bibenzimidazole), which we called as OPBI throughout this study. Surprisingly, the studies on solution properties and the aggregation behavior of OPBI in polar aprotic and protic medium are almost absent in the literature except only very few superficial reports. We have addressed this issue in Chapter 3. The increase of enormous attention of PBI in recent years is because of their use in PEMFC. Despite the presence of large number of literatures on the PA doped PBI membrane for the use in PEMFC, till today the appropriate PBI membrane has not been achieved. We have designed and developed a new OPBI-FA gel membrane. These topics are discussed in Chapter 4. Very limited efforts have been made in literatures about the PBI nanocomposites. We have prepared OPBI nanocomposites using nanoclays and silica nanoparticles and improved several properties of OPBI which are discussed in Chapter 5 and 6. Therefore the thesis projects development of new generation polymer electrolyte membranes based on PBI for the use in future HT-PEMFC. The aims and objectives of each chapter of this thesis are elaborated at the end of the introductory part of the individual chapters.

References

1. Vogel, H. A.; Marvel, C. S. *J. Polym. Sci.* **1961**, *50*, 511.
2. Vogel, H.; Marvel, C. S. *J. Polym. Sci. A* **1963**, *1*, 1531.
3. Plummer. L.; Marvel, C. S. *J. Polym. Sci. A* **1964**, *2*, 2559.
4. Marvel, C. S.; Ariz, T.; Vogel, H. A. *U. S. Patent* 3 174 947,**1965**.
5. Choe, E. W., Choe, D. D. In *Polymeric Materials Encyclopedia*; Salamone, J. C., Ed.; CRC Press: New York, **1996,** 5619.
6. Lee, H.; Stoffey, D.; Neville, K. *New Linear Polymers;* McGraw-Hill: New York, **1967**, Chapter 9.
7. Frazerr, A. H. High *Temperature Resistant Polymers;* Interscience: New York, **1968**, 138.
8. Critchley, J. P. *Prog. Polym. Sci*. **1970**, *2*, 47.
9. Neuse, E. W. *Adv. Polym. Sci.* **1982**, *47*, 1.
10. Power, E. D.; Serad, G. A. *High Performance Polymer: Their origin and Development*, Elesevier, New York, **1986**.
11. Buckley, A.; Stuetz, D.; Serad, G.A. *Encyclopedia of Polymer Science and Engineering*, Wiley, New York, **1987**, 572.
12. Critchley, J. P.; Knight, G. J.; Wright, W.W. *Heat-resistant Polymers*; Plenum Press: New York, **1983**, 259.
13. Prince A. E. *U. S. Patent* 3 509 108, **1970**.
14. Eguchi, T.; Ohfuji, Y. *U. S. Patent* 3 655 632, **1972**.
15. Neuse, E.W.; Loonat, M. S. *Macromolecule*. **1983**,*16*,128.
16. Brand, R. A.; Bruma, M.; Kellman, R.; Marvel, C. S. *J. Polym. Sci., Polym. Chem. Ed*. **1978**, *16*, 2275.
17. Higgins, J.; Marvel, C. S. *J. Polym. Sci.* **1970**, *A1*, 171.
18. Iwakura,Y.; Uno, K.; Imai, Y. *J. Polym. Sci.* **1964**, *A2*, 2605.
19. Choe, E. W. *J. Appl. Polym. Sci.* **1994**, *53*, 497.
20. Li, Q.; He, R.; Jensen, J. Q.; Bjerrum, N. J. *Chem. Mater.* **2007**, *19*, 350.

21. Xiao, L.; Zhang, H.; Scanlon, E.; Ramanathan, L. S.; Choe, E.-W.; Rogers, D.; Apple, T.; Benicewicz, B. C. *Chem. Mater.* **2005**, *17*, 5328.
22. Li ,Q.; Jensena, J. O.; Savinell, R. F.; Bjerrum, N. J. *Prog. Polym. Sci.* **2009**, *34*, 449.
23. Choe, E. W.; Conciatori, A. B. *U. S. Patent* 4 452 972, **1984**.
24. Choe, E. W.; Conciatori, A. B.; Ward, B. C. *U. S. Patent* 4 463 167, **1984**.
25. Choe, E. W.; Conciatori, A. B. *U. S. Patent* 4 485 232, **1984**.
26. Choe, E. W.; Conciatori, A. B. ; Ward, B. C. *U. S. Patent* 4 506 068, **1985**.
27. Choe, E. W.; Conciatori, A. B. *U. S. Patent* 4 533 725, **1985**.
28. Choe, E. W.; Conciatori, A. B. *U. S. Patent* 4 535 144, **1985**.
29. Lobato, J.; Caenizares, P.; Rodrigo, M. A.; Linares, J. J.; Manjavacas, G. *J. Membr. Sci.* **2006**, *280*, 351.
30. Xu, H.; Chen, K.; Guo, X.; Fang, J. *Polymer* **2007**, *48*, 5541.
31. Chen, C. C.; Wang, L. F.; Wang, J. J.; Hsu, T. C.; Chen, C. F. *J. Mater. Sci.* **2002**, *37*, 4109.
32. Sannigrahi, A.; Ghosh, S.; Lalnuntluanga, J.; Jana, T. *J. Appl. Polym. Sci.* **2009**, *111*, 2194.
33. Asensio, J. N.; Borro´s, S.; Go´mez-Romero, P. *J. Electrochem. Soc. A* **2004**, *151*, 304.
34. Xiao, L.; Zhang, H.; Jana, T.; Scanlon, E.; Chen, R.; Choe, E. W.; Ramanathan, L. S.; Yu, S.; Benicewicz, B. C. *Fuel Cells* **2005**, *5*, 287.
35. Sannigrahi, A.; Ghosh, S.; Maity, S.; Jana, T. *Polymer* **2010**, *51*, 5929.
36. Jouanneau, J.; Mercier, R.; Gonon, L.; Gebel, G. *Macromolecules* **2007**, *40*, 983.
37. Li, Z. X.; Liu, J. H.; Yang, S. Y.; Huang, S. H.; Lu, J. D.; Pu, J. L. *J. Polym. Sci., Part A: Polym. Chem.* **2006**, *44*, 5729.
38. Chen, C. C.; Wang, L. F.; Wang, J. J.; Hsu, T. C.; Chen, C. F. *J. Mater. Sci.* **2002**, *37*, 4109.
39. Chuang, S. W.; Hsu, S. L. C. *J. Polym. Sci., Part A: Polym. Chem.* **2006**, *44*, 4508.

40. Sannigrahi, A.; Arunbabu, D.; Sankar, R. M.; Jana, T. *J. Phys. Chem. B* **2007,** *111*, 12124.
41. Qing, S.; Huang, W.; Yan, D. *Euro. Poly. J.* **2005,** *41*,1589.
42. Pu, H.; Liu, Q.; Liu, G. *J. Membr. Sci.* **2004**, *241*, 169.
43. Scariah, K. J.; Krishnamurthy, V. N.; Rao, K. V. C.; Srinivasan, M. *J. Polym. Sci., Part A: Polym. Chem.* **1987**, *25*, 2675.
44. Persson, J. C.; Jannasch, P. *Chem Mater.* **2006**, *18*, 3096.
45. Pu, H. T.; Liu, Q. Z. ; Liu, G. H. *J. Membr. Sci.* **2004,** *241*,169.
46. Klaehn, J. R.; Luther, T. A.; Orme, C. J.; Jones, M. G.; Wertsching, A. K.; Peterson, E. S. *Macromolecules* **2007,** *40,* 7487.
47. Gieselman, M.; Reynolds, J. R. *Macromolecules* **1992**, *25*, 4832.
48. Kojima, T. *J. Polym. Sci., Polym.Phys.Ed*.**1980**, *8*, 1685.
49. Shogbon, C. B.; Brousseau, J. L.; Zhang, H.; Benicewicz, B. C.; Akpalu, Y. *Macromolecules* **2006**, 36, 9409.
50. Sannigrahi, A.; Arunbabu, D.; Sankar, R. M.; Jana, T. *Macromolecules* 2007, *40*, 2844.
51. Ghosh, S.; Sannigrahi, A.; Maity, S.; Jana, T. *J. Phys. Chem. B* 2010, 114, 3122.
52. Kulkarni, M.; Potrekar,R.; Kulkarni,R. A.; Vernekar, S. P. *J. Polym. Sci., Part A: Polym. Chem.* **2008**, *46*, 5776.
53. Varma, I. K.; Veena. *J. Polym. Sci., Polym. Chem. Ed.* **1976**, *14*, 973.
54. Varma, I. K.; Veena. *J. Macromol. Sci., Chem.* **1977**, *11*, 845.
55. Scariah, K. J.; Krishnamurthy, V. N.; Rao, K. V. C. *J. Polym. Sci., Part A: Polym. Chem.* **1987**, *25*, 2675.
56. Korshak, V. V.; Teplyakov, M. M.; Fedorova, R. D. *J. Polym. Sci., Part A: Polym. Chem.* **1971**, *9*, 1027.
57. Tsur, Y.; Levine, H. H.; Levy, M. *J. Polym. Sci., Polym. Chem. Ed*. **1974**, *12*, 1515.
58. Srinivasan, P. R.; Mahadevan, V.; Srinivasan, M. *J. Polym. Sci., Polym. Chem. Ed.* **1982**, *20*, 3095.

59. Lyoo, W. S.; Choi, J. H.; Han, S. S.; Yoon, W. S.; Park, M. S.; Ji, B. C. *J. Appl. Polym. Sci.* **2000**, *78*, 438.

60. Nakajima, T.; Marvel, C. S. *J. Polym. Sci., Part A: Polym. Chem.* **1969**, *7*, 1295.

61. Kovacs, H. N.; Delman, A. D.; Simms, B. B. *J. Polym. Sci., Part A: Polym. Chem.* **1968**, *6*, 2103.

62. Saegusa, Y.; Horikiri, M.; Nakurmura, S. *Macromol. Chem. Phys.* **1997**, *198*, 619.

63. Hedberg, F. L. ; Marvel, C. S. *J. Polymer Sci., Polym. Chem. Ed.* **1974**,*12*, 1823.

64. Brooks, N. W.; Duckett, R. A.; Rose, J.; Ward, I. M.; Clements, J. *Polymer* **1993**, *34*, 4038.

65. Arunbabu, D.; Sannigrahi, A.; Jana, T. *J. Phys. Chem. B* **2008,** *112*, 5305.

66. Deimede, V.; Voyiatzis, G. A.; Kallitsis, J. K.; Qingfeng, L.; Bjerrum, N. J. *Macromolecules* **2000**, *33*, 7609.

67. Menczel, J. D. *J. Them. Analys. Calmetry,* **2000**,*59*,1023.

68. (a) Kumbharkar, S.C.; Islam, Md. Nazrul.; Potrekar, R.A.; Kharul, U. K. *Polymer* **2009**, *50*, 1403, (b) Kumbharkar, S.C.; Kharul, U. K. *J. Membr Sci.* **2010**, *357*, 134.

69. Noye, P.; Li, Q.; Pan, C.; Bjerrum, N. J. *Polym. Adv. Technol.* **2008**, *19*, 1270.

70. Xu, H.; Chen, K.; Guo, X.; Fang, J.; Yin, J. *J. Polym. Sci., Part A: Polym. Chem.* **2007**, *45*, 1150.

71. Kim, T. A.; Jo, W. H. *Chem. Mater.* **2010**, *22*, 3646.

72. Hubner, G.; Roduner, E. *J. Mater. Chem.* **1999**, *9*, 409.

73. Gaudiana, R. A.; Conley, R. T. *J. Polym. Sci.* **1969**, *B7*, 793.

74. Musto, P.; Karasz, F. E.; Macknight, W. J. *Polymer* **1993**, *34*, 2934.

75. Kosmala, B.; Schauer, J. J. *Appl. Polym. Sci.* **2002**, *85*, 1118.

76. Daletou, M. K.; Gourdoupi, N.; Kallitsis, J. K. *J. Membr. Sci.* **2005**, *252*, 115.

77. Chang, Z. H.; Pu, H. T.; Wan, D. C.; Liu, L.; Yuan, J. J.; Yang, Z. L. *Polym. Degrada. Stab.* **2009**, *94*, 1206.

78. Jousset, S. ; Bellissent, H.; Galin, J. C. *Macromolecules* **1998**, *31*, 4520.

79. Antonietti, M.; Briel, A.; Forster, S. *Macromolecules* **1997**, *30*, 2700.
80. Dobrynin, A. V.; Colby, R. H.; Rubintein, M. *Macromolecules* **1995**, *28*, 1859.
81. Ennari, J.; Elomaa, M.; Sundholm, F. *Polymer* **1999**, *40*, 5035.
82. Schwarz, S.; Buchhamer, H. M.; Lunkwitz, K.; Jacobasch, H. -J. *Colloids Surf. A* **1998**, *140*, 377.
83. Schwarz, S.; Lunkwitz, K.; Keßler, B.; Spiegler, U.; Killmann, E.; Jaeger, W. *Colloids Surf. A* **2000**, *163*, 17.
84. Walker, H. W.; Grant, S. B. *Colloids Surf. A* **1996**, *119*, 229.
85. Antonietti, M.; Briel, A.; Forster, S. *J. Chem. Phys.* **1996**, *105*, 7795.
86. Roure, I.; Rinaudo, M.; Milas, M.; Frollini, E. *Polymer* **1998**, *39*, 5441.
87. Skolnick, J.; Fixman, M. *Macromolecules* **1977**, *10*, 944.
88. Huggins, H. L. *J. Phys. Chem.* **1938**, *42*, 911.
89. Schaefgen, J. R.; Trivisonno, C. F. *J. Am. Chem. Soc.* **1952**, *74*, 2715.
90. Saunders, P. R. *J. Polym. Sci.* **1962**, *57*, 131.
91. McCormick, C. L.; Elliot, D. L. *Macromolecules* **1966**, *19*, 52.
92. McCormick, C. L.; Newman, J. K. *Macromolecules* **1994**, *27*, 5114.
93. Ikawa, T.; Abe, K.; Honda, K.; Tsuchida, E. *J. Polym. Sci., Polym. Chem. Ed.* **1975**, *13*, 1505.
94. Osada, Y.; Sato, M. *J. Polym. Sci., Polym. Lett. Ed.* **1976**, *14*, 129.
95. Bednar, B.; Li, Z.; Huang, Y.; Chang, L. C. P.; Morawetz, H. *Macromolecules* **1985**, *18*, 1829.
96. Hemker, D. J.; Garza, V.; Frank, C. W. *Macromolecules* **1990**, *23*, 4411.
97. Bokias, G.; Staikos, G.; Iliopoulos, I.; Audebert, R. *Macromolecules* **1994**, *27*, 427.
98. Iliopoulos, I.; Audebert, R. *Eur. Polym. J.* **1988**, *24*, 71.
99. Fuoss, R. M.; Strauss, U. P. *J. Polym. Sci.* **1948**, *3*, 602.
100. Pals, D. T. E.; Hermans, J. J. *J. Polym. Sci.* **1948**, *3*, 898.
101. Pals, D. T. E.; Hermans, J. J. *J. Polym. Sci.* **1950**, *5*, 773.
102. Pals, D. T. E.; Hermans, J. J. *Rec. Trav. Chim. Pays-Bas.* **1952**, *71*, 458.
103. Roure, I.; Rinaudo, M.; Milas, M. *Ber. Bunsenges. Phys. Chem.* **1996**, *100*, 703.

104. (a) Nandi, P.; Bhattarai, A.; Das, B. *J. Polym. Sci., Part B : Polym. Phys.* **2007**, *45*, 1765, (b) Sharma, R.; Das, B.; Nandi, P.; Das, C. *J. Polym. Sci., Part B : Polym. Phys.* **2010**, *48*, 1196.
105. Freed, K. F. *Adv. Chem. Phys.***1972**, *22*, 1.
106. Yamakawa, H. *Helical Wormlike Chains in Polymer Solutions*; Springer: New York, **1997**.
107. Schmitz, K. S. *Macroions in Solution and Colloidal Suspension*; VCH: New York, **1993**.
108. Forster, S.; Schmidt, M. *Adv. Polym. Sci.* **1995**, *120*, 51.
109. Odijk, T. *Macromolecules* **1979**, *12*, 688.
110. Skolnick, J.; Fixman, M. *Macromolecules* **1977**, *10*, 944.
111. Muthukumar, M. *J. Chem. Phys.* **1996**, *105*, 5183.
112. Muthukumar, M. *J. Chem. Phys.* **1987**, *86*, 7230.
113. Lehn, J. *Angew. Chem. Int. Ed. Engl.* **1988**, *27*, 89.
114. Lehn, J. *Angew. Chem. Int. Ed. Engl.* **1990**, *29*, 1304.
115. Ky Hirschberg, J. H. K.; Brunsveld, L.; Ramzi, A.; Vekemans, J. A. J. M.; Sijbesma, R. P.; Meijer, E. W. *Nature* **2000**, *407*, 167.
116. Bekturov, E. V.; Bimendina, L. A. *Adv. Polym. Sci.* **1981**, *41*, 99.
117. Tschuchida, E.; Abe, K. *Adv. Polym. Sci.* **1982**, *45*, 1.
118. Deepak, V. D.; Asha, S. K. *J. Phys. Chem. B* **2009**, *113*, 11887.
119. Simon, S.; Dugast, J. Y.; Le Cerf, D.; Picton, L.; Muller, G. *Polymer* **2003**, *44*, 7917.
120. (a) Hong, P. -D.; Chou, C. -M.; He, C. -H. *Polymer* **2001**, *42*, 6105, (b) Hong, P. -D.; Chou, C. -M.; Chen, J. -H. *Polymer* **2000**, *41*, 5847.
121. Ogata, Y.; Mogi, T.; Makita, Y. *J. Polym. Sci., Part B: Polym. Phys.* **2010**, *48*, 588.
122. Nuopponen, M.; Ojala, J.; Tenhu, H. *Polymer* **2004**, *45*, 3643.
123. Russo, P. S. *Reversible Polymeric Gels and Related Systems*; Ed, ACS Symposium Series, American Chemical Society: New York, **1986**.

124. Guenet, J. M. *Thermoreversible Gelation of Polymers and Biopolymers*; Academic Press: London, **1992**.
125. Paul, D. R. *J. Appl. Polym. Sci.* **1967**, *11*, 439.
126. Kawanishi, K.; Komatsu, M.; Inoue, T. *Polymer* **1987**, *28*, 980.
127. Mal, S.; Maiti, P.; Nandi, A. K. *Macromolecules* **1995**, *28*, 2371.
128. Mal, S.; Nandi, A. K. *Polymer* **1998**, *30*, 6301.
129. Dikshit, A. K.; Nandi, A. K. *Macromolecules* **2000**, *33*, 2616.
130. Dasgupta, D.; Nandi, A. K. *Macromolecules* **2005**, *38*, 6504.
131. Dikshit, A. K.; Nandi, A. K. *Langmuir* **2001**, *17*, 3607.
132. Giannelis, E. P. *Adv. Mater.* **1996**, *8*, 29.
133. Burnside, S. D.; Giannelis, E. P. *Chem. Mater.* **1995**, *7*, 1597.
134. Gilman, J. W. *Appl. Clay. Sci.* **1999**, *15*, 31.
135. Gilman, J. W.; Jackson, C. L.; Morgan, A. B.; Harris, R., Jr.; Manias, E.; Giannelis, E. P.; Wuthenow, M.; Hilton, D.; Phillips, S. H. *Chem. Mater.* **2000**, *12*, 1866.
136. Giannelis, E. P. *Appl. Organomet. Chem.* **1998**, *12*, 675.
137. Xu, R.; Manias, E.; Snyder, A. J.; Runt, J. *Macromolecules* **2001**, *34*, 337.
138. Ghosh, S.; Sannigrahi, A.; Maity, S.; Jana, T. *J. Phys. Chem. C* **2011**, *115*, 11474.
139. Yano, K.; Usuki, A.; Okada, A.; Kurauchi, T.; Kamigaito, O. *J. Polym. Sci., Part A: Polym. Chem.* **1993**, *31*, 2493.
140. Sinha Ray, S.; Yamada, K.; Okamoto, M.; Ueda, K. *Nano Lett.* **2002**, *2*, 1093.
141. Chen, X. G.; Li, Z.; Zhou, H. Q.; Wang, T. J.; Qin, J. G.; Inokuchi, M. *Polymer* **2007**, *48*, 3256.
142. Cao, T.; Webber, S. E. *Macromolecules* **1995**, *28*, 3826.
143. Loy, D. A.; Assink, R. A. *J. Am. Chem. Soc.* **1992**, *114*, 3977.
144. Ajayan, P. M.; Stephen, O.; Colliex, C.; Trauth, D. *Science* **1994**, *265*, 1212.
145. Ajayan, P. M.; Schadler, L. S.; Giannaris, C.; Rubio, A. *Adv. Mater.* **2000**, *12*, 750.

146. Vaia, R. A.; Krishnamoorti, R. *In Polymer Nanocomposites: Synthesis Characterization and Modeling*; American Chemical Society: Washington, DC, **2001**, 1.

147. (a) Jung, D. H.; Cho, S. Y.; Peck, D. H.; Shin, D. R.; Kim, J. S. *J. Power Sources* **2002**, *106*, 173, (b) Althues, H.; Henle, J.; Kaskel, S. *Chem. Soc. Rev.* **2007**, *36*, 1454, (c) Kickelbick, G. *Prog. Polym. Sci.* **2003**, *28*, 83.

148. (a) Antonucci, P. L.; Arico, A. S.; Creti, P.; Ramunni, E.; Antonucci, V. *Solid State Ionics* **1999**, *125*, 431, (b) Kickelbick, G. *In Hybrid Materials. Synthesis, Characterization, and Applications*; Kickelbick, G., Ed. Wiley-VCH: Weinheim, Germany, **2007**; Chapter 1.

149. (a) Shao, Z.; Joghee, P.; Hsing, I. *J. Membr. Sci.* **2004**, *229*, 43, (b) Akcora, P.; Liu, H.; Kumar, S. K.; Moll, J.; Li, Y.; Benicewicz, B. C.; Schadler, L. S.; Acehan, D.; Panagiotopoulos, A. Z.; Pryamitsyn, V.; Ganesan, V.; Ilavsky, J.; Thiyagarajan, P.; Colby, R. H.; Douglas, J. F. *Nat. Mater.* **2009**, *8*, 354.

150. Verdejo, R.; Bernal, M. M.; Romasanta, L. J.; Lopez-Manchado, M. A. *J. Mater. Chem.* **2011**, *21*, 3301.

151. Zou, H.; Wu, S.; Shen, J. *Chem. Rev.* **2008**, *108*, 3893.

152. Gu, A.; Kuo, S. W.; Chang, F. C. *J. Appl. Polym. Sci.* **2001**, *79*, 1902.

153. Sasaki, A.; White, J. L. *J. Appl. Polym. Sci.* **2004**, *91*, 1951.

154. Vora, R. H.; Pallathadka, P. K.; Goh, S. H.; Chung, T. S.; Lim, Y. X.; Bang, T. K. *Macromol. Mater. Eng.* **2003**, *288*, 337.

155. Homminga, D.; Goderis, B.; Dolbnya, I.; Reynaers, H.; Groeninckx, G. *Polymer* **2005**, *46*, 11359.

156. Gardolinski, J. E.; Carrera, L. C. M.; Cantao, M. P.; Wypych, F. *J. Mater. Sci.* **2000**, *35*, 3113.

157. Romero-Guzmán, M. E.; Flores, O.; Flores, A.; Romo-Uribe, A.; Alvarado-Tenorio, B.; Campillo, B. *Polym. Adv. Tech.* **2011**, *22*, 836.

158. Mishra, A. K.; Chattopadhyay, S.; Nando, G. B. *J. Appl. Polym. Sci.* **2010**, *115*, 558.

159. Yang, C.; Liu, P.; Zhao, Y. *Electrochim. Acta* **2010**, *55*, 6857.

160. Alkan, M.; Demirbas¸, Ö; Doğan, M., *Microporous Mesoporous Mater.* **2005**, *83*, 51.
161. Weiss, A.; Thielepape, W.; Göring, G.; Ritter W.; Schäfer, W. *Int. Clay Conf.* **1963**, *1*, 287.
162. Thompson, J. G.; Cuff, C. *Clays Clay Miner.* **1985**, *33*, 490.
163. Maiti, P.; Nam, P. H.; Okamoto, M.; Hasegawa, N.; Usuki, A. *Macromolecules* **2002**, *35*, 2042.
164. Zhu, J.; Morgan, A. B.; Lamelas, F. J.; Wilkie, C. A. *Chem. Mater.* **2001**, *13*, 3774.
165. Uddin, F. *Metallurgical and Materials Transactions A* **2008**, *39*, 2804.
166. Komori, Y.; Sugahara, Y.; Kuroda, K. *Chem. Mater.* **1999**, *11*, 3.
167. Theng, B. K. G. *The Chemistry of Clay–Organic Reactions*; Adam Hilger: London, **1974**.
168. Paiva, L. B.; Morales, A. R.; Díaz. F. R. V. *Appl. Clay Sci.* **2008**, *42*, 8.
169. Krishnamoorti, R.; Vaia, R. A.; Giannelis, E. P. *Chem. Mater.* **1996**, *8*, 1728.
170. Vaia, R. A.; Ishii, H.; Giannelis, E. P. *Chem. Mater.* **1993**, *5*, 1694.
171. Vaia, R. A.; Vasudevan, S.; Krawiec, W.; Scanlon, L. G.; Giannelis, E. P. *Adv. Mater.* **1995**, *7*, 154.
172. Vaia, R. A.; Jandt, K. D; Kramer, E. J.; Giannelis, E. P. *Macromolecules* **1995**, *28*, 8080.
173. Vaia, R. A.; Giannelis, E. P. *Macromolecules* **1997**, *30*, 8000.
174. Ogata, N.; Jimenez, G.; Kawai, H.; Ogihara, T. *J. Polym. Sci., Part B: Polym. Phys.* **1997**, *35*, 389.
175. Lee, D. C.; Jang, L. W. *J. Appl. Polym. Sci.* **1998**, *68*, 1997.
176. Jeon, H. G.; Jung. H.-T.; Lee, S. W.; Hudson, S. D. *Polym. Bult.* **1998**, *41*, 107.
177. Kim, Y. S.; Wang, F.; Hickner, M.; Zawodzinski, T. A.; McGrath, J. E. *J. Membr. Sci.* **2003**, *212*, 263.
178. Ponce, M. L.; Prado, L.; Ruffmann, B.; Richau, K.; Mohr, R.; Nunes, S. P. *J. Membr. Sci.* **2003**, *217*, 5.
179. McKeen, J. C.; Yan, Y. S.; Davis, M. E. *Chem. Mater.* **2008**, *20*, 5122.

180. Stankovich, S.; Dikin, D. A.; Dommett, G. H. B.; Kohlhaas, K. M.; Zimney, E. J.; Stach, E. A.; Piner, R. D.; Nguye, S. T.; Ruoff, R. S. *Nature* **2006**, *442*, 282.
181. Rafiee, M. A.; Rafiee, J.; Wang, Z.; Song, H.; Yu, Z. -Z.; Koratkar, N. *ACS Nano* **2009**, *3*, 3884.
182. Balazs, A. C.; Emrick, T.; Russell, T. P. *Science* **2006**, *314*, 1107.
183. Darbandi, M.; Thomann, R.; Nann, T. *Chem. Mater.* **2007**, *19*, 1700.
184. Stöber, W.; Fink, A.; Bohn, E. *J. Colloid Interface Sci.* **1968**, *26*, 62.
185. Vassiliou, A. A.; Papageorgiou, G. Z.; Achilias, D. S.; Bikiaris, D. N. *Macromol. Chem. Phys.* **2007**, *208*, 364.
186. Zhang, M. Q.; Rong, M. Z.; Friedrich, K. *In Handbook of Organic- Inorganic Hybrid Materials and Nanocomposites*; Nalwa, H. S., Ed. Ameican Scientific Publishers: Stevenson Ranch, CA, **2003**, *2*, 113.
187. Novak, B. M. *Adv. Mater.* **1993**, *5*, 422.
188. Schubert, U.; Hüsing, N.; Lorenz, A. *Chem. Mater.* **1995**, *7*, 2010.
189. Judeinstein, P.; Sanchez, C. *J. Mater. Chem.* **1996**, *6*, 511.
190. Wen, J. Y.; Wilkes, G. L. *Chem. Mater.* **1996**, *8*, 1667.
191. Schottner, G. *Chem. Mater.* **2001**, *13*, 3422.
192. Huang, S. L.; Chin, W. K.; Yang, W. P. *Polymer* **2005**, *46*, 1865.
193. Yu, Y. Y.; Chen, W. C. *Polym. Int.* **2005**, *54*, 500.
194. He, Z. J.; Pinnau, I.; Morisato, A. *Desalination* **2002**, *146*, 11.
195. Merkel, T. C.; He, Z.; Pinnau, I.; Freeman, B. D.; Meakin, P.; Hill, A. J. *Macromolecules* **2003**, *36*, 8406.
196. Jana, S. C.; Jain, S. *Polymer* **2001**, *42*, 6897.
197. Kang, S.; Hong, S. I.; Choe, C. R.; Park, M.; Rim, S.; Kim, J. *Polymer* **2001**, *42*, 879.
198. Wu, T. M.; Chu, M. S. *J. Appl. Polym. Sci.* **2005**, *98*, 2058.
199. Yang, X. M.; Dai, T. Y.; Lu, Y. *Polymer* **2006**, *47*, 441.
200. Savinell, R.; Yeager, E.; Tryk, D.; Landau, U.; Wainright, J.; Weng, D.; Lux, K.; Litt, M.; Rogers, C. *J. Electrochem. Soc.* **1994**, *141*, L46.

201. Samms, S. R.; Wusmus, S.; Savinell, R. F. *J. Electrochem. Soc.* **1996**, *143*, 1225.
202. Weng, D.; Wainright, J. S.; Landau, U.; Savinell, R. F. *J. Electrochem. Soc.* **1996**, *143*, 1260.
203. Helminiak, T. E.; Benner, C. L.; Gibbs, W. E. *Polym. Prepr., Am. Chem. Soc. Div. Polym. Chem.* **1970**, *11*, 291.
204. Kojima, T.; Yokota, R.; Kochi, M.; Kambe, H. *J. Polym. Sci., Part B: Polym. Phys.* **1980**, *18*, 1673.
205. Mader, J.; Xiao, L.; Schmidt, T, J.; Benicewicz, B, C. *Adv Polym Sci.* **2008**, *216*, 63.
206. Yu, S.; Benicewicz, B.C. *Macromolecules.* **2009,** *42*, 8640.
207. Mecerreyes, D.; Grande, H.; Miguel, O.; Ochoteco, E.; Marcilla, R.; Cantero, I. *Chem. Mater.* **2004**, *16*, 604.
208. Sannigrahi, A.; Arunbabu, D.; Jana, T. *Macromol. Rapid Commun.* **2006**, *27*, 1962.
209. (a) Emsley, J.; Reza, N. M.; Dawes, H. M.; Hursthouse, M. B.; Kuroda, R. *Phosphorus & Sulphur*, **1988**, *35*, 141, (b) Sannigrahi, A. *Ph.D. Thesis*; University of Hyderabad: Hyderabad, India, **2010.**
210. He, R.; Li, Q.; Xiao, G.; Bjerrum, N. J. *J. Membr Sci.* **2003**, *226*, 169.
211. Staiti, P.; Minutoli, M.; Hocevar, S. *J. Power. Sources.* **2000**, *90*, 231.
212. Staiti, P. *Mater. Lett.* **2001**, *47*, 241.
213. Javaid Zaidi, S.M. *Electrochim. Acta.* **2005**, *50*, 4771.
214. Jang, M.Y.; Yamazaki, Y. *J. Power Sources* **2005**, *139*, 2.
215. Guerra; G.; Cheo, S.; Williams, D. J.; Karasz, F. E.; Macknight, W. J. *Macromolecules* **1988**, *21*, 231.
216. Chuang, S. -W.; Hsu, S. L. -C.; Hsu, C. -L. *J. Power Sources* **2007**, *168*, 172.
217. Chuang, S. -W.; Hsu, S. L. -C.; Liu, Y. -H. *J. Membr. Sci.* **2007**, *305*, 353.
218. Suryani; Liu, Y. -L. *J. Membr. Sci.* **2009**, *332*, 121.
219. Pu, H.; Liua, L.; Changa, Z.; Yuana, J. *Electrochim. Acta* **2009**, *54*, 7536.
220. Shao, H.; Shi, Z.; Fang, J.; Yin, J. *Polymer* **2009**, *50*, 5987.

221. (a) Wang, Y.; Shi, Z.; Fang, J.; Xu, H.; Ma, X.; Yin, J. *J. Mater. Chem.* **2011**, *21*, 505, (b) Wang, Y.; Shi, Z.; Fang, J.; Yin, J. *Carbon* **2011**, *49*, 1199.

222. (a) Kannan, R.; Kagalwala, H. N.; Chaudhari, H. D.; Kharul, U. K.; Kurungot, S.; Pillai, V.K. *J. Mater. Chem.* **2011**, *21*, 7223, (b) Fijigaya, T.; Okamaoto, M.; Nakashima, N. *Carbon* **2009**, *47*, 3227, (c) Shao, H.; Shi, Z.; Fans, J.; Yin, J. *Polymer* **2009**, *50*, 5987.

223. Jaffe, M.; Chen, Paul.; Choe, E-W.; Chang, T. S.; Makhija, S. *Adv. Polym. Sci.* **1994**, *117*, 297.

224. Chang, T. S.; Herold, F. K. *Polym. Eng. Sci.* **1991**, *31*, 1950.

225. Musto, P.; Karasz, F. E., MacKnight, W. J. *Macromolecules* **1991**, *24*, 4762.

226. Chang, T. S. *Polym. Rev.* **1997**, *37*, 277.

227. Chang, T. S. *Handbook of Thermoplastics, Marcel Dekker. Inc,* **1997**, 703.

228. Wycisk, R.; Chisholm, J.; Lee, J.; Lin, J.; Pintauro, P. N. *J. Power Sources* **2006**, *163*, 9.

229. Hazarika, M.; Arunbabu, D.; Jana, T. *J. Colloid Interf. Sci.* **2010**, *351*, 374.

230. Heo, P.; Kajiyama, N.; Kobayashi, K.; Nagao, M.; Sano, M.; Hibino, T. *Electrochem. Solid State Lett.* **2008**, *11*, B91.

231. Yeager, E. *Science* **1961**, *134*, 1178.

232. Mench, M. M. *Fuel Cell Engines*; John Wiley & sons, Inc.: **2008**

233. Rikukawa, M.; Sanui, K. *Prog. Polym. Sci.* **2000**, *25*, 1463.

234. Winter, M.; Brodd, R. J. *Chem. Rev.* **2004**, *104*, 4245.

235. An article on *Fuel cells; Green Power*; Los Alamos National Laboratory: U.S.

236. *Fuel Cell Handbook*; 6 th. Ed., EG & G Technical Services, Inc.: U.S. Department of Energy, **2002**.

237. Blomen, L. J. M. J. *Fuel Cell Systems*; Plenum Press: New York, **1993**.

238. Hickner, M. A.; Ghassemi, H.; Kim, S. Y.; Einsla, B. R.; McGrath, J. E. *Chem. Rev.* **2004,** *104*, 4587.

239. Kerres, J. A. *J. Membr Sci.* **2001**, *185*, 3.

240. Li, Q.; He, R.; Jensen, J. Q.; Bjerrum, N. J. *Chem. Mater.* **2003**, *15*, 4896.

241. Roziere, J.; Jones, D. J. *Annu. Rev. Mater. Res.* **2003**, *33*, 503.

242. Smitha, B.; Sridhar, S.; Khan, A. A. *J. Membr. Sci.* **2005**, *259*, 10.
243. Maier, G.; Meier-Haack, J. *Adv. Polym. Sci*. **2008**, *216*, 1.
244. Xiao, L. *Ph.D. Thesis*; Rensselaer Polytechnic Institute: Troy, New York, **2003**.
245. Einsla, B. R. *Ph.D.Thesis*; Virginia Polytechnic: Blackburg, Virginia, **2005**.
246. Mauritz, K. A.; Moore, R. B. *Chem. Rev*. **2004,** *104*, 4535.
247. Yoshitake, M.; Watakabe, A. *Adv. Polym. Sci*. **2008**, *215*, 127.
248. Mehta, V.; Cooper, J. S. *J. Power Sources* **2003**, *114*, 32.
249. Shao, Y.; Yin, G.; Wang, Z.; Gao, Y. *J. Power Sources* **2007**,*167*, 235.
250. Gubler, L.; Scherer, G. G. *Adv. Polym. Sci.* **2008**, *215*, 1.
251. Gasa, J. V.; Weiss,R. A.; Shaw, M. T. *J. Polym. Sci., Part B: Polym. Phys.* **2006**, *44*, 2253.
252. Gilchrist, T. L. *Heterocyclic Chemistry, 3rd Edition*, **1997**.
253. Iwakura, Y.; Uno, K.; Nume, K. *US Patent*, 3741938, **1973**.
254. Arnold, F. E. *US Patent*, 495452, **1974**.
255. Reynolds, J. R.; Lee, Y.; Kim, S.; Bartling, R. L.; Gieselman, M. B.; Savage, C. S. *Polym. Prepr., Am. Chem. Soc. Div. Polym. Chem.* **1993**, *34*, 1065.
256. Litt, M.; Ameri, R.; Wang, Y.; Savinell, R.; Wainwright, J. *Mater. Res. Soc. Symp. Proc.* **1999**, *548*, 313.
257. Li, Q.; Hjuler, H. A.; Bjerrum, N. J. *J. Appl. Electrochem.* **2001**, *31*, 773.
258. Schechter, A.; Savinell, R. F. *Solid State Ionics* **2002**, *147*, 181-187.
259. Wainright, J. S.; Wang, J. T.; Savinell, R. F.; Litt, M.; Moaddel, H.; Rogers, C. *Proc. - Electrochem. Soc.* **1994**, *94-23*, 255.
260. Kreuer, K. D.; Fuchs, A.; Ise, M.; Spaeth, M.; Maier, J. *Electrochim. Acta* **1998**, *43*, 1281.
261. Susan, M. A. B. H.; Noda, A.; Mitsushima, S.; Watanabe, M. *Chem. Commun.* **2003**, 938.
262. Alberti, G.; Casciola, M.; Massinelli, L.; Bauer, B. *J. Membr. Sci.* **2001**, *185*, 73.
263. Yang, C.; Costamagna, P.; Srinivasan, S.; Benziger, J.; Bocarsly, A. B. *J. Power Sources* **2001**, *103*, 1.

264. Dippel, T.; Kreuer, K. D.; Lassegues, J. C.; Rodriguez, D. *Solid State Ionics* **2003**, *61*, 41.

265. Xing, B.; Savadogo, O. *J. New. Mater. Electrochem. Syst.* **1999**, *2*, 95.

266. Wasmus, S.; Duch, B. A.; Moaddel, H.; Rinaldi, P. L.; Litt, M. H.; Rogers, C.; Valeriu, A.; Mateescu, G. D.; Tryk, D. A.; Savinell, R. F. *The Electrochem. Soc. Extended Abstracts*, **1995,** *95-1***,** 716.

267. Glipa, X.; Bonnet, B.; Mula, B. ; Jones, D. J. ; RozieÁre, J. *J. Mater. Chem*, **1999**, *9*, 3045.

268. Kawahara, M.; Morita, J.; Rikukawa, M.; Sanui, K.; Ogata, N. *Electrochim. Acta* **2000**, *45*, 1395.

269. Bouchet, R.; Siebert, E. *Solid State Ionics* **1999**, *118*, 287.

270. Pu, H.; Meyer, W.; Wegner, G. *J. Polym. Sci., Part B: Polym. Phys.* **2002**, *40*, 663.

Chapter 2

How the Monomer Concentration of Polymerization Influences Various Properties of Polybenzimidazole: A Case Study with Poly(4,4'-diphenylether-5,5'-bibenzimidazole)

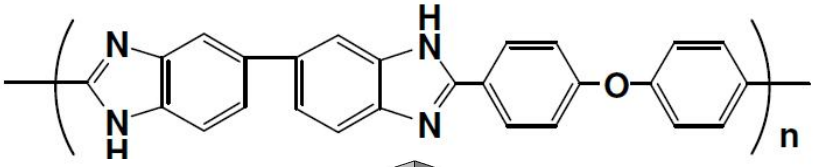

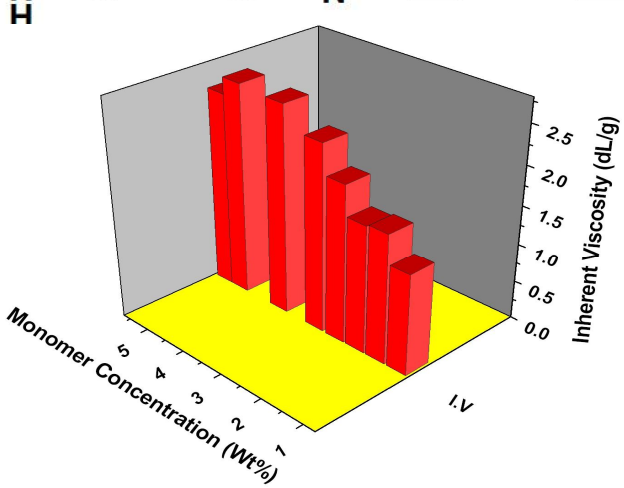

A series of poly(4,4'-diphenylether-5,5'-bibenzimidazole) an aryl ether linked polybenzimidazole (OPBI) polymers were synthesized by varying the initial monomer concentration. The effects of the initial monomer concentration on the various properties of the synthesized OPBI polymers were investigated.

2.1. Introduction

A fuel cell is an electrochemical energy conversion device for the production of efficient, environmentally friendly, and economical power supplies.[1] Polymer electrolyte membrane fuel cells are the most promising alternatives for portable power applications.[2] In recent years, much effort has been focused on developing new and low-cost polymer electrolyte membranes as substitutes for the very expensive sulfonated perfluoropolymers.[3–9] Also, many of these efforts have been focused on how to increase the operating temperature beyond 100°C, which is the main drawback of the Nafion membrane.[5,6,10] Recently, phosphoric acid (PA) doped polybenzimidazole (PBI) membranes have emerged as promising candidates for low-cost and high-performance polymer electrolyte membrane materials for high-temperature polymer electrolyte membrane fuel cells operating above 120°C.[11–15] Large numbers of high-temperature PBI polymer membranes have been synthesized, and their properties have been explored.[11,12,16–22] PBI has excellent thermochemical resistance, fire-retarding capacity, and insulating properties, and it forms good textile fibers.[16] PBI possesses both proton-donor (-NH-) and proton-acceptor (-N=) hydrogen bonding sites that exhibit specific interactions with polar solvents,[23–26] and it forms miscible blends with a variety of polymers.[27–30] PBI is used for various purposes, especially high-temperature applications, fiber spinning, reverse osmosis membranes, and fluorescence sensors for halide ions.[16,31] A variety of PBI polymers have been synthesized and reported in the literature, such as poly[2, 2'-(m-phenylene)-5, 5'-benzimidazole] (*m*-PBI), poly(2,5-benzimidazole),[32] pyridine-based PBI,[11] sulfonated PBI,[22] hyperbranched PBI,[33] fluorinated PBI,[18] and naphthalene-based PBI.[34]

PBI polymers are thermomechanically stable heterocyclic polymers, and they have potential for various industrial applications.[16] However, the major hindrance to their efficient use is their processability, and this arises from the poor solubility and infusibility of the polymers. Hence, several attempts have been carried out to improve the solubility, including incorporating a side chain into the polymer backbone and

making the polymer with flexible monomer units.[35–37] 4, 4'-Oxybis(benzoic acid) (OBA) is an example of a flexible dicarboxylic acid monomer because the two benzoic acid units in this monomer are connected by an ether linkage. Previously, the synthesis of PBI with this monomer was reported.[19,34,38] However, a detailed study of this type of PBI polymer has not been reported so far.

Polyelectrolytes are the polymer or biopolymer bearing charged or ionizable electrolyte group, which have attracted the concentration of the researchers for many years.[39] In presence of polar protic solvents polybenzimidazole also shows the polyelectrolyte nature. Due to this peculiar polyelectrolyte behavior of polybenzimidazole in polar protic solvent, it is very difficult to determine the intrinsic viscosity, which is very important parameter to enable the configuration and the conformational change of polymer in solution. Isoionic dilution method[40,41] is the very unique technique to measure the intrinsic viscosity of any polyelectrolyte.

In this study, we synthesized a series of poly(4,4'-diphenylether-5,5'-bibenzimidazole) an aryl ether linked polybenzimidazole polymers (abbreviated as OPBI troughout this thesis) by varying the initial monomer concentration [total amount of 3,3',4,4'-tetraaminobiphenyl (TAB) and OBA in poly(phosphoric acid) (PPA)] in the polymerization mixture and using PPA as a polycondensation reagent. We studied the effect of the initial monomer concentration on the various molecular properties of the synthesized OPBI polymers. The synthesized polymers were characterized by the determination of the inherent viscosity (IV) as a measurement of the polymer molecular weight, and by thermogravimetric analysis (TGA) for the thermal stability. Fourier transforms infrared (FT-IR) and proton nuclear magnetic resonance (^{1}H-NMR) spectroscopy techniques were used to establish the polymer structure. Wide-angle X-ray diffraction was carried out to determine the crystalline nature of these polymers. We studied the thermomechanical properties of polymers of various molecular weights with dynamic mechanical analysis (DMA). Finally, we studied the photophysical properties of these polymers in both solution and solid states. We have also characterized the polyelectrolyte nature of OPBI in polar protic formic acid (FA) and methanesulfonic

acid (MSA) and measured the intrinsic viscosity of the OPBI in both the solvents by isoionic dilution method.

2.2. Experimental Section

2.2.1. Materials

TAB (polymer-grade), OBA, and PPA (115%) were purchased from Aldrich. Dimethylacetamide (DMAc), formic acid (99%), Methane sulfonic acid (MSA) and sulfuric acid (98%) were purchased from Merck (India). The NMR solvent hexadeuterated dimethyl sulfoxide (DMSO-d_6) was also obtained from Merck. Lithium chloride (LiCl) was purchased from SRL, India. All the chemicals were used without further purification.

2.2.2. Polymer Synthesis

Equal molar amounts of TAB and OBA were placed in a three-necked, round-bottom flask along with PPA. The reaction mixture was stirred with a mechanical overhead stirrer, and a slow stream of purged nitrogen gas was maintained throughout the reaction. The reaction mixture was placed in an oil bath, and the temperature was controlled with a temperature controller. Typically, polymerization was carried out at 190–220°C for approximately 26 h. The reaction mixture became more viscous and developed a dark brown color at the end of the polymerization. A small amount of the reaction mixture was poured into double-distilled water and isolated as a brown mass. The mass was pulverized, neutralized with sodium bicarbonate, washed thoroughly with water, and finally dried in a vacuum oven for 24 h at 100°C to obtain dry OPBI for further characterization. The reaction scheme of OPBI synthesis is presented in Scheme 2.1(A). The initial monomer concentration (total amount of TAB and OBA in PPA) in the polymerization reaction mixture was varied by the placement of the required amounts of TAB and OBA in a fixed quantity of PPA.

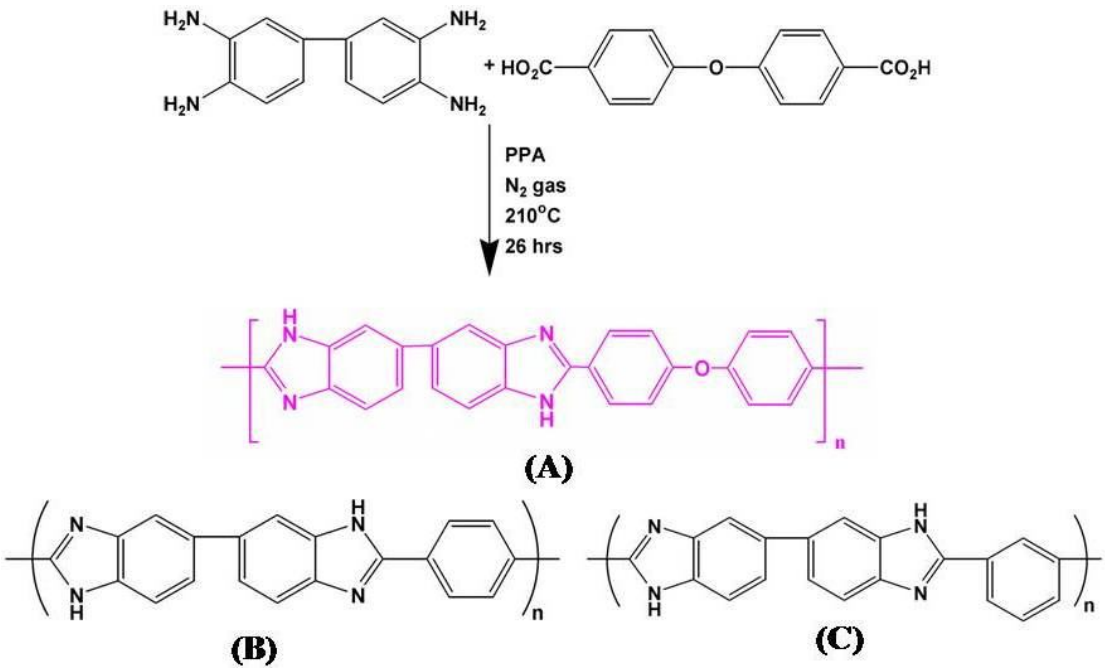

Scheme 2.1. *Synthesis of (A) poly(4,4'-diphenylether-5,5'-bibenzimidazole) (OPBI) (B) poly[2,2'-(1,4-phenylene)-5,5'-bibenzimidazole] (p-PBI), and (C) poly[2,2'-(1,3-phenylene)-5,5'-bibenzimidazole] (m-PBI).*

2.2.3. Viscosity

The viscosity of the polymers was measured in H_2SO_4 (98%) solutions at 30°C in a constant-temperature water bath with a Cannon model F725 Ubbelohde capillary dilution viscometer, and the inherent viscosity (I.V.) values were calculated from the flow time data. The concentration of the polymer solution in H_2SO_4 was 0.2 g/dL for the viscosity measurements.

The OPBI solutions in both the solvents FA and MSA of the specified concentrations were made carefully with different concentrations of LiCl. The measurements have been done in the temperature controlled viscometric water bath at

different concentrations and temperature ranges 30-70°C. The reduced viscosity is measured from the following equation (Eq. 2.1):

$$\eta_{red} = \frac{\eta_{sp}}{C} = \frac{t - t_0}{t_0}\frac{1}{C} \tag{2.1}$$

where, t and t_0 are the measured flow times of the polyelectrolyte solution and the pure solvent respectively. η_{sp}, η_{red}, and C are the specific viscosity, reduced viscosity and concentration of the solution, respectively. The intrinsic viscosity [η] is determined by plotting the reduced viscosity (dL/g) against concentration (g/dL) of the OPBI solution using the following Huggins equation[42] (Eq. 2.2) and extrapolating to OPBI concentration zero to get the intercept.

$$\frac{\eta_{sp}}{C} = \eta_{red} = [\eta] + k_H[\eta]^2 C \tag{2.2}$$

where, [η] and k_H are the intrinsic viscosity and Huggins constant, respectively.

2.2.4. Infrared (IR) and NMR Spectroscopy

The IR spectra of the OPBI films were recorded on a Nicolet 5700 FTIR spectrometer. OPBI films 30–40 μm thick were made from DMAc (2 wt %) solutions. All the NMR spectra were recorded with a Bruker AV 400-MHz NMR spectrometer at room temperature with DMSO-d_6 as an NMR solvent.

2.2.5. Thermal Study

Thermogravimetry/differential thermal analysis (TG–DTA) was carried out on a Netzsch STA 409PC TG–DTA instrument from 100 to 900°C at a scanning rate of 10°C/min in the presence of a nitrogen flow. Before the heating scan, the samples were kept isothermally at 100°C for 20 min inside the TG–DTA furnace.

2.2.6. Mechanical Property Study

The mechanical properties of the OPBI films were measured with DMA (model Q-800, TA Instruments). OPBI films obtained from DMAc solutions (2 wt %) were boiled repeatedly with distilled water for washing and finally dried in an oven at 100°C for 24 h. Films [25 mm × 5 mm × 0.05 mm (length × width × thickness)] were cut and clamped onto the film tension clamp of the precalibrated instrument. The samples were annealed at 420°C for 10 min, then kept at 100°C isothermally for 20 min inside the DMA machine, and finally scanned from 100 to 430°C at a heating rate of 4°C/min. The storage modulus (E'), loss modulus (E''), and tan δ values were measured at a constant frequency of 10 Hz and a preload force of 0.01 N.

2.2.7. X-ray Diffraction

The wide-angle X-ray diffraction patterns of the dry OPBI powders were collected in a Philips model PW 1830 powder diffraction apparatus. The powders were placed on a glass slide, and the diffractograms were recorded with nickel-filtered Cu Kα radiation at a scanning rate of 0.6°/min (2θ).

2.2.8. Photophysical Study

Electronic absorption spectra of both the solution and solid were recorded on a Varian Cary-100 Bio ultraviolet–visible spectrometer. Steady-state fluorescence emission spectra of both the solid and solution were recorded on a Jobin Yvon Horiba Fluoromax-3 spectrofluorometer. A dilute OPBI solution in DMAc was prepared, and the solution spectrum was recorded. The dilute OPBI solution in DMAc was spin-coated onto an optically transparent quartz plate, and then the spectrum was recorded from the spin-coated plate.

2.2.9. PA Doping Level

The dried membranes made from DMAc solutions were immersed into PA (85%) for 7 days and then titrated against NaOH with a Metrohm 702 autotitrator. The PA doping level was calculated as the moles of PA per OPBI repeat unit.

2.3. Results and Discussion

2.3.1. OPBI Synthesis and Molecular Weight

A series of OPBIs of various molecular weights were synthesized with TAB and OBA monomers in a PPA medium at 190–210°C. The initial monomer concentrations (total amount of TAB and OBA in PPA) in the polymerization reaction mixtures were varied from 1 to 5.5% (w/w), and this resulted in a series of OPBI polymers with different molecular weights. A plot of I.V. against the initial monomer concentration is shown in Figure 2.1. I.V. of the polymer solution is a measure of the polymer molecular weight. A higher value of I.V. indicates a higher molecular weight of the polymer.[43] The quantification of the PBI molecular weight by the measurement of I.V. in H_2SO_4 has been demonstrated in the literature extensively.[16,38] Figure 2.1 shows that I.V. increased with the initial monomer concentration increasing up to 4%, and then I.V. saturated and finally dropped at a very high initial monomer concentration (5.5%).

In a recent article, we have shown that the dicarboxylic acid architecture determines the molecular weights of PBI polymers. Para-structure dicarboxylic acid results in higher molecular weight PBI; we also demonstrated that a relatively low initial monomer concentration is required to obtain a high I.V. polymer because of its low solubility in PPA.[17] Because in OBA carboxylic acids are para-structure, we would expect to get a high-I.V. polymer with a low initial monomer concentration. However, Figure 2.1 shows the opposite: I.V. increased with the initial monomer concentration increasing. The presence of the ether linkage in the OBA molecule induced flexibility in OBA, and this resulted in the higher solubility of OBA in PPA. Therefore, more and more OBA molecules were participating in the reaction with the monomer concentration

increasing in the polymerization mixture, and high I.V. polymers were yielded. After a certain concentration such as 4% (w/w), I.V. saturated and then fell, probably because of the super-saturation of OBA molecules in PPA. Hence, from these results, it is clearly evident that the molecular weight of OPBI polymers can be easily tuned through the control of the initial monomer concentration in the polymerization mixture. Another notable observation from this result is that the solubility of dicarboxylic acid plays a vital role in the PBI polymerization, and this observation is in good agreement with our earlier results.[17]

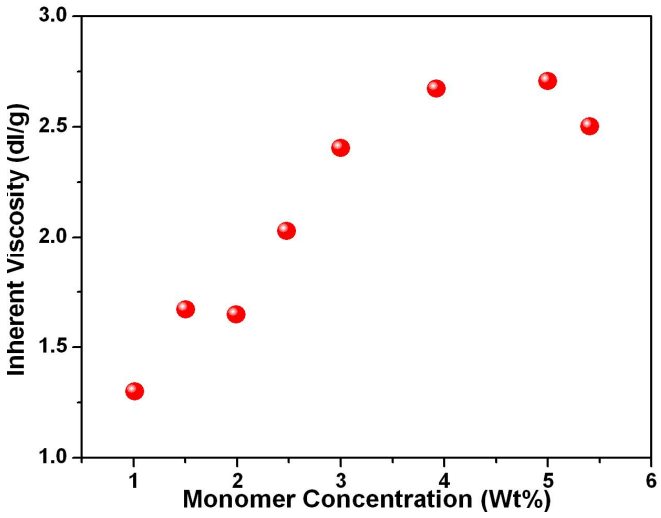

Figure 2.1. *I.V. of the OPBI polymer versus the initial monomer concentration (total amount of TAB and OBA in PPA) in the polymerization mixtures.*

2.3.2. IR and NMR Studies

FT-IR measurements of OPBI films approximately 30 µm thick were performed with an FT-IR spectrometer, and a representative spectrum is shown in Figure 2.2. The thin films of the OPBI polymers were prepared from dilute solutions of the polymers in DMAc. The films were boiled in hot water thoroughly and dried in a vacuum oven at 100°C for 2 days before the recording of the IR spectra. The absence of C-H stretching

of -CH_3 at 2940 cm^{-1} due to DMAc in Figure 2.2 proves the efficiency of the drying process. The presence of O-H stretching of H_2O at 3620 cm^{-1} in the spectrum is due to the moisture in the film absorbed during the sample handling process. FT-IR spectra of PBI polymers were widely discussed earlier by several authors.[20,30,44]

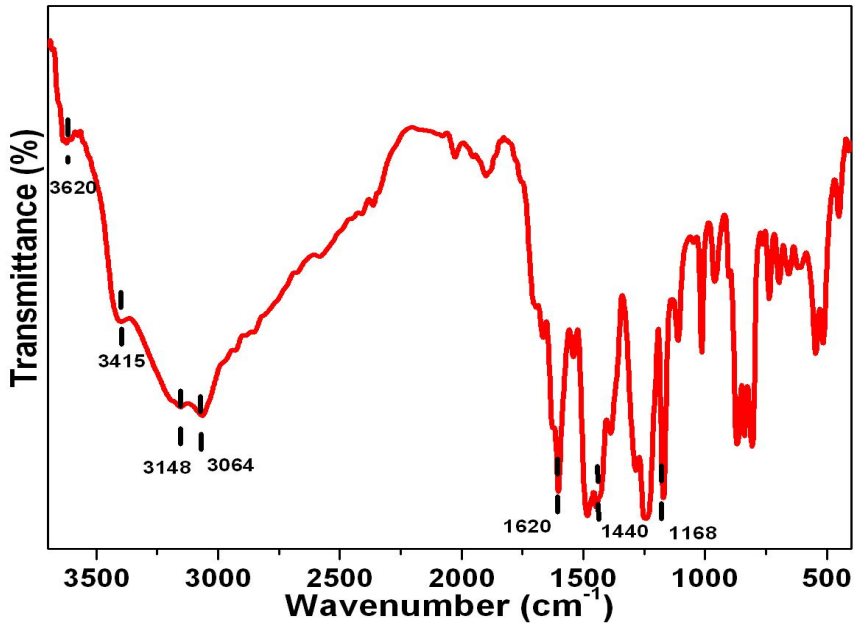

Figure 2.2. *IR spectrum of an OPBI film (thickness ~ 30 µm) made from a DMAc solution. I.V. of this OPBI polymer was 2.40 dL/g.*

The spectrum in Figure 2.2 shows similar types of bands that have been discussed earlier. The characteristic transmission band around 3415 cm^{-1} due to the N-H stretching frequency of the free -NH groups, the broad transmission at 3148 cm^{-1} due to hydrogen-bonded NH groups, and a low intense peak at 3064 cm^{-1} have been assigned to the stretching frequency of aromatic C-H groups. The C=C/C=N stretching vibration can be observed at 1620 cm^{-1}. The band around 1440 cm^{-1} belongs to the in-plane deformation of 2, 6-disubstituted benzimidazole rings. The peak at 1168 cm^{-1} has been assigned to the ether linkage of OPBI.[45] Figure 2.3 shows the IR spectra of OPBI films at various temperatures. The OPBI films were kept inside the oven at the indicated temperatures for 2 hrs, and then IR spectra were immediately recorded with the fast-

scan mode. The gradual disappearance of O-H stretching due to absorbed H_2O at 3620 cm^{-1} with increasing temperature is clearly visible in Figure 2.3. The free N-H stretching band at 3415 cm^{-1} became more intense at a higher temperature. This observation indicates that the water molecules must have hydrated the -NH moiety of the imidazole ring with some kind of weak force, such as hydrogen bonding, at a lower temperature. This possible weak force broke down as the temperature increased because the water molecules evaporated. Therefore, at a higher temperature, the -NH group stretched freely, and this resulted in an intense peak at 3415 cm^{-1}.

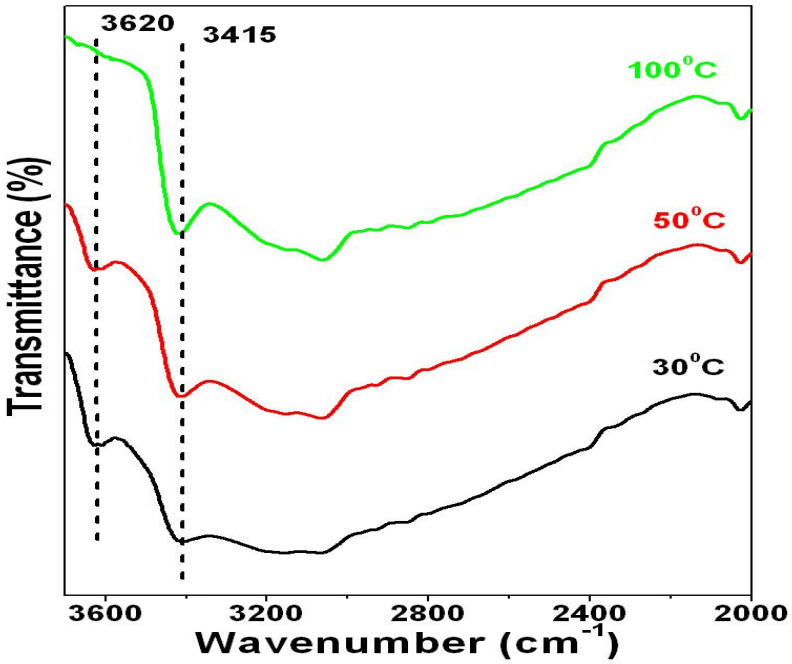

Figure 2.3. *IR spectra of an OPBI (I.V. = 2.40 dL/g) film (thickness ~ 30 µm) at various temperatures.*

Figure 2.4 shows the ^{1}H-NMR spectrum of OPBI in DMSO-d_6 along with the structure of OPBI and the peak assignment. The assigned peaks in Figure 2.4 are in good agreement with the anticipated chemical structure. The imidazole peak can be observed at 13.2 ppm, and all the aromatic protons are at 7–8.5 ppm. The large downfield shift of the imidazole proton is due to the hydrogen bonding of the -NH group with the sulfoxide group of the NMR solvent (DMSO-d_6).[25,46]

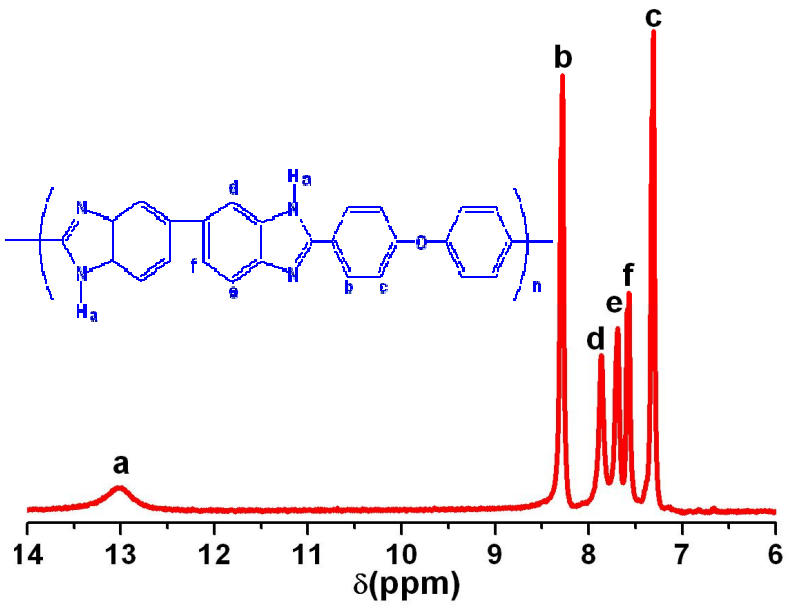

Figure 2.4. *^{1}H-NMR spectrum of OPBI (I.V. = 1.67 dL/g) in DMSO-d_6.*

2.3.3. Thermal Stability

The thermal stability of the synthesized OPBI samples was measured in TG–DTA. In all cases, we observed approximately 5% weight loss in the isothermal scan at 100°C. This first weight loss was associated with the loss of loosely bound absorbed water molecules. The samples were subjected to exhaustive drying in a vacuum oven at 100°C before the TGA and IR experiments. Despite this thorough drying process, we observed the weight loss due to absorbed water in TGA and O-H stretching for water molecules in IR (Figure 2.2). We also noticed that the O-H stretching frequency of the water molecules decreased with increasing temperature (Figure 2.3), and it vanished at 100°C. These observations show that OPBI absorbs moisture readily from the atmosphere and can even absorb moisture during the sample handling time. The TGA curves of OPBI samples of different I.V.s are shown in Figure 2.5. A distinct weight loss can be observed (Figure 2.5) around 510– 530°C for all the samples. This second weight loss was due to the degradation of the polymer backbone, which started at a

temperature greater than 510°C. Less than 10% weight loss (Table I) was observed at 510°C, and this indicated the remarkable thermal stability of the OPBI polymers. The thermal stability of the OPBI polymer increased with the molecular weight (I.V.) of the polymer increasing (Figure 2.5 and Table 2.1). Table 2.1 shows that the temperature at which the 10% weight loss was observed increased with increasing molecular weight (I.V.), and the weight loss at the final temperature (890°C) became less for the higher molecular weight polymer. The enhancement of the thermal stability for the high-I.V. polymer occurred because the bigger molecule (polymer chain) needed a higher temperature to degrade. Also, higher I.V. polymers may have crosslinking that influences the thermal stability.

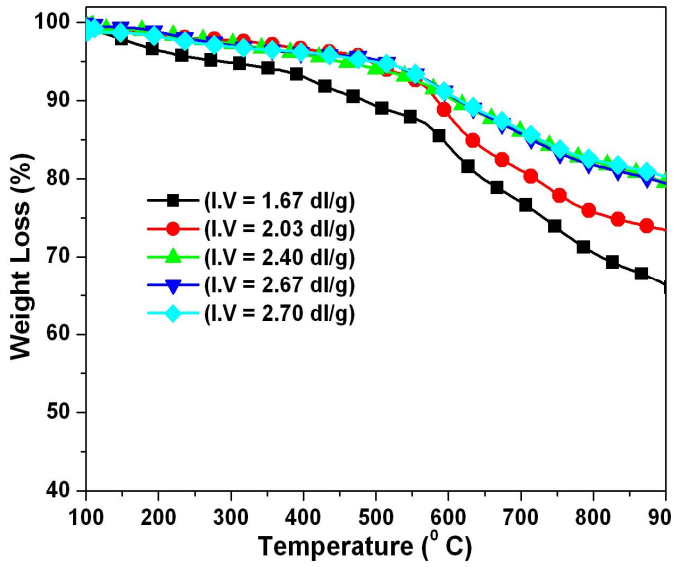

Figure 2.5. *TGA curves of OPBI polymers of various I.V.s.*

Interestingly, we have observed that the OPBI polymers were less thermally stable (Figure 2.6) than the para-structure PBI, poly[4,4'-(*p*-phenylene)-5,5'-bibenzimidazole] (*p*-PBI). The thermal stability data for p-PBI (I.V. = 2.16 dL/g) were higher (residual weight percentage at 510°C = 97.25, temperature at which 10% weight loss was observed = 709.07, residual weight percentage at 890°C = 84.09) in comparison with OPBI (I.V. = 2.03 dL/g; Table 2.1). This observation suggests that the

incorporation of an ether linkage into the polymer backbone leads to a polymer of lower thermal stability. This is due to the enhancement of the flexibility of the polymer chains from the ether linkages.

Table 2.1. *Thermal stability data for all the OPBI polymers.*

IV (dL/g)	$W_{510°C}(\%)^a$	$T_{10\%}{}^b$	$W_{890°C}(\%)^c$
1.67	88.95	484.00	66.78
2.03	94.20	584.29	73.82
2.40	93.86	609.10	79.78
2.67	95.02	614.27	79.55
2.70	94.80	619.03	80.69

[a] Residual weight percentage at 510°C.
[b] Temperature at which 10% weight loss is observed.
[c] Residual weight percentage at 890°C.

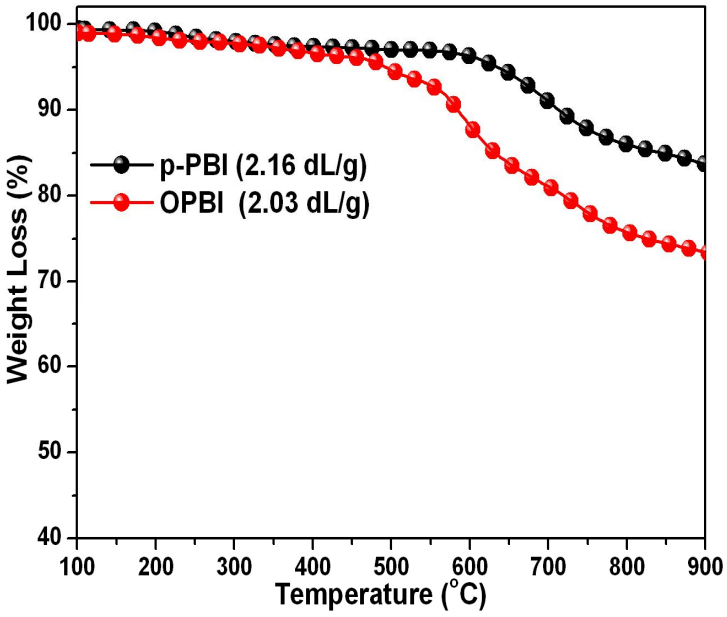

Figure 2.6. *TGA curves of OPBI (I.V. = 2.03 dL/g) and p-PBI (I.V. = 2.16 dL/g).*

2.3.4. Thermal Transitions and Mechanical Properties of OPBI

The thermal transition of a polymer from a glassy state to a rubbery state is recognized by the glass transition temperature (T_g); in other words, T_g is related to the freezing of the segmental motions of polymer chains.[47] DMA is the most reliable and efficient technique for determining T_g of PBI polymers. The T_g values of all the OPBI and p-PBI polymer samples were measured with DMA. The pre-annealing method for DMA scanning was chosen to eliminate the various unidentified, less intense transitions that arose during the first heating run with unannealed samples. Earlier studies on PBI blend system showed that the first DMA heating run results in a complicated structure because of the involvement of various processes such as removal of the residual solvent, glass transitions, and phase separation.[48] Also, it has been proved by IR and TGA studies (discussed earlier) that OPBI is very hygroscopic in nature and can easily absorb approximately 5% (by weight) moisture from the atmosphere. The absorbed moisture may affect the mechanical properties and hence T_g. Therefore, we choose the aforementioned method and could set reproducible T_g values from the DMA study. The T_g values of OPBI and p-PBI were 330–352°C and 370–382°C, respectively (Figure 2.7). The T_g values obtained from the tan δ–temperature plot were 10–20°C more than those from the E''–temperature plot. Several authors have reported similar kinds of differences in T_g measurements from E' and tan δ for various systems.[20,48,49] Hence, T_g of OPBI was 30–40°C lower than that of *p*-PBI as observed from both E'' and tan δ plots of the DMA study (Figure 2.7). OPBI (2.03 dL/g) and *p*-PBI (2.16 dL/ g) samples of similar IVs were used for the experiments. This means that the difference in T_g between OPBI and *p*-PBI is due to their structural differences. The incorporation of the ether linkage into the OPBI backbone significantly improves the bond rotation probability of the chain. This enhances the flexibility of the polymer chains and thus reduces the glass transition of OPBI in comparison with *p*-PBI.

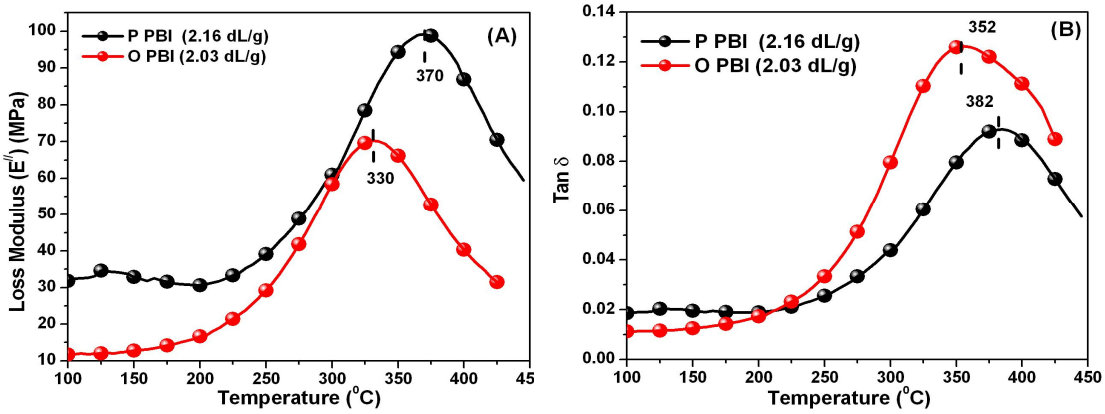

Figure 2.7. *T_g of OPBI (I.V. = 2.03 dL/g) and p-PBI (I.V. = 2.16 dL/g): (A) E'' versus temperature and (B) tan δ versus temperature (from the DMA study).*

Figure 2.8 compares *E'* values of OPBI and *p*-PBI. In both cases, it decreased slightly with increasing temperature, providing evidence for the high thermomechanical stability of the PBI polymers. From Figure 2.8, it is clear that *E'* of OPBI is always less than that of *p*-PBI, especially at high temperatures, and this suggests that OPBI has inferior mechanical properties in comparison with *p*-PBI. The enhanced flexibility of the OPBI chains due to the ether linkage could be the answer to the poor mechanical properties in comparison with *p*-PBI.

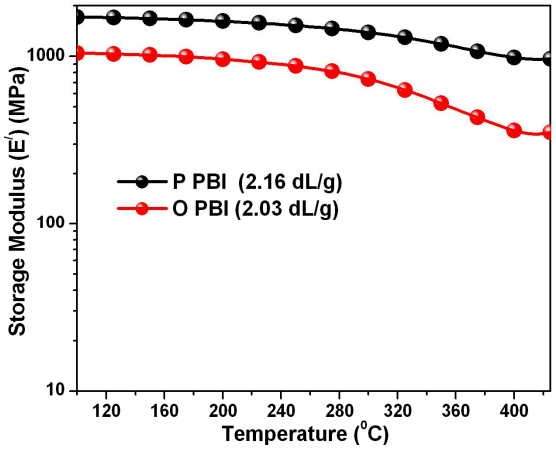

Figure 2.8. *Comparison of mechanical properties (e.g., E') of OPBI (I.V. = 2.03 dL/g) and p-PBI (I.V. = 2.16 dL/g) films made from DMAc.*

Temperature dependent plots of *E'*, *E''*, and tan δ for all the OPBI membranes are presented in Figure 2.9 (A–C). The high E' values of all the prepared membranes justify the rigid backbone of the OPBI polymers. The *E'*–temperature plot in Figure 2.9 (A) clearly indicates the presence of significant differences in the mechanical properties with the molecular weight of the polymer increasing. In all cases, *E'* decreased with increasing temperature, with a little shoulder near T_g. However, the decrease in *E'* was very low with increasing temperature. *E'* had a very high value even at 400°C [Fig. 2.9 (A)], indicating the high thermomechanical stability of the OPBI polymers. A careful analysis of Figure 2.9 (A) reveals that the mechanical property depends on the IV values of the OPBI samples. Table 2.2 compares the *E'* values of OPBI samples of various IVs at different temperature. From Figure 2.9 (A) and Table 2.2, it is clear that the bigger polymer chain (higher IV) had superior mechanical properties. The temperature at which the maximum in *E''* and tan δ plots was observed corresponded to the T_g value of the respective OPBI polymer.[47] Figure 2.9 (B,C) shows T_g values for representative OPBI samples of various IVs. T_g of the polymer is closely related to the flexibility of the polymer chains, and a high value of T_g essentially means a high barrier of bond rotations. The energy barrier of bond rotation depends not only on the type of bond but also on the supramolecular organizations of the polymer chains.[50] We observed that T_g increased with the increasing molecular weight (I.V.) of the OPBI polymer [Figure 2.9 (B,C)]. Hence, we can conclude that with the increasing molecular weight (I.V.) of OPBI polymers, the polymer chains start overlapping very easily, and this produces bigger supramolecular organization, which leads to an increase in T_g of the OPBI polymers.

Table 2.2. *Thermomechanical data for OPBI films obtained from the DMA study.*

I.V. (dL/g)	*E' (MPa) at 100°C*	*E' (MPa) at 300°C*	*E' (MPa) at 420°C*
2.03	1046.20	735.69	345.94
2.40	1100.17	855.52	530.51
2.70	1645.24	1295.57	783.43

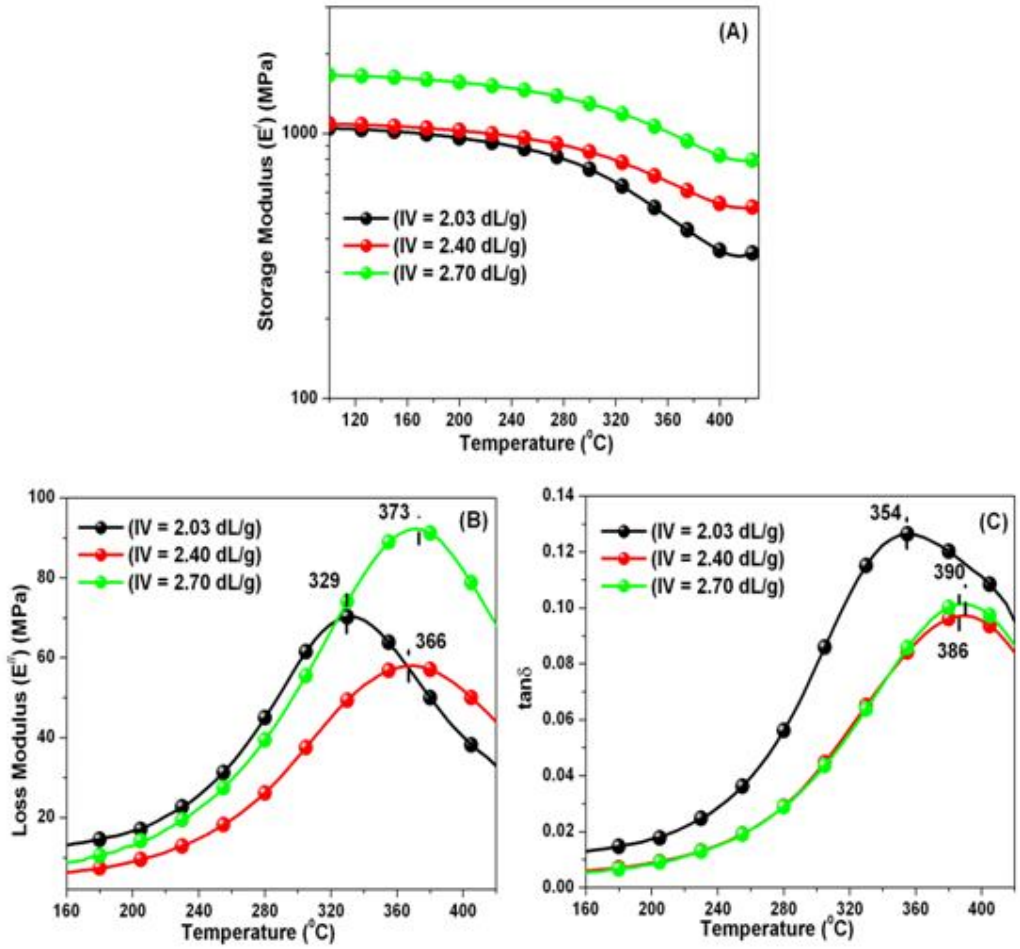

Figure 2.9. *Temperature-dependent plot of mechanical properties obtained from DMA studies of OPBI samples of different I.V.s: (A) E', (B) E'', and (C) tan δ.*

2.3.5. X-ray Diffraction

Wide-angle X-ray diffraction patterns of representative OPBI samples are presented in Figure 2.10. From the figure, it is evident that all the samples were amorphous in nature. In all cases, two broad peaks around 11.5 and 21.3° (2θ) were observed. The existence of the broad peaks resulted from a convolution of amorphous and crystalline scattering. Earlier, several authors reported similar observations for PBI type polymers.[17,34,36,51] However, no sharp peak was observed in any of the cases.

Therefore, we can conclude that the molecular weight does not influence the packing capacity of the polymer chains. All the polymers studied here were completely noncrystalline, and so we did not observe any crystalline melting. We obtained a single T_g because of the amorphous nature of the polymers.

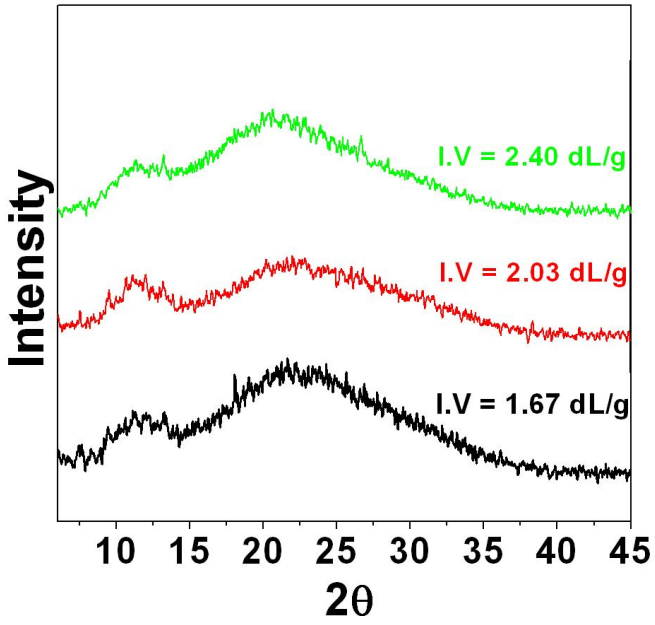

Figure 2.10. *Wide-angle X-ray diffraction patterns of OPBI samples of various I.V.s.*

2.3.6. Photophysical Studies

The absorption and fluorescence emission spectra of OPBI samples were studied from dilute solutions in DMAc and in the solid state. To our knowledge, until now no efforts have been made to study the photophysical behavior of PBI-type polymers in the solid state. The electronic absorption spectra of both the solid and solution are presented in Figure 2.11. Both spectra show two distinct peaks: a lower wavelength peak around 260 nm and higher wavelength absorption around 345 nm. The absorption maxima at ~ 345 nm correspond to the π–π^* transition peak of the PBI polymers.[17,25] The OPBI polymer showed identical absorption behavior in both the solid and solution states (Figure 2.11).

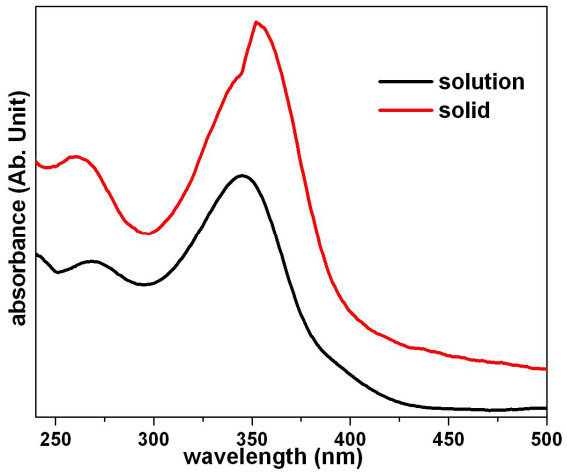

Figure 2.11. *Absorption spectra of OPBI in a DMAc solution and in the solid state.*

Figure 2.12 shows the steady-state emission spectra of OPBI in a DMAc solution and in the solid state. The excitation wavelength was chosen on the basis of the π–π^* absorption maxima (λ_{max}) in Figure 2.11. We recorded the emission spectra (Fig. 2.12) of both the DMAc solution and the solid state with exactly identical optical densities of these samples at their respective λ_{max} wavelengths. The solution spectrum in Figure 2.12 shows two closely located emission bands at 390 and 410 nm. Earlier, these peaks were assigned to the *0–0* and *0–1* transitions from the excited ^1L_b state of the benzimidazole ring of the PBI molecules.[17,23,25] The nature and shapes of OPBI in the DMAc solution spectrum are consistent with the earlier reports. The emission band of the solid spectrum is slightly red-shifted, and a single broad band can be observed. The most notable feature in Figure 2.12 is the difference in the fluorescence intensity between the solid and solution spectra. Figure 2.12 shows that the solution fluorescence was much stronger than that of the solid state. The broad emission band and weak fluorescence of the solid OPBI sample demonstrated the existence of the perturbed vibrational relaxation process in the case of the solid OPBI sample.

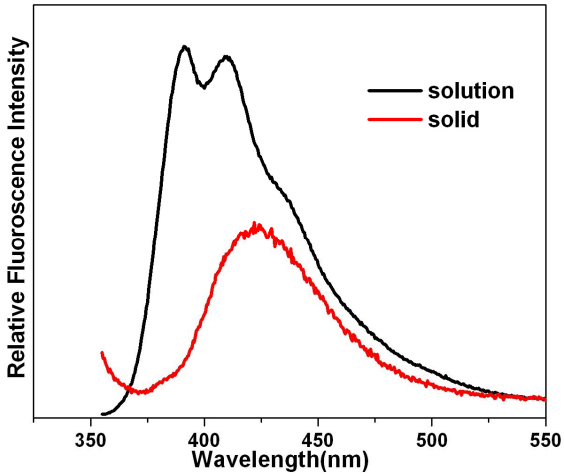

Figure 2.12. *Fluorescence emission spectra of OPBI in a DMAc solution (excitation wavelength = 345 nm) and in the solid state (excitation wavelength = 350 nm).*

2.3.7. PA Loading

The PA loading capacity of a membrane has a significant influence on the performance of the polymer electrolyte membrane fuel cell. Typically, better cell efficiency is expected with a high PA loading.[11,12] A higher acid content facilitates the transport of the protons, and this significantly improves the fuel cell efficiency.[11,12] The PA doping level of the membrane is expressed as the moles of PA per PBI repeat unit. A large number of efforts have been made to improve the PA doping level of m-PBI. Benicewicz et al.[11,12] showed that the PA doping level can be significantly increased by direct casting from the polymerization mixture in PPA. Earlier, we reported that an m-PBI membrane made from an m-PBI gel in PA showed a very high PA doping level (35–40 mol of PA per PBI repeat unit).[26] The doping level also depends on the molecular weight of OPBI.[12] However, there is no report in the literature on the PA doping level of OPBI. Therefore, we made an effort to study the effect of the molecular weight on the PA loading of OPBI membranes. We prepared an OPBI film from a DMAc solution and then washed it with hot water and kept it in a vacuum oven at 120°C for 24 h. The dried membrane was dipped in 85% PA for 7 days. After that, the PA-doped OPBI film was titrated against 0.1(*N)* NaOH solutions. The film prepared

from the DMAc solution held 4–5 mol of PA per repeat unit, and this did not depend on the I.V. of the polymer. Unfortunately, the PA loading is too low, and in the later chapters we have addressed this issue.

2.3.8. Polyelectrolyte Behavior

The reduced viscosity (η_{red}) of OPBI in both the polar protic solvents (FA and MSA), and polar aprotic solvent (DMAc) measured at different concentrations (C) and temperatures. The plots of η_{red} vs. C for all two solvents are shown in Figure 2.13 (A), (B) and (C), respectively. From the Figure 2.13 (A) and (B), it is observed that the curves move upward, giving the steady increase of reduced viscosity with dilution or decreasing the concentrations of the solution, which is the characteristic nature of polyelectrolyte solutions. On the other hand from Figure 2.13 (C), it is clear that there is no such type of anomalous behavior of OPBI in DMAc which follows the Huggins equation (Eq. 2.2). The reason behind the fact is due to the development of the ionic charges along the polyelectrolyte chains which is caused by the enhancing the dissociation of ionizable groups and hence electrostatic repulsive interactions between the ionized groups is more and more along the chains. The reduced viscosity of the polyelectrolyte is largely dependent on the environment i.e. the polarity of the solvent, the ionic strength of the polyelectrolyte solution, etc. which actually affects the electrostatic interactions between the charged species of polyelectrolyte.[52] Careful investigation of Figure 2.13 (A) and (B) demonstrate that the reduced viscosity of OPBI in FA solvent is more than that of OPBI in MSA solvent. As we have told earlier the dependency of solvent polarity plays an important role upon the reduced viscosity of the polyelectrolyte solution as well as the conformation of the polyelectrolyte chains. This is because of the ionization constant or acidity constant of MSA ($K_a = 3\times10^{2}$) is more than that of FA ($K_a = 1.77\times10^{-4}$) and also the higher dielectric constant of MSA than that of FA increases the polarity of the medium which attributes the dissociation becomes very weak along the polyelectrolyte chains. As a result, the electrostatic repulsive interactions between the ionized groups of the polyelectrolyte become decrease by allowing the coiled conformation more easily in FA whereas in MSA, the

polyelectrolyte chains take an expanded conformation due to the high electrostatic repulsive interactions between the ionized groups. Therefore, the higher ability to polarize of OPBI chains to generate huge ionic species in MSA than in FA actually restricts the steep rise in reduced viscosity with dilution.

Temperature has also an impact on the reduced viscosity and the conformation of the polyelectrolyte. The decrease of reduced viscosity of polyelectrolyte solution for a particular concentration is altering more in MSA than that of FA with increasing the temperature, shown in Figure 2.13 (A) and (B). This resembles that the conformation of the polyelectrolyte chains expand and the repulsion between the ionized groups become increases in greater extent in MSA (expanded coil to linear rod), whereas in FA, there is no such type of changing the conformation of polyelectrolyte chains with increasing the temperature.

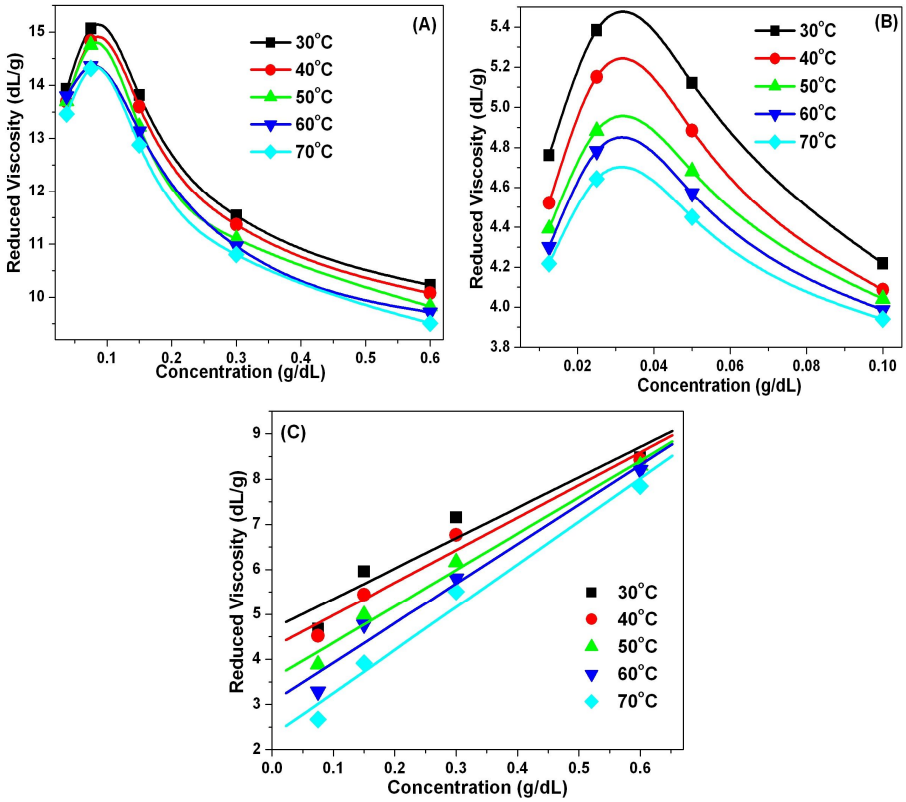

Figure 2.13. *Reduced viscosity vs. concentration plot of OPBI in (A) FA, (B) MSA and (C) DMAc at the indicated temperatures.*

Now the question arises how the polyelectrolyte solution of OPBI in both the protic polar solvent (FA and MSA) could be diluted to generate such type of performance or behavior that is usually observed for non-electrolytic nature of OPBI in DMAc. We have used isoionic dilution technique for the above. This type dilution technique usually has been done by keeping the effective ionic strength of polyelectrolyte solution constant.[40,41] The main idea of this dilution technique is to restrict the continuous change of conformation of the polyelectrolyte in solution through counter ion binding and this counter ion binding has to be kept constant for each dilution of the polyelectrolyte solution which actually helps to measure the intrinsic viscosity of the polyelectrolyte. We have carried out the isoionic dilution of OPBI solutions in both the solvents (FA and MSA) with four different ionic strengths (6×10^{-3} and 3×10^{-3} mol/L for FA and 2×10^{-3} and 10^{-3} mol/L for MSA) by using the LiCl salt at various temperature ranges (30 to 70°C). The dependency of polyelectrolyte concentrations upon the reduced viscosity by using the isoionic dilution in both the solvents (FA and MSA) of different ionic strength of LiCl are shown in Figure 2.14. From the Figure 2.14, it is observed that the reduced viscosity, obtained from isoionic dilution method, has a dependence upon concentrations of polyelectrolyte and is well fitted linearly which actually obeys the Huggins equation[42] (Eq. 2.2) and behaves like a non-electrolyte polymer. Figure 2.14 clearly demonstrates that there is a huge dependency of effective ionic strength of the solution, temperature of the medium, polarity of the solvent upon the intrinsic viscosity and Huggins constant which actually explains the frequent change of the conformation of the polyelectrolyte chains with temperature and solvent polarity (or dielectric constant).

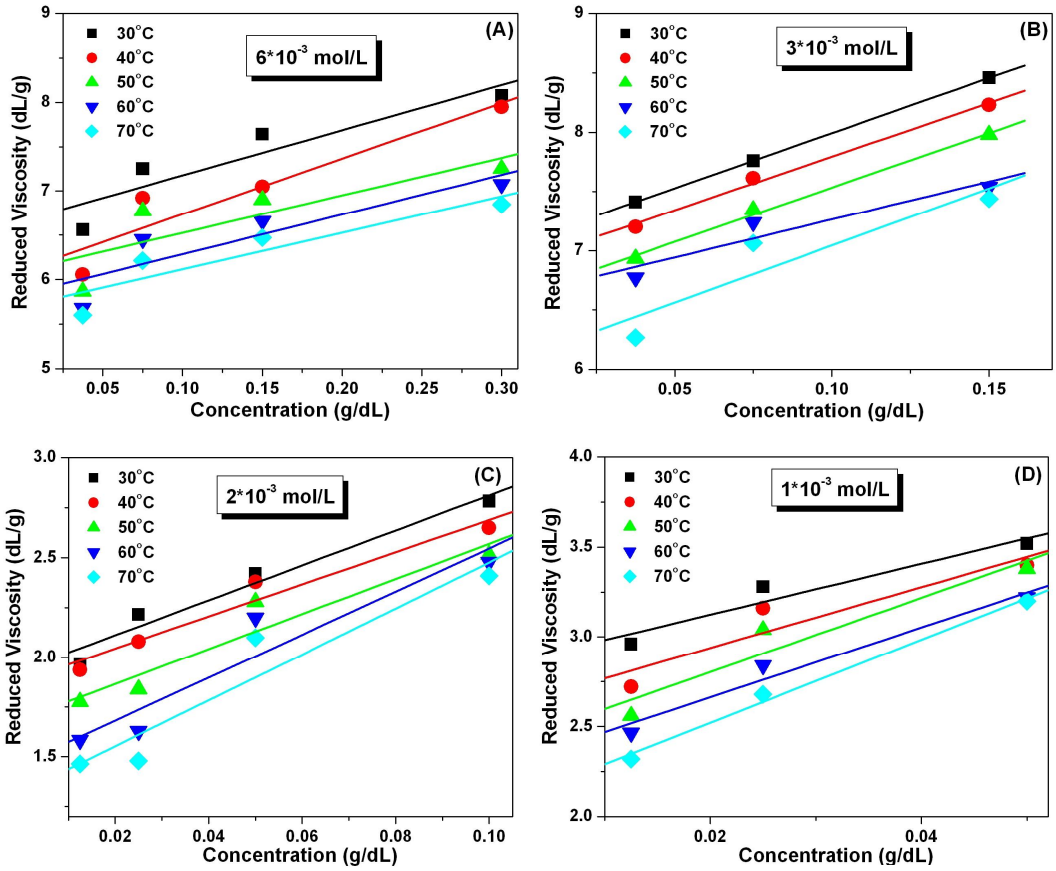

Figure 2.14. *Reduced Viscosity vs. concentration plot, measured by isoionic dilution method of OPBI in both the protic polar solvent with different ionic strength of LiCl (A) FA (6×10^{-3} mol/L), (B) FA (3×10^{-3} mol/L), (C) MSA (2×10^{-3} mol/L) and (D) MSA (1×10^{-3} mol/L) at the indicated temperatures.*

Table 2.3. *Intrinsic viscosities [η] (dL/g) of OPBI in FA and MSA at the indicated ionic strengths and temperatures.*

	Intrinsic Viscosity (dL/g)			
	Formic acid (FA)		**Methanesulfonic acid (MSA)**	
	6×10^{-3} *mol/L*	3×10^{-3} *mol/L*	2×10^{-3} *mol/L*	1×10^{-3} *mol/L*
30°C	6.66	7.06	1.94	2.84
40°C	6.11	6.89	1.88	2.6
50°C	6.10	6.62	1.69	2.39
60°C	5.84	6.62	1.47	2.27
70°C	5.70	6.08	1.32	2.06

It is observed from Figure 2.14 and Table 2.3 that, the intrinsic viscosity of the polyelectrolyte in formic acid is more than that of methanesulfonic acid at the entire temperature region. As we know that the intrinsic viscosity is directly proportional with the hydrodynamic volume of the polymer in solution.[53] Therefore, higher value of intrinsic viscosity corresponds to the end to end distance of a polyelectrolyte chain or the effective persistence length of the chain is more which suggests the higher intramolecular electrostatic repulsion of the individual coil of the polyelectrolyte chains rather than that of methanesulfonic acid. Also with increasing the ionic strength of the solution, the concentrations of the counter ions is increasing as well as the degree of counter ion binding of the polyelectrolyte chains are enhancing considerably which restricts the continuous change of the conformation of polyelectrolyte chain and decreases the intrinsic viscosity of the polyions. This is because of the lowering down of repulsive forces between ionized groups along the polymer chains. Therefore, the effective hydrodynamic volume of the polymer molecules decreases which leads to lower electrostatic interactions between ionized groups of polymer chains and the

couterions by allowing the chains more and more in coiled conformation. This influences the decrease of the intrinsic viscosity of the polyelectrolyte.

2.4. Conclusions

We synthesized and characterized a series of OPBIs consisting of an ether linkage in the polymer backbone by changing the initial monomer concentration in the polymerization reaction mixture. Higher molecular weight polymers were obtained from a higher initial monomer concentration in the polymerization reaction mixture. The thermal stability of the dry polymer powders increased with the molecular weight (IV) of the polymer increasing. The incorporation of an ether linkage into the polymer backbone enhanced the flexibility of the backbone, which influenced the various thermal and thermomechanical properties of this type of PBI (OPBI) in comparison with other PBIs. The OPBI polymer membranes showed excellent thermomechanical stability. T_g increased with increasing molecular weight (IV). All the OPBI polymers synthesized here were completely amorphous in nature. Photophysical studies were carried out both in DMAc solutions and in the solid state. In summary, we conclude that the molecular weight, thermal stability, T_g, and other thermomechanical properties of OPBI polymers can be efficiently controlled by the variation of the initial monomer concentration in the polymerization mixture. We have also characterized the polyelectrolyte nature of OPBI in polar protic formic acid (FA) and methanesulfonic acid (MSA) and the polyelectrolyte (OPBI) solution in both the protic polar solvents (FA and MSA) behaved like non-electrolyte by using isoionic dilution method in presence of LiCl salt.

References

1. *Fuel Cell Handbook, 6th ed.*; EG&G Technical Services: Gaithersburg, MD, **2002**.
2. Blomen, L. J. M. J. *Fuel Cell Systems*; Plenum: New York, **1993**.
3. Hickner, M. A.; Ghassemi, H.; Kim, S. Y.; Einsla, B. R.; McGrath, J. E. *Chem. Rev*. **2004**, *104*, 4587.
4. Kerres, J. *J. Membr. Sci.* **2001**, *185*, 3.
5. Gottesfeld, S.; Pafford, J. *J. Electrochem. Soc*. **1998**, *135*, 2651.
6. Yang, C.; Costamagna, P.; Srinivasan, S.; Benziger, J.; Bocarsly, A. B. *J. Power Sources* **2001**, *103*, 1.
7. Savadogo, O. *J. New Mater. Electrochem. Syst*. **1998**, *1*, 47.
8. Roziere, J.; Jones, D. *J. Annu. Rev. Mater. Res.* **2003**, *33*, 503.
9. Saxena, A.; Tripathi, B. P.; Shahi, V. K. *J. Phys. Chem. B* **2007**, *111*, 12454.
10. Cho, C. G.; Kim, Y. S.; Yu, X.; Hill, M.; McGrath, J. E. *J. Polym. Sci., Part A: Polym. Chem*. **2006**, *44*, 6007.
11. Xiao, L.; Zhang, H.; Jana, T.; Scanlon, E.; Chen, R.; Choe, E. W.; Ramanathan, L. S.; Yu, S.; Benicewicz, B. C. *Fuel Cells* **2005**, *5*, 287.
12. Xiao, L.; Zhang, H.; Scanlon, E.; Ramanathan, L. S.; Choe, E. W.; Rogers, D.; Apple, T.; Benicewicz, B. C. *Chem. Mater.* **2005**, *17*, 5328.
13. Savinell, R.; Yeager, E.; Tryk, D.; Landau, U.; Wainright, J.; Weng, D.; Lux, K.; Litt, M.; Rogers, C. *J. Electrochem. Soc.* **1994**, *141*, L46.
14. Samms, S. R.; Wsmus, S.; Savinell, R. F. *J. Electrochem. Soc.* **1996**, *143*, 1225.
15. Weng, D.; Wainright, J. S.; Landau, U.; Savinell, R. F. *J. Electrochem. Soc.* **1996**, *143*, 1260.
16. Choe, E. W.; Choe, D. D. *In Polymeric Materials Encyclopedia*; Salamone, J. C. CRC: New York, **1996**.
17. Sannigrahi, A.; Arunbabu, D.; Sankar, R. M.; Jana, T. *J. Phys. Chem. B* **2007**, *111*, 12124.

18. Chuang, S. W.; Hsu, S. L. C. *J .Polym. Sci., Part A: Polym. Chem.* **2006**, *44*, 4508.
19. Xu, H.; Chen, K.; Guo, X.; Fang, J. *Polymer* **2007**, *48*, 5541.
20. Qing, S.; Huang, W.; Yan, D. *Euro. Poly. J.* **2005**, *41*, 1589.
21. Osaheni, J. A.; Jenekhe, S. A. *Macromolecules* **1995**, *28*, 1172.
22. Jouanneau, J.; Mercier, R.; Gonon, L.; Gebel, G. *Macromolecules* **2007**, *40*, 983.
23. Kojima, T. *J. Polym. Sci., Polym. Phys. Ed.* **1980**, *18*, 1685.
24. Shogbon, C. B.; Brousseau, J. L.; Zhang, H.; Benicewicz, B. C.; Akpalu, Y. *Macromolecules* **2006**, *39*, 9409.
25. Sannigrahi, A.; Arunbabu, D.; Sankar, R. M.; Jana, T. *Macromolecules* **2007**, *40*, 2844.
26. Sannigrahi, A.; Arunbabu, D.; Jana, T. *Macromol. Rapid Commun.* **2006**, *27*, 1962.
27. Musto, P.; Karasz, F. E.; MacKnight, W. J. *Macromolecules* **1991**, *24*, 4762.
28. Deimede, V.; Voyiatzis, G. A.; Kallitsis, J. K.; Qingfeng, L.; Bjerrum, N. J. *Macromolecules* **2000**, *33*, 7609.
29. Wang, Y.; Goh, S. H.; Chung, T. S. *Polymer* **2007**, *48*, 2901.
30. Musto, P.; Karasz, F. E.; MacKnight, W. J. *Polymer* **1993**, *34*, 2934.
31. Yang, N. C.; Sang, M. L.; Suh, D. H. *Polym. Bull.* **2003**, *49*, 371.
32. Asensio, J. N.; Borrós, S.; Gómez- Romero, P. *J. Electrochem. Soc.* **2004**, *151*, A304.
33. Li, Z. X.; Liu, J. H.; Yang, S. Y.; Huang, S. H.; Lu, J. D.; Pu, J. L. *J. Polym. Sci., Part A: Polym. Chem.* **2006**, *44*, 5729.
34. Chen, C. C.; Wang, L. F.; Wang, J. J.; Hsu, T. C.; Chen, C. F. *J. Mater. Sci.* **2002**, *37*, 4109.
35. Pu, H.; Liu, Q.; Liu, G. *J. Membr. Sci.* **2004**, *241*, 169.
36. Scariah, K. J.; Krishnamurthy, V. N.; Rao, K. V. C.; Srinivasan, M. *J. Polym. Sci., Part A: Polym. Chem.* **1987**, *25*, 2675.
37. Persson, J. C.; Jannasch, P. *Chem. Mater.* **2006**, *18*, 3096.
38. Neuse, E. W. *Adv. Polym. Sci.* **1982**, *47*, 1.

39. Dobrynin, A. V. *Curr. Opini. Colloid. Inter. Sci.* **2008**, *13*, 376.
40. Pals, D. T. E.; Hermans, J. J. J Polym Sci 1950, 5, 773.
41. Pals, D. T. E.; Hermans, J. J. Rec Trav Chim Pays-Bas 1952, 71, 458.
42. Huggins, M. L. *J. Am. Chem. Soc.* **1942**, *64*, 2716
43. Sun, S. F. *Physical Chemistry of Macromolecules: Basic Principles and Issues*; John Wiley & sons, Inc.: New York **1994**.
44. Lobato, J.; Cañizares, P.; Rodrigo, M. A.; Linares, J. J.; Manjavacas, G. *J. Membr. Sci.* **2006**, *280*, 351.
45. Silverstein, R. M.; Webster, F. X. *Spectroscopic Identification of Organic compounds*; John Wiley & Sons, Inc.: New York **2002**.
46. Kojima, T. *J. Polym. Sci., Polym. Phys. Ed.* **1980**, *18*, 1673.
47. Sperling, L. H. *Introduction to Physical Polymer Science*; John Wiley & Sons, Inc.: New York **1992**.
48. Liang, K.; Bánhegyi, G.; Karasz, F. E.; MacKnight, W. J. *J. Polym. Sci., Part B: Polym. Phys.* **1991**, *29*, 649.
49. Manna, S.; Batabyal, S. K.; Nandi, A. K. *J. Phys. Chem. B* **2006**, *110*, 12318.
50. Fernández-Blázquez, J. P.; Bello, A.; Pérez, E. *Polymer* **2005**, *46*, 10004.
51. Kumbharkar, S. C.; Karadkar, P. B.; Kharul, U. K. *J. Membr. Sci.* **2006**, *286*, 161.
52. Alfrey, T.; Bartovics, A.; Mark, H. *J. Am. Chem. Soc.* **1942**, *64*, 1557.
53. Weill, G.; Des Cloiseaux, J. *J. Phys. (Paris)* **1979**, *40*, 99.

Chapter 3

Role of Solvent Protic Character on the Aggregation Behavior of Aryl Ether LinkedPolybenzimidazole in Solution

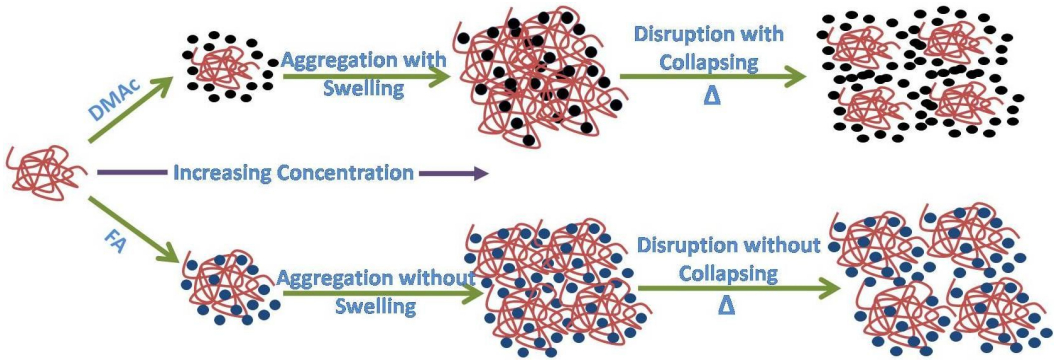

The effects of solvents protic character on aggregation behavior of the poly(4,4′-diphenylether-5,5′-bibenzimidazole), an aryl ether linked polybenzimidazole (OPBI) were studied. The nature of conformational change during the aggregation process was monitored.

3.1. Introduction

Molecular aggregation of polymers and biopolymers in solution represents an important phenomenon in material science and molecular biology. These macromolecules have capabilities to form self-organized structures by interacting with each other in solution and solid state. The self-organization of the macromolecules is predominantly driven by inter- and intramolecular interactions such as hydrogen bonding, electrostatic, van der Waals, and hydrophobic interactions.[1-3] All of these driving forces for the self-organization processes are noncovalent type interactions, and hence, these processes become reversible in nature with concentration, temperature, etc.[4] The molecular aggregated structures of macromolecules created from the self-organization process display very fascinating molecular properties, and these properties can be altered as per the desire by tuning the nature and extent of the self-organization process. Self-organizing systems are widely represented in nature, such as double-helical structures of nucleic acids and bi-layers of lipids within the cell membranes.[5-7] There are plenty of investigations reported in the literature on the molecular aggregation of the synthetic polymers.[5,6,8-11] However, most of these reports were focused on vinyl polymers, polypeptides, and other simple structure polymers.[5,6,8-11] MacKnight et al. have demonstrated and studied extensively the polymer chain conformation, conformational transition due to self-organization in the case of polyelectrolyte-surfactant complexes in the solution.[12] The aggregation of synthetic polymers in solutions, polyelectrolyte/surfactant complexes were also studied extensively by Guenet and co-workers.[13] A very limited number of efforts have been attempted in recent years to study the aggregation behavior of the polymers in solution with highly complex molecular structure.[14-17] Very recently, we have carried out a systematic study on the aggregation behavior of meta structured polybenzimidazole (*m*-PBI) [Scheme 3.1 (A)] in polar aprotic solvent, dimethyl acetamide (DMAc).[14] Our group has demonstrated that the polybenzimidazole (*m*-PBI) chains undergo a coil to rod like conformational transition in solution with increasing concentration due to the molecular aggregation driven by the self-organization process. The degree of molecular aggregation is strongly

dependent upon the molecular orientations of the polymer chains as well as the nature of the solvent.[18,19] Very few attempts have been made in the literature to study the effect of solvents on the aggregation behavior of the macromolecules, and those are mostly with vinyl polymers such as polyvinyl alcohol, etc.[18] However, as per our knowledge, there have been no attempts in the literature to date for heterocyclic polymers, such as polybenzimidazole. Hence, it becomes absolutely necessary to study the effects of solvents on the aggregation behavior of the polybenzimidazole. Polybenzimidazole [*m*-PBI, Scheme 3.1 (A)], known as Celazole, is an aromatic heterocyclic polymer which is resistant to strong acids, bases, a variety of chemicals, and high temperatures. Due to these unique properties, PBI is being used in numerous areas, especially in high temperature applications, reverse osmosis membranes, fire-resistant materials, ultrafilters, and other types of separatory media.[20] PBI possesses both proton donor (-NH-) and acceptor (-N=) hydrogen bonding sites which favor the formation of the miscible blends[21-23] with a variety of polymers and also exhibit specific interaction with both protic and aprotic polar solvents.[16,24,25] Phosphoric acid (PA) doped PBI membrane is a promising candidate to prepare cheap and high performance polymer electrolyte membrane materials for polymer electrolyte membrane fuel cells (PEMFCs).[26-29] Several methods have been developed for the fabrication of PA doped PBI membranes.[25,27-31] The superiorities of the membranes obtained from many of these methods relied on the interactions of PBI chains with the solvent molecules in which the PBI molecules are dissolved.[25,31] Earlier, we had demonstrated that PBI chains form aggregated structure in the DMAc solution with increasing concentrations and we have observed a conformational transition during the aggregation process.[14] This above study helped us to design and develop the thermoreversible gel of PBI in PA from where we could fabricate PBI membrane with very high PA loading.[25] Our goal of this chapter is to study the aggregation behavior of poly(4,4′-diphenylether- 5,5′-bibenzimidazole), an aryl ether linked polybenzimidazole (abbreviated as OPBI throughout the thesis) [Scheme 3.1 (B)] in polar protic formic acid (FA) and polar aprotic N,N-dimethyl acetamide (DMAc) solvents. For the current study, we have chosen OPBI [Scheme 3.1 (B)] instead of *m*-PBI [Scheme 3.1 (A)] due to the flexible nature of the OPBI arising

for the ether linkage in the OPBI polymer backbone.[32,33] OPBI has very good solubility in both polar protic and aprotic solvents such as FA, DMAc, etc. In this chapter, we wish to study the effect of solvents on the OPBI aggregation behavior and also want to explore the possible outcome due to the flexible nature of OPBI on the aggregation. This study may give us a clue to prepare a superior quality of OPBI membrane in protic solvent.

Photophysical studies of polymers have been utilized as a potential approach for the exploration of inter- and intramolecular interactions and molecular motions of the polymer chains and their aggregations.[9,11,16,17,19,34-41] These photophysical studies showed that most of the vinylic polymers bearing aromatic side groups such as styrene, vinylnaphthalene, vinylanthracene, N-vinylcarbazole, vinylpyrene, and their copolymers form interand intramolecular excimers and exciplexes.[38-42] These excimers and exciplexes were used as a degree of molecular interactions. Huang et al. reported that polyquinolines form excimers in acidic solution, resulting in concentration quenching, and showed that excimer formation is forbidden by intermolecular repulsion between the polymer chains.[17] Recently, it has been reported that side chain urethane methacrylate polymer having pendent pyrene units on each side chain form intramolecular excimers in dilute THF solution and form stable intermolecular aggregated structures at higher concentration.[11] Earlier, molecular aggregation of OPBI in DMAc solution due to the overlapping of polymer chains was studied by Kojima et al.[16] However, Kojima could not predict aggregation in FA medium. Hence, there is a lack of enough thorough investigation in the literature on the aggregation behavior of OPBI in different solvents. This detailed study perhaps can guide us about the chain conformation and the nature of OPBI aggregation in various solvents. Therefore, the current study becomes absolutely necessary for the future development of PBI chemistry. In this chapter, we have studied the intra- and intermolecular interactions of dilute OPBI in DMAc and FA solutions by using steady-state and time-resolved fluorescence spectroscopy, viscosity at different temperatures. Also, transmission electron microscopy (TEM) and circular dichroism spectroscopy are employed to

understand the morphological and conformational changes of the OPBI chains in solutions.

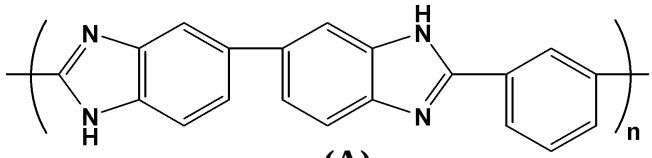

(A)

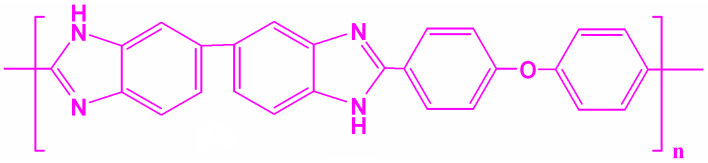

(B)

Scheme 3.1. *(A) Poly(2,2′-(m-phenylene)-5,5′-bibenzimidazole); called as m-PBI and (B) Poly(4,4′- diphenylether-5,5′-bibenzimidazole); called as OPBI.*

3.2. Experimental Section

3.2.1. Materials

3, 3', 4, 4'-tetraaminobiphenyl (TAB, polymer grade), 4, 4'-oxybis(benzoic acid) (OBA), and polyphosphoric acid (PPA, 115%) were purchased from Sigma-Aldrich. Dimethyl acetamide (DMAc) and formic acid (99%) were purchased from Qualigens and SRL India, respectively. All chemicals were used as received.

3.2.2. OPBI Synthesis

The synthesis of OPBI was carried out as per our method reported previously.[33] Briefly, equal moles of TAB and OBA were taken into a three-neck round-bottom flask along with polyphosphoric acid (PPA). The reaction mixture was stirred by using a mechanical overhead stirrer, and a slow stream of purged nitrogen gas was maintained throughout the reaction. The polymerization was carried out at 190-220°C for approximately 26 hrs. The OPBI polymer was isolated, neutralized with sodium bicarbonate, washed thoroughly with water, and finally dried in a vacuum oven for 48

hrs at 100°C. The dried polymer was characterized by measuring the viscosity in concentrated sulfuric acid (98%) by using a Cannon Ubbelohde capillary dilution viscometer (model F725). The synthesized OPBI has an inherent viscosity (IV) value of 2.29 dL/g at 30°C. The concentration of the polymer solution for the viscosity measurement was 0.2 g/dL. The intrinsic viscosity ([η]) of the synthesized OPBI was obtained by using the Kuwahra[43] single point method with the help of the following equation

$$[\eta] = \frac{\eta_{sp} + 3\ln \eta_{rel}}{4C} \tag{3.1}$$

where η_{sp} and η_{rel} are the specific and relative viscosity of the polymer solution, respectively, and C is the concentration of polymer in g/dL. The calculated intrinsic viscosity for the synthesized OPBI sample using eq. 3.1 was 2.50 dL/g at 30°C. The viscosity average molecular weight ($\overline{M_v}$) was obtained by using the Mark-Houwnik equation, $[\eta] = K\overline{M_v}^{a}$, where K = 5.2 × 10^{-5} dL/g and a = 0.92 for H_2SO_4 (98%) solvent at 27°C.[44] The ($\overline{M_v}$) obtained for the OPBI using the above constants is 21091.

3.2.3. Dilute Solution Viscometry (DSV)

A Cannon Ubbelohde capillary dilution viscometer (model F725) was used to measure the viscosity of OPBI solutions in DMAc and FA. The measurement was carried out at various temperatures (303-343 K) by immersing the viscometer into a temperature controlled water bath. Stock solutions of OPBI were prepared in DMAc and FA. These stock solutions were filtered through the 0.25 μm PTFE filter membrane to remove any microgels or large contaminants. Final solutions were made by the appropriate dilution of the stock solutions with filtered solvent. Flow time readings were recorded at least three times until the difference between two readings was found to be within 0.5 s. The Huggins equation (3.2) was utilized to analyze the viscosity data.

$$\frac{t - t_0}{C} = \frac{\eta_{sp}}{C} = \eta_{red} = [\eta] + k_H[\eta]^2 C \tag{3.2}$$

where t and t_0 are the flow time of the polymer solution and solvent, respectively, C is the concentration of polymer in g/dL, η_{sp}, η_{red}, and [η] are the specific, reduced, and intrinsic viscosities of the polymer solution, respectively, and k_H is the Huggins constant. In the case of FA solution, ηred increases with decreasing solution concentration, indicating that the OPBI behaves as a polyelectrolyte in FA solvent.[45] Therefore, the Huggins equation could not be applied to obtain k_H and [η]. We have utilized the isoionic dilution method to obtain [η] and k_H for OPBI in FA.[46] We have used LiBr as a salt for the isoionic dilution method.

3.2.4. Spectroscopy

Electronic absorption spectra were recorded on a UV-visible spectrophotometer (model, Cary-100Bio; make, VARIAN). Steady-state fluorescence emission spectra were recorded on a Jobin Yvon Horiba spectrofluorimeter (model Fluoromax-4). A Peltier temperature controller (model LFI-3751) was used for temperature dependent study. Time resolved fluorescence measurements were carried out using a time-correlated single-photon counting (TCSPC) spectrophotometer (IBH Nano LED). A diode laser (λ_{exc} = 374 nm) was used as the excitation source, and the instrument response time was 75 ps (fwhm). The emission was detected at a right angle to the excitation beam using a Hamamatsu 323P MCP photomultiplier. A dilute solution of Ludox in water was used to record the lamp profile. The decay curves were analyzed by nonlinear least-squares iteration using IBH DAS6 (version 2.2) decay analysis software. The circular dichroism (CD) spectra of polymer solutions were recorded on a spectropolarimeter (Jasco-810) at 30 °C using a 2 mm quartz cuvette.

3.2.5. Microscopy

A transmission electron microscope (TEM, FEI Tecnai Model No. 2083) operating at 120 kV was used to study the morphological features of the OPBI samples prepared from the various solution concentrations in both DMAc and FA solvents. The TEM samples were prepared by dropping the appropriate concentrated solutions in a carbon coated copper (200 mesh) grid and then scanned for imaging in TEM.

3.3. Results and Discussion

3.3.1. Absorption Spectroscopy

The absorption spectra of OPBI [Scheme 3.1 (B)] solutions in two different solvents, namely, dimethyl acetamide (DMAc, polar aprotic solvent) and formic acid (FA, polar protic solvent), are studied. OPBI solutions of two different concentrations (0.2 g/dL or 5×10^{-3} M and 2×10^{-3} g/dL or 5×10^{-5} M) in both of the solvents are prepared, and their absorption spectra are presented in Figure 3.1. The OPBI concentrations in molar concentration units are calculated by considering one repeat unit molecular weight as 1 mol of OPBI. In both of the solvent systems, the absorption bands (λ_{max}) of the OPBI dilute solutions owing to the π-π^* transitions of the imidazole moiety are observed at 345 nm. Therefore, it is noted that the λ_{max} value for the π-π^* transition does not differ for the two solvents used in this study. This observation is in agreement with the previous reports.[47,48] However, the longer wavelength absorption band (low energy band) due to the n-π^* transition of the imidazole ring depends on the solvents (Figure 3.1). In the case of DMAc solution (0.2 g/dL), the n-π^* transition is observed at 440 nm, whereas the same transition band appears as dual bands at 424 and 482 nm in the case of FA solution (0.2 g/dL). The reason for this solvent dependence is because of the fact that the FA is a protic solvent which consumes the nonbonding electron available in the nitrogen atoms of the imidazole rings present in the OPBI polymer backbone and yielding an imidazolium cationic species. Hence, in FA medium, the nature of the n-π^* transition is significantly different from the DMAc medium. It must be noted that all of the OPBI spectra presented in Figure 3.1 exhibit a very long tail toward the higher wavelength which becomes more prominent as the concentration of the solution increases. This observation implies the possibility of aggregation of the OPBI polymer chains.[14] A careful comparison between the DMAc and FA spectra for the higher concentration (0.2 g/dL) OPBI solutions shows significant differences between the two spectra in the higher wavelength region, suggesting that the nature of the OPBI polymer chain aggregation in the two solvents is not of similar type. This is quite logical considering the fact that the protic solvent FA produces polyelectrolyte

species in the solution[16,25] whereas DMAc does not. A more detailed discussion will follow in a later section in this chapter.

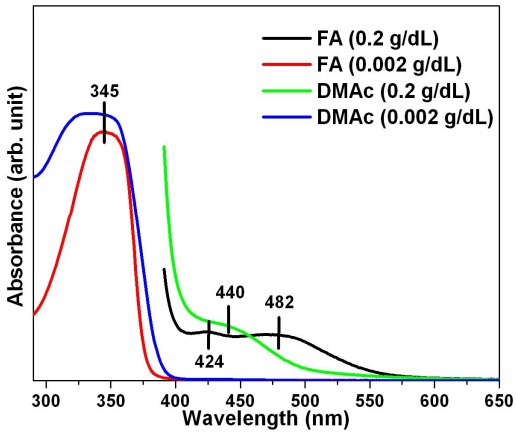

Figure 3.1. *Absorption spectra of OPBI solutions in formic acid (FA) and dimethyl acetamide (DMAc). The concentrations of the solutions are shown in the figure. The spectra are recorded using a cuvette with 1 cm path length.*

3.3.2. Steady-State Fluorescence Spectroscopy

Studies of molecular aggregation of polybenzimidazole [*m*-PBI, Scheme 3.1 (A)] in solution using fluorescence spectroscopy have been reported in the literature, and the emission bands (398 and 410 nm) are assigned to the *0-0* and *0-1* transitions from the excited ^1L_b state of the benzimidazole rings present in the *m*-PBI chain.[16,49] Figure 3.2 represents the emission spectra of OPBI solutions in DMAc and FA at various concentrations. The spectral nature, shapes, and their concentration dependence are consistent with the previous reports on *m*-PBI.[14,16,33] The presence of concentration quenching of OPBI, i.e., the decrease of emission intensity with increasing OPBI solution concentration, is observed in both of the solvents (Figure 3.2), suggesting the formation of aggregated structures of the OPBI chains in both of the solvents at higher concentrations. Very recently, we observed a similar kind of spectral feature for *m*-PBI in DMAc solution and confirmed conformational transition (compact coil to extended helical rodlike) of the *m*-PBI chains due to the molecular aggregation of the polymer chains with increasing concentration in solution.[14] Earlier, Kojima[16] showed that the

critical quenching volume for OPBI chains in DMAc is greater compared to the OPBI chains in FA and suggested very negligible or almost zero aggregation in the FA medium. However, our observation is not in agreement with the Kojima report and we have observed aggregations of OPBI chains both in DMAc and in FA mediums. We believe the nature of the aggregation processes in two different solvents is not similar and hence a thorough comparison of the aggregation behaviors in the two solvents is absolutely necessary. A broad emission peak at longer wavelength (~550 nm) appears with increasing concentration of the OPBI solution in both of the solvent systems, as observed in Figure 3.2 [(A) and (B)]. In our previous studies on the aggregation behavior of m-PBI solution in DMAc, we have assigned this longer wavelength peak (~550 nm) to the intermolecular aggregation/excimer formation at higher concentration. It must be noted from Figure 3.2 that the increase of the longer wavelength (~550 nm) peak intensity with increasing solution concentration is very much prominent for the DMAc solution compared to the FA solution. Figure 3.3 represents a plot of the intensity ratio (I_{550}/I_{410}) between the longer wavelength (550 nm) and lower wavelength (410 nm) emission bands against the solution concentration. A linear increase of the intensity ratio (I_{550}/I_{410}) with the concentration of the solution is observed in the case of the DMAc solution, whereas negligible concentration dependence is obtained for the FA solution. The observation for the DMAc solution is in agreement with our previous results, hence indicating the presence of intermolecular aggregation of OPBI chains in DMAc solution at higher concentration. On the other hand, the Figure 3.3 result for OPBI in FA solution brings two obvious conclusions: either the aggregation of OPBI chains in FA is not intermolecular or OPBI chains do not form any aggregated structure in the FA solution. Incidentally, the later conclusion was also drawn by Kojima previously.[16] At this point, it becomes necessary to validate the later conclusion. If the later conclusion drawn by Kojima is found to be wrong, then efforts should be made to understand the nature of aggregation of OPBI chains in the FA solution, which has to be remarkably different from the aggregation of OPBI chains in the DMAc solution.

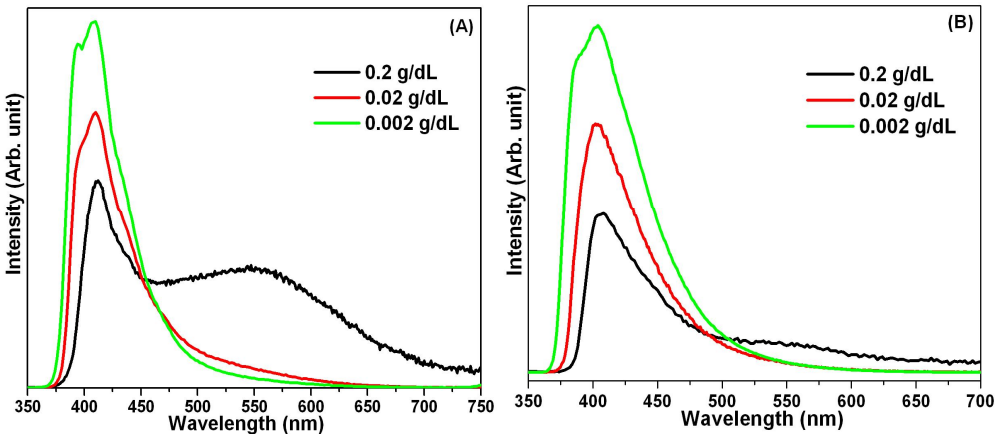

Figure 3.2. *Steady-state fluorescence emission spectra of OPBI in (A) DMAc and (B) FA solution at their indicated concentrations. The excitation wavelength (λ_{exc}) for all of these emission spectra is 340 nm.*

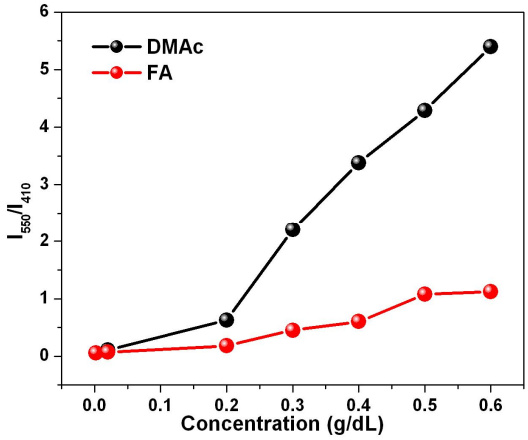

Figure 3.3. *Dependence of longer wavelength (550 nm) to lower wavelength (410 nm) intensity ratio (I_{550}/I_{410}) on the concentration of OPBI in DMAc and FA solutions.*

Long tails in the absorption spectra in both of the solvent systems (Figure 3.1) are attributed to the presence of aggregated species in the ground state that are energetically different. Also, significant differences are seen in the nature of the long absorption tails between the solvent systems, indicating the presence of different kinds of aggregated species in two different solvents. Each of these aggregated species is characterized by its own absorption and emission maxima. Hence, when the excitation

wavelength (λ_{exc}) is shifted, a different species is excited and an emission characteristic of that species is obtained. Therefore, if the fluorescence emission (λ_{em}) of OPBI solution in any particular solvent depends upon the excitation wavelength (λ_{exc}), then it can be concluded that the OPBI chains are forming an aggregated structure in that solvent. On the basis of this argument, we have studied the dependence of fluorescence emission on excitation wavelength for OPBI in both DMAc and FA solutions and the results are presented in Figure 3.4. The emission maxima gradually shift toward longer wavelength with the change in the excitation wavelength. The dependence of λ_{em} on λ_{exc} is presented in the Figure 3.4 (B) and (D). λ_{em} is highly dependent on λ_{exc} in the case of both solvent systems, as observed in Figure 3.4 (B) and (D). These results clearly show that the OPBI aggregation is taking place in both of the solvents at higher concentration. Therefore, the presence of OPBI aggregation in both of the solvents is confirmed. Hence, the conclusion, "OPBI chains do not form any aggregated structure in FA solution", obtained from Figure 3.3 and also suggested by Kojima[16] is not correct. Indeed, OPBI chains form aggregated structure in FA solution. However, the Figure 3.3 results clearly suggest that aggregation of OPBI in FA is not intermolecular in nature, since I_{550}/I_{410} is almost independent of the solution concentration. On the other hand, intermolecular aggregation is observed in the case of DMAc solution which is in agreement with our previous observation.[14] Also, it is worthwhile to note that the extent and nature of λ_{em} dependence on λ_{exc} is not similar for the two solvents (Figure 3.4 B and D). These observations attribute that the nature of the aggregation process is not similar in both of the solvent systems. Now the following question arises: if the OPBI aggregation in FA solvent is not intermolecular in nature (as evident from Figure 3.3), then how do the OPBI chains form aggregated structure with increasing concentration in the FA solution? The immediate answer to this question would be "the aggregation is intramolecular". However, intramolecular aggregation is not possible in this case, since the different parts of OPBI chains repel each other due to the polyelectrolyte nature of the chain in FA.[50] Also, it must be noted that the changes in the photophysical features of the OPBI in FA solutions are observed only when the concentrations of the solutions are gradually increased. Hence, the aggregation of the OPBI in FA indeed is an

intermolecular process, although it does not show the concentration dependence in Figure 3.3. The reason behind the concentration independency in Figure 3.3 may be explained by considering the polyelectrolyte nature of OPBI in FA. The OPBI chains repel each other for the polyelectrolyte nature, and simultaneously, the chains try to overlap each other due to the intermolecular attraction arising from the hydrogen bonding of OPBI chains with the FA solvent molecules.[25] Hence, the system compromises itself to a balanced situation and as a result of this we do not see the concentration dependency, although the aggregation is intermolecular. In a later section of this chapter, we have made efforts to proof the intermolecular aggregation of OPBI in FA using viscometric results.

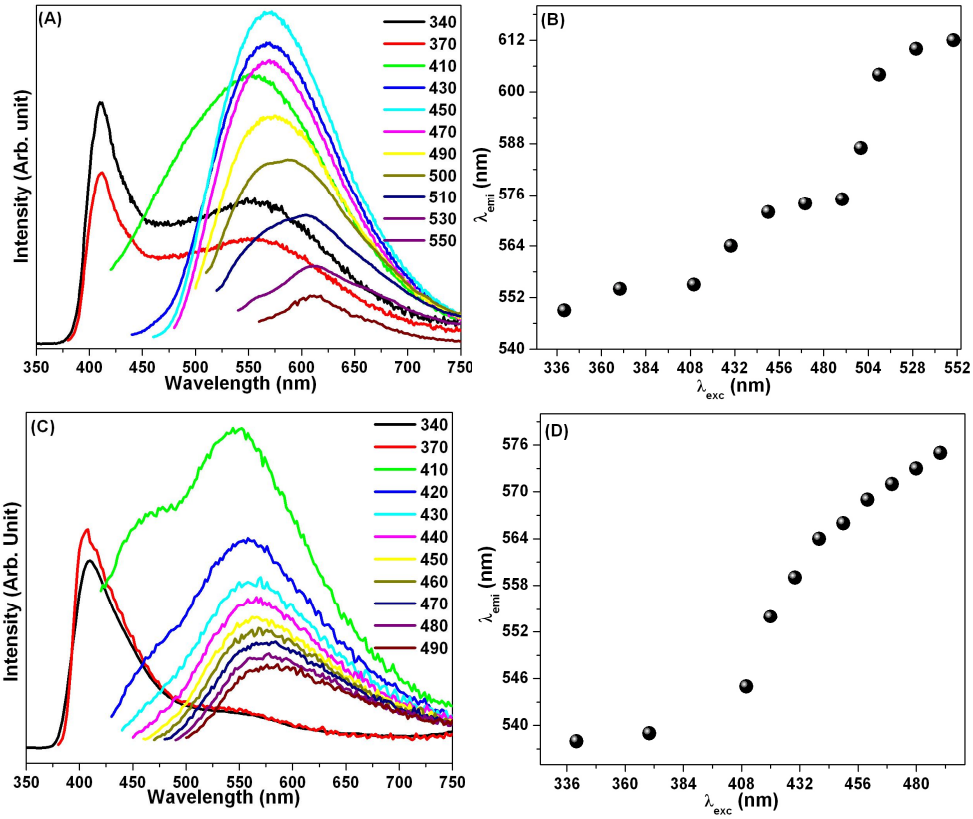

Figure 3.4. *Dependence of steady-state fluorescence emission spectra on the excitation wavelength (indicated in the figure) for OPBI in (A) DMAc [plot of λ_{em} against λ_{exc} (B) for DMAc] and (C) FA solution [plot of λ_{em} against λ_{exc} (D) for FA] (the concentrations of both of the solutions is 0.2 g/dL).*

3.3.3. Time-Resolved Fluorescence Spectroscopy

We have carried out time-resolved fluorescence lifetime measurements of OPBI in DMAc and FA solutions at dilute (0.002 g/dL) and high (0.2 g/dL) concentrations. The decay profiles of all OPBI solutions are recorded by exciting the samples at 374 nm and monitoring the fluorescence at 417 nm. The decay profiles of OPBI in DMAc and FA solutions are presented in Figure 3.5 (A,B) and Figure 3.5 (C,D), respectively. The decay and best fit parameters for all of the samples are presented in Table 3.1. The data recorded and shown in Figure 3.5 for all of the samples are fit quite well, as is evident from the quality of fitting parameter (χ^2) presented in Table 3.1. All of the decay profiles for OPBI solutions exhibit a triexponential decay function, as is evident from Table 3.1. A triexponential decay behavior for *m*-PBI solution in DMAc has been reported by us recently. A negative fractional contribution (α_1) is obtained from the concentrated solutions in both of the solvent systems (Table 3.1), which is attributed to the fact that the decay behavior for the concentrated solutions is different from that of the dilute solution.[51] Figure 3.5 clearly shows that the nature of the decay profiles for the concentrated solutions is quite different from that of the corresponding dilute solutions. The measured excited state lifetimes for the concentrated solutions in both of the solvents are longer than the dilute solutions (Table 3.1). Previously, we observed a longer excited state lifetime, negative pre-exponential factor (fractional contribution), and growth in decay profile in the case of concentrated m-PBI solution in DMAc where the m-PBI chains are aggregated.[14] Therefore, based on previous observation and the results obtained (Figure 3.5 and Table 3.1) from the time-resolved fluorescence lifetime measurement of OPBI in DMAc and FA solutions at dilute (0.002 g/dL) and high (0.2 g/dL) concentrations, we can conclude that OPBI chains aggregate at higher concentration in both DMAc and FA media. The excited state lifetime (τ_{av}) for dilute solution (0.002 g/dL) in both of the solvents are almost the same; however, τ_{av} for concentrated solution (0.2 g/dL) in DMAc (1708 ps) is significantly longer than that for the FA solution (1271 ps) at an identical concentration (Table 3.1). This difference in

excited state lifetime indicates that the nature of the aggregations in the two solvent a system is not similar.

Table 3.1. *Fluorescence Decay Parameters for OPBI in DMAc and FA Solutions at Different Concentrations*[a]

PBI Concentration (g/ dL)	τ_1 ***(ps)***	α_1	τ_2 ***(ps)***	α_2	τ_3 ***(ps)***	α_3	τ_{avg} ***(ps)***	χ^2
0.002 in DMAc	596	0.277	960	0.37	78	0.352	548	1.153
0.2 in DMAc	448	-0.685	1147	1.665	5321	0.0197	1708	1.338
0.002 in FA	480	0.138	909	0.461	79	0.399	518	1.245
0.2 in FA	513	-0.331	1036	1.317	5589	0.0135	1271	1.721

[a] The three lifetimes (τ_1, τ_2, and τ_3) and the respective fractional contributions (α_1, α_2, and α_3), the weighted average lifetime (τ_{avg}), and the quality of fitting (χ^2) for the data in Figure 3.5 are shown.

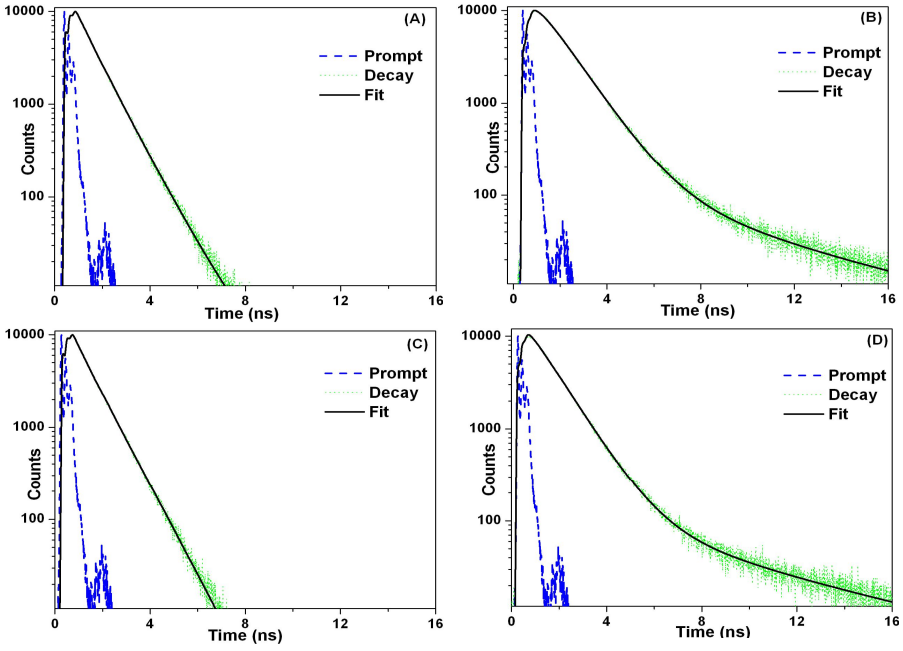

Figure 3.5. *Time-resolved fluorescence decay profiles of OPBI in DMAc and FA solutions: (A) 0.002 g/dL in DMAc; (B) 0.2 g/dL in DMAc; (C) 0.002 g/dL in FA; (D) 0.2 g/dL in FA.* λ_{exc} *= 374 nm.*

3.3.4. Temperature Dependent Fluorescence Spectroscopy

In the previous sections, we have demonstrated that the OPBI chains form aggregated structure at higher concentration in both the FA and DMAc media. The nature of the aggregations in these two solvents is different owing to the fact that the OPBI acts as a polyelectrolyte in the acidic medium (FA), whereas it is not a polyelectrolyte in DMAc. Figure 3.6 compares the steady-state fluorescence emission intensity of OPBI solution (0.2 g/dL) in FA and DMAc. At an exactly identical solution concentration (0.2 g/dL), the emission intensity for FA solution is much higher than that of DMAc solution (Figure 3.6). The larger emission intensity attributes the fact that the access to the chromophoric units (here, the imidazole moiety) is easier in the case of FA compared to the case of DMAc. The OPBI chains in FA medium repel each other and stay apart due to the polyelectrolyte nature, and therefore, the choromophoric imidazole units are more exposed and easily accessible. On the other hand, in the case of DMAc, the OPBI chains are more compact and hence the access to the imidazole units is low compared to the FA, resulting in lower emission intensity than the FA.

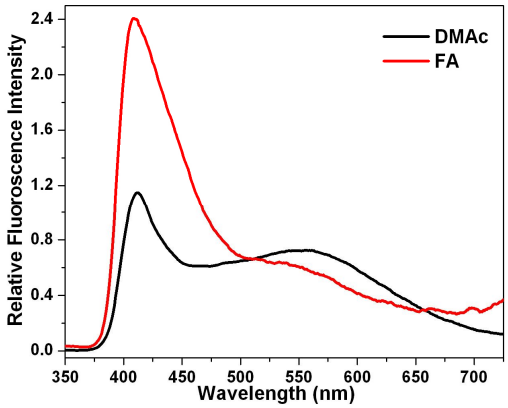

Figure 3.6. *Steady-state fluorescence emission spectra of OPBI solution in FA and DMAc. The concentration of both of the solutions is kept constant at 0.2 g/dL.*

We have recorded the temperature dependent fluorescence emission spectra of OPBI solution (0.2 g/dL) in FA and DMAc to study the effect of temperature on the aggregation behavior of the OPBI chains in these two different media. The emission

intensity decreases with increasing temperature in both cases (Figure 3.7). This shows that the OPBI chain aggregation is disrupted with increasing temperature. In the earlier sections, we have said that the broad peak at longer wavelength (~ 550 nm) is due to the fluorescence of the aggregated species (A) of the OPBI chains and the lower wavelength (~ 410 nm) is the contribution of the molecular/monomer fluorescence (M). Figure 3.7 clearly suggests that both intensities I_A (fluorescence intensity of aggregates) and I_M (fluorescence intensity of monomer) for both of the solvents decrease with increasing temperature. It is important to note from Figure 3.8 that the temperature dependence of I_M for FA is much sharper among all others. A strong solvent proton quenching of the imidazole moiety takes place at higher temperature because of the polyelectrolyte nature of the OPBI in FA, and therefore, I_M sharply decreases with increasing temperature in the case of FA solution, as observed in Figure 3.8. It is evident from Figures 3.7 and 3.8 that the OPBI aggregations in both of the solutions are temperature dependent and hence the aggregation processes must obey the Arrhenius relationship with activation energy (E_A) for the processes. E_A can be obtained from the following equation:

$$\frac{I_M}{I_A} = constnat \times e^{-E_A/RT} \tag{3.3}$$

where I_A and I_M are the fluorescence intensities for the aggregates and monomer emission, respectively.

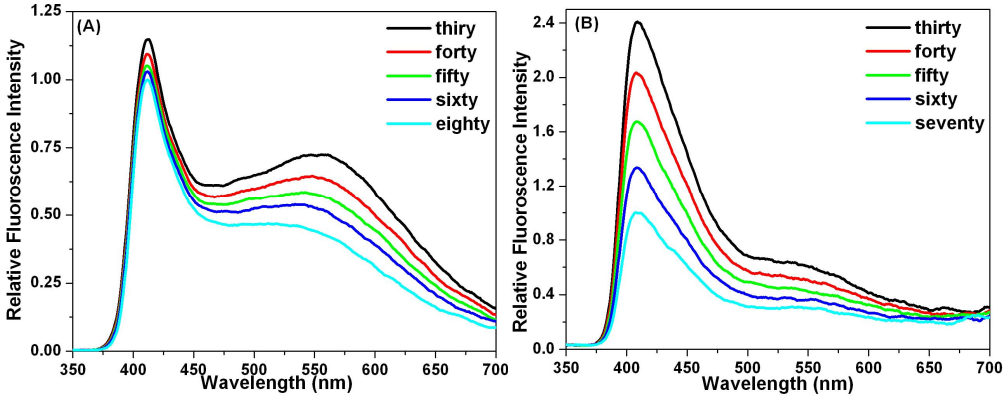

Figure 3.7. *Temperature dependent fluorescence emission spectra of OPBI solution (0.2 g/dL) in (A) DMAc and (B) FA.*

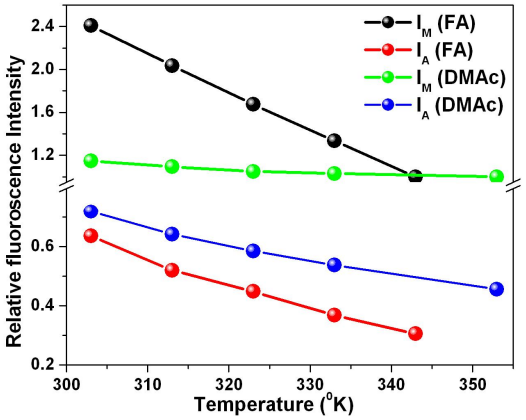

Figure 3.8. *Dependence of monomer (I_M) and aggregate (I_A) intensities of OPBI solution (0.2 g/dL) in FA and DMAc with temperature.*

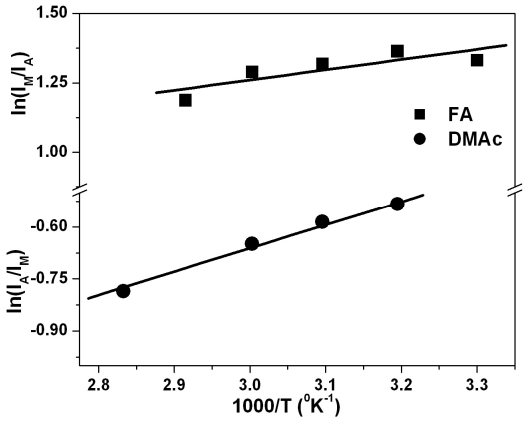

Figure 3.9. *Arrhenius plots for activation energies of the OPBI solutions (0.2 g/dL) in FA and DMAc.*

Hence, the activation energies for the aggregation processes of OPBI in FA and DMAc solutions can be obtained from the suitable plots (Figure 3.9) of the fluorescence intensities as a function of temperature.[42,52] The activation energies obtained from the Arrhenius plot (Figure 3.9) are 3.07 and 5.62 kJ/mol for FA and DMAc solution, respectively. The smaller activation energy for the FA solution than the DMAc solution suggests that in the former case aggregation is not as strong as it is in the later case. The weaker aggregation in the case of FA than the DMAc is indeed due to the

polyelectrolyte nature of the OPBI in this medium which directs the OPBI chains to aggregate in a different manner in FA so that it requires smaller energy. Hence, the nature of the aggregation processes of OPBI in both solvents is not similar.

3.3.5. Viscosity Study

The dilute solution viscosity (DSV) studies have been used in the literature very often to assess the interaction between polymer molecules and solvent in the solution.[9,10,18,53] The DSV measurements of polymer solutions give two well-known important parameters: the Huggins constant (k_H) and the intrinsic viscosity ([η]). The values of these two parameters are frequently used to determine the degree of polymer-solvent interactions and the polymer chain conformation in the solution. The intrinsic viscosities ([η]) obtained from the DSV measurements are often used to predict the polymer chain dimension and therefore can be utilized to study the chain conformation in the solution.[53,54] The hydrodynamic radius (R_h) or radius of gyration (R_g) corresponds to the chain dimension of the polymer in solution. The chain dimension (R_h or R_g) for a fixed molecular weight polymer is directly proportional to [η] as per the relation[55] $[\eta] \approx R_g^2 R_h / M$ .Hence, smaller [η] values suggest compact dimensions, whereas bigger [η] values indicate extended dimensions of polymer in solution. Therefore, the above discussion clearly suggests that the value of [η], obtained from the DSV method, can very well predict the chain conformation of polymer in solution. In short, smaller [η] suggests a collapsed compact conformation, whereas an extended conformation is obtained for larger [η] values.

The [η] values obtained from the DSV measurements at 30°C for OPBI solutions in DMAc and FA are 3.921 and 7.063 dL/g, respectively. The smaller [η] of OPBI solution in DMAc than FA suggests that the OPBI chains exhibit stronger intermolecular interaction in the latter solvent rather than the former one. Hence, the OPBI chains exist in a more extended form in FA than in DMAc. In other words, the chain dimension of OPBI is bigger in FA solvent than DMAc solvent. Hence, OPBI is more swollen in FA than in DMAc. Our spectroscopic studies described in the previous

sections demonstrated that the OPBI chains form aggregated structure with increasing polymer concentration in the solution in both of the solvents; however, the nature of the aggregation could be different. We have observed from the DSV measurements that the [η] value is not altered by the concentration of the OPBI solution in FA; in contrast, it increases significantly from lower concentration to higher concentration regions in DMAc solution. The [η] values of OPBI solution in DMAc at 30°C for the concentration ranges 0.6-0.075 g/dL (higher) and 0.0375-0.0047 g/dL (lower) are 4.659 and 2.585 dL/g, respectively. This result attributes a conformational transition of OPBI chains from compact collapsed conformer to extended conformer in DMAc solution to increasing solution concentration. In contrast, no such conformational transition of OPBI chains is predicted in FA solution with increasing concentration. At lower concentration in DMAc, due to the strong intramolecular interactions between the OPBI chains, the solvent molecules are not able to penetrate inside the polymer coil for swelling, hence resulting in a compact collapsed conformation. However, with increasing concentration, the intermolecular interactions between the OPBI chains are increased significantly, which allows solvent molecules to diffuse inside the coil and produce an extended structure. A schematic presentation of this process is depicted in Figure 3.10. In contrast to the OPBI behavior in DMAc solution, OPBI chains in FA solvent do not show any conformational transition upon aggregation, as depicted in the schematic presentation given in Figure 3.10. The polyelectrolyte character of the OPBI in FA medium is the driving force for this unaltered conformation. The various parts of the OPBI chains repel each other due to the electrolyte nature which helps the solvent molecule go inside the polymer chain easily and results in an extended conformation even at low concentration. As the concentration increases, interchain repulsion due to polyelectrolytic behavior and interchain attraction owing to the hydrogen bonding attraction between the chains through the solvents molecules[25] oppose each other. Finally, these two opposing forces counter balance each other to get the stabilization and form aggregates without disturbing the chain conformation. Hence, all of the above discussion clearly agrees with our spectroscopic results and proves that the aggregation in both solvents takes place with increasing concentration; however, their mechanisms

of formation are different. In the next section, we deal with the morphological features of the OPBI in both of the solvents, arising due to the aggregation process.

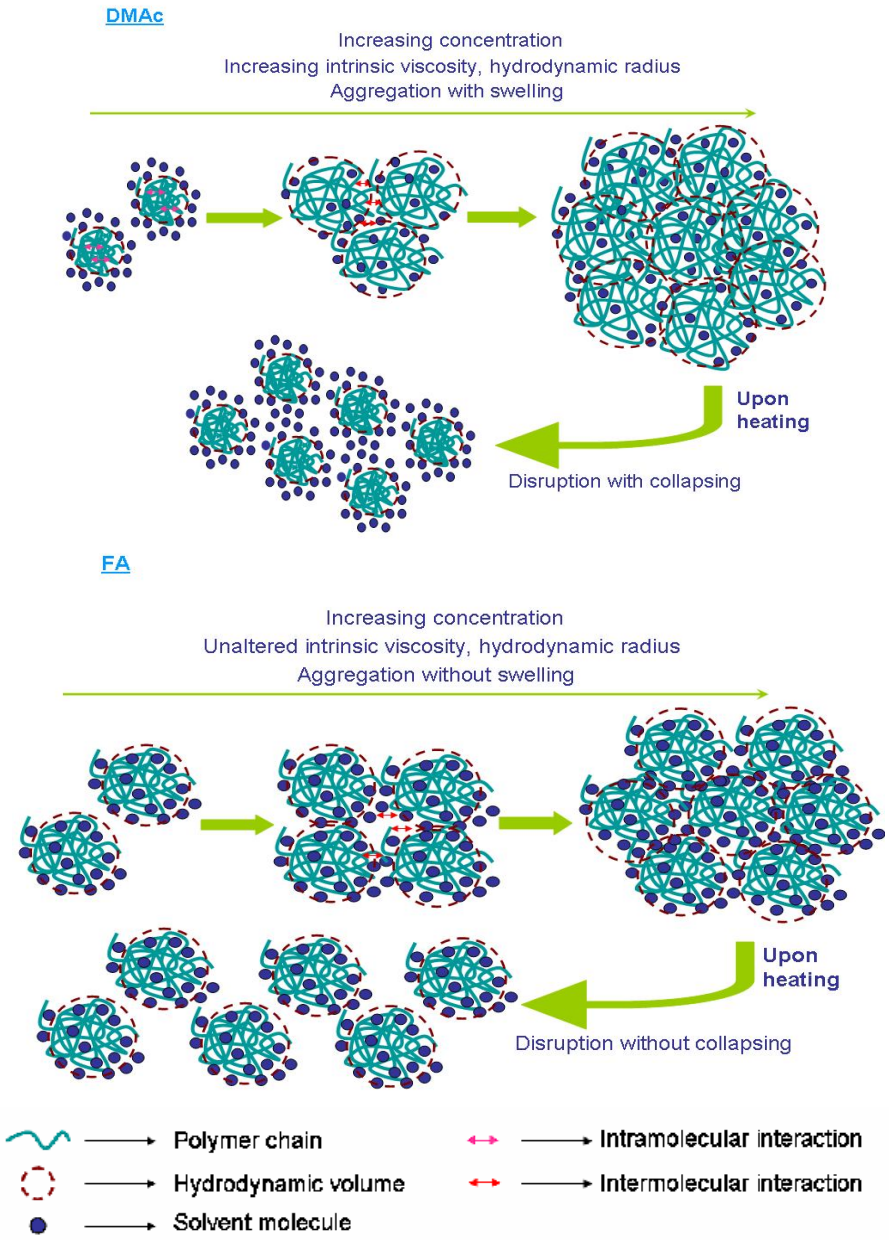

Figure 3.10. *Schematic representation of the aggregation behavior of OPBI in DMAc and FA solvent with increasing concentration. Also, the stability of aggregated structures upon heating is shown.*

Temperature dependent DSV measurements of polymer solution can help us understand the effect of temperature on the polymer chain conformation and the polymer-solvent interaction.[14,56] Recently, we utilized the temperature dependent DSV method to study the stability of the aggregation of m-PBI in a polar aprotic solvent such as DMAc.[14] In Figure 3.11, we plotted intrinsic viscosity ([η]) as a function of temperature for OPBI in both solvent systems. The most striking observation in Figure 3.11 is that [η] does not vary at all with temperature for the FA solvent and, on the other hand, exhibits significant variation with temperature in the case of DMAc medium. Our temperature dependent fluorescence study shows that with increasing temperature aggregation for both cases breaks down. Hence, these results (Figure 3.11) suggest that the disruption of aggregation in the case of FA is not associated with any conformational transition; however, the disruption of aggregation in DMAc solution is associated with conformational transition (Figure 3.10). The intrinsic viscosity of OPBI in DMAc solution is much smaller than that in FA for the entire temperature range studied here and decreases sharply with increasing temperature only in the case of DMAc solution (Figure 3.11). This observation reveals that OPBI chains in FA exhibit a more swollen structure than the DMAc. This result also suggests the presence of a conformational transition in the case of DMAc from extended conformer to compact collapsed structure with increasing temperature, since [η] is temperature dependent, and the absence of any conformational change for FA solution, since [η] is temperature independent in the later case. The schematic diagram presented in Figure 3.10 describes the aggregation processes, conformational transition, and thermal stability of the aggregates in both solvents. Therefore, all of our above results suggest that the aggregation mechanisms for two different solvents are not similar; in DMAc, the aggregation is driven by conformational transition, whereas, in FA, no transition is observed.

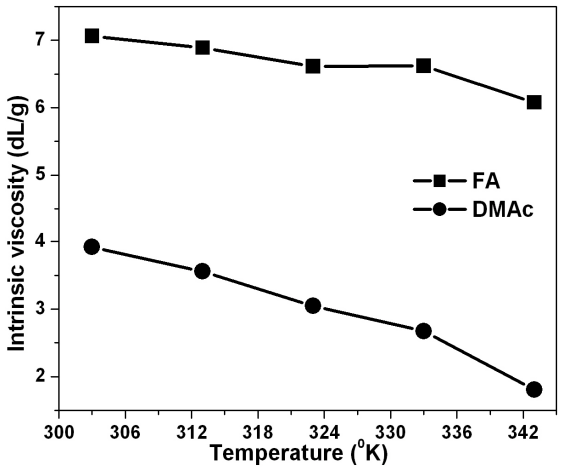

Figure 3.11. *Effect of temperature on the intrinsic viscosity ([η]) of OPBI in FA and DMAc solutions for the concentration region from 0.3 to 0.0375 g/dL.*

3.3.6. Electron Microscopy

In the above discussions, we have demonstrated that the OPBI chain undergoes a structural conformation transition (compact collapsed to swelled extended) with increasing concentration in DMAc solvent and it exhibits extended dimensions in all of the concentrations in FA solvent, indicating that it does not undergo any conformational transition in this solvent (FA). To strengthen our above observations, we have studied the morphology of the OPBI samples made from dilute (0.002 g/dL) and concentrated (0.2 g/dL) solutions in both DMAc and FA solvents using transmission electron microscopy (TEM). The TEM micrographs of various OPBI samples are presented in Figure 3.12. The micrograph of the dilute DMAc sample [Figure 3.12 (A)] consists of closely packed smaller entities which look like triangles. This is expected, since, at this concentration in DMAc, the OPBI chain exhibits a compact collapsed structure. Figure 3.12 (B) is the TEM micrograph obtained from the concentrated (0.2 g/dL) OPBI solution in DMAc. The morphological feature of this image is distinctly different from the dilute solution morphology [Figure 3.12 (A)]. This TEM image clearly shows the extended or swelled structures. Hence, our prediction about the conformation transition of OPBI in DMAc solution with increasing concentration is indeed true and has gotten

real proof from the TEM study. In contrast to the results obtained for DMAc solutions, the morphological observations are quite different for the samples made from OPBI solution in FA [Figure 3.12 (C) and (D)]. In these cases, we have obtained the extended structures type morphology in both the case of dilute and concentrated solutions, as observed in the TEM images presented in Figure 3.12 (C) and (D). These TEM results are in agreement with our earlier conclusion that the OPBI does not undergo any conformation structural transition during the aggregation process with increasing solution concentration in FA solvent. Hence, the morphological features of dilute and concentrated solutions in FA are quite similar.

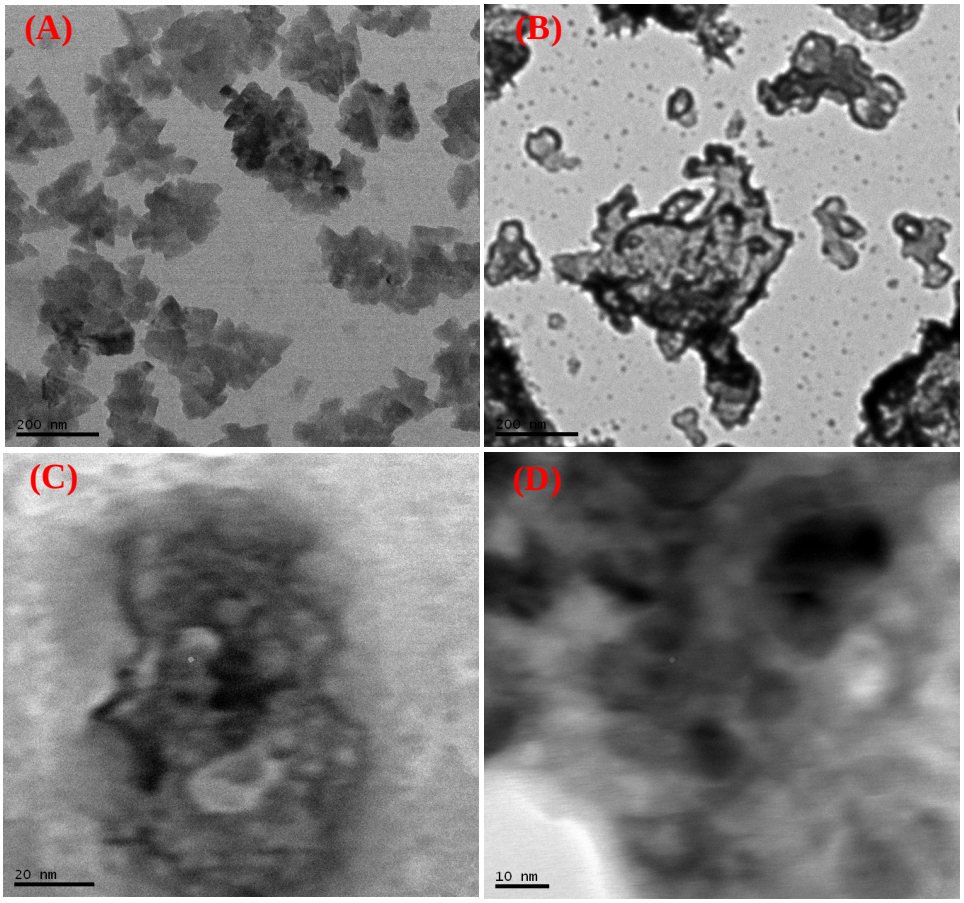

Figure 3.12. *TEM micrographs of OPBI samples made from different concentrations in DMAc and FA: (A) 0.002 g/dL in DMAc; (B) 0.2 g/dL in DMAc; (C) 0.002 g/dL in FA; (D) 0.2 g/dL in FA.*

We have also carried out circular dichroism (CD) studies of the OPBI solutions in both solvents to understand and monitor the conformational changes of the OPBI chains. Figure 3.13 represents the CD spectra of OPBI solutions in FA and DMAc at their indicated concentration. The most important observation that needs to be noted from Figure 3.13 is that both the dilute and concentrated solutions of OPBI in FA are CD active. However, only the concentrated OPBI solution in DMAc is CD active and dilute solution is inactive. A similar observation for m-PBI in DMAc has been observed very recently.[14,24] Thus, the above results clearly are attributed to the fact that OPBI aggregates with increasing concentration both in FA and DMAc but it undergoes a conformational transition in the case of DMAc and not in the case of FA. Hence, we can summarize that the aggregation processes in both solvents do not follow similar mechanisms.

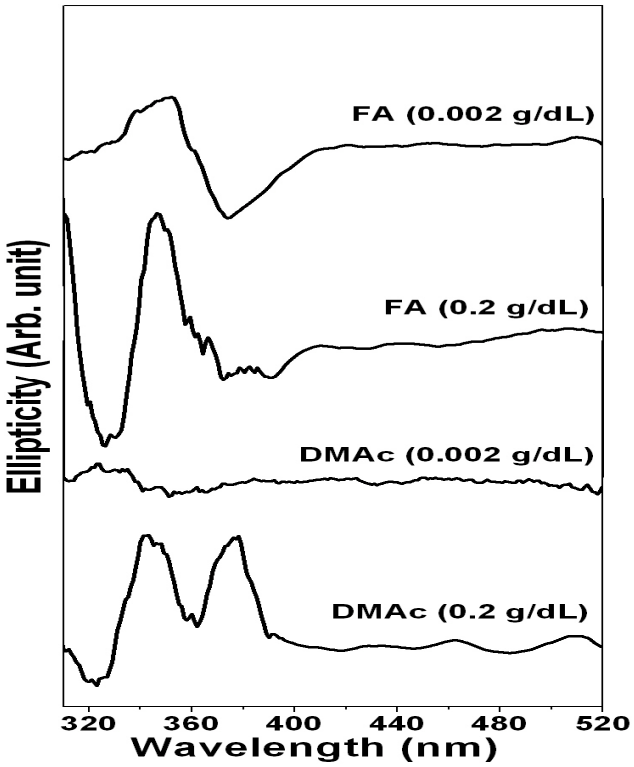

Figure 3.13. *Circular dichroism spectra of OPBI in both DMAc and FA solution at their indicated concentrations.*

3.4. Conclusion

The aggregation behavior of OPBI in polar aprotic solvent such as dimethyl acetamide (DMAc) and polar protic solvent such as formic acid (FA) is studied by varying the polymer concentration in the solution. The role of solvent protic character on the aggregation behavior of OPBI and the associated conformational transitions are elucidated by employing various methods such as photophysical, dilute solution viscosity (DSV), microscopy, and circular dichroism. Steady-state and timeresolved fluorescence spectroscopy studies demonstrated the formation of an aggregated structure of OPBI chain in both DMAc and FA solvents at higher concentration. The concentration dependent photophysical study proved that the aggregation is an intermolecular process in both solvent systems; however, the mechanisms of aggregate formation in both solvent systems are not similar. It has also been shown that stronger aggregates are formed in DMAc compared to FA solvent, since the activation energy of aggregation (E_a) in DMAc is higher than that in FA. DSV studies revealed that with increasing polymer concentration in solution OPBI chains undergo a conformational transition from a compact collapsed conformer to extended structure in DMAc solvent, whereas no such transition is observed in FA solvent. The presence of strong intramolecular repulsion of OPBI chains in FA due to the polyelectrolyte behavior of OPBI in this solvent is the driving force for the unaltered conformation. TEM images and CD spectra obtained from various polymer concentrations also supported the conformational transition of OPBI in DMAc and the absence of any such transition in FA. The temperature dependent studies (steady-state fluorescence and DSV) proved that the aggregated structure dissociated into non-aggregated species with increasing temperature in both DMAc and FA solvent. Temperature dependent DSV studies confirmed that the disruptions of the aggregates are accompanied by a conformational transition (extended to collapsed) in the case of DMAc, whereas an unaltered conformation is obtained in the case of FA. Therefore, in summary, we can conclude that OPBI chains form aggregated structures in both polar aprotic (DMAc) and polar protic (FA) solvents with increasing polymer concentration in the solutions and these

aggregates dissociate at higher temperature in both cases. Most importantly, the nature of the aggregation and its disruptions is driven by different mechanisms due to the protic and aprotic nature of the solvents.

References

1. Lehn, J. *Angew. Chem., Int. Ed. Engl.* **1988**, *27*, 89.
2. Lehn, J. *Angew. Chem., Int. Ed. Engl.* **1990**, *29*, 1304.
3. Ky Hirschberg, J. H. K.; Brunsveld, L; Ramzi, A.; Vekemans, J. A. J. M.; Sijbesma, R. P.; Meijer, E.W. *Nature* **2000**, *407*, 167.
4. Sijbesma, R. P.; Beijer, F.H.; Brunsveld, L.; Folmer, B. J. B.; Ky Hirschberg, J. H. K.; Lange, R. F. M.; Lowe, J. K. L.; Meijer, E. W. *Science* **1997**, *278*, 1601.
5. Bekturov, E. V.; Bimendina, L. A. *Adv. Polym. Sci.* **1981**, *41*, 99.
6. Tschuchida, E.; Abe, K. *Adv. Polym. Sci.* **1982**, *45*, 1.
7. Whitesides, G.; Mathias, J.; Seto, C. *Science* **1991**, *254*, 1312.
8. Minato, K. I.; Ohkawa, K.; Yamamoto, H. *Macromol. Biosci.* **2006**, *6*, 487.
9. Sivadasan, K.; Somasundaran, P.; Turro, N, *J. Colloid. Polym. Sci*. **1991**, *269*, 131.
10. Simon, S.; Dugast, J.Y.; Le Cerf, D.; Picton, L.; Muller, G. *Polymer* **2003**, *44*, 7917.
11. Deepak, V. D; Asha, S. K. *J. Phys. Chem. B* **2009**, *113*, 11887.
12. MacKnight, W. J.; Ponomarenko, E. A.; Tirrell, D. A. *Acc. Chem. Res.* **1998**, *31*, 781.
13. Sannigrahi, A.; Arunbabu, D.; Sankar, R. M.; Jana, T. *Macromolecules* **2007**, *40*, 2844.
14. Tazuke, S.; Matsuyama, Y. *Macromolecules* **1975**, *8*, 280.
15. Kojima, T. *J. Polym. Sci., Polym. Phys. Ed.* **1980**, *18*, 1685.
16. Huang, H.Y.; Yun, H.; Lin, H. S.; Kwei, T. K.; Okamoto, Y. *Macromolecules* **1999**, *32*, 8089.
17. Hong, P. –D.; Chou, C. –M.; He, C. -H. *Polymer* **2001**, *42*, 6105.
18. Fakis, M.; Anestopoulos, D.; Giannetas, V.; Persephonis, P. *J. Phys. Chem. B* **2006**, *110*, 24897.
19. Choe, E. W., Choe, D. D. *In Polymeric Materials Encyclopedia*; Salamone, J. C., Ed., CRC Press: New York, **1996**.

20. Arunbabu, D.; Sannigrahi, A.; Jana, T. *J. Phys. Chem. B* **2008**, *112*, 5305
21. Deimede, V.; Voyiatzis, G. A.; Kallitsis, J. K.; Qingfeng, L.; Bjerrum, N. J. *Macromolecules* **2000**, *33*, 7609.
22. Musto, P.; Karasz, F. E.; MacKnight, W. J. *Macromolecules* **1991**, *24*, 4762.
23. Shogbon, C. B.; Brousseau, J.-L.; Zhang, H.; Benicewicz, B. C.; Akpalu, Y. *Macromolecules* **2006**, *39*, 9409.
24. Sannigrahi, A.; Arunbabu, D.; Jana, T. *Macromol. Rapid Commun.* **2006**, *27*, 1962.
25. Hickner, M. A.; Ghassemi, H.; Kim, S. Y.; Einsla, B. R.; McGrath, J. E. *Chem. Rev.* **2004**, *104*, 4587.
26. Xiao, L.; Zhang, H.; Jana, T.; Scanlon, E.; Chen, R.; Choe, E.-W. ; Ramanathan, L. S.; Yu, S.; Benicewicz, B. C. *Fuel Cells* **2005**, *5*, 287.
27. Savinell, R.; Yeager, E.; Tryk, D.; Landau, U.; Wainright, J.; Weng, D.; Lux, K.; Litt, M.; Rogers, C. *J. Electrochem. Soc.* **1994**, *141*, L46.
28. Samms, S. R.; Wsmus, S.; Savinell, R. F. *J. Electrochem. Soc.* **1996**, *143*, 1225.
29. Mecerreyes, D.; Grande, H.; Miguel, O.; Ochoteco, E.; Marcilla, R.; Cantero, I. *Chem. Mater.* **2004**, *16*, 604.
30. Xiao, L.; Zhang, H.; Scanlon, E.; Ramanathan, L. S.; Choe, E. W. ; Rogers, D.; Apple, T.; Benicewicz, B. C. *Chem. Mater.* **2005**, *17*, 5328.
31. Xu, H.; Chen, K.; Guo, X.; Fang, J. *Polymer* **2007**, *48*, 5541.
32. Sannigrahi, A.; Ghosh, S.; Lalnuntluanga, J.; Jana, T. *J. Appl. Polym. Sci.* **2009**, *111*, 2194.
33. Marletta, A.; Goncalves, V. C.; Balogh, D. T. J. *Luminescence* **2006**, *116*, 87.
34. Ravindranath, R.; Vijilaa, C.; Ajikumar, P. K.; Hussain, F. S. J.; Ng, K. L.; Wang, H.; Jin, C. S.; Knoll, W.; Valiyaveettil, S. *J. Phys. Chem. B* **2006**, *110*, 25958.
35. Traiphol, R.; Charoenthai, N.; Srikhirin, T.; Kerdcharoen, T.; Osotchan, T.; Maturos, T. *Polymer* **2007**, *48*, 813.
36. Wang, S.; Wu, P.; Han, Z. *Macromolecules* **2003**, *36*, 4567.
37. Aspler, J. S.; Guillet, J. E. *Macromolecules* **1979**, *12*, 1082.

38. Gupta, M. C.; Gupta, A.; Horwitz, J.; Kliger, D. *Macromolecules* **1982**, *15*, 1372.
39. Gatica, N.; Marcelo, G.; Mendicuti, F. *Polymer* **2006**, *47*, 7397.
40. Cuniberti, C.; Perico, A. *Euro Polym J.* **1980**, *16*, 887.
41. Fox, R.B.; Price, T. R.; Cozzens, R. F.; Mcdonald, J. R. *J. Chem. Phys* **1972**, *57*, 534.
42. Kuwahara, N. *J. Polym. Sci.* **1963**, *A1*, 2395.
43. Yuan, Y.; Johnson, F, Cabasso, I. *J. Appl. Polym. Sci.* **2009**, *112*, 3436.
44. Fuoss, R.M. *J. Polym. Sci.* **1948**, *3*, 603.
45. Nandi, P.; Bhattarai, A.; Das, B. *J. Polym. Sci., Part B: Polym. Phys.* **2007**, *45*, 1765.
46. Neuse, E. W. *Adv. Polym. Sci.***1982**, *47*, 1.
47. Sannigrahi, A.; Arunbabu, D.; Sankar, R. M.; Jana, T. *J. Phys. Chem. B* **2007**, *111*, 12124.
48. Zimmermann, H.; Joop, N. *Ber. Bunsenges. Phys. Chem.* **1962**, *66*, 342.
49. The reduced viscosity of the dilute OPBI solution in FA increases sharply and shows a maximum with decreasing concentration, providing a support for the polyelectrolytic character of OPBI in FA solvent in chapter 2.
50. Birks, J. B. *Photophysics of Aromatic Molecules*; Wiley-Interscience: New York, **1970**.
51. Skilton, P. F.; Ghiggino, K. P. *Polym. Photochem.* **1985**, *5*, 179.
52. Sun, S. F. *Physical Chemistry of Macromolecules: Basic Principles and Issues*; John Wiley & sons, Inc.: New York, **1994**.
53. Budhlall, B. M.; Landfester, K.; Sudol, E. D.; Dimonie, V. L.; Klein, A.; El-Aasser, M. S. *Macromolecules* **2003**, *36*, 9477.
54. De Gennes, P. -G. *Scaling Concepts in Polymer Physics*; Cornell University Press: Ithaca, NY, **1979**.
55. Kojima, T.; Yokota, R.; Kochi, M.; Kambe, H. *J. Polym. Sci., Polym. Phys. Ed.* **1980**, *18*, 1673.

Chapter 4

Solvent Induced Porous Polybenzimidazole Membrane: A Facile Route to Enhance Proton Conductivity

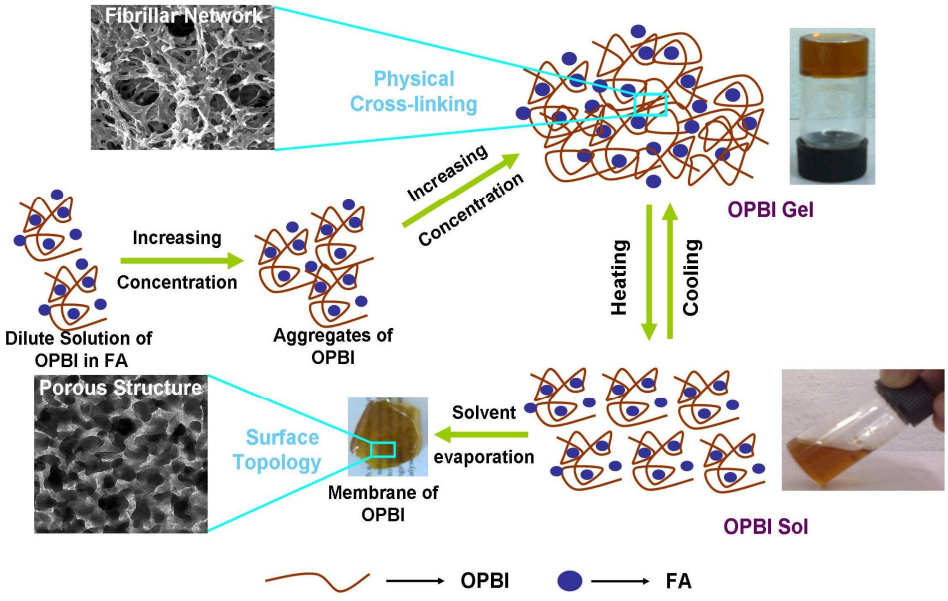

The thermoreversible gel of poly(4,4′-diphenylether-5,5′-bibenzimidazole) (OPBI) in formic acid (FA) was prepared which upon evaporation of FA yielded a porous OPBI membrane. Porous OPBI membrane upon doping with PA displayed very high acid doping level and proton conductivity.

4.1. Introduction

Polymer electrolyte membrane fuel cell (PEMFC) is receiving increasing attention due to their abilities as power generators for both stationary and transportation applications.[1,2] During the past decade, research activities on polymer electrolyte membrane (PEM) have increased progressively.[3-9] The most successful membrane is the Nafion® membrane which offers quite good performance below 100°C under fully hydrated conditions. Consequently, the operational temperature is limited to below 100°C. The Nafion membrane has several drawbacks to operate this membrane at high temperature (>120°C).[5,6,10] For a good membrane to be used for high temperature PEMFC, it should have characteristics, such as high proton conductivity, high thermal and mechanical stability. In recent years, much effort has been focused on developing new cheaper polymer electrolyte membranes (PEMs) to substitute the extremely high cost sulfonated perfluoropolymers and improve the operating temperatures above 100°C. Phosphoric acid (PA) doped polybenzimidazole (PBI) are currently being explored widely because of their potential applications in proton exchange membrane fuel cells (PEMFCs). One of the most important features of PA-doped PBI membranes is that they still have particularly highly proton conductive at low humidification, or at high temperature (150–200°C), so they are the most promising membrane materials for high temperature PEMFC applications.[11-15] Polybenzimidazole (PBI) is an amorphous aromatic heterocyclic polymer which possesses both proton donor (-NH-) and acceptor (-N=) hydrogen bonding sites which shows some specific interactions with both protic and aprotic polar solvents.[16-18] PBI is well-known as an excellent, high performance resin for its good mechanical properties, thermal, and chemical stabilities.[13-15,19]

Various approaches have been reported by several literatures to fabricate PA doped PBI membrane; these includes by casting from dimethyl acetamide (DMAc) organic solvent followed by doping with PA,[13-15] by introducing the porosity in the PBI by leaching out a low molecular weight compound using selective solvent for porogen followed by doping the film in PA,[20] and by using sol-gel process from the polymeric mixture in the polyphosphoric acid (PPA).[11,12,21,22] Besides from the above methods, our

group have developed a novel method to cast PA doped PBI membrane from PBI-PA gel by which the solvents can be fascinated inside the polymer network to make a better mechanical strength membrane due to its highly dense interconnected network.[23] Also several synthetic approaches have been attempted through the modification of the polymer backbone[26-32] as well as the side chain[33-35] to obtain the new PBI and hence the PA doped PBI membranes. The major problem is to get a membrane with high acid doping level with moderately good mechanical stability. Sometime, the acid content of the membrane is too high to process the membrane due to its very poor mechanical stability.[36] Also, the PA doped membrane should have superior thermal stability to avoid the leaching out of the free phosphoric acid from the membrane above 160ºC, to achieve high conductivity of many orders of magnitude during fuel cell operation.[37] Hence to get a superior quality membrane, a compromise between these two important parameters (acid loading and mechanical strength) has to be maintained.

In recent times, the thermoreversible gels of polymers and biopolymers have drawn a significant attention to explore its various properties.[24,25] Thermoreversible gels which are physical gels where solvent mostly stabilize the system through weak electrostatic interactions like hydrogen bonding, van der Waal's forces, hydrophobic interactions. These interactions concerned in the linking domains are of the order of kT, and can therefore be destroyed and transformed reversibly by heating and cooling the system. Due to the non-covalent weak electrostatic interactions these processes become reversible in nature with respect to concentration, temperature, etc. That is why the mechanism of thermoreversible gelation depends upon the polymer and solvent pairs interaction that brings in crystallization, conformation ordering, liquid-liquid phase separation, mesomorphic phase transition.[24,25] In the chapter 2, we had demonstrated that OPBI chains form aggregated structure in the DMAc and FA solution with increasing concentrations and we have observed a conformational transition during the aggregation process in case of DMAc and in case of FA there is no conformational transition. This above study helped us to design and develop the thermoreversible gel of OPBI in FA.

. This study reports the formation of porous structures of OPBI membrane, casted from OPBI-FA gel which can hold huge amount of PA and increase the proton conductivity enormously. Indeed, the multiporous structure of the polymer membrane is one of the convenient tools for ionic transport and enhances ionic conduction.[38] Due to low boiling point of FA, we expect that the solvent evaporates very easily from the OPBI membrane from OPBI-FA gel and this porous membrane is expected to retain display electrochemical properties such as proton conductivity after doping of PA. In past few years, there have been many research devoted to the synthesis and design of materials exhibiting multiscale porosity.[39-41] For this study, we have chosen poly(4, 4′-diphenylether-5, 5′-bibenzimidazole) (named as OPBI) (Scheme 3.1B) due to its flexible nature in the polymer backbone and good solubility in nature.

4.2. Experimental Section

4.2.1. Materials

3, 3′, 4, 4′-tetraaminobiphenyl (TAB, polymer grade), 4, 4′-oxybis (benzoic acid) (OBA) and phosphoric acid (PPA, 115%) were purchased from Aldrich. Formic acid (99%) and sulfuric acid (98%) were purchased from Merck, India. All the chemicals were used without further purification.

4.2.2. OPBI Synthesis and Preparation of OPBI Gel

The OPBI synthesis procedure is same as described elsewhere.[26,32,42] Equal moles of TAB and OBA were taken into a three neck round bottom flask with PPA and the reaction mixture was stirred continuously in nitrogen atmosphere at 190-210°C for 26 h. The OPBI polymer was isolated, neutralized with sodium carbonate, washed thoroughly with water, and dried in a vacuum oven at 100 °C for 24 h. The inherent viscosity (I. V.) of the dried polymer was measured in concentrated sulfuric acid (98%) of polymer concentration 0.2 g/dL by using a Cannon Ubbelohde capillary dilution viscometer (model F725). The I. V. of the synthesized OPBIs were varied by altering the monomer concentration in the polymerization mixture as reported earlier by us.[42]

The gel was prepared by taking required amount of OPBI in measured amount of formic acid (FA) in a sealed glass vial. The glass vial was kept at 65 °C to make the solution homogeneous. After obtaining the homogeneous orange color solution, the solution was kept at room temperature to form the gel. Again, the gel was transformed into solution after keeping at 65°C.

4.2.3. Membrane Fabrication and Doping with Phosphoric Acid (PA)

The OPBI gel in FA was heated at 65^{o}C to make the homogeneous orange solution and then this solution was poured in a glass petridish immediately. After evaporation of FA, OPBI film was obtained which was pilled off from the glass petridish. Then the membrane was washed with acetone and water repeatedly and dried in vacuum oven at 60ºC for 24 hrs. After that, the membrane was dipped in PA bath for 7 days to get a free standing PA loaded OPBI membrane.

4.2.4. Gelation Kinetics

The gelation kinetics was measured by a test tube tilting method. Several homogeneous solutions of different concentrations were prepared in sealed glass vial by taking required amount of OPBI in measured amount of FA at 65°C and quickly transferred to a thermostatic bath preset at different gelation temperature. The time required for complete freezing of the fluid, even after tilting the sealed glass vial, in the glass vial was taken as gelation time (t_{gel}). The gelation rate (t_{gel}^{-1}) is the reciprocal of gelation time (t_{gel}).

4.2.5. Morphology

The morphologies of the gels were examined by scanning electron microscope (SEM), field emission scanning electron microscope (FESEM), transmission electron microscope (TEM) and atomic force microscope (AFM). For SEM study, the gels were dried by the solvent replacement method by leaching with a guest solvent (mixture of acetone + water). Then the sample was gold coated and their micrographs were taken in an SEM apparatus (Philips-XL30ESEM). The surface of membranes, prepared from

different percentage of OPBI in FA and cross-section morphologies of the membrane, prepared by breaking the membrane in liquid nitrogen medium were recorded in FESEM (Carl Zeiss, Model No. ULTRA-55). For TEM study, a drop of sample was placed on a carbon coated copper (200 mesh) grid, dried and observed through the TEM instrument (FEI Tecnai Model No. 2083) operating at 120kV. For AFM study, the sample was prepared by giving one drop of the particular percentage solution of OPBI on the freshly cleared and thoroughly cleaned mica and kept it in vacuum for one day for recording the micrographs in semicontact mode in AFM apparatus (Model: Solver Pro M of NT-MDT). A microcantilever with a spring constant 10 N/m was used to scan the samples.

4.2.6. Spectral Characterization

The FT-IR spectra of the samples were recorded on a (Nicolet 5700 FT-IR) FT-IR spectrometer. The FT-IR spectra of the OPBI and OPBI gel were performed from the KBr pellet of the samples.

4.2.7. Thermal Measurement

Differential scanning calorimetry (DSC) experiments were performed in a Pyris Diamond DSC (Perkin-Elmer) instrument under nitrogen atmosphere. The gel samples were taken in a large volume capsule (LVC) pan. The samples were scanned from 10°C to 70°C at the heating rate of 10°C/min and from 70°C to 10°C at a cooling rate 5°C/min. The DSC instrument was calibrated with indium and zinc before each set of experiments. The thermogravimetric analysis of PA doped and PA undoped gel membranes samples were carried out on a (Netzsch STA 409PC) TG-DTA instrument from 50 to 900°C with a scanning rate of 10° deg/min in the presence of nitrogen flow. The sample weight loss was measured as a function of temperature. Before the heating scan, the samples were kept isothermally at 100ºC for 30 min inside the TG–DTA furnace.

4.2.8. WAXS Study

Wide angle x-ray scattering study was carried out to understand the crystallization and the structure of the gel sample. Bruker D8 Advance diffractometer using Cu-Ka X-radiation (λ =1.54 Å) at 40 kV and 30 mA was used. The gels were taken in a glass slide and Diffraction patterns were collected over a 2θ range of 5–60° at a scan rate of 1° min^{-1}.

4.2.9. PA doping level

The PA doping level of OPBI gel membrane was determined by titrating of a preweighed piece of membrane sample with standardized 0.1 (N) sodium hydroxide solution using Metrohm Titrino Titrator. The acid doping levels are expressed as mols of phosphoric acid per mol of OPBI repeat unit. The acid doping level was calculated using the following equation:

$$\text{Acid doping level} = \frac{V_{NaOH} C_{NaOH}}{W_{dry}} M_w \qquad (4.1)$$

where, V_{NaOH} and C_{NaOH} are the volume and the molar concentration of the sodium hydroxide, respectively. W_{dry} is the dry polymer membrane weight and M_w is the molecular weight of the polymer repeat unit. The acid doping level reported here are the average values obtained from three separate values, measured from three similar size membrane samples.

4.2.10. Dynamic Mechanical Property

The mechanical properties of the OPBI gel membrane in FA, PA doped OPBI gel films and dried OPBI membrane were measured using a dynamic mechanical analyzer (DMA) (TA Instruments, model Q-800). Membranes of 15 mm × 6 mm × 0.05 mm (L × W × T) dimensions were cut and clamped on the film tension clamp of the calibrated instrument. The storage modulus (G'), loss modulus (G") were measured by

frequency sweeping process with a preload force of 0.01N. We have used the frequency sweeping experiment at 30℃ with variation of frequency from 0.01 Hz to 30 Hz.

4.2.11. Stress-Strain Study

The stress-strain relationship of the PA doped OPBI gel membranes were measured utilizing a Universal Testing Machine (Autograph Model AGS 10, ANG, Shimadzu) with 0.3(N) load cell. Dumb-bell specimens were cut following the ASTM standard D653 (Type V specimens). Tensile properties of all films were measured in an air atmosphere at room temperature with a cross head speed of 1 mm min^{-1}.

4.2.12. Conductivity Study

Proton conductivity measurements were performed by four-probe impedance spectroscopy using Zahner Impedance spectrometer (ZENNIUM PP211) over a frequency range from 1 Hz to 100 kHz. The home made conductivity measurement cell made of Teflon was used. Conductivity measurements were performed on PA doped OPBI gel membranes. The membrane sample was sandwiched between two teflon plates with four electrodes. Two outer electrodes (1.5 cm apart) supply current to the cell, while the two inner electrodes 0.5 cm apart on opposite sides of the membrane measure the potential drop. The cell was placed in an oven to measure the temperature dependence of the proton conductivity. All the membranes were dried by heating at 100°C for 2h to avoid the conduction due to presence of water molecule. The membrane sample was then cooled in a vacuum oven and taken out just before conductivity measurement in an effort to keep the sample dry. The conductivities of the membrane sample were measured from 30 to160°C at intervals of 20°C. At every temperature, membrane was kept for 30 minutes to reach the equilibrium and then the measurements were carried out. The conductivity was calculated from the relationship $\sigma = \frac{D}{LBR}$, where D is the distance between the electrodes (here it is 0.5 cm), and B and L are the thickness and width of the gel sample, respectively. In all cases, resistance (R) was

obtained from the Nyquist plot by fitting all the experiments with a two-component model with an ohmic resistance in parallel with a capacitor.

4.3. Results and Discussions

Polymer gels show very discrete morphological features in the gel state. Most often, interconnected fibrils or fibrillar network morphology is observed from gels and this observation has been reported by several authors.[23,43-47] The solid powder OPBI, which is not treated with any solvent, does not exhibit any type of fibrillar morphology, in fact it is almost featureless [Figure 4.1 (A)]. Figure 4.1 (B) and (C) show the morphologies acquired form the SEM and TEM of the dried gel respectively which clearly suggest the network morphology of the gel consisting of well defined interconnected fibrils. In this context, it is important to mention that we have used guest solvents (mixture of acetone + water) as substituting solvent of FA to dry the gel for SEM study which help us to keep the original fibrillar network structure be remain intact as it is in the gel after the removal of the guest solvent by very slow evaporation. Direct evaporation of FA from OPBI-FA gel at higher temperature gives the collapsed structure, showing no interconnected fibrillar networking in the dried gel which is shown in Figure 4.1 (D). These above observations profoundly suggest that the OPBI, which does not have any morphological features in powder state [Figure 4.1 (A)], produces fibrils after treatment with FA and these fibrils form interconnected network structure in the higher concentration. We have discussed in the later section of this chapter how the network density, length, thickness, number of the interconnected fibrils in the dried OPBI gel state influences with changing the concentration of the OPBI-FA gel and the molecular weight of the OPBI.

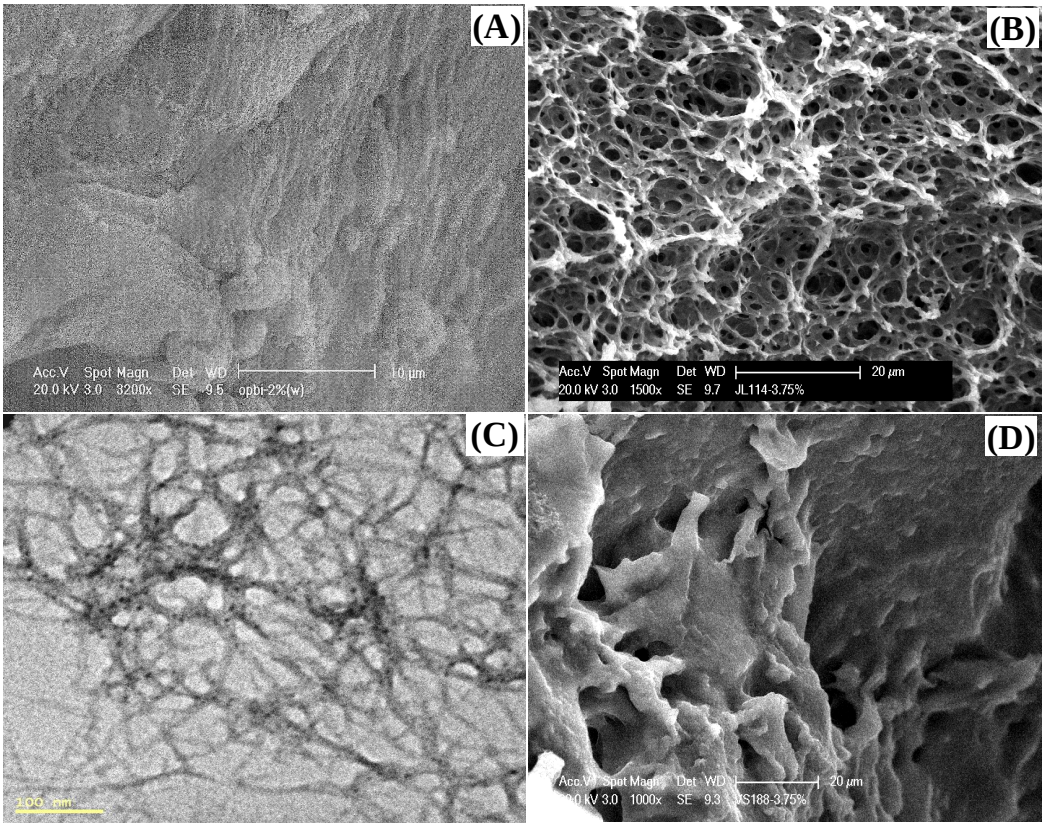

Figure 4.1. *SEM micrographs of (A) OPBI powder (B) 3.75 wt% OPBI-FA gel dried using guest solvent, (C) TEM micrograph of 2% (w/v) OPBI-FA gel and (D) SEM micrograph of OPBI-FA gel dried by direct evaporation of FA (3.75 wt%). The I.V. of OPBI sample used here is 2.3 dL/g.*

The frequency sweep experiments from DMA of the OPBI gel in FA has been carried out to confirm the physical gel nature of the OPBI membrane obtained from FA which will also provide us the support for the above network morphology. Figure 4.2 shows the dependence of storage modulus (E') and loss modulus (E'') on frequency (angular). Both the moduli are parallel over the range of angular frequency region and the magnitude of storage modulus is more than loss modulus which suggests the elastic nature of gel rather than the viscous nature. Both E' and E'' values are in the order of MPa suggesting very strong mechanical stability of the membrane. Higher E' than E'' and both the moduli parallel to the angular frequency attribute the physical gel structure

and hence OPBI-FA gel is a physical gel. Hence our morphological and rheological studies clearly prove that OPBI form physical gel in formic acid medium and the gel have fibrillar network structure.

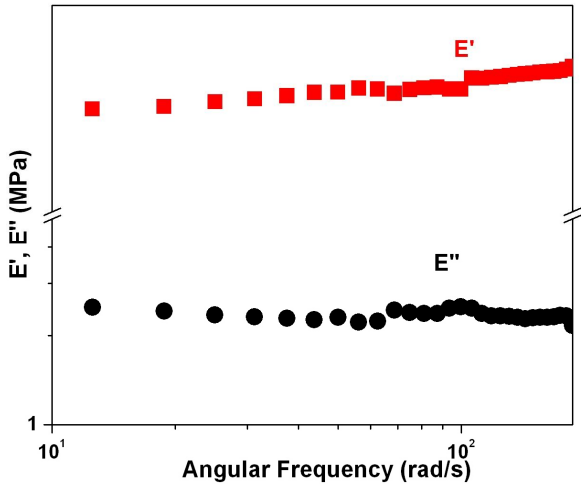

Figure 4.2. *Dependency of moduli on frequency as obtained from DMA: The membrane is obtained from OPBI gel in FA. I.V. of polymer is 2.3 dL/g. The gelation concentration is 2%.*

We also observed that this physical gel can be transformed to homogeneous solution by heating the gel and again transforms to the gel state by cooling the homogeneous solutions. We noticed that this process is reversible, very fast and takes place at 39-49ºC temperatures, which are much lower than FA boiling point. This observation indicates the thermoreversible nature of the gel. We have carried out the DSC studies (Figure 4.3) of the gel and found out that indeed this gel is thermoreversible in nature and shows reversible endothermic and exothermic first order phase transition during heating and cooling cycles, respectively (Figure 4.3).

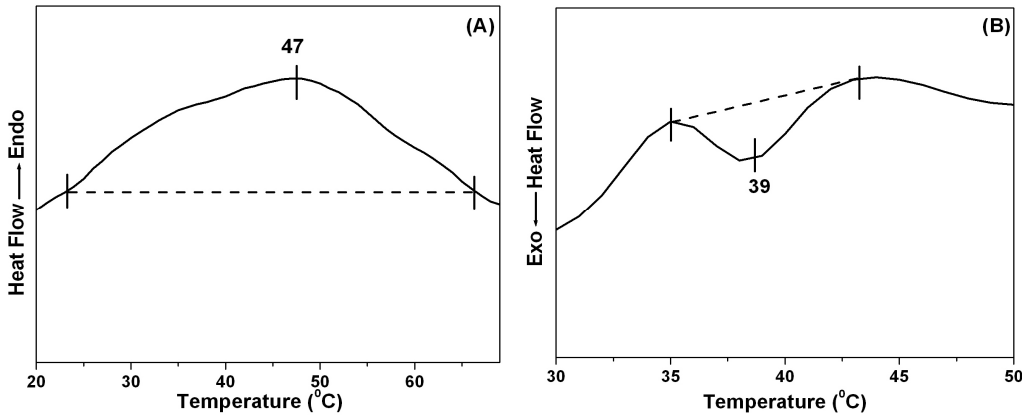

Figure 4.3. *DSC thermogramms of OPBI – FA gel (A) Heating, (B) Cooling.*

4.3.1. Gelation Kinetics

The kinetics of gelation is an important tool to understand the mechanism of gelation. The test tube tilting method for measuring gelation kinetics can only be used if the kinetics is reasonably fast. As mentioned in the experimental section, the current gelation is fast enough to apply this test tube tilting method. The apparent gelation rate (t_{gel}^{-1}) is obtained from the reciprocal of the gelation time (t_{gel})[43,44] which is the time required for the polymer solutions to form the gels. Figure 4.4 shows how the gelation rate (t_{gel}^{-1}) varies with the change in OPBI concentrations (w/v) in FA at different temperatures. There is a non-linear variation of gelation rate (t_{gel}^{-1}) with gelation concentration at different temperatures. Therefore the gelation rate (t_{gel}^{-1}) is a combination of temperature and concentration functions.

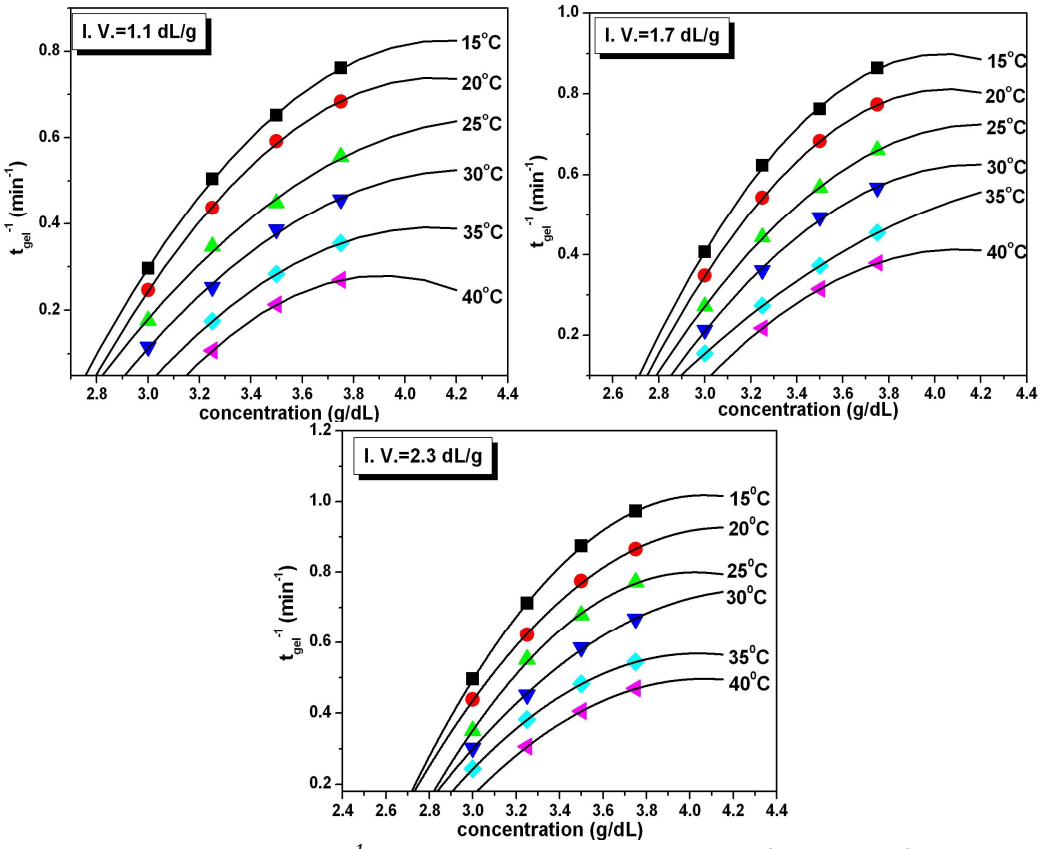

Figure 4.4. *Gelation rate (t_{gel}^{-1}) vs. concentration (g/dL) plots of gelation of OPBI in FA for different I.V. samples at various gelation temperatures.*

A minute observation of Figure 4.4 also indicates the dependency of t_{gel}^{-1} upon the molecular weight of the sample. To check this dependency carefully, we have compared the gelation kinetics data at each gelation temperature for different IV samples as shown in Figure 4.5. From this comparison it is seen that the rate of gelation increases or the time required for the gelation at the particular temperature decreases with increasing the molecular weight (IV) of the OPBI. Therefore, the rate of gelation is not only the function of concentration and temperature, but it is also the function of molecular weight of the polymer.

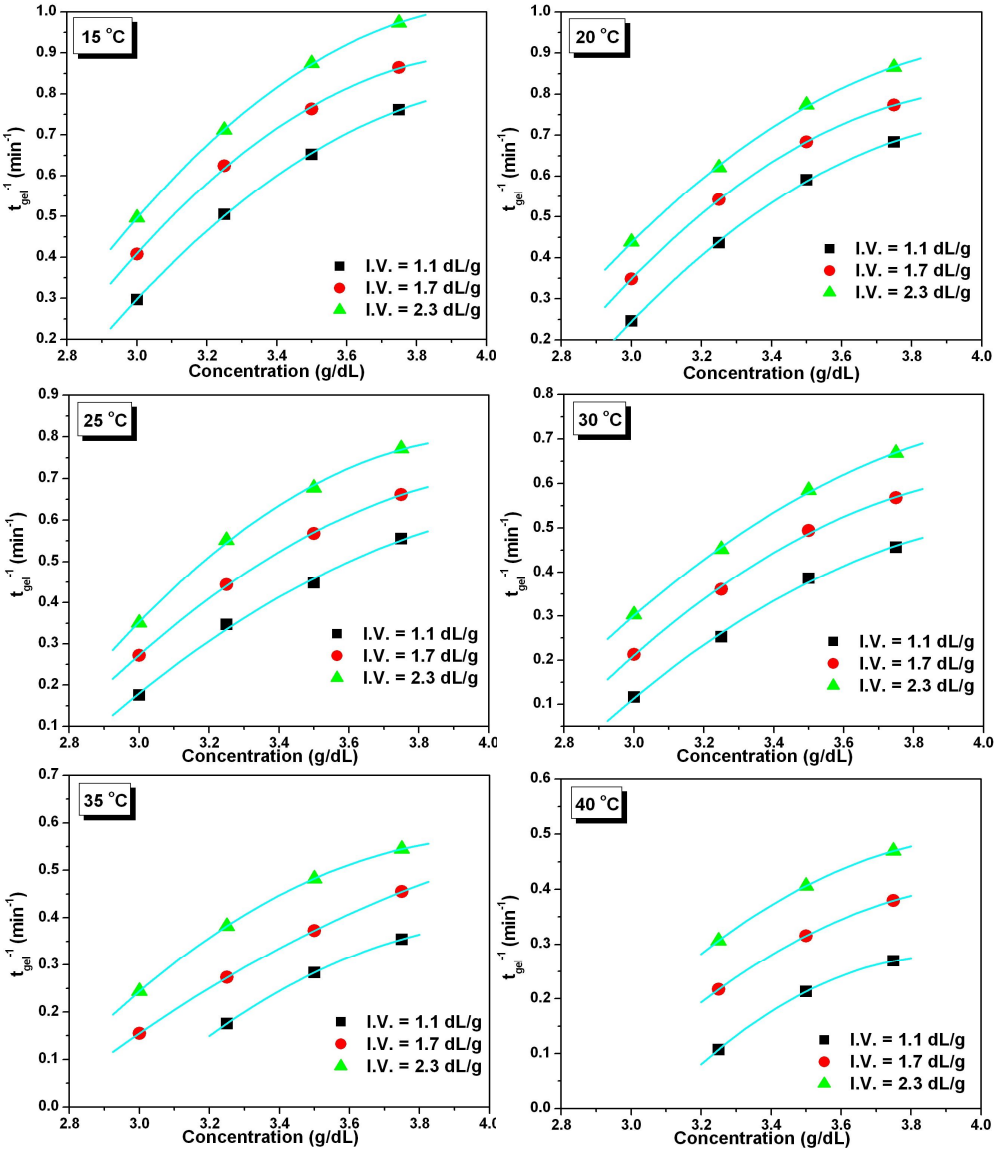

Figure 4.5. *Influence of I.V. (molecular weight) on gelation kinetics of OPBI polymer at different temperature.*

The critical gelation concentrations ($C^*_{t=\infty}$), concentration of OPBI in FA below which gelation is not observed, are obtained by extrapolating each curve (Figure 4.4) to the zero gelation rate. The values of critical gelation concentrations are tabulated in Table 4.1 and plotted in Figure 4.6 to demonstrate the effect of the temperature and I.V. (molecular weight) of the OPBI on the critical gelation temperatures.

Table 4.1. *$C^*_{t=\infty}$ obtained for different molecular weights (I.V.) OPBI polymers at different temperatures from the Figure 4.4.*

I.V.(dL/g)	Critical gelation concentration $C^*_{t=\infty}$ (g /dL)					
	15°C	20°C	25°C	30°C	35°C	40°C
1.1	2.765	2.796	2.823	2.91	3.037	3.151
1.7	2.714	2.754	2.795	2.856	2.896	3.023
2.3	2.71	2.73	2.78	2.83	2.857	3.012

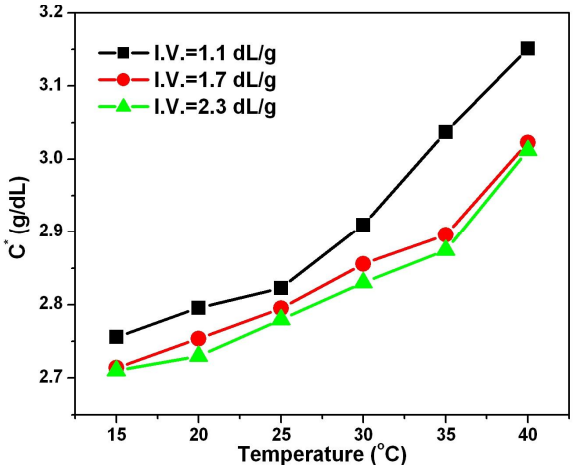

Figure 4.6. *Critical gelation concentration versus temperature plot of OPBI gel obtained from test tube tilting method.*

Therefore, it can be concluded from the Table 4.1 and Figure 4.6 that the critical gelation concentration is the function of temperature and IV (molecular weight of the samples). The above observations demonstrate that the higher molecular weight samples form the gel readily with higher rate of formation. This is due to the size of the molecule since higher I.V. samples are bigger in size, hence they produce gel readily. Figure 4.4 and 4.6 suggest that higher I.V. OPBI sample has lower critical gelation concentration ($C^*_{t=\infty}$) than the low I.V. OPBI and $C^*_{t=\infty}$ varies with temperature. Critical gelation concentration ($C^*_{t=\infty}$) suggests that the higher IV polymer chains (fibrils) are overlap with each other to form dence crosslinking more easily compare to low IV polymer to produce gels at similar kinetics condition.

The information about the heat of formation of crosslinking or overlapping of the polymer chains (fibrils) can be easily understood by plotting log $C^*_{t=\infty}$ vs. 1/T using the following equation as proposed earlier by Eldridge and Ferry.[48,49]

$$\log C^* = \frac{\Delta H^o}{2.303RT_{gel}} + \text{Constant} \qquad (4.2)$$

Where, ΔH^o is the heat of reaction for the gelation process to produce 1 mol of crosslinking in the gel. We have calculated the values of ΔH^o for different I.V. samples from the slopes of log $C^*_{t=\infty}$ vs. $1/T_{gel}$ plots (Figure 4.7).

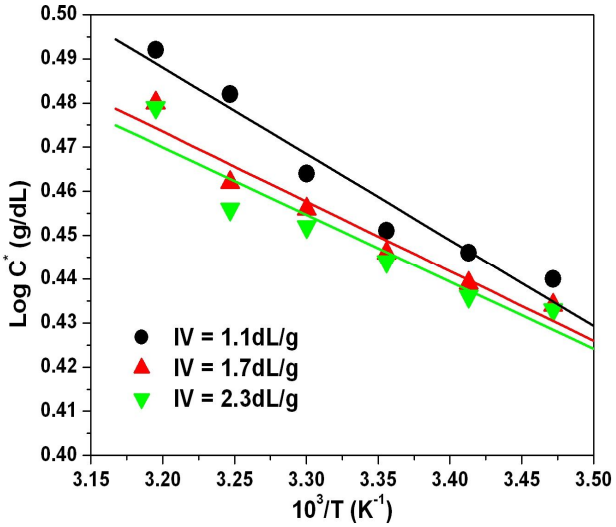

Figure 4.7. *log $C^*_{t=\infty}$ vs. $1/T_{gel}$ plots for OPBI gels in FA. Different straight lines are obtained for the indicated I.V. of the OPBI samples.*

From Figure 4.7, the negative slope of the curves indicates the exothermic nature of the crosslinking to produce fibrillar network. The values of heat of reactions (ΔH°s) are 18.1, 18.3 and 18.6 kJ mol^{-1} for I.V. = 1.1, 1.7, 2.3 dL/g, respectively and are plotted in Figure 4.8 as a function of molecular weight (I.V.).

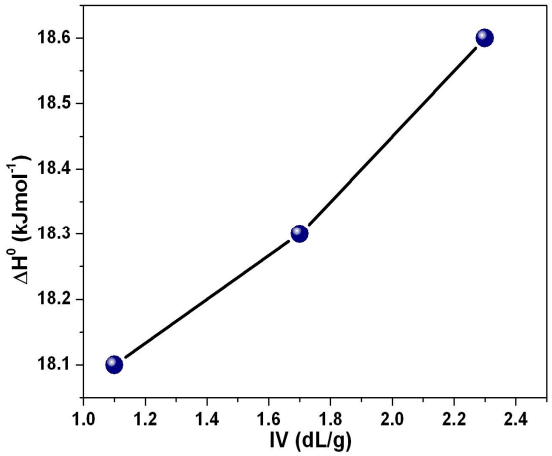

Figure 4.8. *Variation of ΔH^o with the molecular weight (I.V.) of OPBI polymers in FA gel.*

Although the dependency of ΔH^o on I.V. is not much, however, it is clear from the Figure 4.8 that ΔH^o values are increasing with increasing the molecular weight (I.V.) of the polymer. Therefore, the heat of reaction (ΔH^o) values is dependent upon the molecular weight (I.V.) of the polymer, attributing that higher heat of reaction involves for higher molecular weight (I.V.) OPBI. Since OPBI gel crystallites act as most important points of physical junction in these gelation processes, the higher amount of energy is required to produce the crosslinking junction for higher I.V. polymers.

4.3.2. Morphological Investigation

The kinetics study clearly suggests that the morphological feature (inter connected fibrillar network) of the dried OPBI gel has dependency upon the concentration and molecular weight (I.V.) of the OPBI. Because of these, all the parameters of the (network density, length, thickness, number) interconnected fibrils will be changing with concentration and molecular weight (I.V.). Figure 4.9 shows the dependency of gel morphological feature upon the OPBI concentration in the gel sample at fixed molecular weight PBI. An important change in the morphological feature is observed with changing the gelation concentration (Figure 4.9). A careful comparison of the SEM micrographs brings the following observations with increasing gelation

concentrations: increase in number of fibrils, decrease of fibrils thickness, and increase in fibrils length and most importantly significant increase in fibrillar network density (number of fibrils crossing each other per unit area). Also we have noticed that at higher concentration the gels are very stable and the time required for the gelation is very small (discussed previously in the gelation kinetics). An estimation of network density using the *imageJ* software results the density values of the different micrographs as (A) 55, (B) 69, (C) 49, and (D) 58 cross-linked fibrils per unit area of the micrographs. This clearly indicates network density varies with the gelation concentration. Thus the morphological study attributes that the gelation concentration plays an important role for the gel formation. With increasing the polymer concentration, the more and more fibrils overlap or interconnected with each other to make high network density structure.

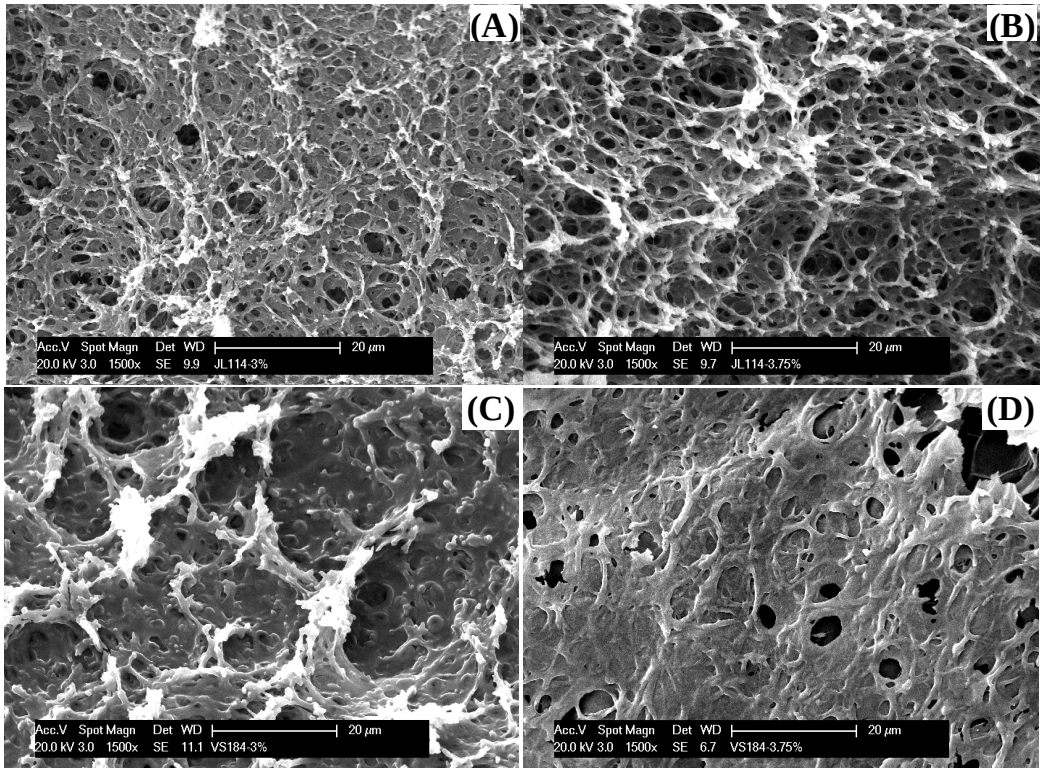

Figure 4.9. *SEM micrographs of OPBI-FA gels of various OPBI concentrations (w/v) (A) 3% and (B) 3.75% of I.V. 2.3 dL/g and (A) 3% and (B) 3.75% of I.V. 1.1 dL/g. Note that all micrographs presented here are in identical magnification (1500X).*

Figure 4.10 shows the effect of molecular weight of the PBI on the gel morphology. The gelation concentration of all the samples is kept fixed at 3.75% (w/v). The fibrils become thinner and longer with increasing molecular weight (I.V.) of OPBI. Also the network/crosslinking density of the fibrils increases with increasing molecular weight (IV) of OPBI (Figure 4.10). Therefore, for higher IV OPBI, the gelation can take place easily which also provides the explanation for the faster gelation rate and lower $C^*_{t=\infty}$ for higher IV OPBI. The calculated network density using *imageJ* software are as follows (A) 56, (B) 63, and (C) 69 cross-linked fibrils per unit area for 1.1, 1.7, and 2.3 dL/g OPBIs, respectively; clearly prove our previous mentioned observations.

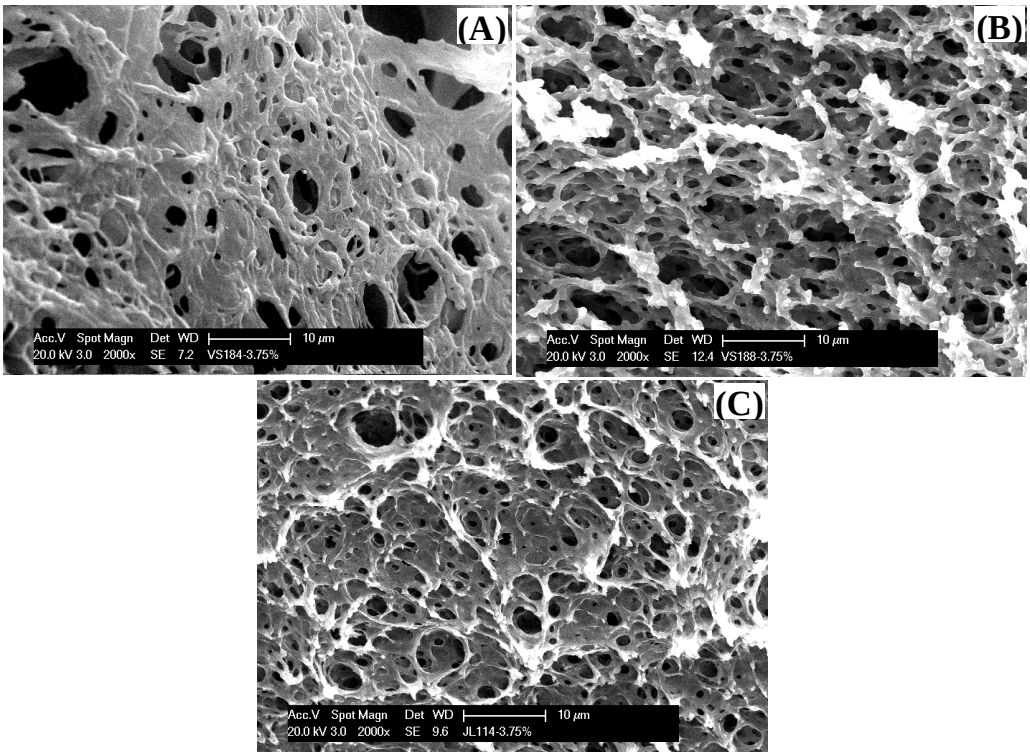

Figure 4.10. *SEM micrographs of 3.75% (w/v) OPBI-FA gels of various molecular weight (IV) OPBI (A) 1.1 dL/g, (B) 1.7 dL/g, (C) 2.03 dL/g. The magnification for the entire image is identical (2000X).*

4.3.3. Thermodynamic Study

To understand the nature of the phase transition of any types of polymer–solvent complexes, thermoreversible gel, etc., Differential Scanning Calorimetry (DSC) is an important tool. It is generally recognized that the endothermic peak appears in DSC when the system changes from the ordered state to disordered state such as melting of crystals, the transition of gel to sol, etc., and the exothermic peak in DSC appears when the system changes from disordered state to ordered state such as crystallization of gel formation, etc. These reversible transitions and the fibrillar network morphology of the gel samples provide the evidence of the thermoreversible nature of the gel.[23,43-47] The DSC thermogramms for heating and cooling scan of a series of different concentrations of the OPBI-FA gel are shown in Figure 4.11 (A) and 4.11 (B), respectively. The DSC heating and cooling thermograms for other I.V. OPBI samples are presented in Figure 4.12. All these DSC results clearly exhibit the endothermic gel melting temperature peak (T_{GM}) for the heating scan and exothermic gelation temperature peak (T_G) for the cooling scan respectively. This certainly indicates that the OPBI-FA system exhibits first-order phase transition during both heating and cooling. It is observed that the endothermic gel melting temperature for the heating scan is higher than the exothermic gelation temperature of the cooling scan. This is occurred due to hysterisis effect of the first order transitions which is commonly observed for many thermoreversible gel systems.[50] In both the cases, the observed peaks are broad in nature and this is due to the semi-crystalline nature of OPBI-FA gel. Therefore, it has been observed that the amorphous OPBI transforms into the partially crystalline in the FA medium and this is due to the strong hydrogen bonding interactions between FA and OPBI which will be discussed later with the help of FT-IR study.

The endothermic gel melting and exothermic gelation temperature and their enthalpy values are shown in Table 4.2. In all the cases, the gel melting temperature (T_{GM}) and gelation temperature (T_G) are almost similar, but the enthalpy change for T_{GM} and T_G are different for all the cases and these are depend upon the IV and the gelation concentration as well. With increasing the molecular weight of the polymer, the

enthalpy change for both the gel melting temperature and gelation temperature increases. It has been shown that the enthalpy changes for endothermic gel melting temperature (ΔH_{GM}) and exothermic gelation temperatures (ΔH_G) increase upto 3.75% and then decrease again for all the cases. The similar T_{GM} and T_G for all the cases might be due to the partial crystalline character of the physical crosslinking junction. However, the sizes of the crosslinking junction may not be the same and hence the enthalpy values alter with changing the IV and the gelation concentrations.

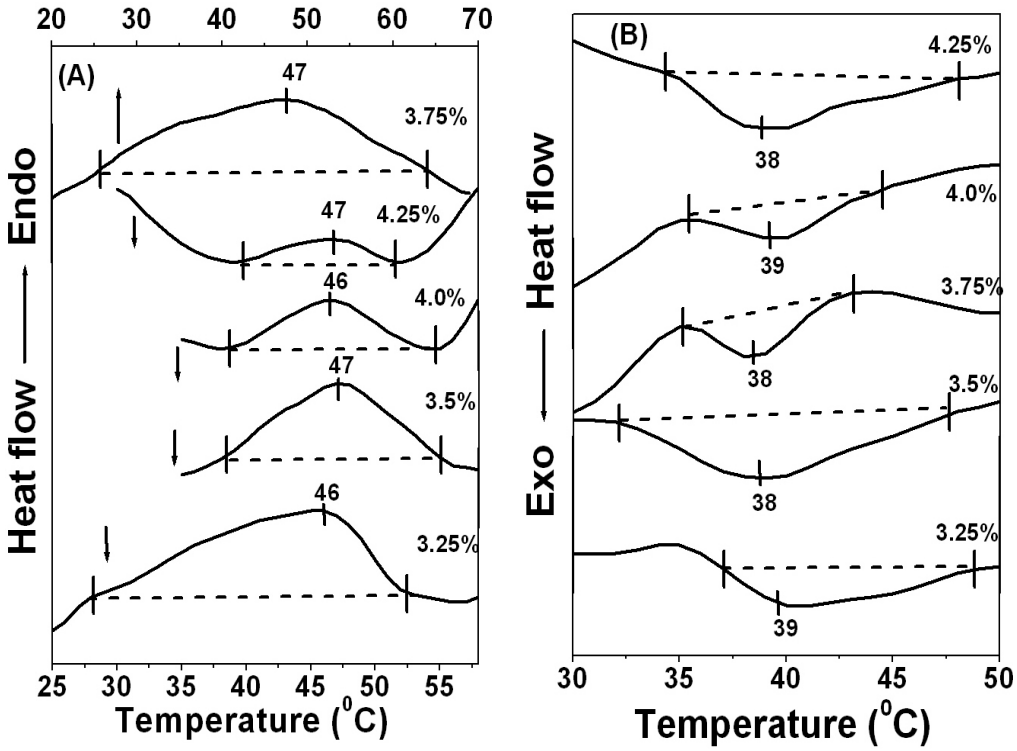

Figure 4.11. *DSC thergrams of the insitu prepapred OPBI-FA (IV = 2.3 g/dL) gel systems (A) heating scan from 10º-70ºC at the rate 10ºC/min. and (B) cooling scan from 70º-10ºC at the rate 5ºC/min.*

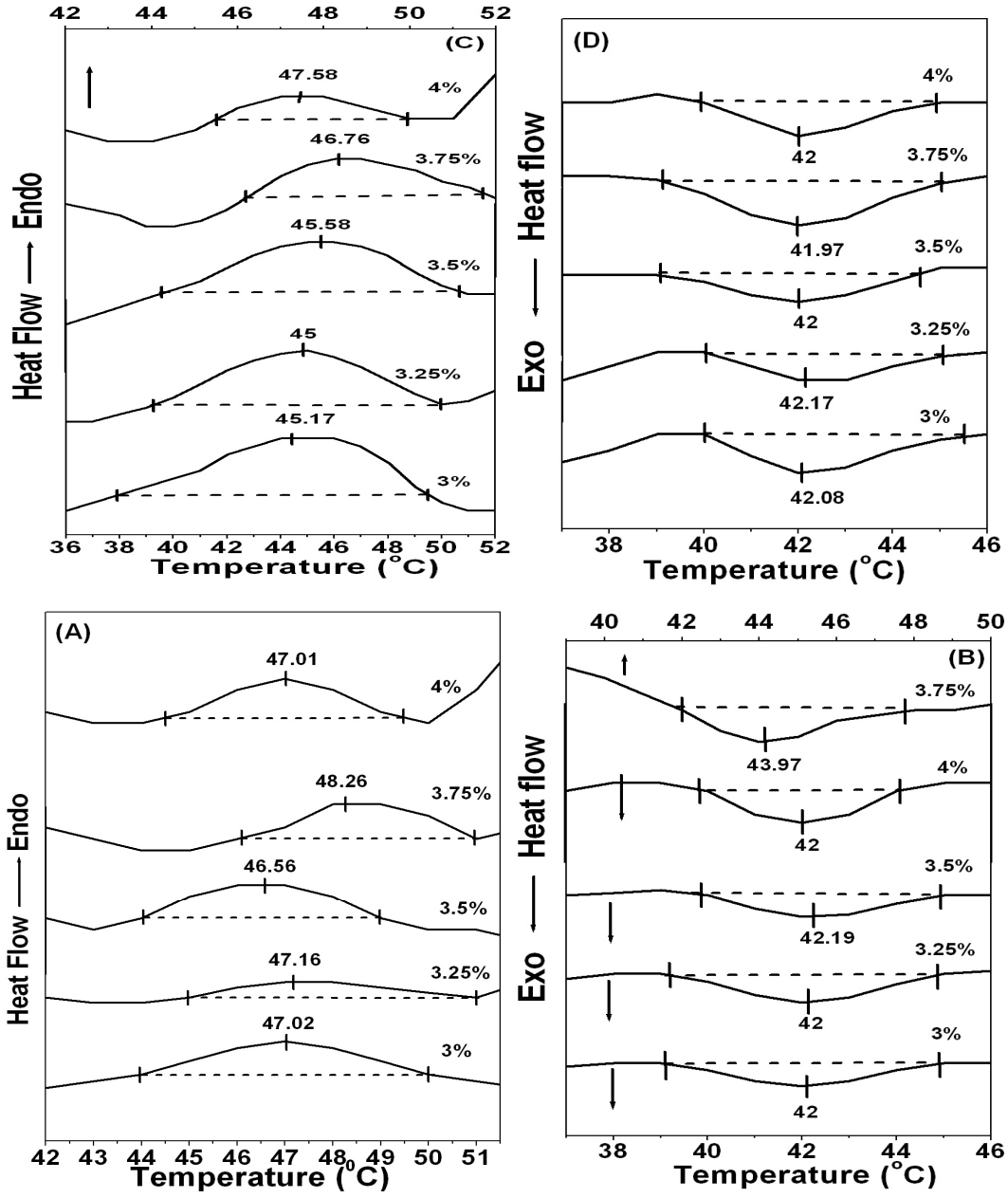

Figure 4.12. *DSC thermogramms of the insitu prepared OPBI-FA gel systems (A) and (C) heating endotherms of IV=1.1 and 1.7 dL/g, respectively and (B) and (D) cooling exotherms of IV=1.1 and 1.7 dL/g, respectively.*

Table 4.2. *Thermodynamic data obtained from the DSC experiments for various OPBI-FA gel samples.*

Concentration (W/V)	T_{GM} (°C)	ΔH_{GM} (J/g)	T_G (°C)	ΔH_G (J/g)
		I.V.=2.3 dL/g		
3.25%	45.96	0.086	39.53	-0.028
3.5%	47.068	0.0699	38.66	-0.0248
3.75%	47.43	1.0825	38.47	-0.0535
4.0%	46.36	0.0431	39.21	-0.0263
4.25%	46.99	0.0193	38.83	-0.0173
		I.V.=1.7 dL/g		
3%	45.17	0.0063	42.08	-0.0056
3.25%	45	0.0179	42.17	-0.0108
3.5%	45.58	0.0182	42	-0.0153
3.75%	46.76	0.0214	41.97	-0.0199
4%	47.58	0.0133	42	-0.0111
		I.V.=1.1 dL/g		
3%	47.02	0.0027	42	-0.0023
3.25%	47.16	0.0132	42	-0.0099
3.5%	46.56	0.0157	42.19	-0.0141
3.75%	48.26	0.0184	42	-0.0152
4%	47.01	0.011	43.97	-0.096

4.3.4. FT-IR spectroscopy

Most of the informations obtained from FT-IR study of OPBI are relied on the N-H stretching frequency region at 3500 to 3000 cm^{-1}. These region can be divided into three distinct parts as: (i) a relatively sharp peak at 3420 cm^{-1} due to isolated, non hydrogen bonded free N–H groups; (ii) a very broad asymmetric peak centered at around 3161 cm^{-1} owing to self-associated, hydrogen bonded N–H groups, and (iii) a third low intensity peak at 3063 cm^{-1} due to the stretching modes of the aromatic C-H groups. OPBI possesses both hydrogen donor (-NH-) and hydrogen acceptor (-N=) sites which can easily take part in hydrogen bonding interaction with suitable solvent molecules.[16-18,51] The FT-IR spectrum of the OPBI gel in FA and dry OPBI film are shown in Figure 4.13. The presence of hydrogen bonding in the OPBI-FA gel sample is clearly observed from the frequency shifts and peaks broadening in the IR spectra. The free N-H and hydrogen bonded N-H stretching frequency of powder OPBI at about 3420 cm^{-1} and 3161 cm^{-1}, respectively, display significant change in case of the OPBI–FA gel sample and appears as a broad single peak of 3171 cm^{-1}. The shifting of free N-

H peak towards lower frequency (from 3420 to 3171) and slight displacement of hydrogen bonded N-H peak towards higher frequency (from 3161 to 3171) attributes that the –NH group undergoes very strong hydrogen bonding with the formic acid by breaking the self-association in the OPBI chains. The band in the range of 2550– 2950 cm^{-1} due to the N^{+}–H stretching mode in case of the OPBI gel in FA which is forming because of the weak electrostatic interactions such as hydrogen bonding between the polar groups in imidazole rings and the FA. In case of OPBI film, the characteristic bands of benzimidazole were clearly observed at 1630 cm^{-1} (C=N and C=C stretching), 1460 cm^{-1} (in-plane ring vibration of 2,6-disubstituted benzimidazole), and 1300 cm^{-1} (in plane C–H deformation of 2,6-disubstituted benzimidazole).[52] But in case of OPBI gel in FA all the stretching frequency bands at lower frequency region (1550-800 cm^{-1}), present in OPBI powder, were not observed since all the ring vibrations of benzimidazole has been shielded due to presence of large quantity of FA in OPBI gel sample. The huge differences of the characteristics bands of OPBI powder and OPBI gel is due to presence of FA in OPBI gel. There is residual stretching frequency at 1720 cm^{-1} is observed in OPBI gel, suggesting the presence of carbonyl group (>C=O) which is due to formate ion (HCO_2^-) in OPBI gel. Also, the bands at 1370 cm^{-1} and 755 cm^{-1} in OPBI gel in FA are due to the characteristics stretching frequency of C–O and O=C–O^- of formate, respectively.

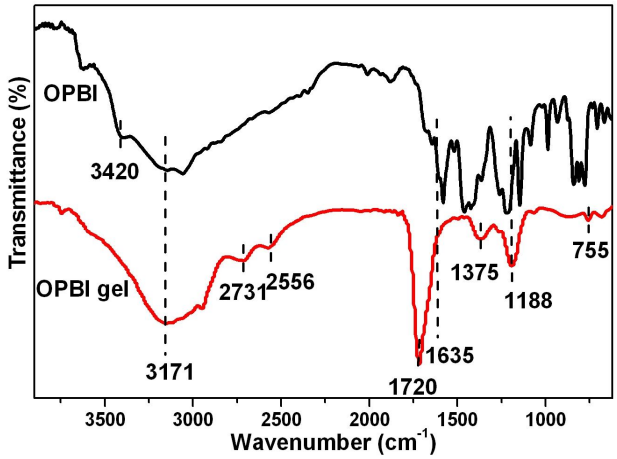

Figure 4.13. *Solvent subtracted FT-IR spectra of OPBI gel and powder sample.*

4.3.5. X-ray Diffraction Study

Figure 4.14 shows the wide-angle x-ray diffraction patters of 2.75% and 3.75% OPBI-FA gels and OPBI powder. OPBI powder has a single broad amorphous peak at ~25º, which is referred to the parallel orientation between the planes of benzimidazole rings. Therefore, there is no sharp distinct peak in case of OPBI sample, whereas on the other hand, several new strong peaks appeared in all the gel samples which were absent in the diffractogramm of the parent polymer. It is well known in the literature that OPBI is an amorphous polymer and hence display only one broad peak at 25º.[42] The 2.75 %(W/V) OPBI-FA gel sample has sharp peaks at 2θ = 20.58, 16.84, 12.68, 8.52º, and broad peak at 28.39º. For 3.75 %(W/V) OPBI-FA gel, sharp peaks appear at 2θ = 19.27, 17.08, 14.46º and broad peak appear at 2θ = 28.44º. It is important to note that the broad amorphous peak at 25º of OPBI has been shifted to the higher angle in case of the gel samples, indicating that in the gel sample the parallel orientation between the plane of the benzimidazole ring has been disturbed. The presence of diffraction peaks, shifting of amorphous peak of OPBI and more importantly alternation of peaks position depending upon the gelation concentration attributes the formation of ordered (partially crystalline) structure in the gel and this degree of ordering highly depend upon the polymer concentration in the gel. It has been observed earlier by us and other authors that the presence of polar protic solvent like FA which is entrapped inside the polymer chain network can introduce semi-crystalline nature to the OPBI polymer. The polyelectrolyte nature of the polymer in the acidic medium is found to be the driving force for the semi-crystalline nature. Earlier, we have observed that meta-structure PBI transforms to a semi-crystalline *m*-PBI in phosphoric acid (PA) medium and the semi-crystalline nature is the responsible for the formation of *m*-PBI-PA gel.[23] Generally thermoreversible gel is formed from solution as a result of the formation of a three dimensional network whose junction points consist of physical bonding. Hence, OPBI forms a three dimensional network whose junction points are crystallites which is molecularly self-associated OPBI chains through various weak interaction such as hydrogen bonding interaction with the solvent molecules. The T_{GM} and T_G obtained in DSC are the melting

and crystallizing of the crystallites in the OPBI-FA gel samples which have interconnected fibrillar morphology due to larger degree of polymer aggregation through hydrogen bonding between the -NH- of benzimidazole rings and oxygen atom of FA.

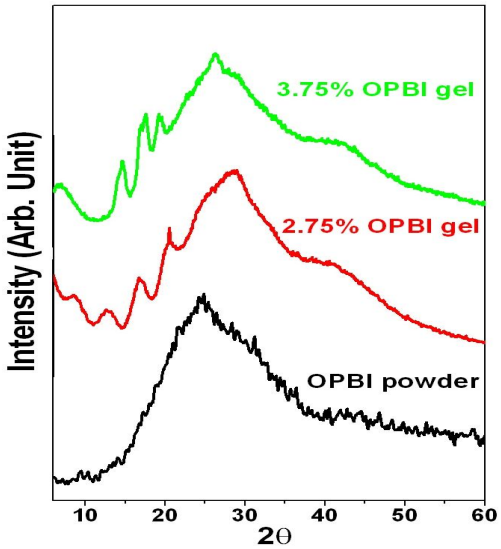

Figure 4.14. *WAXD patterns of OPBI powder, 2.75% and 3.75% OPBI gels in FA.*

However, a question still remains unanswered is "How OPBI crystallite form in FA?" Earlier, we have demonstrated that the in FA medium OPBI undergoes to an aggregated state with increasing concentration, and this aggregation process takes place without any conformational transition. Solvent (FA) swollen OPBI chains partially overlap each other due to the strong hydrogen bonding despite the intermolecular repulsion between the OPBI particles. When the OPBI concentration increased to a larger extent these aggregated OPBI particles further aggregated and results crystalline junction which drives the polymer chain to undergo nucleation and finally yield to gel state. A possible schematic model (Figure 4.15) is proposed for the formation of the semicrystalline OPBI in presence of FA and the driving force of this semicrystalline nature is due to the hydrogen bonding between the -NH- of benzimidazole rings and oxygen atom of FA. We have already proposed a possible mechanism in our last chapter how OPBI is aggregated in FA with increasing the concentration and nature of the OPBI

chains (or fibrils) in FA.[51] Also we proposed that due to polyelectrolyte nature of OPBI in FA, the swelled OPBI coils are repelled each other and with increasing concentration those polymer coils come closer to form an aggregated structure. Therefore, these coils do not show any conformational transition with increasing the concentration of OPBI in FA like our previous report which showed that polymer chains of *m*-PBI undergoes conformational transition during the gelation process.[23] In fact our efforts to monitor this conformational transition using UV-vis like our earlier report proves that there is no growth of 615 nm peak with time.[23] Probably the formate ion present in FA plays an important role to bring OPBI chains (or coils) closer. With increasing the concentration of OPBI in FA, the density of the polymer coils in FA solution is increasing and those coils crosslinked or overlapped each other to form an aggregated structure by compromising the repulsion of the charges due to polyelectrolyte nature. These aggregated structures of polymer chains produce the gel structure at gel concentration which assists to form semi-crystalline OPBI in FA. Hence in the current studies the gelation of OPBI takes place in FA without any conformational transition.

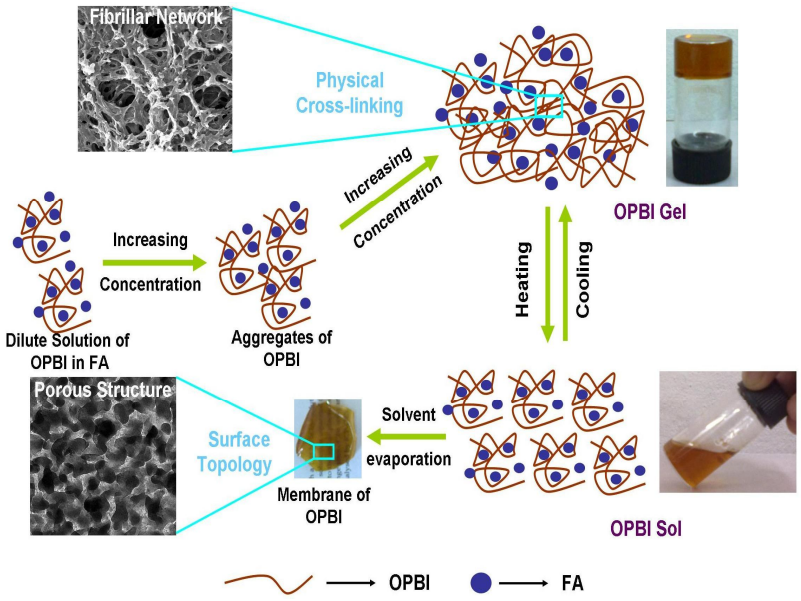

Figure 4.15. *Schematic diagram for the formation of thermoreversible gel of OPBI in FA.*

4.3.6. PA Doping Level

The fuel cell efficiency is largely dependent upon the phosphoric acid (PA) loading of the membrane. It has a huge influence on the cell performance, generally, the higher the PA loading expected to result higher the cell performance since high PA loaded membrane exhibits higher conductivity. The PA doping level of the membrane is expressed as the number of PA mols per OPBI repeat unit. The biggest challenge is to prepare a PA doped OPBI membrane with appropriate thermal and mechanically stabilities. Chemically, OPBI is a basic polymer and can readily react with a strong acid. Among various inorganic acids phosphoric acid is of special interest because of its unique proton conductivity, also under anhydrous conditions, as well as its excellent thermal stability. Several literatures have been reported by many authors about the PA loading of PBI membranes, prepared by the conventional method.[11,12,20,53] Unfortunately, it is very difficult to get all the desired properties such as high PA doping levels and high proton conductivity with high mechanical properties of the membrane simultaneously using the conventional method. From our research group we have shown that the PBI membrane made from the PBI gel in PA shows a very high PA doping level (35-40 mols PA per PBI repeat unit), high conductivity (6.60×10^{-2} S/cm) and high tensile strength (6.05 MPa). The interconnected fibrillar network structure is the driving force for the above fascinating results. Based on this observation, we hypothesized that in this case (OPBI gel in FA), if we remove the FA from the gel then it will result a porous membrane in which we will be able to load a large quantity of PA. The PA doping level of the different IV OPBI gel membranes are shown in Table 4.3. We have also included acid loading data as prepared using conventional method. The most prominent observation from Table 4.3 is that the acid loading has increased dramatically in case of the OPBI membranes obtained from FA compared to DMAc and the increase is almost three folds. Also, acid loading is highly dependent upon the OPBI concentration in the gel and slightly depends on the IV of the OPBI.

Table 4.3. *Phosphoric acid loading obtained from different percentage (w/v) OPBI-FA gel membrane.*

% Gel membrane (w/v)	*% PA (w/w)*	*% PBI (w/w)*	*% H_2O (w/w)*	*Mols of PA/PBI repeat unit*
		I.V.= 2.3 dL/g		
1%	58.09	14.59	27.52	16.379
2%	64.11	11.63	24.27	22.052
3.5%	66.59	10.26	23.16	22.589
1% DMAc	47.56	26.89	25.55	6.14
2% DMAc	49.33	28.65	22.02	7.06
		I.V.= 1.7 dL/g		
1%	59.06	14.81	26.12	17.51
2%	64.52	12.63	22.85	21.86
		I.V.= 1.1 dL/g		
1%	60.67	15.32	24.07	17.11
2%	65.57	11.64	22.84	20.52

This huge enhancement in PA loading is very important since this is obtained by simply making the membrane from FA instead of DMAc. We have demonstrated in this chapter that OPBI forms gel in FA, upon removal of solvent (FA) the gel transforms to porous structure. We have investigated the surface and cross-sectional morphology of the gel sample of several concentrations by using the SEM, TEM and AFM (Figure 4.16). We also compared the surface and cross-sectional morphology of OPBI films obtained from DMAc solution of varieties of concentrations. It is evident from the morphological feature that porous structure is formed in case of FA treated OPBI sample; whereas DMAc treated samples do not exhibit any characteristic morphology. It is important to note that the size of the porosity varies depending on the gelation concentration, attributing that the sample is multi-porous in nature. TEM pictures suggest that with increasing concentration surface morphology transforms from fibrillar to porous. AFM image and height profile support the porosity of the OPBI in FA. We believe due to this multi-porous nature of the OPBI membrane obtained from FA, it loads huge amount of PA in its pores and display very high mechanical strength! The

increase in PA loading with increase in gel concentration is simply due to the increase in number of pores or pore density for higher concentration. After a certain concentration (e.g. 2%) it saturates since pore density is also saturates.

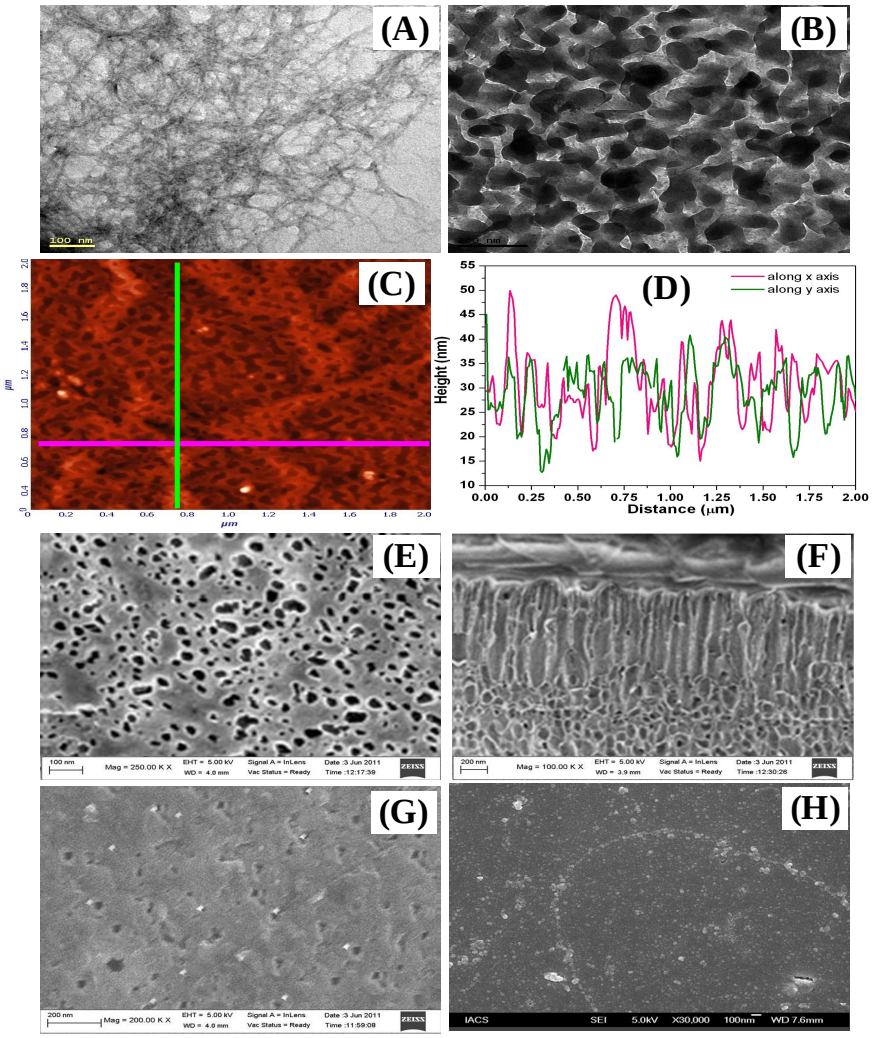

Figure 4.16. *TEM micrographs of (A) 1% (w/v), (B) 3% (w/v) OPBI membrane from FA, (C) AFM micrograph of 3% OPBI membrane from FA, (D) height profile of AFM imagewith appropriate color coding as shown in height profile, FESEM of (E) 3% (w/v) OPBI membrane, (F) cross-section of 3% (w/v) OPBI membrane, (G) 1% (w/v) OPBI membrane from FA and (H) SEM of 2% (w/v) OPBI membrane from DMAc. The IV of OPBI sample used here are 2.3 dL/g.*

4.3.7. Thermal and Mechanical Stability

Thermo gravimetric analysis (TGA) is performed to determine change in weight of the PA doped OPBI membrane with change in temperature. OPBI membrane obtained after evaporation of FA from OPBI-FA gel is scanned in TGA and the same membrane after doping in PA is also scanned in TGA. Both the samples were first preheated to 100°C for 30 minutes in the furnace to remove any moisture. Figure 4.17 shows that the polymer degradation precedes in two stages. The first stage is due to the dehydration of the moisture present in the sample and this continues up to 100°C, where the weight loss is around 5-6% for PA un-doped OPBI membrane and for PA doped OPBI membrane, the weight loss is near about 20% at 100°C followed by a continuous mass decreases due to the condensation of PO_4 units. These weight losses are in agreement with as reported by Savinell and co-workers which have deeply investigated the thermal rearrangement of phosphoric acid in doped-PBI membranes by means of TG-MS measurements.[54] A distinct weight loss can be observed around 510–530ºC for all the samples. This second weight loss is due to the degradation of the polymer backbone.

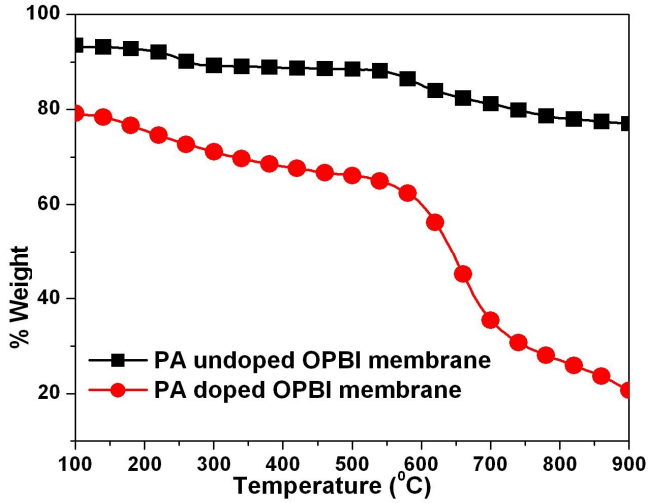

Figure 4.17. *TGA curve of the PBI-based membranes of PA un-doped and doped OPBI membranes. The OPBI membrane was obtained by evaporating the FA from the OPBI-FA gel. The IV of the OPBI sample is 2.3 dL/g.*

Now, a question arises that how long PA doped membrane is stable at temperature above 100ºC? Since long term stability (durability) above 100°C is very important for the fuel cell application. Hence, we performed isothermal heating scan (Figure 4.18) for six hours in N_2 atmosphere at 120, 160 and 180ºC for the gel membrane to check the stability and durability of the membrane. We have not found any weight loss after six hours except the initial weight loss for loosely bound water and phosphoric acids. These observations proof that our membrane has high thermal stability and durability.

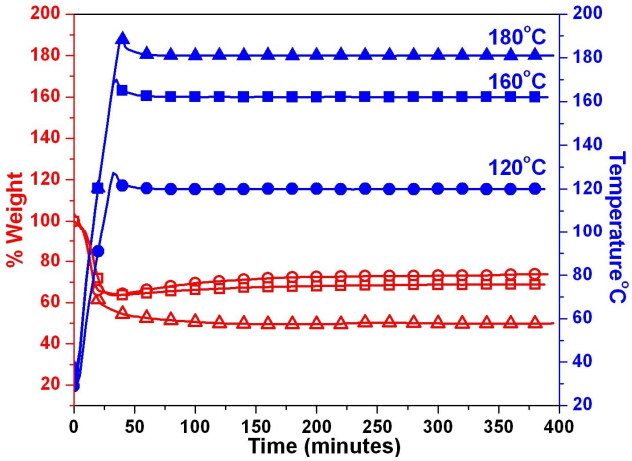

Figure 4.18. *Isothermal TGA curves of the OPBI-FA gel (2%) membrane at 120, 160 and 180°C for 6 hrs. The I.V. of OPBI is 2.3 dL/g. The open symbols represent the change in weight when kept in the corresponding temperature as shown in the figure by close symbol.*

The three dimensional interconnected crosslinked fibrils in the OPBI gel membrane have an impact on the mechanical properties of PA doped gel membrane. The membrane with very good mechanical properties is desirable for the use in operation fuel cell. Figure 4.19 represents the tensile testing plots (plot of stress against strain) for the PA doped OPBI membranes where the OPBI membranes were obtained from the FA solution. Table 4.4 tabulates the tensile data as obtained from stress-strain plots for various IV OPBI samples.

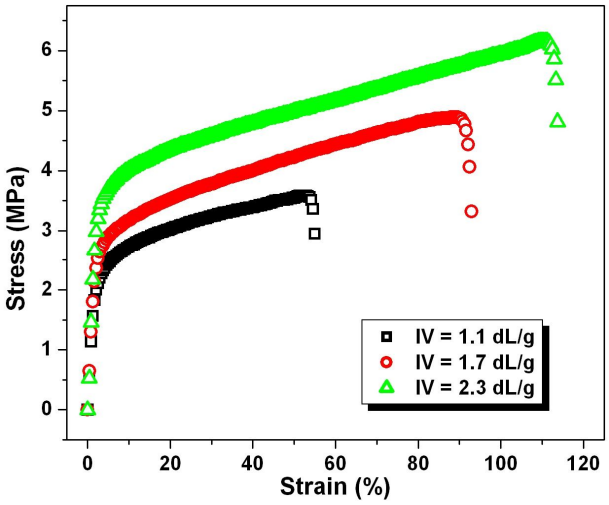

Figure 4.19. *Stress-strain plot of PA doped OPBI-FA gel (3 %) membrane for the mentioned IVs.*

Table 4.4. *Mechanical strength data obtained from stress-strain experiment.*

I.V. (dL/g)	*Yield Stress (MPa)*	*% Elongation*	*Tensile Strength (MPa)*
1.1	3.63	52.63	1.39
1.7	4.94	89.31	2.66
2.3	6.25	110.35	8.79

The data clearly indicates the good tensile strength of PA doped OPBI membrane. However it is important to note for lower I.V. samples mechanical property is not very encouraging. However, for high IV (2.3 dL/g) the tensile strength is very high, suggesting that this membrane was enough mechanical strength for the use in operating fuel cell. In fact there is no literature report where such a high tensile strength is reported for any kind of PBI which holds very high PA.

4.3.8. Conductivity Study

The proton conductivity of the membrane is particularly important since it has a significant role in the performance of the fuel cell. The proton conductivity of the PA doped OPBI membranes are measured by varying the temperature from 30ºC to 160ºC

by using a in-house built conductivity cell. Figure 4.20 shows the impedance plots as real part of impedance (*Z*') vs. imaginary part of impedance (*Z*'') of the PA doped OPBI membrane obtained from OPBI gel in FA at various temperatures and these plots are generally known as Nyquist plots. The Nyquist plots of various IV samples (IV = 1.1, 1.7, and 2.3 dL/g) are shown in Figure 4.20. The Nyquist plot has been fitted with a two component model with a resistor is parallel with a capacitor across the frequency range at all the temperatures which perfectly fit into the semicircle at all temperature. The ohmic resistance of the PA doped OPBI membrane are obtained by extracting the real part of impedance value at point where the semi-circle intersects the *Z*' axis.

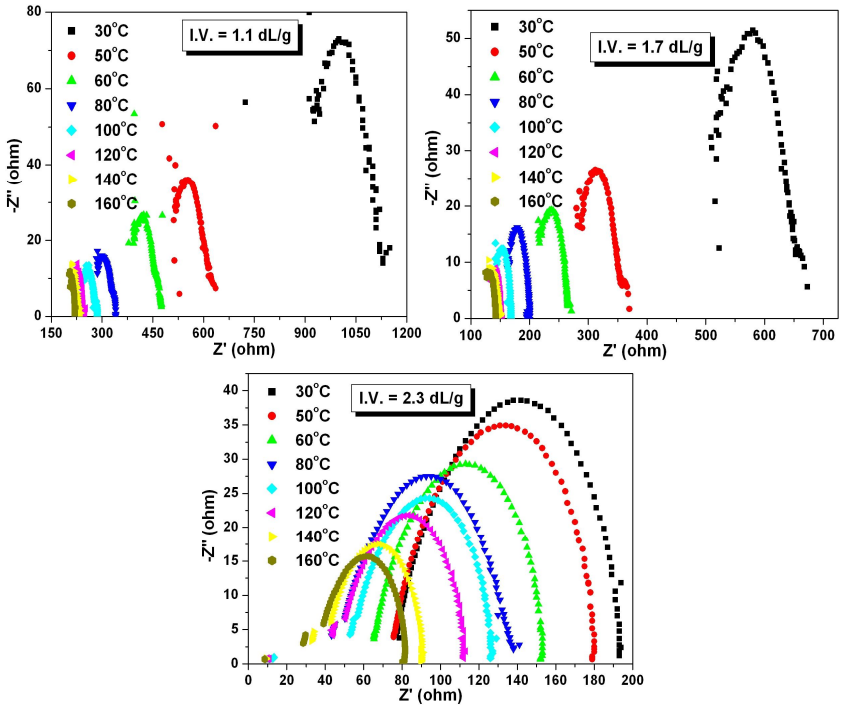

Figure 4.20. *Nyquist plots for PA doped 2% OPBI membrane in FA for the various I.V. (as indicated in the figure) OPBI samples.*

Figure 4.21 shows that the proton conductivity (σ) of PA doped OPBI membrane increases with increasing the temperature. At 160ºC, the proton conductivity of the OPBI gel membrane is 1.117×10^{-1} S.cm^{-1} for OPBI sample with IV = 2.3 dL/g. Proton conductivity increases with temperature.

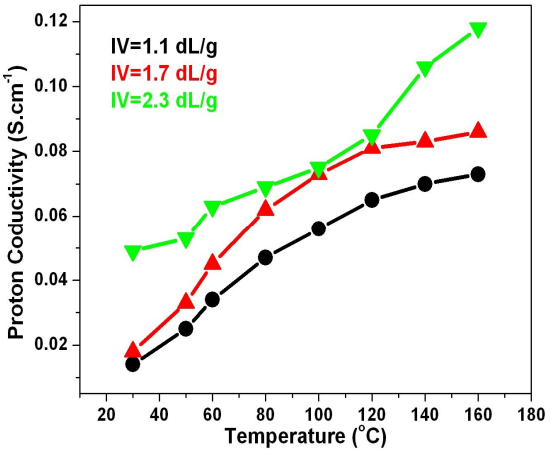

Figure 4.21. *Proton conductivities against temperature for PA doped OPBI membrane for the indicated OPBI samples. Gel concentration in all the cases were 2% (w/v).*

From the Figure 4.22, it has been shown that the proton conductivity is dependent upon the temperature and this dependency of proton conductivity on temperature is well understood by Arrhenius equation[55] which is given as:

$$\ln(\sigma T) = \ln \sigma_0 - \frac{E_a}{RT} \tag{4.3}$$

where σ is the proton conductivity of the membrane (Scm^{-1}), σ_o is the pre-exponential factor ($S\ K^{-1}\ cm^{-1}$), E_a is the proton conducting activation energy (kJ/mol), R is the ideal gas constant ($J\ mol^{-1}K^{-1}$) and T is the temperature (K). The Arrhenius plot for PA doped OPBI membrane showed a straight line, representing an Arrhenius type of proton conducting behavior. This attributes the proton hopping mechanism. The slopes of the Arrhenius plots have been used to analyze the corresponding activation energy (E_a) for the proton conduction method. The activation energy (E_a), which is the minimum energy required for proton conduction through the OPBI gel membranes, was obtained from the slope in the linear fit and is shown in Figure 4.22. The low activation energy means the proton conduction process is very fast. These values are very close to the activation energy obtained for pure H_3PO_4 system (14.29 kJ/mol) as reported in the literature.[56] Generally, E_a value for PA doped PBI ranges between from 20-40 kJ/mol

are reported in the literature depending on the PA loading. This significantly lower activation energy attributes to the presence of free H_3PO_4 and phosphates species in the membrane and these are involved in the transport process.

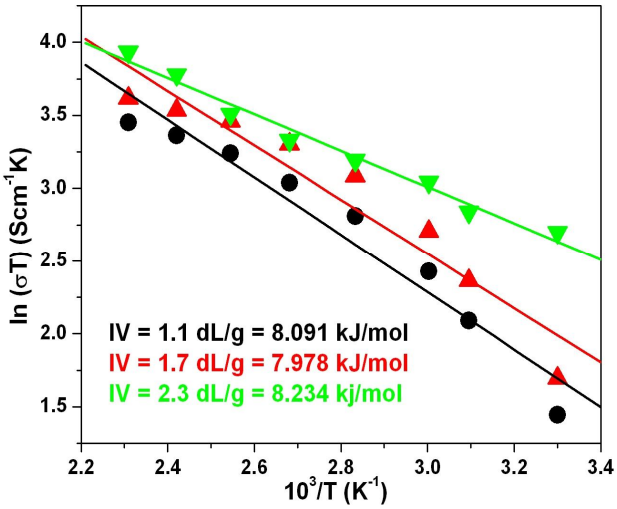

Figure 4.22. *Arrhenius plots for the proton conduction. 2% OPBI gel membrane, I.V. of OPBI are 1.1 dL/g (acid loading = 20.516 mols PA/ OPBI repeat unit), 1.7 dL/g (acid loading = 21.856 mols PA/ OPBI repeat unit) and 2.3 dL/g (acid loading = 22.589 mols PA/ OPBI repeat unit) with their corresponding activation energy values.*

4.4. Conclusion

Thermoreversible gel of OPBI in FA has been developed. Morphology of the dried OPBI-FA gel has been investigated through SEM, TEM and AFM. The physical nature of this gel has been proved by dynamic mechanical analyzer. DSC experiments indicate reversible first order phase transition. A strong hydrogen bonding interaction between OPBI and FA molecules in the gel is the driving force of the gelation and is confirmed from the FT-IR study. WAXS study proves the presence of crystallites in the gel. The gelation rate and critical gelation concentration required for the gelation depend upon the gelation temperature and the molecular weight (IV) of OPBI. The proton conduction of the PA doped OPBI gel membranes obtained from OPBI-FA gels are very high and it depends upon the surface morphology of the OPBI gel membrane.

Interestingly, the activation energies (E_a) for the proton conduction for these membranes are in the range of E_a for pure PA which also supporting the gel structure. In summary, we have developed the PA doped OPBI membrane, which has the remarkably high PA loading with best thermo mechanical stabilities and especially very high and faster proton conduction characteristics.

References

1. *Fuel Cell Handbook, 6 th. Ed*; EG & G Technical Services, Inc. U.S.: Department of Energy **2002**.
2. L. J. M. J. Blomen, "*Fuel Cell Systems*"; Plenum: New York **1993**.
3. Hickner, M. A.; Ghassemi, H.; Kim, S. Y.; Einsla, B. R.; McGrath, J. E. *Chem. Rev.* **2004**, *104*, 4587.
4. Kerres, J. *J. Membr. Sci.* **2001**, *185*, 3.
5. Gottesfeld, S.; Pafford, J. *J. Electrochem. Soc.* **1998**, *135*, 2651.
6. Yang, C.; Costamagna, P.; Srinivasan, S.; Benziger, J.; Bocarsly, A. B. *J. Power Sources* **2001**, *103*, 1.
7. Savadogo, O. *J. New Mater. Electrochem. Syst.* **1998**, *1*, 47.
8. Roziere, J.; Jones, D. J. *Annu. Rev. Mater. Res.* **2003**, *33*, 503.
9. Saxena, A.; Tripathi, B. P.; Shahi, V. K. *J. Phys. Chem. B* **2007**, *111*, 12454.
10. Cho, C. G.; Kim, Y. S.; Yu, X.; Hill, M.; McGrath, J. E. *J. Polym. Sci., Part A: Polym. Chem.* **2006**, *44*, 6007.
11. Xiao, L.; Zhang, H.; Jana, T.; Scanlon, E.; Chen, R.; Choe, E. W.; Ramanathan, L. S.; Yu, S.; Benicewicz, B. C. *Fuel Cells* **2005**, *5*, 287.
12. Xiao, L.; Zhang, H.; Scanlon, E.; Ramanathan, L. S.; Choe, E. W.; Rogers, D.; Apple, T.; Benicewicz, B. C. *Chem. Mater.* **2005**, *17*, 5328.
13. Savinell, R.; Yeager, E.; Tryk, D.; Landau, U.; Wainright, J.; Weng, D.; Lux, K.; Litt, M.; Rogers, C. *J. Electrochem. Soc.* **1994**, *141*, L46.
14. Samms, S. R.; Wsmus, S.; Savinell, R. F. *J. Electrochem. Soc.* **1996**, *143*, 1225.
15. Weng, D.; Wainright, J. S.; Landau, U.; Savinell, R. F. *J. Electrochem. Soc.* **1996**, *143*, 1260.
16. Kojima, T. *J. Polym. Sci., Polym. Phys. Ed.* **1980**, *18*, 1685.
17. Shogbon, C. B.; Brousseau, J.-L.; Zhang, H.; Benicewicz, B. C.; Akpalu, Y. *Macromolecules* **2006,** *39*, 9409.
18. Sannigrahi, A.; Arunbabu, D.; Sankar, R. M.; Jana, T. *Macromolecules* **2007**, *40*, 2844.

19. Choe, E. W.; Choe, D. D. In *Polymeric Materials Encyclopedia*; Salamone, J. C., Ed., CRC Press: New York, 1996
20. Mecerreyes, D.; Grande, H.; Miguel, O.; Ochoteco, E.; Marcilla, R.; Cantero, I.; *Chem. Mater.* **2004**, *16*, 604.
21. Mader, J.; Xiao, L.; Schmidt, T. J.; Benicewicz, B. C. *Adv. Polym. Sci.* **2008**, *216*, 63.
22. Yu, S.; Benicewicz, B. C. *Macromolecules.* **2009,** *42*, 8640.
23. Sannigrahi, A.; Arunbabu, D.; Jana, T. *Macromol. Rapid Commun.* **2006**, *27*, 1962.
24. Russo, P. S. *Reversible Polymeric Gels and Related Systems*; ACS Symposium Series, American Chemical Society: New York, **1986**.
25. Guenet, J. M. *Thermoreversible Gelation of Polymers and Biopolymers*; Academic Press: London, **1992**.
26. Sannigrahi, A.; Arunbabu, D.; Sankar, R. M.; Jana, T. *J. Phys. Chem. B* **2007**, *111*, 12124.
27. Jouanneau, J.; Mercier, R.; Gonon, L.; Gebel, G. *Macromolecules* **2007**, *40*, 983.
28. Li, Z. X.; Liu, J. H.; Yang, S. Y.; Huang, S. H.; Lu, J. D.; Pu, J. L. *J. Polym. Sci., Part A: Polym. Chem.* **2006**, *44*, 5729.
29. Chen, C. C.; Wang, L. F.; Wang, J. J.; Hsu, T. C.; Chen, C. F. *J. Mater. Sci.* **2002**, *37*, 4109.
30. Chuang, S. -W.; Hsu, S. L. -C. *J . Polym. Sci., Part A: Polym. Chem.* **2006**, *44*, 4508.
31. Qian, G.; Benicewicz, B. C. *J. Polym. Sci., Part A: Polym. Chem.* **2009**, *47*, 4064.
32. Sannigrahi, A.; Ghosh, S.; Maity, S.; Jana, T. *Polymer* **2010**, *51*, 5929.
33. Sansone M. J. *US patent* 4,898,917, **1990**.
34. Klaehn, J. R.; Luther, T. A.; Orme, C. J.; Jones, M. G.; Wertsching A. K.; Peterson E. S. *Macromolecules* **2007**, *40*, 7487.
35. Pu, H. T.; Liu, Q. Z.; Liu, G. H. *J. Membr. Sci.* **2004**, *241*, 169.
36. Li , Q.; Jensena, J. O.; Savinell, R. F.; Bjerrum, N. J. *Prog. Polym. Sci.* **2009**, 34, 449.

37. Yu, S.; Xiao, L.;Benicewicz, B. C. *Fuel Cells* **2008**, 3–4, 165.
38. Song, J. Y.; Cheng, C. L.; Wang, Y. Y.; Wan, C. C. *J. Electrochem. Soc.* **2002**, *149*, 1230.
39. Davis, S. A.; Burkett, S. L.; Mendelson, N. H.; Mann, S. *Nature* **1997**, *385*, 420.
40. Antonietti, M.; Berton, B.; Göltner, C.; Hentze, H. *Adv. Mater.* **1998**, *10*, 154.
41. Holland, B. T.; Abrams, L.; Stein, A. *J. Am. Chem. Soc.* **1999**, *121*, 4308.
42. Sannigrahi, A.; Ghosh, S.; Lalnuntluanga, J.; Jana, T. *J. Appl. Polym. Sci.* **2009**, *111*, 2194.
43. Dikshit, A. K.; Nandi, A. K. *Macromolecules* **1998**, *31*, 8886.
44. Yadav, P.; JayPrakash; Aswal, V. K.; Sastry, P. U.; Patra, A. K.; Maity, P. *J. Phys. Chem. B* **2009**, *112*, 13516.
45. Guenet, J. M, *J. Rheol.* **2000**, *44*, 947.
46. Malik, S.; Jana, T.; Nandi, A. K. *Macromolecules* **2001**, *34*, 275.
47. Dikshit, A. K.; Nandi, A. K. *Langmuir* **2001**, *17*, 3607.
48. Eldridge, J. E.; Ferry, J. D. *J. Phys. Chem.* **1954**, *58*, 992.
49. Mal. S.; Maity, P.; Nandi, A. K. *Macromolecules*, **1995**, *28*, 2371.
50. Daniel, C.; Dammer, C.; Guenet, J. M. *Polymer* **1994**, *35*, 4243.
51. Ghosh, S.; Sannigrahi, A.; Maity, S.; Jana, T. *J. Phys. Chem. B* **2010**, *114*, 3122.
52. Silverstein, R. M.; Webster, F. X. *Spectroscopic Identification of Organic compounds*; John Wiley & Sons, Inc.: New York **2002**.
53. Li, Q.; Hjuler, H. A.; Bjerrum, N. J. *J. Appl. Electrochem.* **2001**, *31*, 773.
54. Wainright, J. S.; Wang, J. T.; Savinell, R. F.; Litt, M.; Moaddel, H.; Rogers, C. *Proc. - Electrochem. Soc.* **1994**, *94*, 255.
55. He, R.; Li, Q.; Bach, A.; Jensen, J. O.; Bjerrum, N. J. *J. Membr. Sci.* **2006**, *277*, 38.
56. Ma, Y. -L.; Wainright, J. S.; Litt, M.; Savinell R. F. *J. Electrochem. Soc.* **2004**, *151*, A8.

Chapter 5

Role of Clays Structures on the Nanocomposites of Aryl Ether Linked Polybenzimidazole: Potential Membranes for the Use in Polymer Electrolyte Membrane Fuel Cell

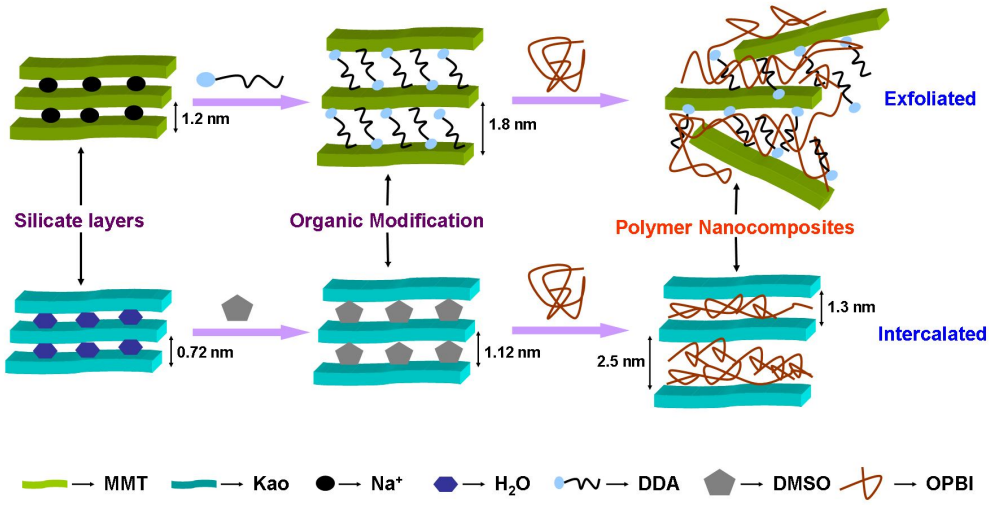

The nanocomposites of poly(4,4′-diphenylether-5,5′-bibenzimidazole) (OPBI) with two structurally different clays (MMT and Kao) were synthesized by solution blending process. The influences of incorporation of nanosized clays on the properties of OPBI were evaluated.

5.1. Introduction

In recent years polymer/layered silicate nanocomposites (PLSNs), typically of the order of a few nanometers, have attracted great interest both in industries and academics owing to the fact that they often exhibit remarkable improvement in various properties when compared with pristine polymer.[1] A large volume of reports have demonstrated that the introduction of very low percentage of layered silicates in to the polymer matrix can lead to an enormous improvement in several properties of the resulting polymer nanocomposite materials.[2-12] Intercalated or exfoliated morphologies are achieved in PLSNs depending on the degree of dispersion of the silicate layers in a polymer matrix. The favorable interactions between the layered silicate (these are often called as clay) and the polymer are the driving forces for these nanocomposites formation. A judicious choice of polymer structure and functionality along with clay structure and appropriate organic modification of layered silicates are the key factors to have favorable interactions. Montmorillonite (MMT) with 2:1 aluminosilicate smectite clay[13-15] structure and kaolinite (Kao) with 1:1 aluminosilicate Illite clay[16-18] have been used extensively for the formation of PLSNs. These clays are used because they have low cation exchange capacity and therefore do not have large amount of ionic interactions holding the clay plates together;[19] hence the silicate layers can be easily separated or delaminated. Organic modification of MMT and Kao make the hydrophilic clays into organophilic clays and more compatible with the polymers.[2,20-25] It has been observed from earlier studies that among the three techniques (in situ polymerization, solution mixing, and melt mixing) for the preparation of PLSNs the solution mixing yields better exfoliation/delamination and dispersion of layered silicates in a polymer. Solution mixing involves dispersion of the filler in an organic solvent followed by dissolution of the polymer matrix and solvent casting.[26-29]

Recently, phosphoric acid (PA)-doped polybenzimidazole (PBI) has been found to be the best polymer electrolyte membrane (PEM) for the use as a PEM in high-temperature PEM fuel cell (HTPEM-FC). There are several methods reported in the literature for the fabrication of PA-doped PBI membrane.[30-35] The biggest challenge for

the fabrication of PA-doped PBI membrane for the use in HTPEM-FC is the preparation of membrane with high acid loading so that high proton conduction can be achieved, with workable mechanical, thermal, and oxidative stabilities. However, many of these reported fabrication methods often fail to achieve high acid loading with suitable mechanical properties. Recently, our laboratory prepared the PA-doped membrane from thermoreversible PBI gel in PA where large quantity of PA solvents are entrapped inside the polymer network.[35] Although our gel method is an important breakthrough for the fabrication of PA-doped PBI membranes, but it has few disadvantages like large scale preparation, leaching out of PA from the membrane with time and more especially the gel formation is very specific to PBI backbone structure not all the PBI forms gel in PA. Therefore, invention of a new method for the fabrication of PA-doped PBI membrane with high acid loading and superb thermomechanical stability remains a challenge. Hence, we hypothesize that the formation of nanostructure with clay might adequately resolve the problems associated with existing methods and results novel PA-doped PBI membrane.

In this study, we have chosen poly(4,4'-diphenylether-5,5'-bibenzimidazole) (OPBI; Scheme 3.1B) as polymer and organically modified MMT (OMMT) and Kao (OKao) as layer silicate components for the preparation of PLSNs. The attractions to opt the OPBI among the various other available PBI structures are readily tunable molecular weight, relatively more flexible backbone due to ether linkage in the backbone compared to other PBI structure[36] as shown in chapter 2 and better solubility in low boiling point volatile solvents such as formic acid.[37] Since pristine OPBI membrane has poor oxidative stability, moderate thermal and mechanical stabilities, higher water uptake, and pathetic acid loading (doping level) capacity compared to other PBI structure, it offers us an opportunity to demonstrate the remarkable improvement of the above properties of OPBI upon formation of nanocomposites with layered silicates (clays). We have chosen two structurally different clays to see the effect of the clay structures on the morphologies and properties of the final resulting PLSNs.

5.2. Experimental Section

5.2.1. Materials

3,3´,4,4´- tetraaminobiphenyl (TAB, polymer grade), 4,4´-oxybis (benzoic acid) (OBA), polyphosphoric acid (PPA, 115 %), montmorillonite (MMT) and kaolinite (Kao) were purchased from Sigma-Aldrich. Dimethyl sulfoxide (DMSO) and formic acid (99%) were purchased from Qualigens, India. Dodecylamine (DDA) was purchased from SRL, India. All chemicals were used as received.

5.2.2. OPBI Synthesis

The synthesis of OPBI was carried out by as per our method reported previously,[36] in short: equal mols of TAB and OBA were taken into three-neck round bottom flask along with polyphosphoric acid (PPA). The reaction mixture was stirred by using a mechanical overhead stirrer and slow stream of purged nitrogen gas was maintained throughout the reaction. The polymerization was carried out at 190-220°C for approximately 26 hours. The OPBI polymer was isolated, neutralized with sodium bicarbonate, washed thoroughly with water and finally dried in vacuum oven for 48 hours at 100°C. The dried polymer was characterized by measuring the viscosity in concentrated sulfuric acid (98%) by using a Cannon Ubbelohde capillary dilution viscometer (model F725). The synthesized OPBI has an inherent viscosity (IV) value of 2.29 dL/g at 30°C. The concentration of the polymer solution for the viscosity measurement was 0.2 g/dL.

5.2.3. Modification of Montmorillonite with Dodecylamine

Organophilic montmorillonite was prepared using alkyl ammonium salts according to the reported methods as described earlier.[20,21] Dodecyl ammonium chloride solution was prepared by reacting dodecylamine (DDA) with hydrochloric acid. The mixture of DDA and HCl was stirred at 80°C until a clear solution was obtained indicating the formation of dodecyl ammonium chloride. To this solution, a suspension

of MMT in distilled water was added; the mixture was mechanically stirred at 80°C for 5 hours. The obtained white precipitate was obtained and collected by filtration and then washed by hot water to remove salt. This process was repeated several times until no chloride was detected in the filtrate by 0.1 (*N*) $AgNO_3$. The resultant precipitate was dried in vacuum oven at 100°C for 3 days, and collected as white powder. The modified MMT was termed as OMMT.

5.2.4. Modification of Kaolinite with DMSO

Kaolinite was modified by treating in solution with various organic solvents as described earlier.[22,23] Kao and DMSO were added into a bottom-flask and the mixture was ultrasonicated for 2 hours to enhance the dispersion of Kao. Then this suspension was stirred for 4 days at 80°C. At last, the solution was filtrated and washed with methanol. The resultant precipitate was dried in vacuum oven at 100°C for 3 days and collected as white powder. The modified Kao was termed as OKao.

5.2.5. Preparation of OPBI/Organoclays (OMMT and OKao) Nanocomposite Membranes

OPBI/OMMT and OPBI/OKao nanocomposites with 3, 5, 7 wt % OMMT and OKao loading with respect to OPBI weight were prepared as follows: required amount of OMMT and OKao were dispersed in 10 ml of formic acid (FA) at room temperature under vigorous stirring for 1 h and then added to the OPBI solution which was already prepared by dissolving 0.2 g of OPBI in 10 mL FA (2 wt% solution). Then the mixtures (OPBI and organoclays) were vigorously stirred overnight to make a homogeneous solution. The solutions were cast onto a petridish, slowly evaporate the FA solvent at 70°C under the airflow and then dried in a vacuum oven at 80°C for 24 h to remove the traces amount of solvent. The thicknesses of the OPBI/OMMT and OPBI/OKao nanocomposite membranes were approximately 40 (±5) μm. The overall process for the formation of nanocomposites is schematically described as shown in Scheme 5.1. The nanocomposite membranes are homogeneous and transparent indicating the well dispersion of organically modified clay inside polymer matrix. We have also made and

effort to prepare the nanocomposite with unmodified clay which produces non-homogeneous, opaque films where clays are phase separated from the polymer (Figure 5.1). Hence, the organic modification of clay is absolutely necessary to prepare the PLSNs.

Figure 5.1. *Photographs of OPBI film, OPBI/modified clay and the OPBI/unmodified clay nanocomposite films.*

5.2.6. Doping of OPBI and Its Nanocomposite Membranes with Phosphoric acid (PA)

The dried OPBI and OPBI/clay nanocomposite membranes with the above mentioned loading of organoclays made from FA were immersed into PA (85%) for 7 days to get free standing PA doped membranes.

5.2.7. Spectral Characterization

The FT-IR spectra of the OPBI and its nanocomposite films were recorded on a FT-IR spectrometer (Nicolet 5700 FT-IR). The infrared spectra were obtained in the region 3900-450 cm^{-1}. Solid state ^{13}C cross polarization magic angle spinning (CPMAS) NMR spectra were obtained on a Bruker AV 400 MHz NMR instrument operating at 100 MHz at a spinning rate of 5 KHz and a contact time of 2 ms.

5.2.8. X-ray Study

X-ray diffraction was used in this study to investigate the structure of the OPBI nanocomposites, specifically the basal spacing or the inter-gallery spacing of the clay. XRD is enable to measure the changes into the clay galleries spacing that occur to the clay due to the intercalation or exfoliation of the polybenzimidazole. The small angle X-ray diffraction (SAXD) experiment of the OPBI film and its nanocomposites with both the organoclays were carried out on a Hecus (S3-Micro System) X-ray diffractometer with Cu Kα radiation (λ = 1.5418 Å) source operated at voltage of 50 kV and 1 mA current and Wide angle Xray diffraction (WAXD) patterns of the samples were performed with an X-ray generator (Model PW 1729, Philips) with Cu Kα radiation (λ = 1.5418 Å) source operated at voltage of 40 kV and 30 mA current.

5.2.9. Morphology

The distributions of both the clay particles into the polymer matrix were examined by transmission electron microscope (TEM) and atomic force microscope (AFM). For TEM study, a drop OPBI/clay nanocomposite samples, prepared from FA was placed on a carbon coated copper (200 mesh) grid, dried and observed through the TEM instrument (FEI Tecnai Model No. 2083) operating at 200kV. For AFM study, a small portion of nanocomposite samples (thin films) were fixed on a glass substrate for recording the micrographs in semicontact mode in AFM apparatus (Model: Solver Pro M of NTMDT). A microcantilever with a spring constant of 10 N/m was used to scan the samples.

5.2.10. Thermal Measurement

Thermogravimeteric analysis was carried out to elucidate thermal decomposition behavior. The thermogravimetric analysis of OPBI film and its nanocomposites films with both the organoclays were carried out on a (Netzsch STA 409PC) TG-DTA instrument from 50 to 800°C with a scanning rate of 10° deg/min in the presence of nitrogen flow.

5.2.11. Dynamic Mechanical Study

Dynamic mechanical analyses (DMA) of OPBI/OMMT and OPBI/OKao nanocomposite membranes were carried out using a TA Instrument Dynamic Mechanical Analyzer (DMA) Q800. The storage modulus, loss modulus, and tan δ were measured at a heating rate of 4°Cmin^{-1} in nitrogen under a preload force of 0.01N at a frequency of 10 Hz. The samples were annealed at 400°C for 30 min, then kept at 100°C isothermally for 20 min inside the DMA machine, and finally scanned from 100 to 400°C at a heating rate of 4°C/min.

5.2.12. Oxidative Stability

The stability of all the nanocomposite membranes to oxidation was investigated by immersing the membranes into Fenton's reagent (30 ppm $FeSO_4$ in 30% H_2O_2) at 70°C. The oxidative stability was characterized by the expanded time variation up to 100 hours. The membranes were taken out at certain time intervals, dried in vacuum oven at 80°C overnight, and weights were recorded. The oxidative stabilities of all the membranes were calculated as a weight remained after taking out the membranes from the Fenton's reagent.

5.2.13. PA Doping Level

The PA doping level of PA doped OPBI nanocomposite membranes with both the organoclays was determined by titrating of a preweighed piece of membrane sample using standardized sodium hydroxide solution with a Metrohm Titrino Titrator. The acid doping levels, expressed as mols of phosphoric acid per mol of PBI repeat unit, were calculated from the equation:

$$\text{Acid doping level} = \frac{V_{NaOH} C_{NaOH}}{W_{dry}} M_w \qquad (5.1)$$

Where, V_{NaOH} and C_{NaOH} are the volume and the molar concentration of the sodium hydroxide, while W_{dry} is the dry polymer membrane weight and M_w is the molecular weight of the polymer repeat unit, respectively. The acid doping level reported here are

the average values obtained from three separate values, measured from three similar size membrane samples.

5.2.14. Conductivity Study

Proton conductivities of all the acid loaded nanocomposites membranes of OPBI were measured with a four-point probe technique. The impedance of the membrane was measured with an impedance analyzer by using a Zahner Impedance spectrometer (ZENNIUM PP211) over a frequency range from 1 Hz to 100 kHz. The rectangular shape acid loaded membranes were mounted onto a homemade teflon conductivity cell. The membranes were dried at 100°C by heating and holding at 100°C isothermally for 2 hours to remove the water from the membrane. The membrane samples were then cooled in a vacuum oven and taken out just before conductivity measurement in an effort to keep the samples dry. The conductivities of the membranes were measured from room temperature to 160°C at 20°C intervals. The samples were kept for 30 minutes in each temperature before the impedance measurement. The conductivity was calculated with the following equation:

$$\sigma = \frac{D}{RBL} \tag{5.2}$$

where, σ is the proton conductivity (S/cm), D is the distance between the electrodes, and B and L are the thickness and width of the membrane samples, respectively. In all cases, R is the measured resistance values which were obtained Nyquist plots.

5.3. Result and Discussions

5.3.1. FT-IR Study

The FT-IR spectra of MMT, OMMT, Kao and OKao are shown in the Figure 5.2. In case of MMT the peaks at around 3422 cm^{-1} and 3242 cm^{-1} are recognized as stretching vibrations of free N-H and hydrogen bonded N-H respectively, and the peak at around 2930 cm^{-1} is attributed to the asymmetric or symmetric stretching vibrations

of C-H of the alkyl ammonium cation. The absorption peak at around 1450 cm^{-1} is due to the in plane bending vibration (scissoring) of methylene (-CH-) group.[38] The appearance of all these peaks in OMMT sample indicating that the dodecylammonium molecules has replaced the alkali metal cation into the galleries of the silicate layers of OMMT. Appearance of the absorption band 3500 cm^{-1} is due the intercalation of dimethyl sulfoxide (DMSO) molecule inside the galleries of silicate layers of kaolinite.[39]

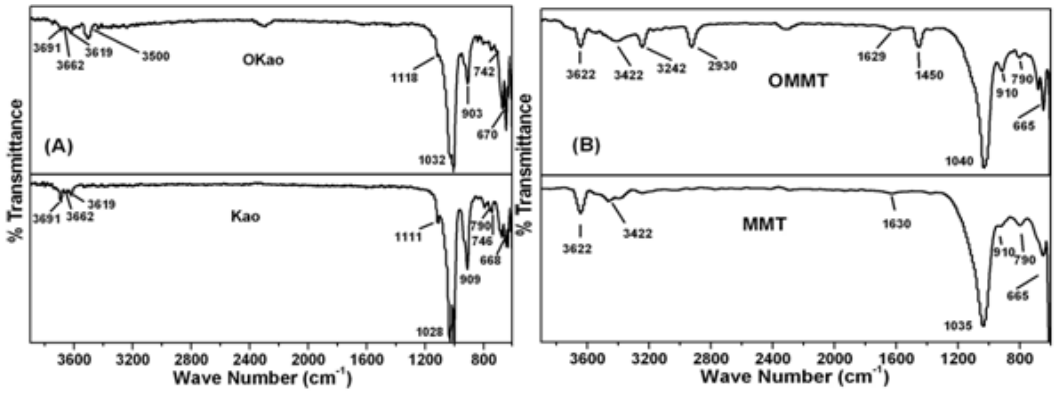

Figure 5.2. *FT-IR spectra of (A) Kao and OKao and (B) MMT and OMMT. All the stretching bands are shown in the figure.*

Figure 5.3 shows the FT-IR spectra of OPBI/OMMT and OPBI/OKao nanocomposites. In both the nanocomposite cases, a peak in the region 1020-1030 cm^{-1} develops gradually along with the other peaks of OPBI with the increasing in clay loading. This peak corresponds to the O-Si-O stretching vibration and with increasing the percentage of nanoclay loading, the intensity of this peak increases for both the nanocomposite systems. Therefore, these results support that the nanocomposites of OPBI with OMMT and OKao have been successfully prepared.

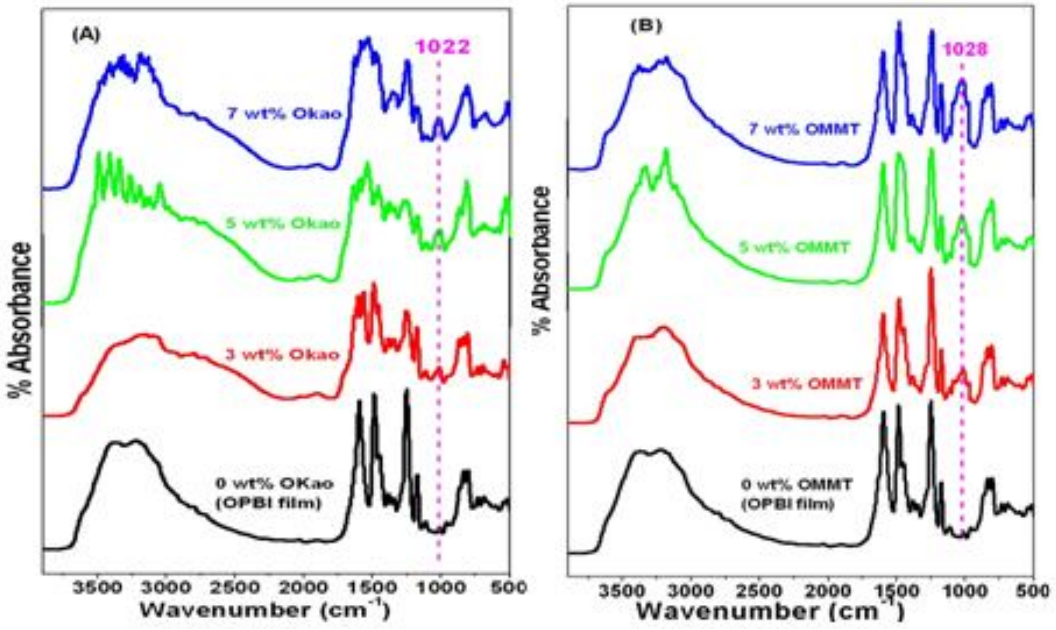

Figure 5.3. *FT-IR spectra of OPBI and its nanocomposite membranes with different percentage loading of (A) OKao and (B) OMMT. The development of O-Si-O peak is shown with dotted line.*

5.3.2. X-ray study

The Small angle X-ray diffraction (SAXD) technique has been used extensively to determine the structure of the nanocomposites; whether the polymer matrixes is intercalated or exfoliated inside the silicate layers and also evaluate how much expansion has occurred of the basal spacing of silicate layer due to the formation of nanocomposites.[40,41] The SAXD patterns of both the OPBI nanocomposites with OMMT and OKao are presented in Figure 5.4. The X-ray patters of the unmodified clays, modified clays and the OPBI are also shown along with the nanocomposites in the Figure 5.4 for the comparison. The Basal spacing (gallery distance between the clay layers) of the unmodified Kao is 0.72 nm[42] (2θ = 12.2°, q = 0.87 Å^{-1}, Figure 5.5) which has increased to 1.12 nm (2θ = 7.9°, q = 0.56 Å^{-1}) after the modification of Kao with the DMSO (Figure 5.4 A). Similarly, the basal spacing of MMT has increased from 1.2 nm (2θ = 7.2°, q = 0.52 Å^{-1}) to 1.8 nm (2θ = 4.9°, q = 0.35 Å^{-1}) after the organic

modification of MMT with the help of dodecylammonium cation (Figure 5.4 B). These increments of clay gallery spacing in both the cases are in well agreement with the previously reported values.[40-43]

From Figure 5.4 (A), it is clear that the characteristic sharp peak of the OKao at $2\theta = 7.9°$ ($d = 1.12$ nm, $q = 0.56$ Å^{-1}) has shifted to lower angle regions at $2\theta = 6.2°$ ($d = 1.38$, $q = 0.45$ Å^{-1}) and 3.57° ($d = 2.54$ nm, $q = 0.25$ Å^{-1}) in case of OPBI-OKao nanocomposites due to the increase in the Basal spacing of OKao. This attributes the formation of intercalated structure of OPBI/Kao nanocomposites in which OPBI chains are intercalated (inserted) between the OKao gallery spacing. In addition it is important to note that the sharp diffraction peak of OKao becomes broad in nature in case of OPBI/OKao nanocomposite. This observation also implies the formation of intercalated structure. The presence of two Basal spacing, broadness, and the low intensity of the peaks in the case of OPBI/OKao nanocomposites is due to variety of nanostructures in the nanocomposite, and also the crystalline nature of the silicate layers is affected due the nanocomposite formation. Although the layer spacing increases, there still exists an attractive force between the silicate layers to stack them in an ordered structure. On the other hand, no peaks are observed in the case of OPBI/OMMT nanocomposites (Figure 5.4 B) which implies the formation of exfoliated structures due to loss of the structural patterns of the silicate layers (OMMT), which is completely dispersed in the OPBI matrix. Hence the above study demonstrates that the two different types of nanocomposites are obtained from the same polymer by varying the clay structure (Scheme 5.1). This attributes that the interaction between OPBI and clay must be depending on the clay structure which is the driving force to determine the final morphologies of the nanocomposites.

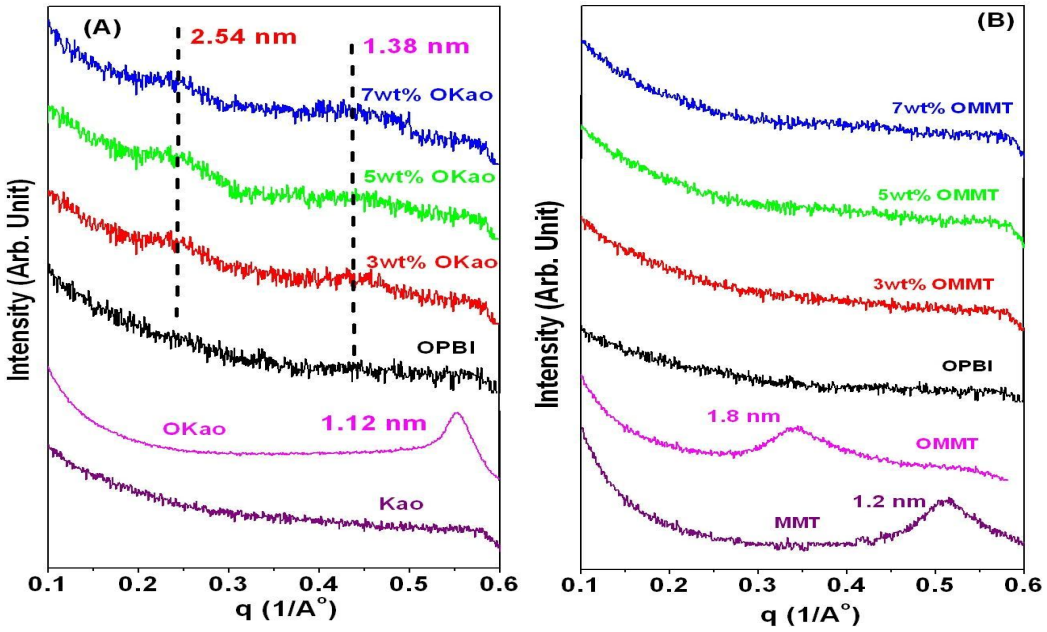

Figure 5.4. *SAXD patterns of OPBI and its nanocomposites with different percentage loadings of (A) OKao and (B) OMMT.*

The wide-angle X-ray diffraction (WAXD) measurement between 5 and 60° was applied to observe the crystalline structure of nanocomposites. Figure 5.5 shows WAXD patterns of OPBI/OKao and OPBI/OMMT nanocomposites. The diffractograms of the OKao and OMMT in Figure 5.5 have very intense, characteristic crystalline peaks, indicating that both the organic modified clays are highly crystalline. The XRD pattern of OPBI usually displays broad peaks attributing the amorphous structure of polymer. In addition to the amorphous broad peaks of OPBI, several crystalline sharp peaks were observed for the OPBI nanocomposites with both organoclays (Figure 5.5). The intensity of these peaks increased with increasing organoclay loading in the OPBI. These diffractograms in Figure 5.5 emerge to specify that all the peak intensities of all the OPBI nanocomposites reduces to a large extent as well as broad compared with the intensity of both the organically modified clays. Several other peaks of both the organoclays in Figure 5.5 (A) and (B) have not been observed in the case of OPBI nanocomposites. This is either because the homogeneous dispersion of the organoclays

in the OPBI matrix breaks of the clay aggregated structures and hence looses its crystalline nature or because of the low percentage of organoclays in the OPBI matrix. It is also proved from this WAXD that nanosized organoclays have very little influence on the amorphous structure of the polymer matrix.

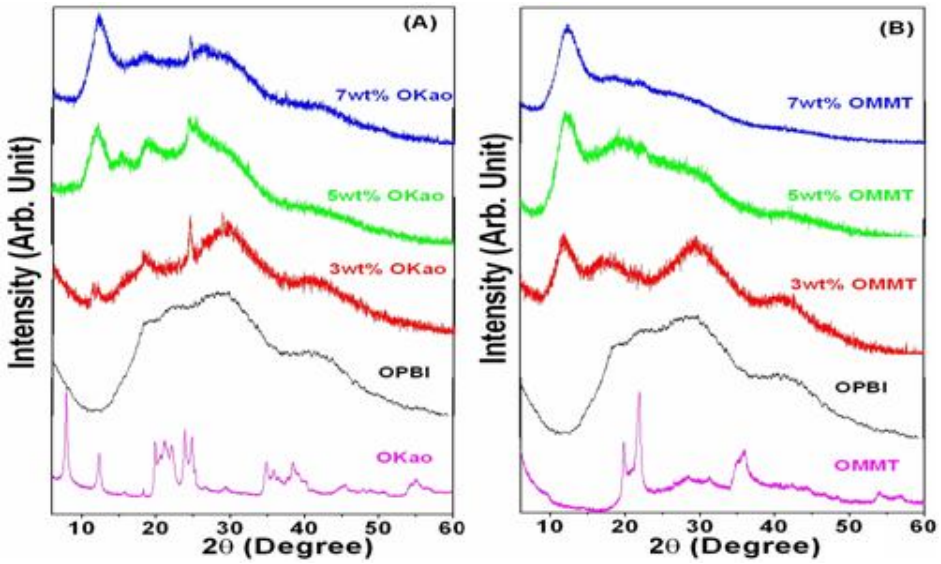

Figure 5.5. *WAXD patterns of OPBI and its nanocomposites with different percentage loadings of (A) OKao and (B) OMMT.*

5.3.3. Morphology Study

TEM can provide useful information in a localized area on the morphology structure, and spatial distribution of the dispersed phase of the nanocomposites.[44,45] XRD, FT-IR studies, and NMR discussed in the previous sections demonstrated the presence of detailed interactions between the OPBI matrix and both the organoclays, which aligns with the intercalated structure of OPBI with OKao and exfoliated structure with OMMT. The TEM images of OPBI nanocomposites with 3 and 7 wt % loading of both the organoclays (OKao and OMMT) are presented in Figure 5.6. It is observed that OPBI nanocomposites show intercalated structure with OKao (Figure 5.6 A and B) and yield exfoliated structures with OMMT (Figure 5.6 C and D). The homogeneous dispersion of the silicate layers along the polymer matrix is increasing with increasing

the percentage loading of both the organoclays. These above studies are well agreement with our SAXD pattern. The inset pictures of Figure 5.6 A and B clearly show that the basal spacings are 1.3 and 2.5 nm which we have also obtained from SAXD pattern presented in Figure 5.4 A. The incorporation of the OPBI chains inside the silicate layers of the organoclays might have diminished the parallel arrangement of the silicate layers of OMMT clay, but in the case of OKao the parallel arrangement of silicate layers could not be separated due to the strong cohesive energy of the kaolinite layer compare to that of MMT layer.

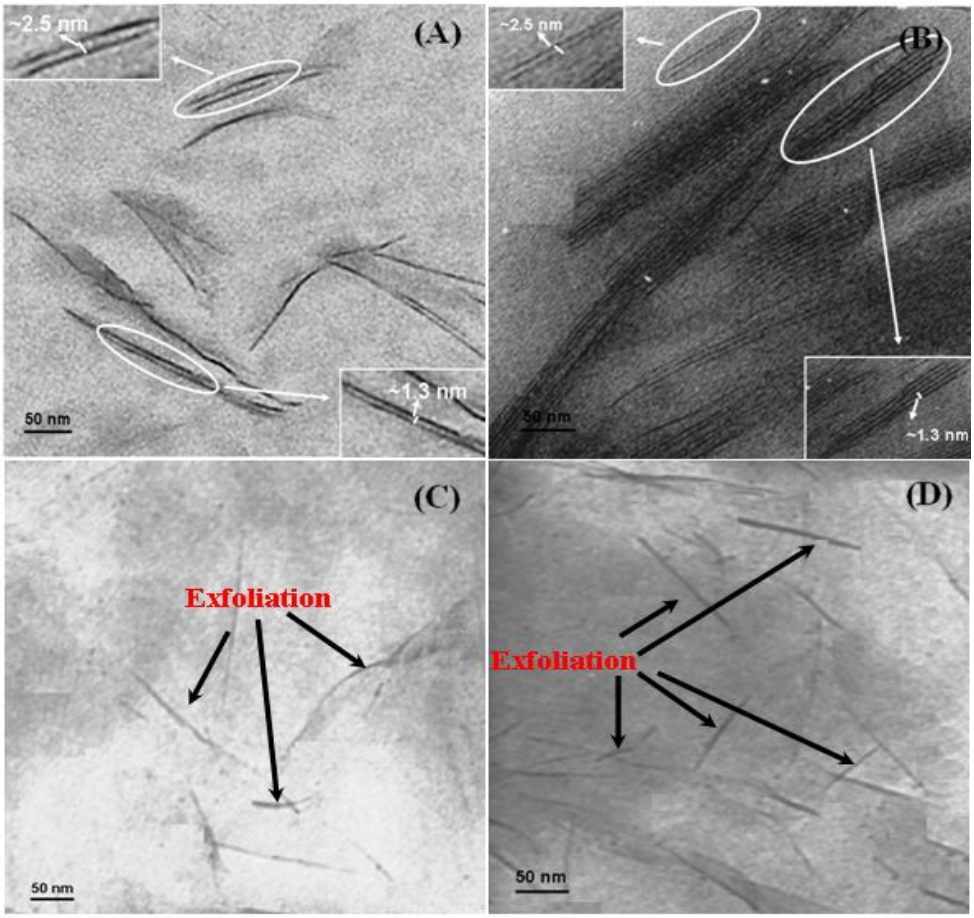

Figure 5.6. *TEM images of (A) 3% OPBI/OKao, (B) 7% OPBI/OKao (inset: magnified images of intercalation), (C) 3% OPBI/OMMT, and (B) 7% OPBI/OMMT nanocomposites prepared by solution blending method.*

The surface morphology of the polymer nanocomposite was imaged using the of atomic force microscopy (AFM) technique operating in semicontact mode. Figure 5.7 shows the AFM images of the OPBI nanocomposites containing 7 wt % loading of both the organoclays (OKao and OMMT). From the AFM images, it is clear that both the organoclays (OKao and OMMT) are uniformly distributed in the OPBI matrix. AFM images also support our observations obtained from TEM and SAXD studies. We have represented the above observations schematically in Scheme 5.1 to illustrate the role of clay structures on the resulting nanocomposites structures and morphology.

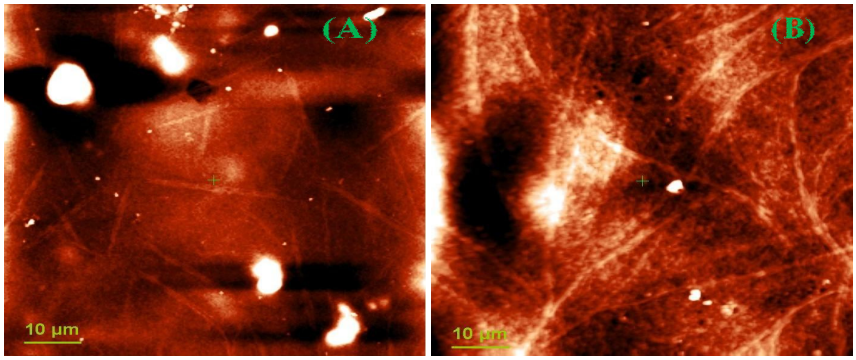

Figure 5.7. *AFM images of the OPBI nanocomposites (A) OMMT and (B) OKao. The percentage loading of both the clays is 7 wt%.*

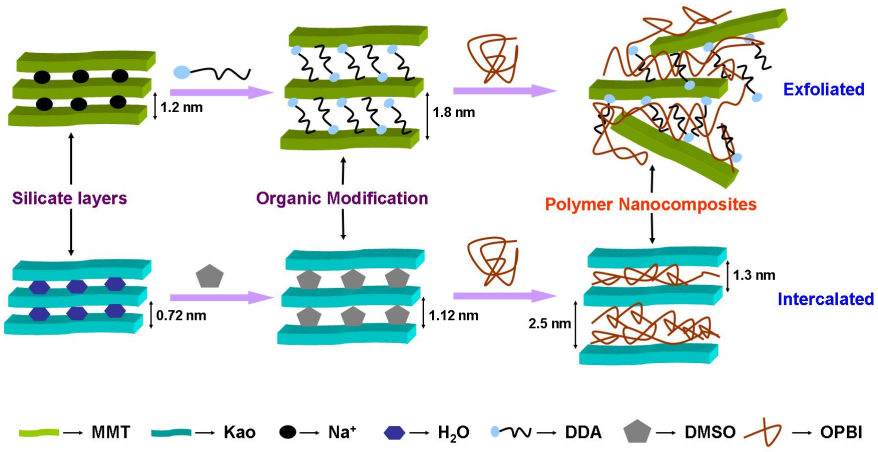

Scheme 5.1. *Schematic representation of OPBI nanocomposites with the organoclays.*

5.3.4 Solid-State NMR Study

The ^{13}C CPMAS NMR spectra of the OPBI, OPBI/OMMT, and OPBI/OKao nanocomposites are given in Figure 5.8. The spectrum of OPBI consists of several lines that can be recognized in order of increasing magnetic field as lines arising from the carbons of imidazole rings attached to phenylene rings (151 ppm), the carbons connecting benzimidazole rings in the bibenzimidazole system (142 ppm), and the aromatic carbons bound to the nitrogen atoms (134 ppm). The three remaining lines (129, 120, and 111 ppm) have also been assigned.

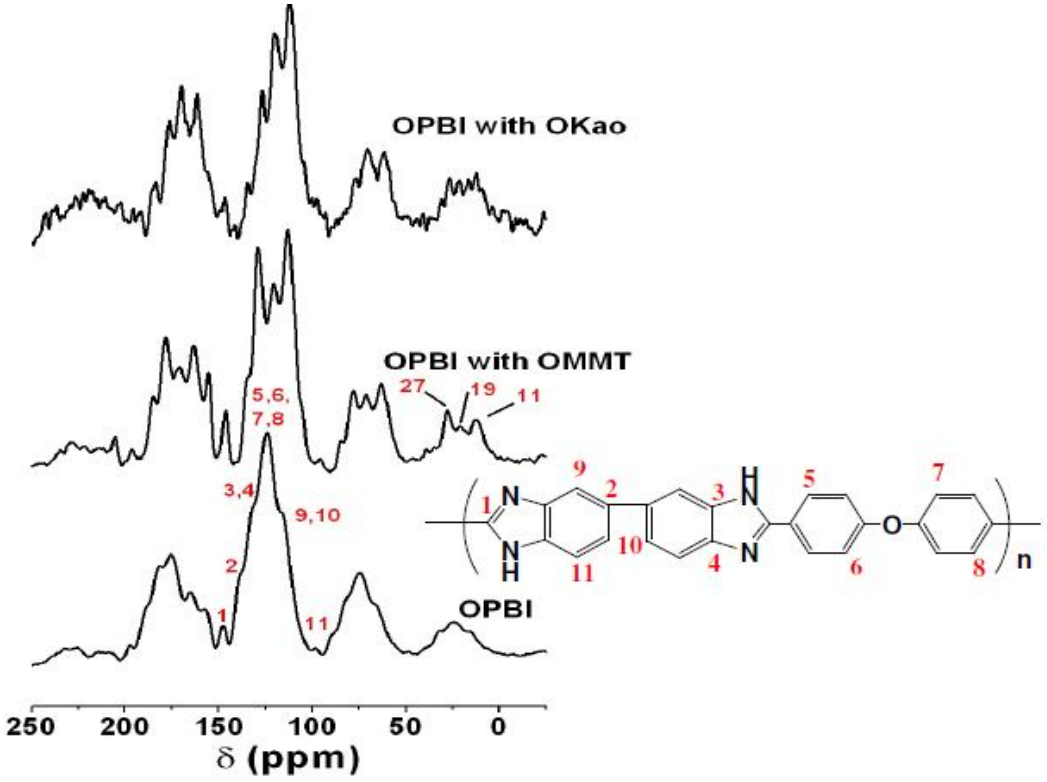

Figure 5.8. *Solid-state 13C CPMAS NMR spectra for OPBI, OPBI/OMMT, and OPBI/OKao nanocomposites. The percentage loading of both clays is 7 wt %.*

The DMSO-intercalated Kao (OKao) shows ^{13}C resonances at 43.9 and 42.8 ppm which are completely gone in the case of the OPBI/OKao nanocomposites, indicating the complete displacement of the DMSO molecules by OPBI or in the other

words the OPBI become intercalated into the silicate layers of Kao.[42] Earlier it was shown[43] that the dodecyl ammonium modified MMT shows three ^{13}C resonances at 16, 23, and 33 ppm corresponding to $–CH_3$, $(–CH_2)_{10}$, and $–CH_2NH_3^+$ groups, respectively. These peaks have been shifted to the higher field at 11, 19, and 27 ppm in the case of the OPBI/OMMT nanocomposites (Figure 5.8), indicating the strong interaction between OPBI and OMMT. The presence of these peaks of dodecyl ammonium cation attributes that OPBI is not intercalated in the clay layer; rather it is exfoliated into the silicate layers of OMMT.

5.3.5. TGA Study

It is observed from the TGA plots shown in the Figure 5.9 that a 10% mass loss was observed between 125 and 800°C for pure MMT and a one step mass loss at 450°C in case of kaolinite, while two-step mass loss is observed at 125 and 380°C in the case of OMMT and 180 and 500°C in the case of OKao. The difference in the mass losses between them is probably due to the presence of different organic modifiers.

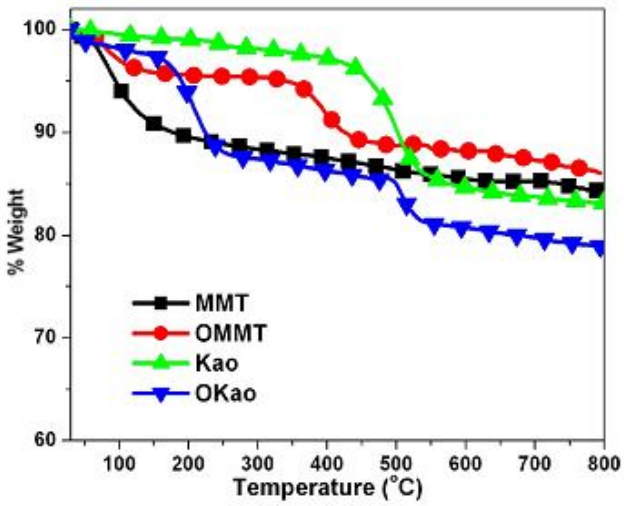

Figure 5.9. *TGA plots of both the clays and organic modified clays.*

Often, the structure and morphology of the nanocomposites affects the thermal stability of the resulting materials and play important roles for enhancing the thermal stability

with the loading of nanofillers.[2-5] The thermal stabilities of OPBI film and nanocomposites containing 3, 5, and 7 wt % of both OMMT and OKao in nitrogen environments are studied. The TGA traces of the OPBI film and its nanocomposite samples are shown in Figure 5.10.

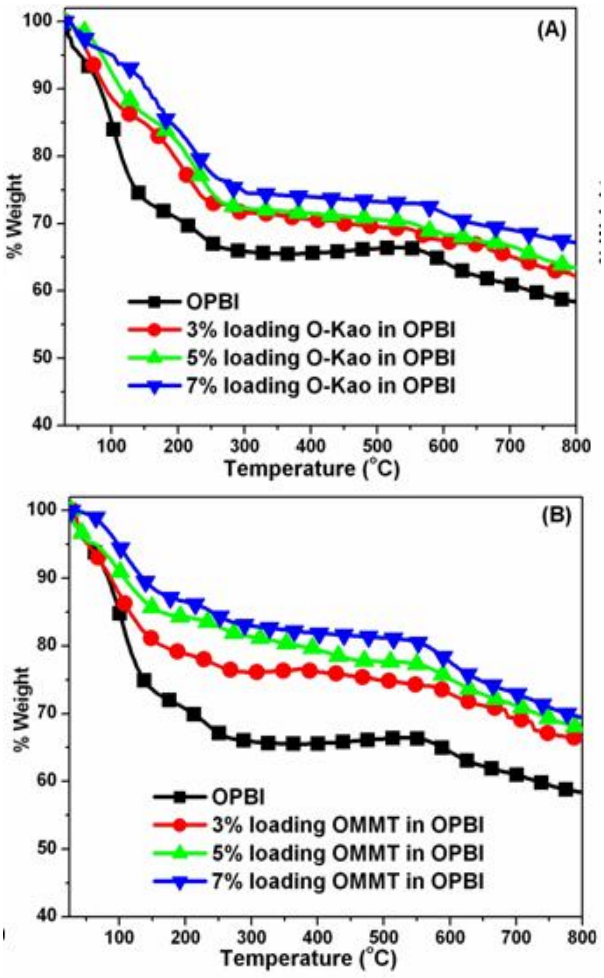

Figure 5.10. *TGA plots of OPBI nanocomposite membranes with (A) OKao and (B) OMMT and their comparisons with OPBI membrane.*

An initial weight loss at around 100-120°C and a second weight loss at around 570-600°C are observed in both the cases. The first weight loss is due to the loosely bound absorbed water molecule to the OPBI film and the second weight loss is due the

degradation of polymer backbone. The thermal degradation data obtained from TGA plots are summarized in the Table 5.1. It is clear from the TGA data that the thermal stability of OPBI film has improved significantly after nanocomposite formation and enhances with the increase of clay loading in both OMMT and OKao cases. This improvement in thermal stability of nanocomposite at all temperature ranges is due to the uniform dispersion of the silicate layers along the OPBI matrix. The silicate layers act as a thermal barrier which actually decelerate the thermal decomposition of the polymer matrixes by forming the silicate char on the surface of the polymer to resist it for further degradation.[46,47] Another reason may be due to the increase in crystalline properties of the OPBI phase in nanocomposite sample with increasing the percentage loading of nanofillers (Figure 5.6). Since the thermal stability of the crystalline phase is much higher than the amorphous one. That is why all the OPBI/OMMT and OPBI/OKao nanocomposites have better thermal stability than pristine OPBI film. It is also interesting to note that the nanocomposite obtained from OMMT have higher thermal stability than OKao nanocomposites (Table 5.1). This is due to the higher degree of dispersion in the case of OMMT than OKao, which results exfoliated structure for OMMT as shown previous sections by SAXD and TEM studies. Also the greater thermal stability of OMMT clay rather than OKao (Figure 5.9) plays a role for the above observation.

Table 5.1. *Thermal stability data for all the OPBI nanocomposite membranes.*

Sample	W_{510^oC} (%)[a]	$T_{20\%}$ (^oC)[b]	W_{790^oC} (%)[c]
OPBI	66.76	116	58.74
3wt% OMMT	74.84	166	66.54
5wt% OMMT	77.62	367	68.21
7wt% OMMT	81.24	564	69.87
3wt% OKao	69.41	192	62.54
5wt% OKao	70.80	215	63.65
7wt% OKao	73.58	230	67.56

[a] Residual weight percentage at 510°C.
[b] Temperature at which 20% weight loss is observed.
[c] Residual weight percentage at 790°C.

5.3.6. Dynamic Mechanical Analysis

The thermomechanical behavior and strengthening effect of the organoclays in the OPBI nanocomposites are evaluated using DMA. The structure, percentage content, and the dispersion pattern of the organoclays and their interaction with the polymer matrix can readily alter the physical and mechanical properties of the polymers.[48] Figure 5.11 and 5.12 show the temperature-dependent storage modulus, loss modulus, and tan δ plots of OPBI nanocomposites with OKao and OMMT. The storage modulus (E') is one of the important parameters of the DMA measurements which corresponds to the elastic response to the deformation and relates the capacity of the material to store when oscillatory load is applied to the sample and the loss modulus (E'') relates the ability to damping and energy dissipation. The storage modulus of both the OPBI-organoclays nanocomposites remarkably increased all over the temperature range than that of OPBI film (Table 5.2) with increasing the clay loading due to the mechanical reinforcement by the clays owing to the large surface area and the high aspect ratio of the nanosized clay particles.[49] The storage modulus (E') for the OPBI/OKao nanocomposites is more than the OPBI/OMMT nanocomposites over the entire region for each percentage loading of organoclays. This is due to the facts that the dispersion patterns of both the organoclays along the polymer matrixes are different and the weak interaction of each silicate layers for the intercalated dispersion of kaolinite clay is more than the exfoliated dispersion of montmorillonite clay since the lateral dimension (bigger aspect ratio) of Kao is higher than the MMT as visible from TEM (Figure 5.6) and AFM (Figure 5.7) images. The extent to which the modulus is increased is different through out the different temperature ranges (Table 5.2). These results show that the effect of clay on mechanical property strengthening is better in rubbery state than that in the glassy state. In the rubbery state the movement of polymer chain division is relatively free so the strengthening effect of clay particles is more effective, causing a large increase in storage modulus.

Table 5.2. *Various thermomechanical data of OPBI nanocomposite membranes obtained from the DMA study.*

Sample	T_g (°C)*	E' (MPa) at 150°C	% increase	E' (MPa) at 300°C	% increase	E' (MPa) at 390°C	% increase
OPBI	327	1174		847		449	
3wt% OMMT	332	1346	14.65	971	14.64	510	13.59
5wt% OMMT	335	1628	38.67	1264	49.23	803	78.84
7wt% OMMT	341	2010	71.20	1496	76.62	838	86.64
3wt% OKao	330	1857	58.17	1549	82.88	1202	167.71
5wt% OKao	332	2364	101.36	1949	130.11	1231	174.16
7wt% OKao	335	2939	150.34	2199	159.62	1261	180.85

* obtained from loss modulus plots

The loss modulus and tan δ (Figure 5.11 and 5.12) plots display only one peak for all the samples, and that peak temperature increases with increasing clay content in both the cases. This peak temperature corresponds to glass transition temperature (T_g) of the polymer. The variation of T_g with clay content can be explained by the existence of the strong interaction between organic layered clay and the OPBI matrix, which limits the movement of the OPBI chain segments. The different T_g values obtained from tan δ and loss modulus plots are also observed by us previously for the PBI systems.[50] To explain the increase in OPBI T_g in the polymer nanocomposites, a possible reason that may be proposed is that the silicate clay layers attract each other in the dispersed state due to the van-der Waals attraction causing the OPBI chains to become more close-packed structures, decreasing the free volume. As a result, higher temperature is required to reach the required free volume fraction segmental motion and hence T_g in the case of all the OPBI nanocomposites with both organoclays are increased.[48,49] The effect of the type of dispersion of the silicate layers of the organoclays on the glass transition temperature is large for exfoliated structure rather than the intercalated structure. That is why the increment of glass transition temperature (T_g) values of

exfoliated structure (OPBI/OMMT) is more than intercalated structure (OPBI/OKao) nanocomposites (Table 5.2).

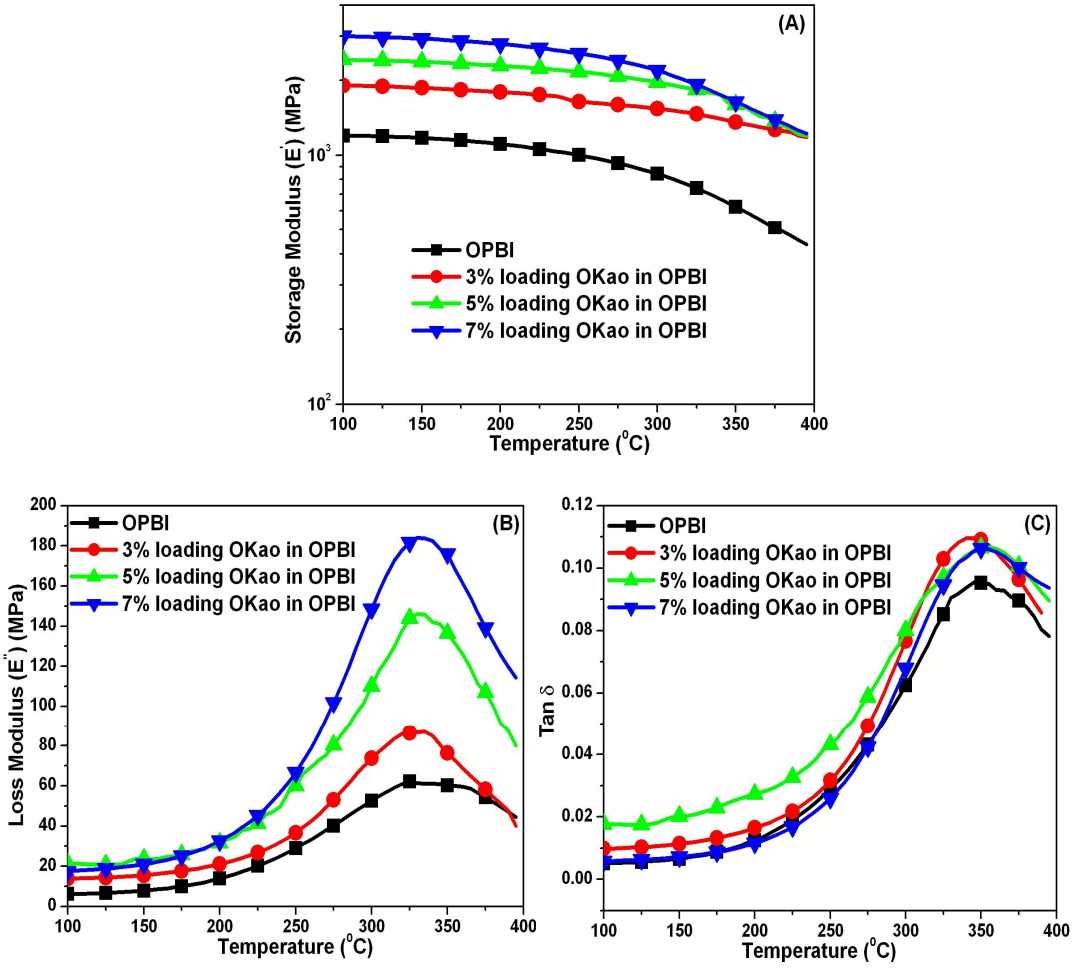

Figure 5.11. *Temperature dependent plot of mechanical properties obtained from DMA studies of OPBI/OKao nanocomposite membranes of different percentage loading: (A) storage modulus (E'), (B) loss modulus (E'') and (C) tan δ.*

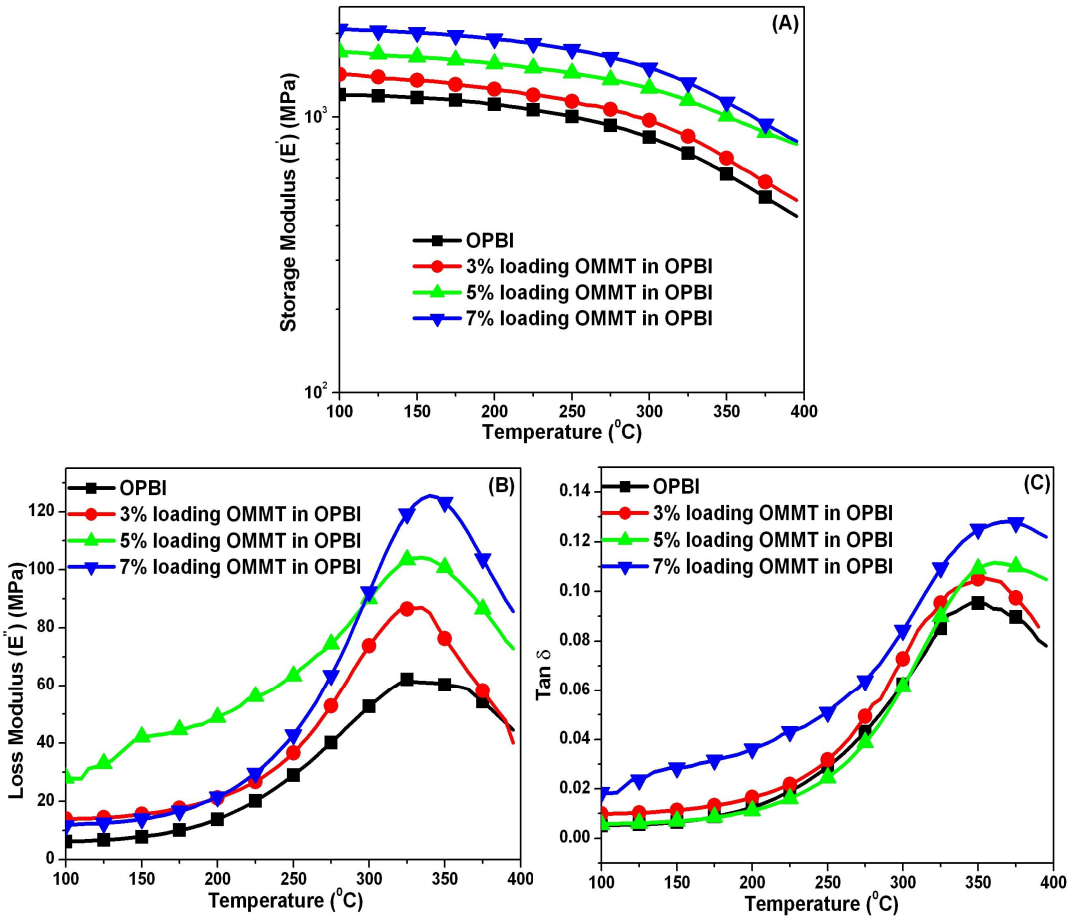

Figure 5.12. *Temperature-dependent plot of mechanical properties obtained from DMA studies of OPBI/OMMT nanocomposite membranes of different percentage loading. (A) Storage modulus (E'), (B) loss modulus (E'') and (C) tan δ.*

5.3.7. Oxidative Stability

The oxidative stability of the membranes is used to estimate the membrane durability in oxidative environment.[51] Here, all the OPBI nanocomposites membranes are subjected to Fenton's reagent to start the oxidative reaction by the attack of hydroxyl and hydroperoxyl radicals species ($HO^{\cdot}$ and $HOO^{\cdot}$), which actually lead either to chain dissociation or to ring-opening of the benzimidazole rings of the OPBI matrix. The influence of both the nanosized organoclays dispersion on the oxidative stability in the

OPBI matrix is shown in Figure 5.13. It is important to note that the oxidative stabilities of the nanocomposite membranes are significantly improved with increasing the percentage of both the nanoclays loading in the OPBI matrix. This implies that the clay layers are incorporating into the OPBI matrix which actually shows an enormous enhancement of the oxidative stability in case of OPBI nanocomposite membranes than the pure OPBI membrane. The incorporated clay particles inside the polymer chains act as barrier controlling the diffusion of radical for oxidation. Hence the $HO^{\cdot}$ and $HOO^{\cdot}$ radical species can not enter into the polymer chains readily and could not destroy the structure of the polymer chains.[52-54] As a result with increasing the clay content in the polymer chains, it becomes tougher for free radicals to attack the polymer chains, resulting higher oxidative stability.

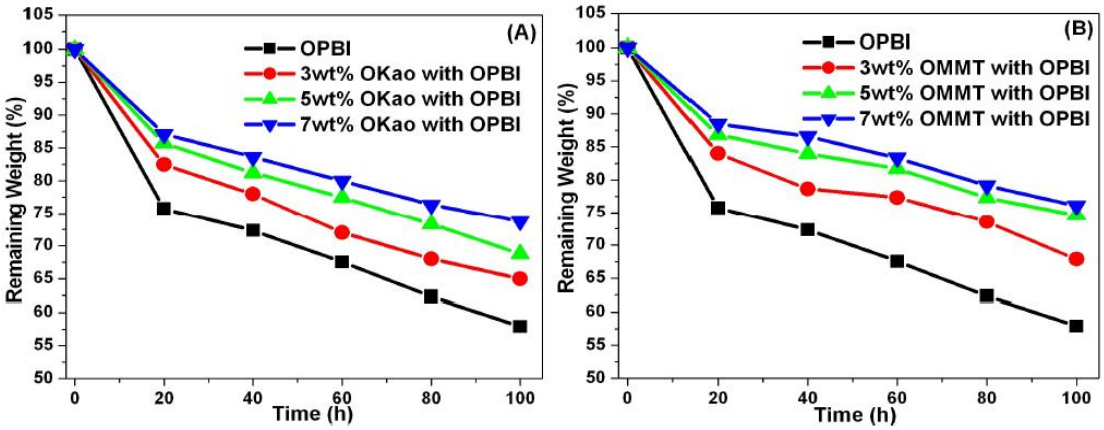

Figure 5.13. *Oxidative stability of OPBI nanocomposite membranes with different percentage loadings of (A) OKao and (B) OMMT.*

5.3.8. PA Loading

The efficiency of the PBI-based PEMFC is largely dependent upon the PA loading capacity of the PBI membranes. Generally, higher acid loading capacity of the membrane corresponds to better performance of the fuel cell by facilitating the transfer of the protons.[34] In the literature, the PA doping level of the membrane is often expressed as the number of PA mols per OPBI repeat unit. Earlier, our research group

has demonstrated that PBI [poly (2, 2'-(m-phenylene)-5, 5'-bibenzimidazole); known as *m*-PBI (scheme 3.1A)] membrane made from *m*-PBI gel in PA showed a very high PA doping level (35–40 mols of PA per PBI repeat unit) owing to the interconnected gel network structure of the PBI gel in PA.[35] It is well known that OPBI absorbs moisture readily up to 5-10% of its weight, and this absorbed moisture is associated themselves with the proton-accepting nitrogen (-N=) of the imidazole backbone of the OPBI. Hence these H_2O molecules probably blocks the passage of acid molecules (PA) to come near the –N= doping the OPBI chain.[36] On the basis of the above observation we expect that the introduction of nanoclay in the OPBI matrix might enhance the hydrophobic character of the OPBI membrane due to the formation of nanostructure, and also it is known that nanoclays can absorb acid molecule. Hence, it is expected that the PA loading will enhance in the OPBI/clay nanocomposite membrane. The PA doping levels of all the OPBI nanocomposites with both the organoclays are tabulated in Table 5.3. The PA loading of OPBI/clay nanocomposite membranes is much higher than the parent OPBI membrane. This clearly attributes the effect of clay and nanocomposite formation in the PA loading. Careful observations from the TGA (Figure 5.10) demonstrate that with the introduction of both the organoclays the first weight loss (due to the presence of absorbed moisture) is decreased or in other words, the hydrophobic nature of the nanocomposite membrane enhanced. Therefore, more and more acid molecules (PA) are entrapped in the OPBI nanocomposite membranes with the addition of organoclays, which is actually assisting the nanocomposite membrane to load more PA molecules. It is observed that with an increase in the percentage loading of the organoclays the PA doping capacity increases in the case of OKao; however it remains the same in the case of OMMT. This observation might be due to the formation of different nanostructures in different clays.

Table 5.3. *PA doping level of the OPBI nanocomposite membranes with different percentage loading of both the organoclays.*

Sample	PA mols/PBI repeat unit
OPBI	16.58
3 wt% OKao	17.284
5 wt% OKao	22.279
7 wt% OKao	24.746
3 wt% OMMT	23.293
5 wt% OMMT	24.104
7 wt% OMMT	25.479

5.3.9. Proton Conductivity

The proton conductivities of all the nanocomposite membranes are studied in the temperature range of 30–160ºC. The representative Nyquist plots of the OPBI and nanocomposite membranes are shown in Figure 5.14. The proton conductivities of the membranes, obtained from the Nyquist plots are plotted against temperature and shown in Figure 5.15. As expected in all the cases the proton conductivity increases with increasing temperature. Also, the proton conductivities of the membranes increase by increasing the nanoclay loading in the polymer matrix in both OMMT and OKao nanocomposites. The improvement of the proton conductivity of the nanocomposites membranes with the nanoclay content is due to the higher PA holding capacity of the nanocomposite membranes (Table 5.3) and the galleries silicate layers play an important role in an additional proton conductor.[55] Already we have shown that with an increase in the percentage loading of the organoclays, the acid (PA) loading capability increases, and therefore the higher acid (PA) doping capacity corresponds to the higher proton conductivity of the OPBI nanocomposite membranes. In addition to the higher PA loading, the other reason for the higher proton conductivity could be due to the nanostructure of organoclays. Since the acid molecules are entrapped inside the gallery

through the weak intermolecular interaction (such as hydrogen bonding) with the organoclays, which serve as vehicles for supporting the transportation of protons through the membrane hence the proton conduction increases. The proton conductivity of OPBI nanocomposite membranes is supported by a continuous "forming–breaking–forming" process of the weak hydrogen bonds of OPBI and the organoclays with PA which accelerates the proton transfer in the nanocomposite membranes.

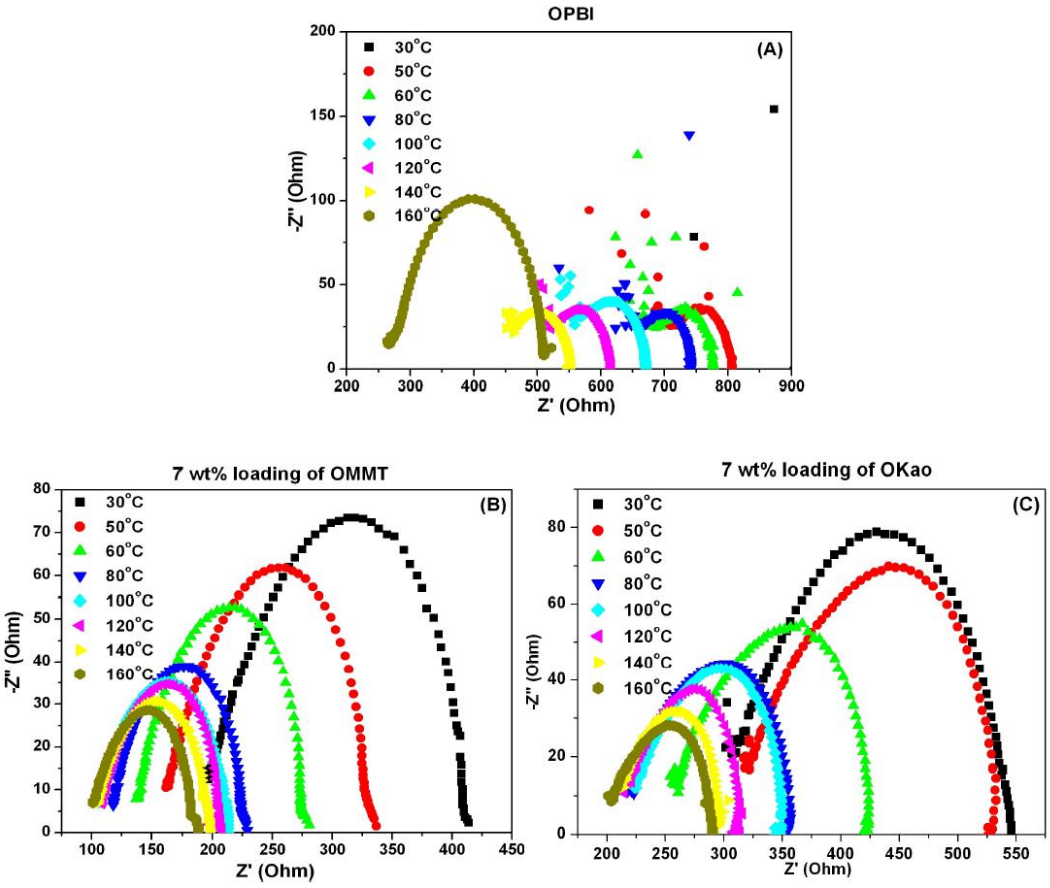

Figure 5.14. *Nyquist plots of (A) OPBI, (B) OPBI-OMMT and (C) OPBI-OKao nanocomposites with 7wt% loading.*

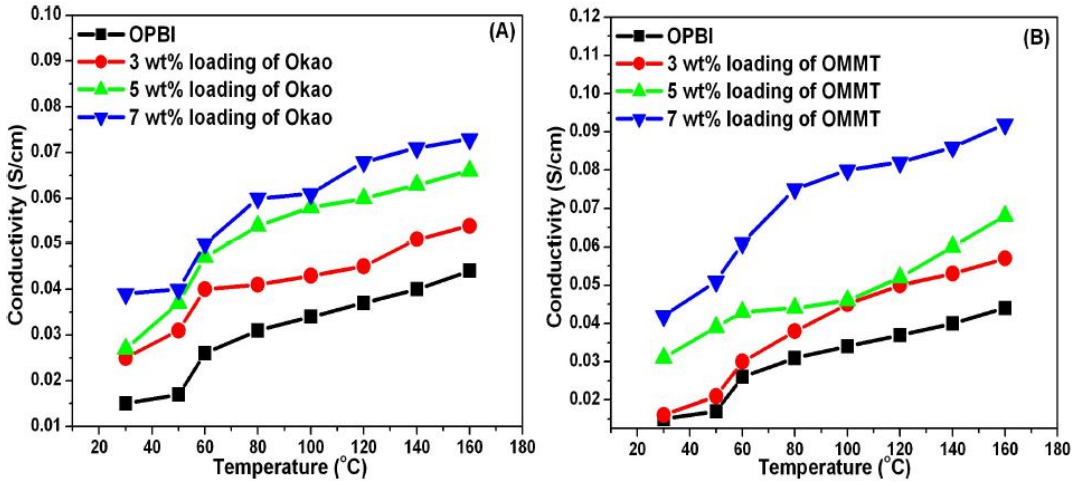

Figure 5.15. *Proton conductivity against temperature for OPBI nanocomposite membranes with various percentages loading of (A) OKao and (B) OMMT.*

The dependency of the temperature (T) on the proton conductivity (σ), measured using the four-probe method is well expressed with the activation energy (E_a) for the proton conduction behavior using the Arrhenius equation[56] as follows

$$\ln(\sigma T) = \ln \sigma_0 - \frac{E_a}{RT} \tag{5.3}$$

where σ is the proton conductivity of the membrane (Scm^{-1}), σ_0 is the pre-exponential factor ($S\ K^{-1}\ cm^{-1}$), E_a is the proton conducting activation energy (kJ/mol), R is the ideal gas constant ($J\ mol^{-1}K^{-1}$) and T is the temperature (K). Our data fits very well with the equation (2) indicating that the Grotthuss mechanism is responsible for the proton conduction process. The activation energy (E_a), which is the minimum energy required for proton conduction through each OPBI nanocomposites membranes, are obtained from the slope in the linear fit as shown in Figure 5.16. The activation energies obtained are quite low and as comparable with the E_a of free PA. The low activation energy corresponds to the fast proton conduction process. The smaller E_a obtained for nanocomposites is due to the contribution from the clay components, which serves as an

extra charge carriers for the conduction. The presence of free hydroxyl groups in the clay layers provides an easy path for the continuous forming-breaking-forming process of weak interaction between the OPBI and PA through the nanoclay structure. Therefore the formations of nanostructure of OPBI/clay nanocomposite provide a very low barrier for the proton conduction, yielding low activation energy and faster proton conduction.

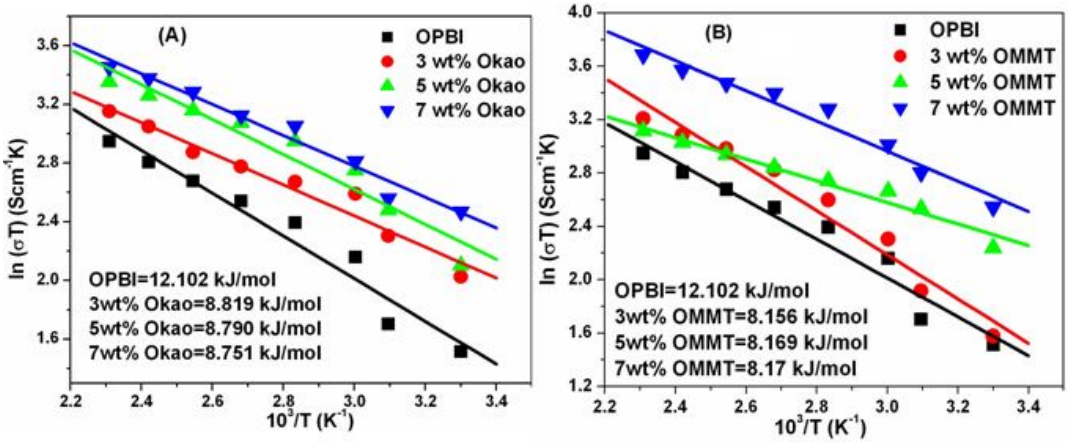

Figure 5.16. *Arrhenius plot for the proton conduction of OPBI nanocomposites with (A) OKao and (B) OMMT.*

5.4. Conclusion

A series of nanocomposite materials consisting of OPBI and two types of organically modified layered clay (MMT and Kao) are prepared by effectively dispersing of the silicate layers in the OPBI matrix by the solution blending method. FT-IR, ^{13}C CPMAS NMR, XRD, TEM, TGA, and DMA experiments are carried out to characterize the morphology and properties of the nanocomposites. The morphologies of the OPBI/Clay nanocomposites are dependent upon the structure of the clay; in the case of MMT, an exfoliated structure is obtained, whereas intercalated morphology is obtained with Kao. The incorporation of nanoclays in OPBI results in an increase in thermal and oxidative stabilities. The storage modulus and glass transition temperature of all the nanocomposites increased much greater than that of pure polymer. The PA loading of the nanocomposites is much higher than the pristine polymer. The proton conductivity of all the nanocomposite membranes increases with increasing percentage

content of the clays. The nanocomposite membranes have small activation energies for the proton conduction. These nanocomposite membranes have all the characteristics that are required to be efficient PEM for HT-PEMFC application. Hence, we believe these nanocomposite membrane can be used in HT-PEMFC as PEM.

Referrences

1. Vaia, R. A.; Krishnamoorti, R. *In Polymer Nanocomposites: Synthesis Characterization and Modeling*; American Chemical Society: Washington, DC, 2001.
2. Giannelis, E. P. *Adv. Mater.* **1996**, *8*, 29.
3. Wang, Z.; Pinnavaia, T. J. *Chem. Mater.* **1998**, *10*, 1820.
4. Burnside, S. D.; Giannelis, E. P. *Chem. Mater.* **1995**, *7*, 1597.
5. Alexandre, M.; Dubois, P. *Mater. Sci. Eng.* **2000**, *28*, 1.
6. Gilman, J. W. *Appl. Clay. Sci.* **1999**, *15*, 31.
7. Ray, S. S.; Yamada, K; Okamoto, M; Ueda, K *Nano Lett.* **2002**, *2*, 1093.
8. Gilman, J. W.; Jackson, C. L.; Morgan, A. B.; Harris, R., Jr.; Manias, E.; Giannelis, E. P.; Wuthenow, M.; Hilton, D.; Phillips, S. H. *Chem. Mater.* **2000**, *12*, 1866.
9. Chang, J. H.; Park, J. H.; Park, G. G.; Kim, C. S.; Park, O. O. *J. Power Sources* **2003**, *124*, 18.
10. Giannelis, E. P. *Appl. Organomet. Chem.* **1998**, *12*, 675.
11. Zhang, G. W.; Zhou, Z. T. *J. Membr. Sci.* **2005**, *261*, 107.
12. Xu, R.; Manias, E.; Snyder, A. J.; Runt, J. *Macromolecules* **2001**, *34*, 337.
13. Yano, K.; Usuki, A.; Okada, A.; Kurauchi, T.; Kamigaito, O. *J. Polym. Sci., Part A: Polym. Chem.* **1993**, *31*, 2493.
14. Gu, A.; Kuo, S. W.; Chang, F. C. *J. Appl. Polym. Sci.* **2001**, *79*, 1902.
15. Tyan, H. L.; Liu, Y. C.; Wei, K. H. *Chem. Mater.* **1999**, *11*, 1942.
16. Gardolinski, J. E.; Carrera, L. C. M.; Cantao, M. P.; Wypych, F. *J. Mater. Sci.* **2000**, *35*, 3113.
17. Alkan, M.; Demirbas, Ö; Doğan, M., *Microporous Mesoporous Mater.* **2005**, *83*, 51.
18. Thompson, J. G.; Cuff, C. *Clays Clay Miner.* **1985**, *33*, 490.
19. Alexandre, M.; Dubois, P. *Mater. Sci. Eng. R* **2000**, *28*, 1.

20. Maiti, P.; Nam, P. H.; Okamoto, M.; Hasegawa, N.; Usuki, A. *Macromolecules* **2002**, *35*, 2042.
21. Zhu, J.; Morgan, A. B.; Lamelas, F. J.; Wilkie, C. A. *Chem. Mater.* **2001**, *13*, 3774.
22. Komori, Y.; Sugahara, Y.; Kuroda, K. *Chem. Mater.* **1999**, *11*, 3.
23. Theng, B. K. G. *The Chemistry of Clay–Organic Reactions;* Adam Hilger: London, 1974.
24. Paiva, L. B.; Morales, A. R.; Díaz. F. R. V. *Appl. Clay Sci.* **2008**, *42*, 8.
25. Krishnamoorti, R.; Vaia, R. A.; Giannelis, E. P. *Chem. Mater.* **1996**, *8*, 1728.
26. Wu. J.; Lerner, M. M. *Chem. Mater.* **1993**, *6*, 835.
27. Ogata, N.; Jimenez, G.; Kawai, H.; Ogihara, T. *J. Polym. Sci., Part B: Polym. Phys.* **1997**, *35*, 389.
28. Yano, K.; Usuki, A.; Karauchi T.; Kamigaito, O. *J. Polym. Sci., Part A: Polym. Chem.* **1993**, *31*, 2493.
29. Lee, D. C.; Jang, L. W. *J. Appl. Polym. Sci.* **1998**, *68*, 1997.
30. Samms, S. R.; Wsmus, S.; Savinell, R. F. *J. Electrochem. Soc.* **1996**, *143*, 1225.
31. Weng, D.; Wainright, J. S.; Landau, U.; Savinell, R. F. *J. Electrochem. Soc.* **1996**, *143*, 1260.
32. Savinell, R.; Yeager, E.; Tryk, D.; Landau, U.; Wainright, J.; Weng, D.; Lux, K.; Litt, M.; Rogers, C. *J. Electrochem. Soc.* **1994**, *141*, L46.
33. Mecerreyes, D.; Grande, H.; Miguel, O.; Ochoteco, E.; Marcilla, R.; Cantero, I. *Chem. Mater.* **2004**, *16*, 604.
34. (a) Xiao, L.; Zhang, H.; Scanlon, E.; Ramanathan, L. S.; Choe, E.-W.; Rogers, D.; Apple, T.; Benicewicz, B. C. *Chem. Mater.* **2005**, *17*, 5328. (b) Xiao, L.; Zhang, H.; Jana, T.; Scanlon, E.; Chen, R.; Choe, E.-W.; Ramanathan, L. S.; Yu, S.; Benicewicz, B. C. *Fuel Cells* **2005**, *5*, 287
35. Sannigrahi, A.; Arunbabu, D.; Jana, T. *Macromol. Rapid Commun.* **2006**, *27*, 1962.
36. Sannigrahi, A.; Ghosh, S.; Lalnuntluanga, J.; Jana, T. *J. Appl. Polym. Sci.* **2008**, *111*, 2194.

37. Ghosh, S.; Sannigrahi, A.; Maity, S.; Jana, T. *J. Phys. Chem. B*, **2010**, *114*, 3122.
38. Kuila, B. K.; Nandi, A. K. *Macromolecules* **2004**, *37*, 8577.
39. Turhan, Y.; Doğan, M.; Alkan, M. *Ind. Eng. Chem. Res.* **2010**, *49*, 1503.
40. Causin, V.; Marega, C.; Mariog, A.; Ferrara, G. *Polymer* **2005**, *46*, 9533.
41. Vaia, R. A.; Liu, W.; Koerner, H. *J. Polym. Sci. B: Polym. Phys.* **2003**, *41*, 3214.
42. Letaief, S.; Elbokl, T. A.; Detellier, C. *J. Colloid Interface Sci.* **2007**, *302*, 254.
43. Zhang, L.; Xu, J.; Hou, G.; Tang, H.; Deng, F. *J. Colloid Interface Sci.* **2007**, *311*, 38.
44. Morgan, A. B.; Gilman, J. W. *J. Appl. Polym. Sci.* **2003**, *87*, 1329.
45. Eckel, D. F.; Balogh, M. P.; Fasulo, P. D.; Rodgers, W. R. *J. App. Polym. Sci.* **2004**, *93*, 1110.
46. Ray, S. S.; Okamoto, M. *Prog. Polym. Sci.* **2003**, *28*, 1539.
47. Becker, O.; Varley, R. J.; Simon, G. P. *Eur. Polym. J.* **2004**, *40*, 187.
48. Satapathy, B. K.; Weidisch, R.; Potschke, P.; Janke, A. *Compos. Sci. Technol.* **2007**, *67*, 867.
49. Kuila B. K.; Nandi, A. K. *J. Phys. Chem. B* **2006**, *110*, 1621.
50. Sannigrahi, A.; Ghosh, S.; Maity, S.; Jana, T. *Polymer* **2010**, *51*, 5929.
51. Gosalawit, R.; Chirachanchaia, S.; Shishatskiy, S.; Nunes, S. P. *J. Membr. Sci.* **2008**, *323*, 337.
52. Asano, N.; Aoki, M; Suzuki, S; Miyatake, K. *J. Am. Chem. Soc.* **2006**, *128*, 1762.
53. Hübner, G; Roduner, E. *J. Mater. Chem.* **1999**, *9*, 409.
54. Li, Q; He, R; Jensen, J. O.; Bjerrum, N. J. *Fuel Cells* **2004**, *4*, 147.
55. Karthikeyan, C. N.; Nunes, S. P.; Prado, L. A. S. A.; Ponce, M. L.; Silva, H.; Ruffmann, B.; Schulte, K. *J. Membr. Sci.* **2005**, *254*, 139.
56. He, R.; Li, Q.; Bach, A.; Jensen, J. O.; Bjerrum, N. J. *J. Membr. Sci.* **2006**, *277*, 38.

Chapter 6

Aryl Ether Linked Polybenzimidazole/Silica Nanocomposites: Organic-Inorganic Hybrid Membranes for Polymer Electrolyte Membrane Fuel Cell

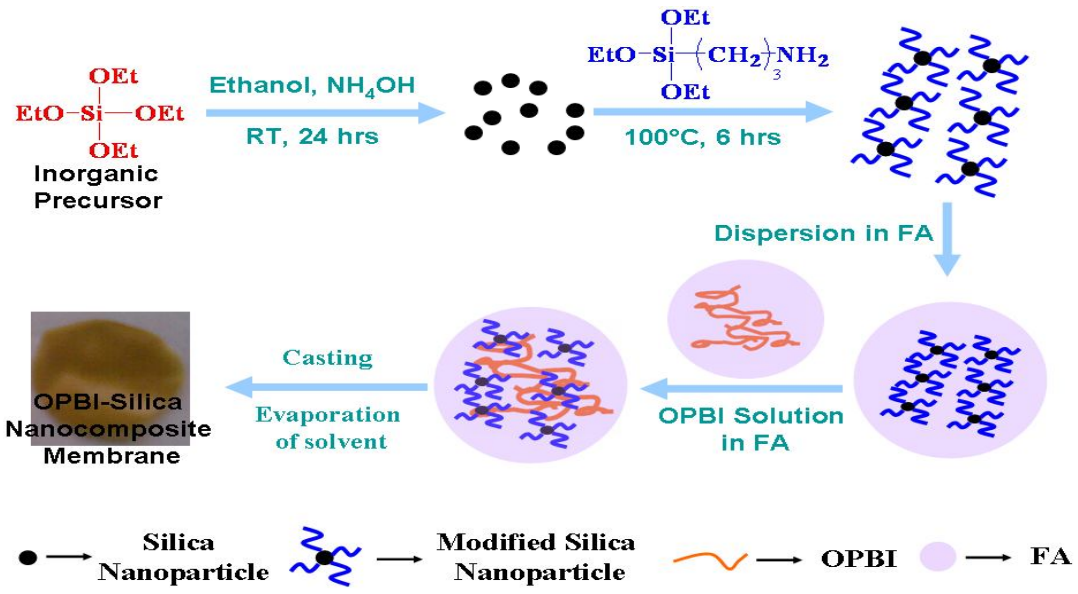

Nanocomposites of poly(4,4′-diphenylether-5,5′-bibenzimidazole) (OPBI) with silica nanoparticle were synthesized by solution blending process. The influences of incorporation of nanosized silica particle on the properties of OPBI were evaluated.

6.1. Introduction

Recently, organic/inorganic hybrid nanocomposites where the inorganic part is nanosized fillers and the organic part is the polymer matrix [1-4] have been studied widely owing to their unique properties and application potentials. These hybrid materials display extraordinary improvement of several properties than the pure polymer due to presence of inorganic fillers inside the polymer matrix.[4] Among various types of inorganic nanofillers which include heteropoly acids,[5,6] carbon nanotube,[7,8] fullerene,[9,10] zeolite,[11] graphene[12] and many others, the applications of silica nanoparticles is continuously increasing due to their high specific surface area, large porous volume, high mechanical and thermal stability, and easy surface modification.[13] The organic modification of the silica particle surface can readily induce the weak interaction between the nanofiller and the polymeric matrix. The dispersion pattern of silica in the polymer matrix usually has a significant impact on the properties of nanocomposites. Nanosized silica particles have strong tendency to aggregate particularly at very high particle concentrations, therefore effective incorporation and homogeneous dispersion of silica nanoparticles within the polymer matrix are the key challenges to be addressed.[14,15] Among many methods, solution blending method has been found to be very useful to provide a well uniform dispersion of inorganic nanoparticles in the polymer matrix.[16,17,18]

Polybenzimidazole (PBI) loaded with phosphoric acid (PA) is the most promising polymer electrolyte membrane (PEM) material for the use in high-temperature PEM fuel cell (HT-PEMFC) applications.[19] Various attempts have been made so far for the fabrication of PA doped PBI membranes in the literature.[20-23] However the major drawback of PBI is that the mechanical stability of the membranes significantly decreases as the content of phosphoric acid in the membranes increases.[24] Also, PA leaches out from the membrane easily when PA content is high, which leads to the decrease of the proton conductivity by many orders of magnitude during fuel cell operation.[25] Therefore the fabrication of highly proton conducting, mechanically stable PA loaded PBI membrane remains prime challenge to be solved. In order to address this

issue, PBI composite with variety of inorganic additives e.g. clay,[26] nanotubes,[27] graphenes,[28] heteropolyacids[29] and silica particles[30] have been developed in last couple of years. Although it was shown that the SiO_2 incorporation in the PBI matrix reinforces the mechanical properties of PBI membranes, but these methods often exhibit poor proton conductivity.[30]

Substantial increment of both mechanical properties and proton conductivity of poly (4,4′-diphenylether-5,5′-bibenzimidazole) (OPBI as shown in Scheme 3.1B)-clay nanocomposites[26] membranes have been observed by us very recently. This encourages us to develop OPBI-SiO_2 nanocomposite membranes in this study. The flexible nature of the OPBI backbone and good solubility in solvent like formic acid (FA) and readily tunable molecular weight are the attractions to choose the OPBI structure.[31,32] This nanocomposite formation is expected to yield completely new materials in which good characteristics of organic polymer and inorganic materials are combined. Our goal in this study to fabricate PA doped OPBI nanocomposite membranes with enhanced mechanical and proton conducting properties for the future HT-PEMFC application.

6.2. Experimental Section

6.2.1. Materials

3,3´,4,4´- tetraaminobiphenyl (TAB, polymer grade), 4,4´-oxybis (benzoic acid) (OBA) and polyphosphoric acid (PPA, 115 %) were purchased from Sigma-Aldrich. Formic acid (FA) (99%) was purchased from Qualigens, India and tetraethylortho silicate (TEOS) was purchased from Merck, India. 3-aminopropyltriethoxy silane (APTES) was purchased from Sigma-Aldrich. All chemicals were used as received.

6.2.2. OPBI Synthesis

The synthesis of OPBI was carried out by as per our method reported previously,[31] in short: equal mols of TAB and OBA were taken into three-neck round bottom flask along with polyphosphoric acid (PPA). The reaction mixture was stirred by using a mechanical overhead stirrer and slow stream of purged nitrogen gas was

maintained throughout the reaction. The polymerization was carried out at 190-220°C for approximately 26 hours. The OPBI polymer was isolated, neutralized with sodium bicarbonate, washed thoroughly with water and finally dried in vacuum oven for 48 hours at 100°C. The dried polymer was characterized by measuring the viscosity in concentrated sulfuric acid (98%) by using a Cannon Ubbelohde capillary dilution viscometer (model F725). The synthesized OPBI has an inherent viscosity (I.V.) value of 2.29 dL/g at 30°C. The concentration of the polymer solution for the viscosity measurement was 0.2 g/dL.

6.2.3. Synthesis of Silica Nanoparticle and Its Surface Modification

Silica nanoparticles were prepared by hydrolysis and condensation of TEOS (10.7 mmol) in ethanol, and in presence of 28% ammonia as catalyst, as described by Stöber et al.[33] First, solution containing appropriate quantities of absolute ethanol, ammonia and deionized water were stirred for 5 minutes to ensure complete mixing. Then a certain amount of TEOS in absolute ethanol was added to the above solution and the reaction was carried out at ambient temperature for 24 hours. The colloidal solution was separated by centrifugation, and the silica nanoparticles were washed by absolute ethanol for three times, followed by drying in oven at 100°C for 6 hrs. The average size of the silica nanoparticle is ~50 nm as obtained from TEM images. The silica nanoparticles were dispersed in ethanol followed by the addition of APTES (12.9 mmol) as described earlier.[34] The above mixture was stirred for 6 h at reflux conditions. Again the surface modified silica nanoparticles were separated from dispersed solution of ethanol in a similar way as it was done in case of silica particles described above. The modified surface of the silica particle consists of amine functionality; hence this amine modified silica particle is referred as AMS. The average size of the silica nanoparticle is ~90 nm as obtained from TEM images.

6.2.4. Preparation of PBI/silica Nanocomposite Membranes

Representative 4, 7, 10, 15, 20 wt% loading of the amine modified silica nanoparticle (AMS) with respect to OPBI were prepared as follows: required amount of

AMS were dispersed in 10 ml of formic acid (FA) at room temperature under vigorous stirring for 1 hr and then added to a OPBI solution, which was already prepared by dissolving 0.2 g in 10 ml FA to form a 2 wt% solution. The mixture was vigorously stirred 24 hours to make a homogeneous solution. The solution was cast onto a Petridis and solvent was removed slowly by applying heat at 60ºC under the air flow. The samples were dried in a vacuum oven at 100°C for 24 h to remove the traces of solvent. OPBI composites with unmodified silica (UMS), silica particles as obtained from the Stöber's process, were also made with variety of loading using exactly the similar method as mentioned above for comparison with OPBI/AMS. The thickness of the OPBI/silica nanocomposite membranes were approximately 40 (±5) μm. A schematic representation of the nanocomposites preparation is shown in Scheme 6.2.

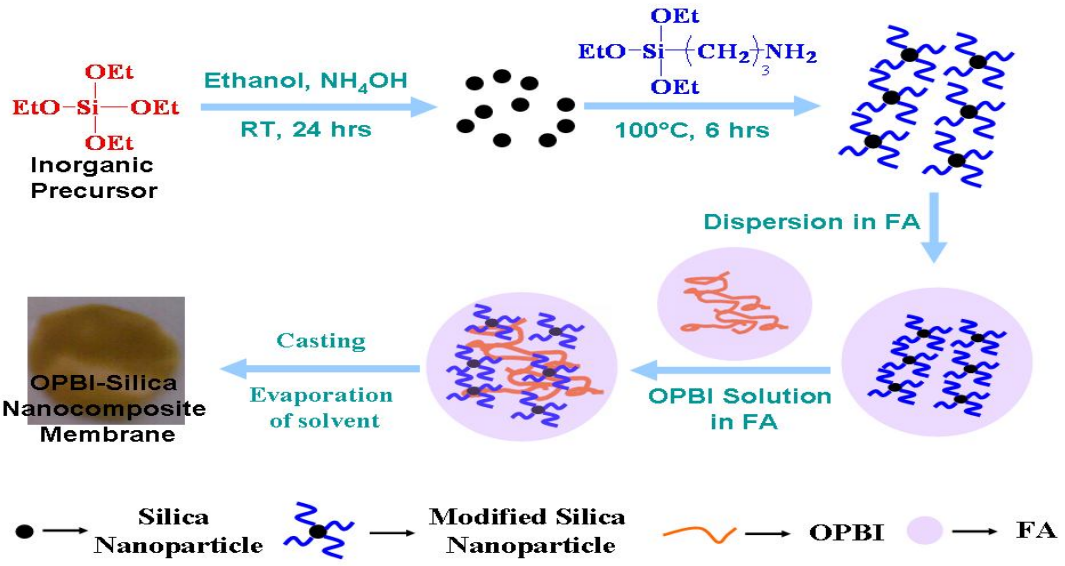

Scheme 6.2. *Preparation of OPBI nanocomposites with amine modified silica nanoparticles (AMS) by solution blending process.*

6.2.5. Doping of OPBI and Its Nanocomposite Membranes with Phosphoric acid (PA)

The dried OPBI, OPBI/AMS and OPBI/UMS nanocomposite membranes with the above mentioned loading of silica nanoparticles made from FA were immersed into PA (85%) for 7 days to get free standing PA doped membranes.

6.2.6. Spectral Characterization

The FT-IR spectra of the OPBI and its nanocomposite membranes were recorded on a (Nicolet 5700 FT-IR) FT-IR spectrometer. The infrared spectra were obtained in the region 3900-600 cm^{-1}. Solid state ^{13}C cross polarization magic angle spinning (CPMAS) NMR spectra were obtained on a Bruker AV 400 MHz NMR instrument operating at 100 MHz at a spinning rate of 5 kHz and a contact time of 2 ms.

6.2.7. X-ray Study

X-ray diffraction was used in this study to investigate the structure of the OPBI nanocomposites. The small angle X-ray diffraction (SAXD) experiment of the OPBI film and its nanocomposites were carried out on a Hecus X-ray diffractometer with Cu Kα radiation (λ = 1.5418 Å) source operated at voltage of 50 kV and 1 mA current and the wide angle X-ray diffraction (WAXD) patterns of the samples were performed in an X-ray generator (Model PW 1729, Philips, Holland) with Cu Kα radiation (λ = 1.5418 Å) source operated at voltage of 40 kV and 30 mA current in the angular range (2θ) of 5-40°.

6.2.8. Morphology

The distributions of the silica nanoparticles into the polymer matrix were examined by transmission electron microscope (TEM). For TEM study, a drop of samples prepared from FA was placed on a carbon coated copper (200 mesh) grid, dried and observed through the TEM instrument (FEI Tecnai Model No. 2083) operating at 200kV.

6.2.9. Thermal Measurement

Thermogravimeteric analysis was done to explain thermal decomposition behavior. The thermogravimetric analysis of OPBI and its nanocomposites membranes were carried out on a (Netzsch STA 409PC) TG-DTA instrument from 50 to 800°C with a scanning rate of 10° deg/min in the presence of nitrogen flow.

6.2.10. Dynamic Mechanical Study

Dynamic mechanical analyses (DMA) of all the OPBI nanocomposite membranes were determined using a TA Instrument Mechanical Analyzer (DMA) Q800. The storage modulus, loss modulus, and tan δ were measured at a heating rate of $4°Cmin^{-1}$ under a preload force of 0.01N at a frequency of 10 Hz. The samples were annealed at 400°C for 30 min, then kept at 100°C isothermally for 20 min inside the DMA machine, and finally scanned from 100 to 400°C at a heating rate of 4°C/min.

6.2.11. Oxidative Stability

The stability of all the OPBI nanocomposite membranes to oxidation was investigated by immersing the membranes into Fenton's reagent (30 ppm $FeSO_4$ in 30% H_2O_2) at 70°C. The oxidative stability was characterized by the expanded time variation up to 100 hours. The membranes were taken out at certain time intervals, dried in vacuum oven at 80°C overnight, and weights were recorded. The oxidative stabilities of all the membranes were calculated as a weight remained after taking out the membranes from the Fenton's reagent.

6.2.12. PA Doping Level

The PA doping level of PA doped OPBI nanocomposite membranes with both the organoclays was determined by titrating of a preweighed piece of membrane sample using standardized sodium hydroxide solution with a Metrohm Titrino Titrator. The acid doping levels, expressed as mols of phosphoric acid per mol of PBI repeat unit, were calculated from the equation:

$$\text{Acid doping level} = \frac{V_{NaOH} C_{NaOH}}{W_{dry}} M_w \quad (6.1)$$

Where, V_{NaOH} and C_{NaOH} are the volume and the molar concentration of the sodium hydroxide, while W_{dry} is the dry polymer membrane weight and M_w is the molecular weight of the polymer repeat unit, respectively. The acid doping level reported here are the average values obtained from three separate values, measured from three similar size membrane samples.

6.2.13. Water Uptake and Swelling Ratio

Water uptake and swelling ratio of the nanocomposite membranes were obtained by immersing the membranes in water for three days. The nanocomposite membranes were thoroughly vacuum dried for three days at 100°C. The length and weight of the membrane were measured. Then the membranes were immersed in water for three days at room temperature. The wet membranes were quickly wiped to remove the surface water. Again the length and weight of the wet membrane were noted. Water uptake of the membranes were calculated as

$$\text{Water Uptake} = \frac{W_w - W_d}{W_d} \times 100\% \quad (6.2)$$

where, W_w and W_d are the weights of the wet and dry membranes, respectively. The swelling ratio of the membranes were calculated as

$$\text{Swelling Ratio} = \frac{L_w - L_d}{L_d} \times 100\% \quad (6.3)$$

where, L_w and L_d are the lengths of the wet and dry membranes, respectively. The water uptake and swelling ratio measurements of the membranes were carried out in triplicate independently with different pieces of membranes to check the reproducibility of the results.

6.2.14. Conductivity Study

Proton conductivities of all the acid loaded nanocomposites membranes of OPBI were measured with a four-point probe technique. The impedance of the membrane was measured with an impedance analyzer by using a Zahner Impedance spectrometer (ZENNIUM PP211) over a frequency range from 1 Hz to 100 kHz. The rectangular shape acid loaded membranes were mounted onto a homemade teflon conductivity cell. The membranes were dried at 100°C by heating and holding at 100°C isothermally for 2 hours to remove the water from the membrane. The membrane samples were then cooled in a vacuum oven and taken out just before conductivity measurement in an effort to keep the samples dry. The conductivities of the membranes were measured from room temperature to 160°C at 20°C intervals. The samples were kept for 30 minutes in each temperature before the impedance measurement. The conductivity was calculated with the following equation:

$$\sigma = \frac{D}{RBL} \tag{6.4}$$

where, σ is the proton conductivity (S/cm), D is the distance between the electrodes, and B and L are the thickness and width of the membrane samples, respectively. In all cases, R is the measured resistance values which were obtained Nyquist plots.

6.3. Results and Discussion

6.3.1. Spectroscopic study

FT-IR spectra of pure OPBI, amine modified silica nanoparticles (AMS) and OPBI nanocomposites with AMS are shown in Figure 6.1. In case of pure OPBI, the characteristic peaks at 3415, 3148 and 3064 $cm^{-1}$are assigned to the stretching frequency of the free –NH groups, the broad transmission due to the hydrogen bonded –NH groups and a low intense peak due to the stretching frequency of aromatic CH groups, respectively.[31] In nanocomposites, these peaks are not distinguishable and appears as a

very broad signal. The broad peaks between 2500 cm^{-1} to 3500 cm^{-1} of OPBI nanocomposites indicates the existence of hydrogen bonding interactions between OPBI and silica nanoparticles. The increasing peak intensity of Si-O-Si stretching vibration at 1035 cm^{-1} with the increasing loading of silica nanoparticle in the OPBI matrix confirms that the AMS nanoparticles are incorporated into the OPBI matrix and yielded the nanocomposites.

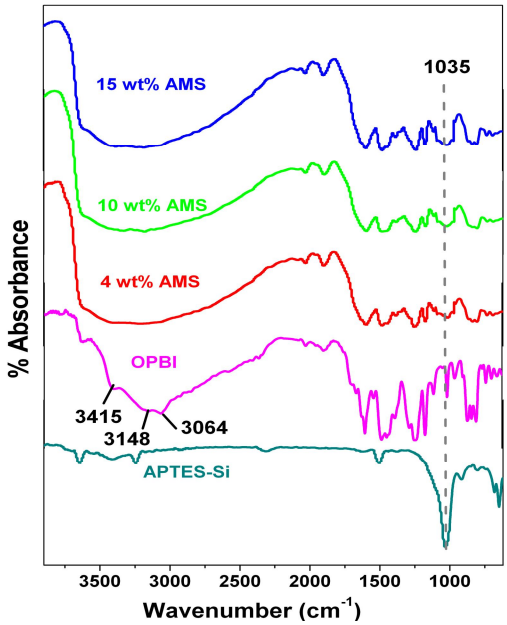

Figure 6.1. *FT-IR spectra of the APTES-Si (AMS), OPBI and OPBI nanocomposite membranes with the indicated AMS loading.*

The ^{13}C CPMAS NMR spectra of the OPBI and OPBI/15 wt% AMS nanocomposite are shown in Figure 6.2. The spectrum of OPBI consists of several lines that can be recognized in order of increasing magnetic field as lines arising from the carbons of imidazole rings attached to phenylene rings (151 ppm), the carbons connecting benzimidazole rings in the bibenzimidazole system (142 ppm), and the aromatic carbons bound to the nitrogen atoms (134 ppm). The three remaining lines (129, 120, and 111 ppm) have also been assigned. Earlier it was shown[35] that the amine modified silica nanoparticle (AMS) shows three ^{13}C resonances at 9.6, 21.1, and 42.7 ppm corresponding to $-CH_2NH_2$, $-CH_2-$, and $-CH_2-Si$ groups, respectively. These peaks

have been shifted to the higher field at 7.65, 17.35 and 35.42 ppm in case of OPBI/AMS nanocomposite (Figure 6.2), indicating the presence of the strong intermolecular interaction between the OPBI and amine modified silica nanoparticles.

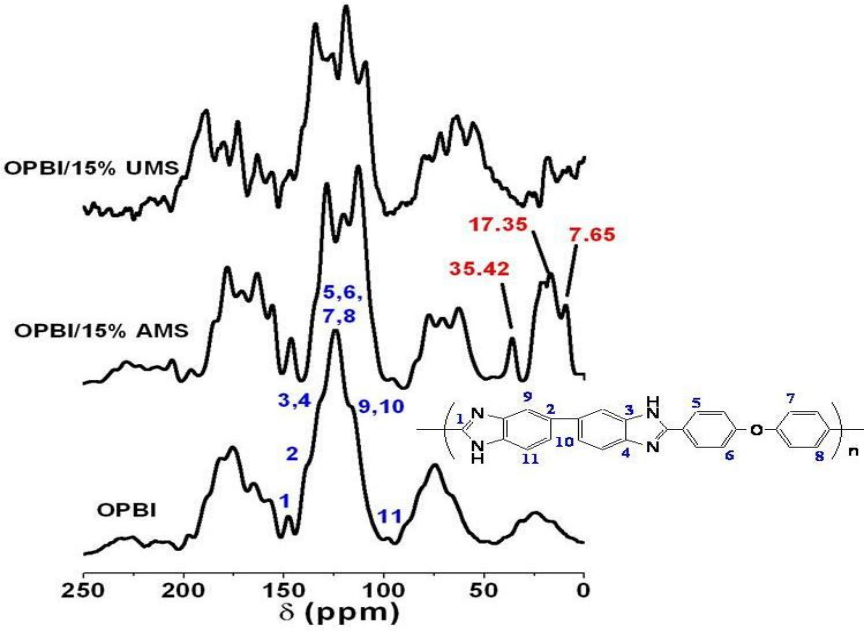

Figure 6.2. *Solid state ^{13}C CPMAS NMR spectra of OPBI and its nanocomposites.*

6.3.2. X-ray Study

Small angle x-ray scattering (SAXS) and wide angle x-ray diffraction (WAXD) are used for the characterization of the structure and to evaluate the crystallinity of OPBI/AMS nanocomposites. The WAXD patterns of the OPBI, AMS, UMS and their nanocomposites are presented in the Figure 6.3. Both the OPBI and AMS display a broad diffraction at 2θ = 20-30º, attributing that both are amorphous in nature and this observation matches well with the literature.[31] Several sharp crystalline peaks are observed for the OPBI nanocomposites along with the amorphous broad peak of OPBI and the intensities of these peaks are altering with increasing the percentage loading of AMS (Figure 6.3A). The appearance of crystalline peaks in the nanocomposites despite of the fact that both polymer and nanofiller are amorphous in nature is the indication of formation of ordered structure. This ordering in nanocomposites is probably because of

the fact that the OPBI chains drive the highly dispersed silica nanoparticles in an ordered state in the OPBI matrix with the help of interaction between the surface $–NH_2$ functionality of AMS and imidazole moieties of OPBI. Hence it can be concluded that the partial crystalline (ordered) nature of OPBI/AMS nanocomposite is achieved by introducing AMS in OPBI. However, it is interesting to note that the modification of silica particle surface with amine functionality using APTES is very important to bring this ordered structure in the nanocomposites. We have observed that composites of OPBI with unmodified silica (UMS) particles prepared in similar manner as it was done with AMS do not display any ordered structure (Figure 6.3B) like in Figure 6.3A. The WAXD patterns of OPBI/UMS composites have only amorphous broad peaks. Comparison of membranes photographs (Figure 6.4) clearly demonstrates that a very transparent homogeneous nanocomposites membrane is obtained in case of AMS whereas the film obtained using UMS has phase separated zones. Hence the modification of silica with APTES is the key step for the whole process since the amine functionality on the silica surface brings the interaction with OPBI.

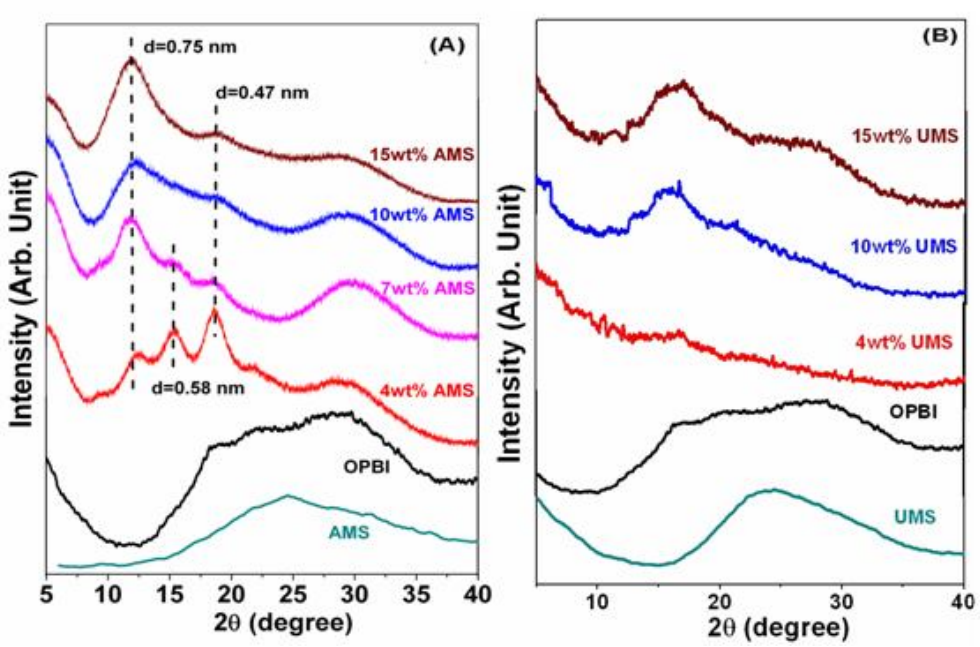

Figure 6.3. *WAXD patterns of OPBI, AMS, UMS and their nanocomposites with different percentage loading of (A) AMS and (B) UMS .*

Figure 6.4. *Photographs of OPBI/AMS and the OPBI/UMS nanocomposite membranes.*

Figure 6.5 represents the SAXS profiles of the nanocomposites of OPBI/AMS and OPBI/UMS along with OPBI, AMS and UMS. OPBI and AMS do not have any peaks, but all the OPBI/AMS nanocomposites display peaks in the SAXS patterns (Figure 6.5A). The position and the intensity of the peaks vary depending upon the nanofiller loading. This result once again attributes the formation of ordered structure in the nanocomposites although the polymer and nanofiller are amorphous. The necessity of the surface modification of silica particle with $–NH_2$ functionality using APTES is again proved by the appearance of peaks in the SAXS patter in case of OPBI/AMS whereas absence of any peaks in the SAXS patterns of OPBI/UMS as shown in Figure 6.5B.

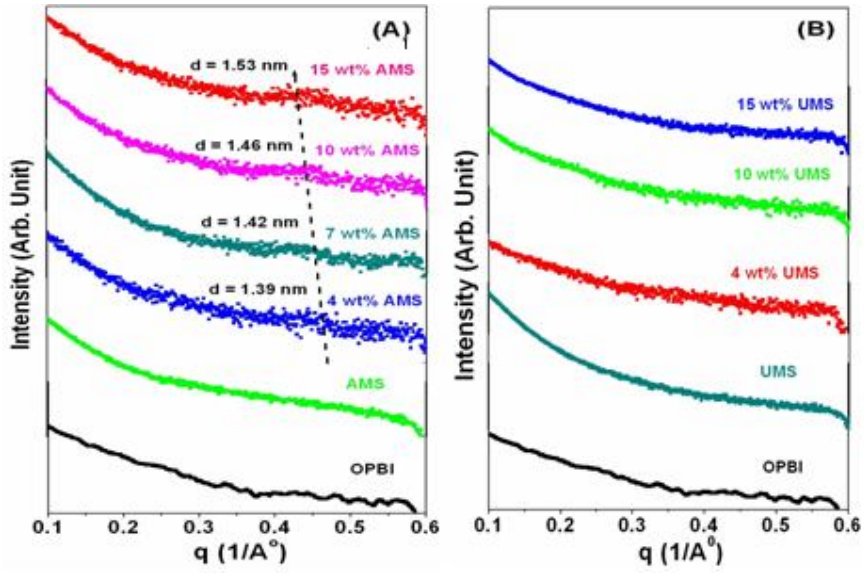

Figure 6.5. *SAXS patterns of OPBI, AMS, UMS and their nanocomposites with different percentage loading of (A) AMS and (B) UMS .*

A careful analysis of WAXD and SAXS data shown in Figure 6.3A and 6.5A respectively bring to our notice that the positions and intensities of the diffraction peaks depend upon the nanofiller loading. Few peaks have stronger intensity when the loading is low and they almost disappear for higher loading, instead a new peak appears (Figure 6.3 A). For example peak at 2θ = 15.22º (0.58 nm) in case of 4 wt% nanocomposite is sharp bur disappears for 10 and 15 wt% nanocomposites and similarly peak at 2θ = 12.2º (d = 0.75 nm) is not intense in 4 wt% nanocomposite but gradually become sharper in 15 wt% nanocomposites. This observation suggests the formation of ordered structure of AMS particles through a self-assembly process through the interaction with polymer chain in the OPBI matrix. This result attributes that the ordering of the AMS in OPBI matrix is governed by the loading of nanofiller and different structure are formed for different loading. Similar kind of observation was made earlier by Akcora et al.[36] in case of nanocomposite of polystyrene grafted silica on polystyrene matrix and they have predicted, both theoretically and experimentally, a structural anisotropy super structure formation due to the self-assembly. In the present case also similar process is happening by yielding self-assembled clusters of AMS particles depending upon the loading. In next section we will get prove from the TEM study. However, it is interesting to note that the nanocomposites obtained from UMS do not show the variation in their WAXD pattern with loading (Figure 6.3 B); reinforcing our claim that modification of silica surface plays an important role in the self-assembly process. In fact we noticed that OPBI/UMS nanocomposites do not display any self-assembled clusters in TEM images. Similarly SAXS (Figure 6.5 A) data clearly shows that the peak position and intensity varies as a function of the AMS loading. Hence the self-assembly of particles in the OPBI matrix is completely governed by the loading in the nanocomposite. Again the SAXD data (Figure 6.5 B) of nanocomposites obtained from UMS samples do not show any scattering peaks, confirming the absence of self-assembled structures.

6.3.3. Morphology Study

TEM is used to examine the quality of the homogeneous dispersion of silica nanoparticles in OPBI and the any possible cluster or structure formation owing to the

self-assembly of silica nanoparticles. Figure 6.6 shows the TEM micrographs of the OPBI/silica nanocomposites with the indicated weight percentage loading of both the UMS and AMS along with both the pristine silica particles. Both the pristine silica nanoparticles (Figure 6.6 A and B) are well dispersed, not in aggregated states and almost spherical in size. The size of the AMS is found to be bigger than the UMS. In all the nanocomposite cases silica particles are distributed uniformly in the OPBI matrix. We observed the morphological features (as presented in Figure 6.6) all over the TEM grids. It is worthwhile to note that in case of OPBI/AMS nanocomposite, the particles are aggregated and the domain size and the shape of the aggregates are different for different loading (Figure 6.6 C-F) but in case of OPBI/UMS nanocomposites, the particles are not aggregated and they are well dispersed (Figure 6.6 G-I). It can be clearly seen that the AMS are tightly bonded to the matrix, indicating a very well interfacial adhesion between the two phases. The FT-IR (Figure 6.1) and ^{13}C CPMAS NMR (Figure 6.2) studies demonstrated the presence of interactions between the silica nanoparticles and the benzimidazole moiety of OPBI polymer. These interactions are believed to be accountable for the formation of the nanosized silica domains within the OPBI matrix and the relatively high level of mixing between the OPBI matrix and silica nanoparticles. The interesting observation is that the domain size and shape (collection of silica nanoparticles) of silica nanoparticles increases with increasing the percentage loading. This attributes that the interactions between the polymer and AMS not only enhances the compatibility of the organic–inorganic system it also facilitates the attractive interactions between the particles themselves, which causes them to aggregates in different size and shapes. The different size and shapes of the self-assembled AMS in the OPBI matrix resulted in clusters formation. This structure formation leads to the ordering and hence we observed variation of crystalline peaks depending on the loading as observed from WAXD and SAXD data shown in Figure 6.3A and 6.5A, respectively. However, in case of OPBI/UMS nanocomposite, since particles do not undergo any self-assembled structure formation, hence no ordering takes place and no peaks appear in WAXD and SAXD as shown in Figure 6.3B and 6.5B, respectively.

Now question remains why the self-aggregated cluster formation takes place in the OPBI matrix in case of AMS but not for UMS. In case of UMS, the surfaces are decorated with hydroxyl groups and hence the particles tend to repel each other resulting non-aggregated structure. However, in AMS the surface of the particles are decorated by the hydroxyl as well as $-NH_2$ functionality and hence the particles do not repel each other in presence of OPBI, which acts as a driving bridge for the particles to come close each other with the help of hydrogen bonding interaction with the OPBI to form the cluster.[15] The size and the shape of the cluster are probably due to the synergistic effect of the loading. It is important to note that this cluster formation significantly influences the various properties especially mechanical and ion conducting property of the OPBI nanocomposites, as presented in the next few sections.

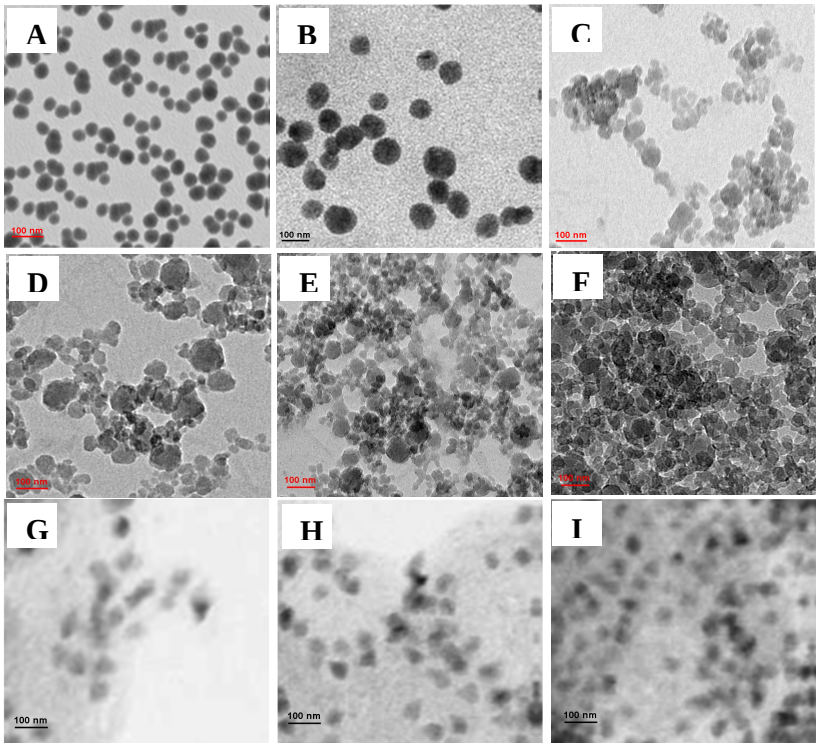

Figure 6.6. *Transmission electron micrographs of (A) silica nanoparticles (UMS), (B) amine modified silica nanoparticles (AMS), the OPBI nanocomposite with (C) 4 wt%, (D) 7 wt%, (E) 10 wt%, (F) 20 wt% AMS loading and (G) 4 wt%, (D) 10 wt% and (E) 15 wt% UMS loading.*

6.3.4. Thermal Stabilities

TGA data for OPBI and all the OPBI nanocomposites with different percentage loading of the AMS are shown in Figure 6.7. An initial weight loss at around 100-120°C and a second weight loss at around 570-600°C are observed in all the cases. The first weight loss is due to the loosely bound absorbed water molecule to the OPBI film and the second weight losses are due the degradation of polymer backbone. Table 6.1 summarizes thermal stability data. The TGA data obtained clearly indicates that the thermal stability of OPBI film improved after nanocomposite formation with the AMS and stability increases with increasing the loading of silica nanoparticles in the OPBI matrix. Very recently, we have observed similar kinds of influence of various types of nanoclays in the thermal stabilities of OPBI.[26] Interfacial interaction between OPBI and silica nanoparticles have a very significant function in the thermal degradation of polymeric nanocomposites. A suitable interfacial interaction permits silica nanoparticles to play as thermal barrier in the OPBI matrix which actually restricts the decomposition of the material by the uniform dispersion of nanosized particles inside the OPBI matrix by accumulating to the surface of the molten polymer and creating a sort of shield that acts as physical protection from heat for the remaining polymer and slowing down the volatilization of the polymer fragments.[37] The shielding ability depends on the dispersion patters of the silica nanoparticles in the polymer matrix. This aspect is related to both the nature and morphological features of the silica nanoparticles in the OPBI matrix. Since in the current nanocomposites, the morphological and structural feature changes with the silica loading (as seen in Figure 6.3, 6.5 and 6.6) hence we obtained different level of thermal stability. It is interesting to note that nanocomposite obtained from UMS sample does not display significant improvement in the thermal stability (Figure 6.7 and Table 6.1) even though the particles are well dispersed in the OPBI matrix (Figure 6.6G-I). This clearly proves the effect of morphologies in thermal stability. We believe the self-assembled clusters obtained in case of OPBI/AMS nanocomposite is the responsible for the dramatic change in thermal stabilities of OPBI.

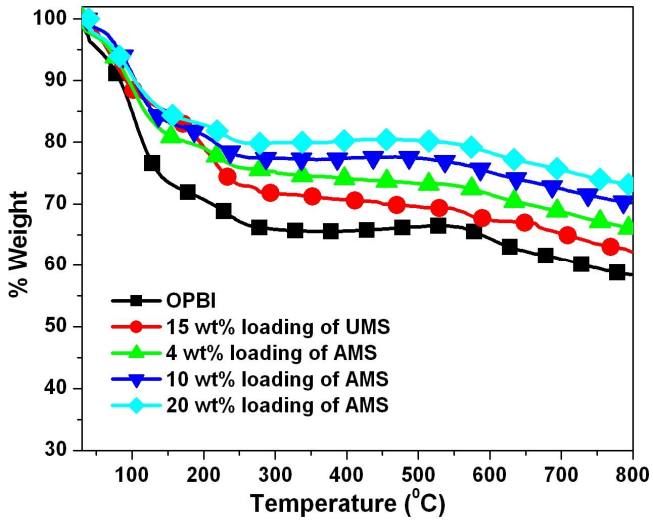

Figure 6.7. *TGA plots of OPBI and its nanocomposite membranes with AMS and UMS at various percentages of loading.*

Table 6.1. *Thermal stability data for all the OPBI nanocomposite membranes with the silica nanoparticles.*

Sample	$W_{510°C}$ (%)[a]	$T_{20\%}$ (°C)[b]	$W_{790°C}$ (%)[c]
OPBI	66.76	116	58.74
OPBI/4wt% AMS	73.47	158	66.24
OPBI/7wt% AMS	75.58	205	68.05
OPBI/10wt% AMS	77.09	210	69.86
OPBI/15wt% AMS	77.99	226	70.46
OPBI/20wt% AMS	80.41	249	73.48
OPBI/15wt% UMS	69.46	191	62.35

[a] Residual weight percentage at 510°C.
[b] Temperature at which 20% weight loss is observed.
[c] Residual weight percentage at 790°C.

6.3.5. Dynamic Mechanical Properties

The effect of large surface area of silica nanoparticles on the thermo-mechanical properties of OPBI matrix in the nanocomposite can be studied well using DMA. The storage modulus (E', the elastic component of the materials) as a function of temperature for the OPBI nanocomposites with AMS are shown in Figure 6.8. We have extracted few important data from Figure 6.8 and tabulated in Table 6.2 for comparison. The E' of the nanocomposites are higher than that of neat OPBI and OPBI/UMS nanocomposites and are increasing with increasing the percentage loading of AMS (Figure 6.8 and Table 6.2). Hence, substantial mechanical reinforcements are observed in case of OPBI/AMS nanocomposites whereas the negligible reinforcement took place when UMS particles are used. This result clearly attributes that the morphology and structural features of the resulting nanocomposites are the deciding factors for the modification of mechanical strength of the final materials. The presence of AMS on the OPBI matrix increases the rigidity of the matrix by reducing the segmental mobility due to physical interactions between inorganic and organic phases which brings the ordering in the composite by yielding AMS clusters which in turn helps to enhance E' of the nanocomposites. Also with increasing the AMS content in the OPBI matrix, the interfacial adhesion increases due to interactions between silica nanoparticles and OPBI. Table 6.2 compares the E' values of OPBI and OPBI nanocomposites with the silica nanoparticles at various temperatures. From the table it is seen that % of increase of E' enhances with increasing loading all over the temperature range. However, it is important to note that even 15 wt% UMS (last row in Table 6.2) only increase by ~5-17 % depending on the temperature range whereas 15 wt% of AMS enhances E' by more than 110-140 % (5^{th} row in the Table 6.2). This huge difference between UMS and AMS nanocomposites is because of their morphological and structural features. Despite the uniform dispersion of UMS in OPBI (Figure 6.6G-I) the resulting materials do not show much improvement since the interaction between the OPBI and UMS is not enough to reinforce the mechanical properties. On the other hand the self-assembly of AMS particles resulted clusters formation (Figure 6.3A, 6.5A, and 6.6C-F) owing to the

strong interaction between the particles trough the OPBI, which acts as a bridging, boosted the mechanical property enormously.

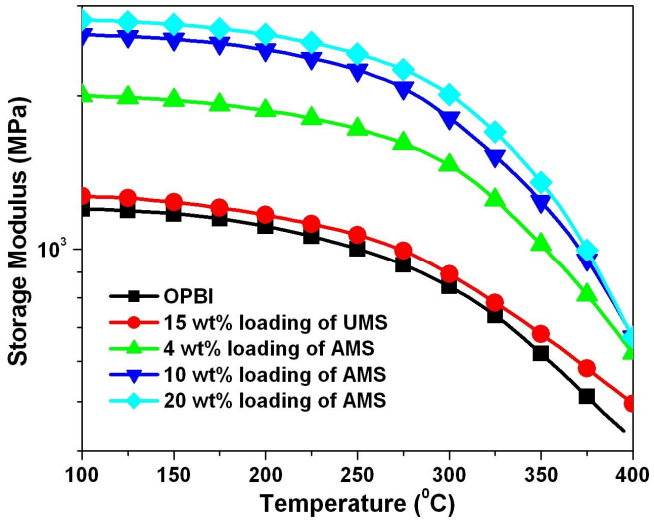

Figure 6.8. *Temperature dependent storage modulus plots of OPBI nanocomposites obtained from DMA studies.*

Table 6.2. *Various thermo mechanical data of OPBI nanocomposite membranes obtained from the DMA study.*

Sample	*E' (MPa) at 150°C*	*% increase*	*E' (MPa) at 300°C*	*% increase*	*E' (MPa) at 390°C*	*% increase*
OPBI	*1174*		*847*		*449*	
OPBI/4wt% AMS	1965	67.37	1466	73.08	799	77.95
OPBI/7wt% AMS	2475	110.81	1798	112.28	871	93.99
OPBI/10wt% AMS	2587	120.36	1814	114.17	1025	128.29
OPBI/15wt% AMS	2681	128.36	1830	116.06	1082	140.98
OPBI/20wt% AMS	2777	136.54	2018	138.25	1167	159.91
OPBI/15wt% UMS	1246	6.13	891	5.19	529	17.81

The tan δ curves of neat OPBI and its nanocomposites with both the silica nanoparticles (UMS and AMS) as a function of temperature are shown in Figure 6.9. All the nanocomposite membranes exhibit single relaxation point which corresponds to

the glass transition temperature (T_g). With the increase of percentage loading of AMS in OPBI matrix, the glass transition temperature (T_g) of the nanocomposites shifts towards the higher temperature. However, the T_g in case of UMS show very negligible shift. The T_g of OPBI has shifted by 63°C (from 344°C to 407°C) when nanocomposite is made with 15% AMS whereas 15% UMS loading in OPBI displays only 8°C (344°C to 352°C) shift. Since OPBI and AMS interact each other and bring certain degree of ordering in the nanocomposite, as proved by structural and morphological study in the earlier sections, hence the significant decrease in free volume occurs in the AMS nanocomposites. As a result, higher temperature is required to reach the required free volume fraction segmental mobility and the T_gs increases with loading of AMS. Because of these above facts T_gs in case of all the OPBI nanocomposites with AMS are increased. However, since in case of UMS interactions are not much so it is expected T_g will not change substantially.

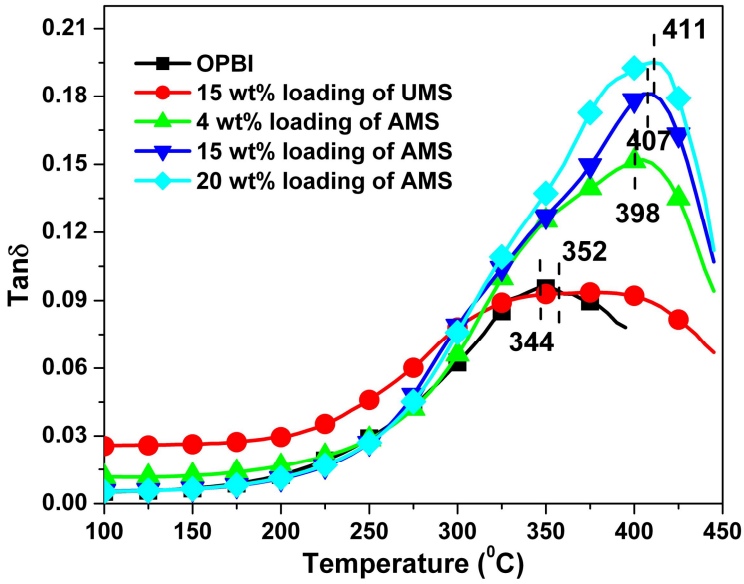

Figure 6.9. *Temperature dependent tan δ plots of OPBI nanocomposites obtained from DMA studies.*

6.3.6. Oxidative stability

The oxidative stabilities of the membranes are used to estimate the membranes durability in oxidative environment.[38] All the nanocomposite membranes were tested in oxidizing condition, in presence of Fenton's reagent (3% H_2O_2 containing 2 ppm $FeSO_4$) at 70°C to check their stability. The effect of the nano-sized AMS dispersion on the oxidative stability of OPBI membranes is shown in Figure 6.10. It is observed that the introduction of AMS particles in the OPBI matrix improve the oxidative stability quite significantly than the pristine OPBI. The hydroxyl and hydroperoxyl radicals species (HO· and HOO·)[39, 40] produced from the Fenton's reagent can not penetrate the silica nanoparticles to attack the polar group of polymer matrix due to the presence of homogeneous dispersion of AMS in the OPBI matrix. The presence of hydroxyl and amine groups in the surface of the silica nanoparticles contribute in hydrogen bonding with polymer chains as shown in FT-IR study (Figure 6.1), which probably shields the polar groups of OPBI from attack by free radical species. With increasing the silica content in the polymer matrix, the shielding is better and it becomes difficult for free radicals to attack the polymer chain.

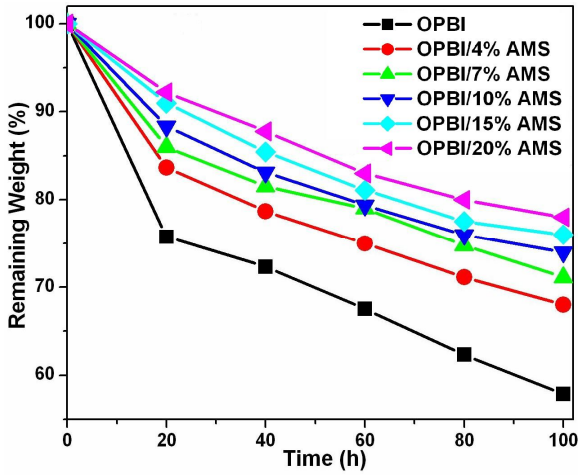

Figure 6.10. *Oxidative stability of OPBI nanocomposite membranes with different percentage loading of AMS nanoparticles.*

6.3.7. Water uptake and phosphoric acid (PA) doping level

Table 6.3 displays the water uptake, swelling ratio and PA doping level of OPBI nanocomposite membranes obtained with AMS. The water uptake and swelling ratio of the OPBI nanocomposite membranes are lower than that of the pristine OPBI membrane and decreases significantly with increasing the nanofiller content in the nanocomposite. TGA data (Figure 6.7 and Table 6.1) also is agreement with this observation where the initial weight loss due to the water molecule is decreasing with increasing the percentage loading of AMS in the nanocomposite. The hydrophobic nature of the silica particles increases after the modification of silica surfaces by APTES and therefore the AMS nanofiller enhances the hydrophobic character of OPBI/AMS nanocomposites, which results in decrease in water uptake and swelling ratio. Also we noticed that due to the interaction between the nanofiller and OPBI which yields some degree of structural ordering by producing cluster (Figure 6.6C-F), reducing the free volume of the OPBI chain which is reflected in their high T_g value (Figure 6.9). Therefore, the water molecules could not trap themselves inside the nanocomposite membranes because of small free volume resulting low water uptake and swelling ratio.

The PA doping capacity of the polymer membrane is the important screening parameter which has a huge influence upon the fuel cell efficiency.[20] The PA doping level of the membrane is expressed as the number of PA mols per OPBI repeat unit. PA doping levels of all OPBI nanocomposite membranes are shown in Table 6.3. The OPBI nanocomposite membranes show the remarkably higher PA doping levels than that of pristine OPBI membrane and it increases with increasing nanofiller loading. Earlier in several occasions, we have found out that the increase in hydrophobic character (low water uptake and swelling ratio) enhances the PA loading capacity. The reason behind this is because the hydrophobic nature of the membrane does not allow water molecule to block the proton accepter (-N=) groups of OPBI and hence facilitates the PA molecule to diffuse and dope the –N= group readily.[41] Therefore it is expected that with increasing silica loading, the PA loading should increase since hydrophobic character decreases. Table 6.3 data clearly reflects our above observations. In addition the amine

modified silica has an amphoteric character, and in PA media silica nanoparticle acts as a base and can absorb phosphoric acid, which might help the nanocomposite membranes to dope more PA molecules.[25]

Table 6.3. *Water uptake, swelling ratio and PA doping level of the OPBI/AMS nanocomposite membranes.*

Sample	*Water Uptake (Wt %)*	*Swelling Ratio (%)*	*PA mols/PBI repeat unit*
OPBI	16.25	4.06	16.18
OPBI/4 wt% AMS	14.52	3.99	21.75
OPBI/7 wt% AMS	13.21	3.73	22.75
OPBI/10 wt% AMS	9.32	3.41	24.43
OPBI/15 wt% AMS	7.06	2.44	26.60
OPBI/20 wt% AMS	6.19	1.17	31.25

6.3.8. Proton conductivity

Proton conductivity (σ) of the PA doped OPBI membrane is an important parameter to be evaluated because the fuel cell efficiency is strongly dependent upon this property. The representative Nyquist plots of the OPBI and nanocomposite membranes are shown in supporting information Figure 6.11. Figure 6.12 shows the proton conductivities of the pristine OPBI, the OPBI/AMS nanocomposites and OPBI/UMS membranes as a function of temperature. It must be noted that proton conductivities reported here were measured in complete dry condition i.e. in zero relative humidity (RH). We have taken appropriate precaution as mentioned in the experimental section to measure the conductivities at 0% RH. Very often, it has been observed and reported by several authors that the PA doped PBI membranes obtained from the dipping of PBI membrane in PA bath do not conduct protons above 100^{o}C in 0% RH.[42] However, in this case we could measure the proton conductivities in 0% RH at above 100^{o}C and obtain perfect semicircle Nyquist plots (as shown in Figure 6.11).

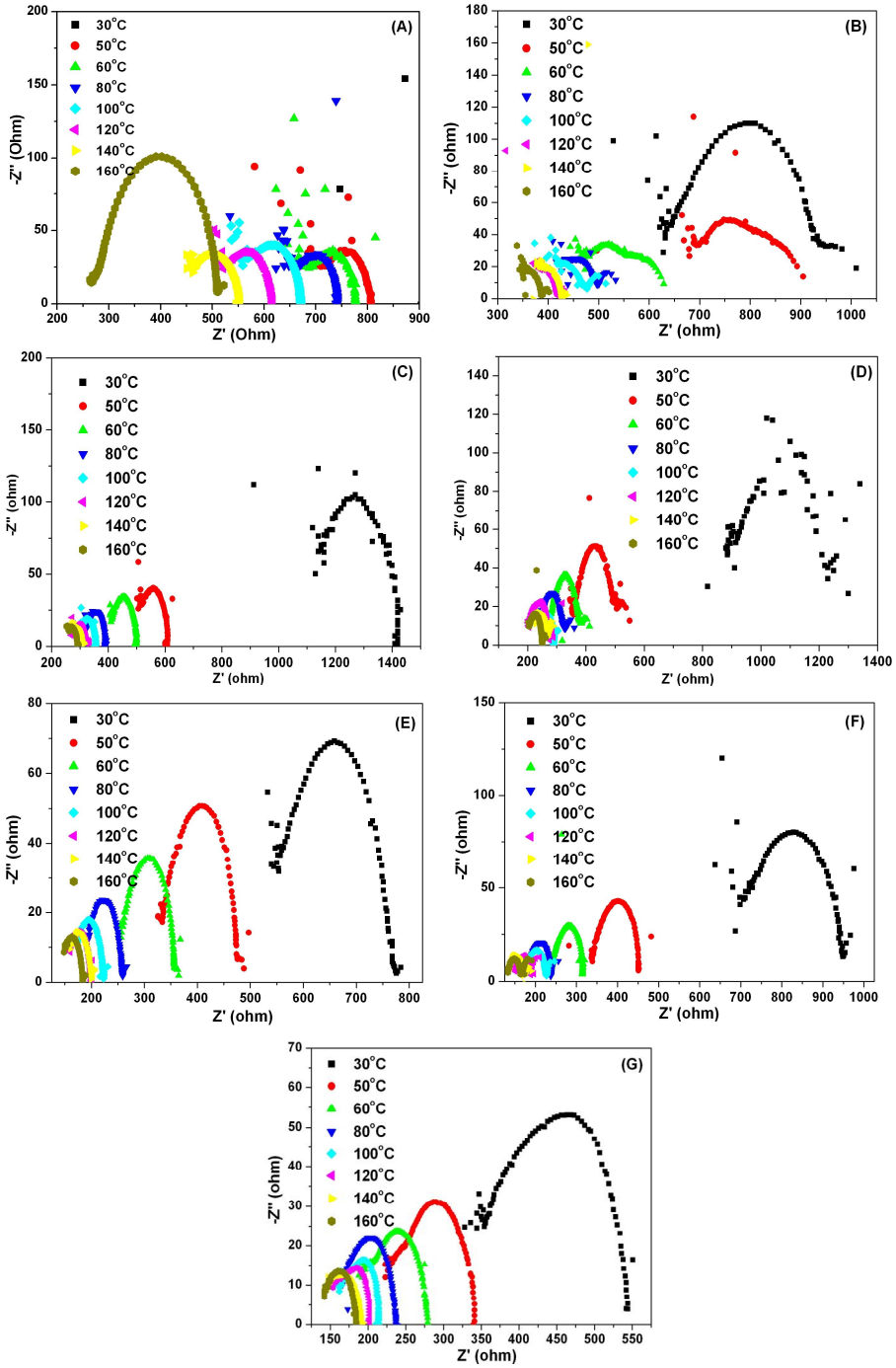

Figure 6.11. *Nyquist plots of (A) OPBI, (B) OPBI/4 wt% AMS, (C) OPBI/7 wt% AMS, (D) OPBI/10 wt% AMS, (E) OPBI/15 wt% AMS, (F) OPBI/20 wt% AMS and (G) OPBI/15 wt% UMS nanocomposites.*

Figure 6.12 clearly suggests that the proton conductivities of nanocomposite hybrid membranes are much higher than the pristine OPBI membrane and increases with increasing the nanofiller content. At 160ºC, the σ of pristine OPBI is 4.4×10^{-2} S/cm whereas at the same temperature the σ of OPBI/20 wt% AMS membrane is 1.25×10^{-1} S/cm. Hence the σ increases by an order of magnitude from OPBI to nanocomposite membrane with 20 wt% loading. The substantial increase in σ with increase in AMS loading is expected since the PA loading (Table 6.3) of nanocomposite membranes are very high. Generally, the proton transport in organic-inorganic nanocomposite materials under anhydrous condition takes place through a Grotthuss mechanism (the proton moves in an infinite network of hydrogen bonds) and supported by vehicle mechanism (protons form hydrogen bonding with silica nanoparticle acting as proton carriers) in which the inorganic component acts as a vehicle for the proton conductive process.[43,44] The OPBI/15 wt% UMS has σ = 6.9×10^{-2} S/cm whereas OPBI/15 wt% AMS has 1.03×10^{-1} S/cm at 160ºC. The presence of AMS nanoparticles and their self-assembled clusters facilitates the proton transport process much better than the UMS where particles are more dispersed. Hence, our σ data once again reinforces the fact that the clusters formation in case of AMS owing to the interaction between OPBI and nanofiller influences the properties of nanocomposite membrane.

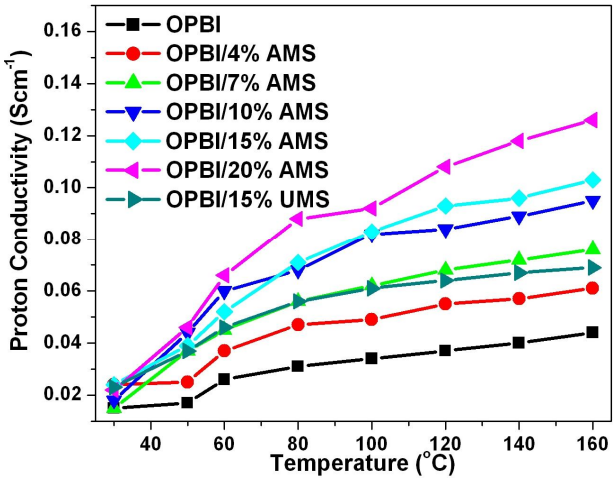

Figure 6.12. *Proton conductivity against temperature for OPBI nanocomposite membranes with various percentages loading of nanofillers.*

The temperature dependency of proton conductivity is well expressed by Arrhenius equation[45] as follows:

$$\ln(\sigma T) = \ln \sigma_0 - \frac{E_a}{RT} \tag{6.5}$$

Where σ is the proton conductivity of the membrane (Scm^{-1}), σ_o is the pre-exponential factor ($S\ K^{-1}\ cm^{-1}$), E_a is the proton conducting activation energy (kJ/mol), R is the ideal gas constant ($J\ mol^{-1}K^{-1}$) and T is the temperature (K). The activation energy (E_a), which is the minimum energy required for proton conduction are obtained from the slope at the linear fit of equation 6.5 and is shown in Figure 6.13. In all the cases the data fit well with the Equation 6.5 indicates that the proton conduction is primarily governed by the Grotthuss mechanism. However a careful look in the Figure 6.13, suggests deviations at different points from the linear plots in nanocomposite cases; attributing that the proton conduction mechanism not only governed by Grotthuss process some contribution from vehicle type process might be involved. This is possible since nanofillers are acting as bridging carrier of proton since they form self-assembled clusters in case of OPBI/AMS nanocomposite membranes. Higher activation energy value means high energy is required to conduct proton through the membrane. Table 6.4 list all the E_a values and exhibits that E_a value for nanocomposites are higher than the pristine OPBI. This is expected since nanofillers act as carrier bridge for proton therefore little more energy is required for the process. However, the E_a values are quite close to the E_a of free PA,[46] hence faster conduction process will take place.

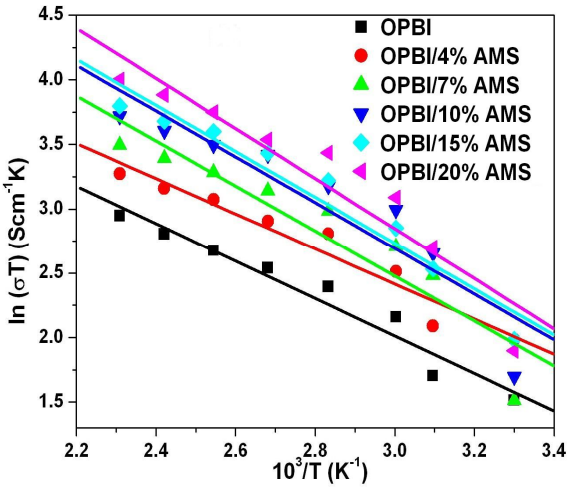

Figure 6.13. *Arrhenius plots for the proton conduction of OPBI and its nanocomposites with AMS nanoparticles.*

Table 6.4. *Activation energy (E_a) of the OPBI and OPBI/AMS nanocomposite membranes.*

Sample	***Activation Energy (E_a) (kJ/mol)***
OPBI	12.102
OPBI/4wt% AMS	11.34
OPBI/7wt% AMS	14.52
OPBI/10wt% AMS	14.75
OPBI/15wt% AMS	14.81
OPBI/20wt% AMS	16.15

6.4. Conclusions

A series of organic/inorganic hybrid nanocomposite materials consisting of OPBI with amine modified and unmodified silica nanoparticles (AMS and UMS) are prepared by the solution blending method. FT-IR, ^{13}C CPMAS NMR, XRD, TEM,

TGA, DMA experiments are carried out to characterize the morphology and properties of the nanocomposites. The morphology of the OPBI/silica nanocomposites are largely dependent upon the functional groups of the silica surface; in case of amine modified surface (AMS) self-assembled clusters formation is observed whereas well dispersed morphology is obtained with unmodified surface (UMS). The incorporation of AMS in OPBI results in an increase in thermal and oxidative stabilities. The storage modulus and glass transition temperature of the OPBI/AMS nanocomposites are increased greatly than that of pure polymer. The phosphoric acid (PA) loading of the nanocomposites are much higher than the pristine polymer. The proton conductivity of all the nanocomposite membranes increases with increasing percentage content of the silica nanoparticle. These nanocomposite membranes have all the characteristics which are required to be an efficient polymer electrolyte membrane (PEM) for HT-PEMFC application.

Referrences

1. Jung, D. H.; Cho, S. Y.; Peck, D. H.; Shin, D. R.; Kim, J. S. *J. Power Sources* **2002**, *106*, 173.
2. Antonucci, P. L.; Arico, A. S.; Creti, P.; Ramunni, E.; Antonucci, V. *Solid State Ionics* **1999**, *125*, 431.
3. Kannan, R.; Kakade, B. A.; Pillai, V. K. *Angew. Chem*. **2008**, *120*, 2693.
4. Zou, H.; Wu, S.; Shen, J. *Chem. Rev*. **2008**, *108*, 3893.
5. Kim, Y. S.; Wang, F.; Hickner, M.; Zawodzinski, T. A.; McGrath, J. E. *J. Membr. Sci.* **2003**, *212*, 263.
6. Ponce, M. L.; Prado, L.; Ruffmann, B.; Richau, K.; Mohr, R.; Nunes, S. P. *J. Membr. Sci.* **2003**, *217*, 5.
7. Ajayan, P. M.; Stephen, O.; Colliex, C.; Trauth, D. *Science* **1994**, *265*, 1212.
8. Ajayan, P. M.; Schadler, L. S.; Giannaris, C.; Rubio, A. *Adv. Mater.* **2000**, *12*, 750.
9. Chen, X. G.; Li, Z.; Zhou, H. Q.; Wang, T. J.; Qin, J. G.; Inokuchi, M. *Polymer* **2007**, *48*, 3256.
10. Loy, D. A.; Assink, R. A. *J. Am. Chem. Soc.* **1992**, *114*, 3977.
11. McKeen, J. C.; Yan, Y. S.; Davis, M. E. *Chem. Mater*. **2008**, *20*, 5122.
12. Stankovich, S.; Dikin, D. A.; Dommett, G. H. B.; Kohlhaas, K. M.; Zimney, E. J.; Stach, E. A.; Piner, R. D.; Nguye, S. T.; Ruoff, R. S. *Nature* **2006**, *442*, 282.
13. Balazs, A. C.; Emrick, T.; Russell, T. P. *Science* **2006**, *314*, 1107.
14. Yang, F.; Ou, Y.; Yu, Z.-Z. *J. Appl. Polym. Sci.* **1998**, *69*, 355.
15. Bagwe, R. P.; Hilliard, L. R.; Tan, W. *Langmuir* **2006**, *22*, 4357.
16. Chen, Y.; Iroh, J. O. *Chem. Mater*. **1999**, *11*, 1218.
17. Zhang, M. Q.; Rong, M. Z.; Friedrich, K. *In Handbook of Organic-Inorganic Hybrid Materials and Nanocomposites*; American Scientific Publishers: Stevenson Ranch, CA, **2003**, *2*, 113.
18. Schadler, L. S. *Nanocomposite Science and Technology*; Wiley-VCH: Weinheim, Germany, **2003**.

19. Savadogo, O. *J. New Mater. Electrochem. Syst.* **1998**, *1*, 47.
20. Samms, S. R.; Wsmus, S.; Savinell, R. F. *J. Electrochem. Soc.* **1996**, *143*, 1225.
21. Xiao, L.; Zhang, H.; Scanlon, E.; Ramanathan, L. S.; Choe, E. -W.; Rogers, D.; Apple, T.; Benicewicz, B. C. *Chem. Mater.* **2005**, *17*, 5328.
22. Mecerreyes, D.; Grande, H.; Miguel, O.; Ochoteco, E.; Marcilla, R.; Cantero, I. *Chem. Mater.* **2004**, *16*, 604.
23. Sannigrahi, A.; Arunbabu, D.; Jana, T. *Macromol. Rapid. Commun.* **2006**, *27*, 1962.
24. Li, Q.; He, R.; Jensen, J. O.; Bjerrum, N. J. *Fuel Cells* **2004**, *4*, 147.
25. Mustarelli, P.; Quartarone, E.; Grandi, S.; Carollo, A.; Magistris, A. *Adv. Mater.* **2008**, *20*, 1339.
26. (a) Ghosh, S.; Sannigrahi, A.; Maity, S.; Jana, T. *J. Phys. Chem. C* **2011**, *115*, 11474, (b) Chung, S. -W.; Hsu, S. L. -C.; Hsu, C. -L *J. Power Sources* **2007**, *168*, 172.
27. (a) Fijigaya, T.; Okamaoto, M.; Nakashima, N. *Carbon* **2009**, *47*, 3227, (b) Shao, H.; Shi, Z.; Fans, J.; Yin, J. *Polymer* **2009**, *50*, 5987, (c) Kannan, R.; Kagaiwale, H. N.; Chaudhari, H. D.; Kharul, U. K.; Kurungot, S.; Pillai, V. K. *J. Mater. Chem.* **2011**, *21*, 7223.
28. (a) Wang, Y.; Shi, Z.; Fang, J.; Yin, J. *Carbon* **2011**, *49*, 1199, (b) Wang, Y.; Shi, Z.; Famg, J.; Hu, H.; Ma, X.; Yin, J. *J. Mater. Chem.* **2011**, *21*, 505.
29. (a) Xu, C.; Wu, X.; Wang, X.; Mamlouk, M.; Scott, K. *J. Mater. Chem.* **2011**, *21*, 6014, (b) He, R.; Li, Q.; Xiao, G.; Bjerrum, N. J. *J. Membr. Sci.* **2003**, *226*, 109.
30. (a) Pu, H.; Liu, L.; Chang, Z.; Yuan, J. *Electrochim. Acta* **2009**, *54*, 7536, (b) Chung, S. -W.; Hsu, S. L. -C.; Liu, Y. -H. *J. Membr. Sci.* **2007**, *305*, 353.
31. Sannigrahi, A.; Ghosh, S.; Lalnuntluanga, J.; Jana, T. *J. Appl. Polym. Sci.* **2008**, *111*, 2194.
32. Ghosh, S.; Sannigrahi, A.; Maity, S.; Jana, T. *J. Phys. Chem. B* **2010**, *114*, 3122.
33. Stober, W.; Fink, A. *J. Colloi. Interf. Sci.* **1968**, *26*, 62.

34. de Haan, J. W.; Van den Bogaert, H. M.; Ponjee, J. J.; Van de Ven, L. J. M. *J. Colloid. Inter. Sci.* **1986**, *110*, 591.
35. Chang, K. C.; Lin, C. Y.; Lin, H. F.; Chiou, S. C.; Huang, W. C.; Yeh, J. M.; Yang, J. C. *J. Appl. Polym. Sci.* **2008**, *108*, 1629.
36. Akcora, P.; Liu, H.; Kumar, S. K.; Moll, J.; Li, Y.; Benicewicz, B. C.; Schadler, L. S.; Acehan, D.; Panagiotopoulos, A. Z.; Pryamitsyn, V.; Ganesan, V.; Ilavsky, J.; Thiyagarajan, P.; Colby, R. H.; Douglas, J. F. *Nat. Mater.* **2009**, *8*, 354.
37. Hsiue, G. H.; Liu, Y. L.; Tsiao, J. *J. Appl. Polym. Sci.* **2000**, *78*, 1.
38. Gosalawit, R.; Chirachanchaia, S.; Shishatskiy, S.; Nunes, S. P. *J. Membr. Sci.* **2008**, *323*, 337.
39. Asano, N.; Aoki, M; Suzuki, S; Miyatake, K. *J. Am. Chem. Soc.* **2006**, *128*, 1762.
40. Hübner, G; Roduner, E. *J. Mater. Chem.* **1999**, *9*, 409.
41. Arunbabu, D.; Sannigrahi, A.; Jana, T. *J. Phys. Chem. B* **2008**, *112*, 5305.
42. He, R.; Li, Q.; Xiao, G.; Bjerrum, N. J. *J. Membr. Sci.* **2003**, *226*, 169.
43. Kreuer, K. D.; Rabenau, A.; Weppner, W. *Angew. Chem., Int. Ed. Engl.* **1982**, *21*, 208.
44. Karthikeyan, C. N.; Nunes, S. P.; Prado, L. A. S. A.; Ponce, M. L.; Silva, H.; Ruffmann, B.; Schulte, K. *J. Membr. Sci.* **2005**, *254*, 139.
45. He, R.; Li, Q.; Bach, A.; Jensen, J. O.; Bjerrum, N. J. *J. Membr. Sci.* **2006**, *277*, 38.
46. Ma, Y. -L.; Wainright, J. S.; Litt, M.; Savinell, R. F. *J. Electrochem. Soc.* **2004**, *151*, A8.

Chapter 7

Summary & Conclusions

7.1 Summary

Thesis entitled *"Studies of Aryl Ether Linked Polybenzimidazole for the Use in Fuel Cell"* describes the synthesis and characterization of polybenzimidazole with ether backbone (OPBI) with tunable molecular weight by varying the initial monomer concentrations. Photo physical properties and the aggregation behavior of OPBI chains in polar protic and aprotic solvent were investigated. Formation of OPBI gel in formic acid (FA) by varying the gelation concentration and the polymer molecular weight were investigated. A detailed investigation has been carried out to monitor the improvement in several properties of OPBI by making the nanocomposites of OPBI using nanoclays and silica nanoparticles. The thesis consists of seven chapters. The summary of the contents of each chapter is given below.

Chapter 1

This chapter deals with a brief introduction of various types of polybenzimidazoles (PBIs) types of polymers, highlighting their different synthetic procedure of preparation and giving a general idea on their physical and chemical properties and polymer nanocomposites. In this chapter we have discussed the historical developments on PBI types of polymer and demonstrates the information about the nanocomposite formation of PBI polymer due to presence of proton donor (-NH-) and proton acceptor (-N=) hydrogen bonding sites in the backbone. This chapter also describes the most advanced application of phosphoric acid (PA) doped polybenzimidazole in high temperature polymer electrolyte membrane fuel cell (HT-PEMFC). A brief introduction about fuel cell, types of fuel cells and challenging involved in PEM fuel cell research are also included.

Chapter 2

A series of poly(4,4'-diphenylether-5,5'-bibenzimidazole)s (OPBIs) were synthesized from 4,4'-oxybis(benzoic acid) and 3,3',4,4'-tetraaminobiphenyl through the variation of the initial monomer concentration with a solution polycondensation

technique in a poly(phosphoric acid) medium. The resulting polymers were characterized by various techniques such as infrared (IR), nuclear magnetic resonance, dynamic mechanical analysis (DMA), and thermogravimetric analysis. The initial monomer concentration in the polymerization mixture played an important role in controlling the molecular weight of the resulting polymers. A temperature-dependent IR study showed that the free movement of the -NH group of the imidazole ring was blocked by the absorbed moisture. The DMA study showed that the glass-transition temperature (T_g) varied with the molecular weight, and the presence of the ether linkage in the OPBI polymer backbone had a significant influence on T_g. A high-molecular-weight OPBI polymer tended to form a supramolecular organization, which influenced the thermal characteristic of the polymer. Photophysical studies demonstrated the fluorescent characteristics of the OPBI polymers in both solid and solution states.

Chapter 3

The aggregation behavior of poly(4,4′-diphenylether-5,5′-bibenzimidazole) (OPBI) in polar aprotic (dimethyl acetamide, DMAc) and protic (formic acid, FA) solvents was studied as a function of the polymer concentration and solution temperature. The effects of solvent protic character on the aggregation behavior of OPBI were elucidated. The photophysical studies suggested that the OPBI chains form aggregated structures in both DMAc and FA solutions when the OPBI concentration is increased. The dependences of the emission spectra on the polymer concentrations in two solvents were not similar in nature, indicating that in both of the solvents the aggregations are intermolecular processes, though their mechanisms were different owing to the polyelectrolytic nature of OPBI in FA medium. The triexponential decay profiles obtained from the time-resolved fluorescence study for the concentrated solutions (both in DMAc and FA) displayed a negative fractional coefficient and longer excited state lifetime, providing support for the aggregations at higher concentration. The temperature dependence emission spectra suggested that the aggregations in both of the solvents destabilize with increasing temperature. The higher activation energy of aggregation (E_a) in DMAc (5.62 kJ/mol) compared with that in FA (3.07 kJ/mol)

revealed that the aggregation formation pathways were different in two solvents and stronger aggregates are formed in the former solvent. The dilute solution viscometry (DSV) studies demonstrated that the OPBI chains adapt a bigger extended conformation in FA compared with DMAc owing to the stronger intramolecular chain repulsion in FA arising due to the polyelectrolyte nature of OPBI in this solvent. A conformation transition of OPBI chains from compact collapsed to extended conformer was observed in DMAc solvent with increasing concentration, whereas any such transition was absent in FA medium. Transmission electron microscope (TEM) images and circular dichroism (CD) spectra were also in agreement with the presence of a conformational transition in DMAc and the absence of it in FA. The temperature dependent DSV studies further supported the disruption of aggregated structure with increasing temperature in both of the solvents. DSV studies exhibited that the deaggregation was driven by a conformation transition (extended to compact collapsed) in DMAc, whereas in FA the disruption happened without conformational transition.

Chapter 4

Thermoreversible gelation of OPBI in formic acid (FA) was explored thoroughly by studying the gel morphology, thermodynamics of the gelation, gelation kinetics utilizing test tube tilting and rheological study. The effect of concentration and molecular weight of the OPBI on the gelation process were probed by gelation kinetics studies reveal that the both gelation rate and critical gelation concentration ($C^*_{t=\infty}$) were function of gelation temperature (t_{gel}) and the molecular weight of OPBI. Fibrillar network morphology of gel was highly influenced by the gelation concentration and molecular weight of OPBI. Both the gel melting (T_{GM}) and gelation (T_G) temperature have been observed in thermodynamic study, showing the first order phase transition and also FA molecules help to produce the OPBI crystallites. The presence of crystallites in the gel was confirmed by WAXS study. FT-IR study provided the proof for the presence of strong hydrogen bonding interaction between the OPBI and FA molecules. The PA loading of OPBI membrane obtained from the OPBI-FA gel found to be significantly high than the conventional imbibing process membrane. The PA

doped OPBI film displayed very high thermal and mechanical stabilities. The porous structure of the membrane after evaporation of FA, which has been proved by SEM, TEM and AFM has been found to be the reason behind high acid loading. The proton conductivity of the membrane at 160^{o}C is ~1.117×10^{-1} S.cm^{-1}.

Chapter 5

Polymer nanocomposites of poly (4,4'-diphenylether-5,5'-bibenzimidazole) (OPBI) were prepared with two structurally different organoclays, namely, montmorillonite (OMMT) and kaolinite (OKao), to evaluate the effect of clay structures on the nanocomposites morphology, structure, and the properties. Solid State ^{13}C cross-polarization magic-angle spinning nuclear magnetic resonance, small-angle X-ray diffraction, and transmission electron microscopy studies suggested the formation of exfoliated structure for OPBI/OMMT, whereas and intercalated structure was obtained for OPBI/OKao. Both the nanocomposites displayed significant enhancement in the thermal stabilities compared to the pristine OPBI, and the higher thermal stability of OPBI/OMMT than that of OPBI/OKao was attributed to the higher degree of dispersion of the nanoclay into the OPBI matrix owing to the exfoliated structure of the former. Both the nanocomposites membranes exhibited large mechanical reinforcement by the clays and the superior mechanical property was obtained in the rubbery state compared to the glassy state. The storage moduli (E') for the OPBI/OKao membranes were found to be higher than that of OPBI/OMMT and recognized to the different dispersion patterns of both the organoclays along the polymer matrixes. The dispersed clay particles in the OPBI matrix shielded the polymer chains from the attack of oxidative radicals and resulted in huge enhancement of oxidative stability of the nanocomposites membranes compared to the pure OPBI membrane. The nanocomposites membranes have significantly higher phosphoric acid (PA) loading compared to the pure OPBI membrane which resulted higher proton conductivities of the formers. A continuous “forming-breaking-forming” process of weak hydrogen bonds of OPBI and the organoclays with PA was found to be the driving force for nearly a one order increase in proton conductivities for nanocomposite membranes. The low activation energy (E_a),

comparable with the E_a of free PA, obtained from the temperature dependent proton conductivities suggested a faster proton conduction process.

Chapter 6

Despite the myriad studies on polybenzimidazole based polymer electrolyte membranes for fuel cell operating above 100ºC, the development of membranes with higher proton conductivity without compromising mechanical stability has continued to be the prime challenge. In this chapter, organic/inorganic hybrid nanocomposites of poly (4,4'-diphenylether-5,5'-bibenzimidazole) (OPBI) were prepared with surface functionalized silica nanoparticles to address this key issue. Structural and morphological studies probed by SAXS, WAXD and TEM, respectively revealed the formation of selfassembled clusters of nanoparticles when OPBI nanocomposites were made with amine modified silica (AMS) whereas and well dispersed structure was obtained for OPBI and unmodified silica (UMS) composite. The OPBI/AMS nanocomposites displayed significant enhancement in the thermal stabilities compared to the pristine OPBI and OPBI/UMS nanocomposite. The OPBI/AMS nanocomposites membranes exhibited large mechanical reinforcement than the pristine OPBI and OPBI/UMS nanocomposite. The formation of nanoparticles clusters into the OPBI matrix in case of OPBI/AMS was found to be the driving force for the higher thermal and mechanical stability of OPBI/AMS than that of OPBI/UMS. The incorporation of AMS in the OPBI matrix shielded the polymer chains from the attack of oxidative radicals, resulted huge enhancement of oxidative stability of the nanocomposites membranes compared to the pure OPBI membrane. The OPBI/AMS nanocomposites membranes have significantly higher phosphoric acid (PA) loading compared to the pure OPBI membrane which resulted higher proton conductivities of the formers. The self-assembled clusters of AMS in OPBI matrix facilitated the proton transport process.

7.2. Conclusions

The following conclusions are drawn from the studies of *Studies of Aryl Ether Linked Polybenzimidazole for the Use in Fuel Cell.*

1. A series of OPBIs consisting of an ether linkage in the polymer backbone by changing the initial monomer concentration in the polymerization reaction mixture are synthesized and characterized.

2. Higher molecular weight polymers are obtained from a higher initial monomer concentration in the polymerization reaction mixture.

3. The incorporation of ether linkage in the polymer backbone enhances the flexibility of the backbone which influences the various thermal and thermo-mechanical properties of this type PBI (OPBI) compare to other PBI.

4. The molecular weight, thermal stability, T_g and other thermo-mechanical properties of the OPBI polymers can be efficiently controlled by varying the initial monomers concentration in the polymerization mixture.

5. The aggregation behavior of OPBI in polar aprotic solvent such as dimethyl acetamide (DMAc) and polar protic solvent such as formic acid (FA) are studied by varying the polymer concentration in the solution.

6. The concentration dependent photophysical study, dilute solution viscosity (DSV), microscopy and circular dichroism proved that the aggregation is an intermolecular process in both the solvent systems; however the mechanisms of aggregate formation in both the solvent systems are not similar.

7. OPBI chains form aggregated structures in both polar aprotic (DMAc) and polar protic (FA) solvents with increasing polymer concentration in the solutions and these aggregates dissociates at higher temperature in both the cases. The most importantly the natures of aggregations and its disruptions are driven by different mechanisms due to the protic and aprotic nature of the solvents.

8. OPBI produces thermoreversible physical gel in formic acid (FA).

9. The polyelectrolyte nature of OPBI in FA, strong hydrogen bonding between OPBI and FA molecule induce the crystallinity in the OPBI-FA gel, which is the driving force for the gelation.

10. PA doped OPBI membrane obtained from the PBI-FA gel shows remarkably high acid doping level as well as good thermo-mechanical stability and relatively high and faster proton conductive characteristics.

11. Nanocomposite materials consisting of OPBI and two types of organically modified layered clay (MMT and Kao) are prepared by dispersing of the silicate layers in the OPBI matrix by the solution blending method.

12. The morphology of the OPBI/Clay nanocomposites are dependent upon the structure of the clay; in case of MMT exfoliated structure is obtained whereas intercalated morphology is obtained with Kao.

13. The incorporation of nanoclays in OPBI results in an increase in thermo-mechanical, oxidative stabilities, acid doping level and huge increase in proton conductivity.

14. A series of organic/inorganic hybrid nanocomposite materials consisting of OPBI with amine modified and unmodified silica nanoparticles (AMS and UMS) are prepared by the solution blending method.

15. The morphology of the OPBI/silica nanocomposites are largely dependent upon the functional groups of the silica surface; in case of amine modified surface (AMS) self-assembled clusters formation is observed whereas well dispersed morphology is obtained with unmodified surface (UMS).

16. The incorporation of silica in OPBI results in an increase in thermo-mechanical, oxidative stabilities, and thermal stabilities.

17. The enhancement of the PA doping level as well as proton conductivity of the all the nanocomposite membranes compared to that of pure OPBI is observed.

7.3. Scope of Future Work

The present thesis has addressed three important aspects of *Aryl Ether Linked Polybenzimidazole: Solution Behavior, Thermoreversible Gelation and Nanocomposites*. We believe the findings of this thesis will have great impact on the future development of polybenzimidazole (PBI) chemistry in general, especially the use of PBI in PEMFC application. The thesis put forward and establish novel concept in the PBI chemistry research. The potential and scope of future work of this thesis are enormous. Few of these are listed below

1. Effort should be made to understand the polymerization mechanism and establish a correlation between the monomer solubility and reactivity ratios of the monomers.

2. Efforts should be made for the introduction of flexible monomer in the polymer backbone for easy processing of PBI.

3. Attempts must be made for the introduction of different kinds of nanofillers in the PBI polymer to enhance its properties.

4. The proton conduction behaviors and fuel cell efficiency of the PA doped PBI polymer membranes require attention.

5. Studied of thermoreversible gelation of verities of PBI may be initiated.

6. Finally, the fuel cell testing of the PA doped OPBI membrane obtained from the OPBI–FA gel can be studied.

Publications & Presentations

Publications

1. ***How the Monomer Concentration of Polymerization Influences Various Properties of Polybenzimidazole: A case Study with Poly (4,4'-diphenylether-5,5'-bibenzimidazole), Arindam Sannigrahi, ***Sandip Ghosh***, Joseph Lalnuntluanga, and Tushar Jana, *J. App. Polym. Sci.* **2009**, *111*, 2194.

2. ***Role of Solvents Protic Character on the Aggregation Behavior of Polybenzimidazole in Solution, ***Sandip Ghosh***, Arindam Sannigrahi, Sudhanshu Maity and Tushar Jana, *J. Phys. Chem. B* **2010**, *114*, 3122.

3. Monomer Structural Isomer Directed Polybenzimidazole Copolymerization and Their Properties, Arindam Sannigrahi, ***Sandip Ghosh***, Sudhangshu Maity and Tushar Jana, *Polymer* **2010**, *51*, 5929.

4. ***Role of Clays Structures on the Polybenzimidazole Nanocomposites: Potential Membranes for the Use in Polymer Electrolyte Membrane Fuel Cell, ***Sandip Ghosh***, Arindam Sannigrahi, Sudhanshu Maity and Tushar Jana, *J. Phys. Chem. C* **2011**, *115*, 11474.

5. ***Polybenzimidazole/Silica Nanocomposites: Organic-Inorganic Hybrid Membranes for Polymer Electrolyte Membrane Fuel Cell, ***Sandip Ghosh***, Sudhanshu Maity and Tushar Jana, Communicated to *Journal of Material Chemistry*.

6. Polybenzimidazole Gel Membrane for the Use in Fuel Cell, Arindam Sannigrahi, ***Sandip Ghosh***, Sudhangshu Maity and Tushar Jana, Revised manuscript submitted in *Polymer*.

7. *****Solvent induced porous polybenzimidazole membrane: A facile route to enhance proton conductivity, ***Sandip Ghosh***, Arindam Sannigrahi, Sudhanshu Maity and Tushar Jana, Manuscript under preparation.

8. *****Investigation of Polyelectrolyte Nature of Polybenzimidazole in Various Acidic Solvents Using the Isoionic Dilution Mthod, ***Sandip Ghosh***, Arindam Sannigrahi, Sudhanshu Maity and Tushar Jana, manuscript under preparation.

Note: Publications indicated by (*) marks are included in this thesis.

Presentations

1. Poster Presented on "*Synthesis and Characterization of Poly (4,4´-diphenylether-5,5´bibenzimidazole) for use in Fuel Cell*" Poly 2008: International Conference on Advances in Polymer Science and Technology January 28-31, 2008, Indian Institute of Technology, New Delhi, India.

2. Poster Presented on "*Synthesis and Characterization of Poly (4,4´-diphenylether-5,5´bibenzimidazole) for use in Fuel Cell*" 5th annual in-house symposium CHEMFEST 2008 of the School of Chemistry, University of Hyderabad, Hyderabad, India.

3. Poster Presented on "*Solvent induced porous polybenzimidazole membrane: A facile route to enhance acid loading capacity*" 6th annual in-house symposium CHEMFEST 2009 of the School of Chemistry, University of Hyderabad, Hyderabad, India.

4. Oral Talk on "*Polybenzimidazole-Clay Nanocomposites*" 8th annual in-house symposium CHEMFEST 2011 of the School of Chemistry, University of Hyderabad, Hyderabad, India.